UNIVERSITÀ
DEGLI STUDI
DI PADOVA

Sede Amministrativa: Università degli Studi di Padova
Dipartimento Territorio e Sistemi Agro-forestali

SCUOLA DI DOTTORATO DI RICERCA IN
"TERRITORIO, AMBIENTE, RISORSE E SALUTE"
INDIRIZZO:
"IDRONOMIA AMBIENTALE"

CICLO XXIV

STABILITY ANALYSIS OF GRAVEL-BED RIVERS: COMPARISON BETWEEN NATURAL RIVERS AND DISTURBED RIVERS DUE TO HUMAN ACTIVITIES

Direttore della Scuola : Ch.mo Prof. MARIO ARISTIDE LENZI
Coordinatore d'indirizzo: Ch.mo Prof. MARIO ARISTIDE LENZI
Supervisore :Ch.mo Prof. MARIO ARISTIDE LENZI
Co-Supervisore: Prof. JUAN J. R. SERRA
Co-Supervisore: Prof. LUCA MAO

Dottorando : GABRIEL KALESS

Contents

Index of Figures

Index of Tables

SOMMARIO

La presente ricerca studia i processi –i flussi dell'acqua e dei sedimenti- che definiscono la forma dei corsi alluviali. Il rapporto tra forme e processi si presenta molto complesso perché queste aspetti interagiscono mutuamente: la forma dell'alveo influisce il flusso delle acque che guida il moto delle particelle sul fondo ed, a sua volta, modifica la forma del canale. Questo studio riprende un vecchio argomento negli studi fluviali, quello di spiegare la forma dei corsi'acqua come risposta a certi controlli esterni e processi interni. Tuttavia, il problema non è risolto e questo studio apporta nuovi elementi.

Il punto di partenza nello studio del rapporto tra forme e processi si trova nelle teorie di regime che consistono in un insieme di equazioni per estimare la larghezza, profondità e pendenza di un corso d'acqua in equilibrio, quando la portata liquida ed il apporto di sedimenti sono conosciuti. Le teorie di regime sono state create nel secolo XIX inquadrate nell'ambito dell'ingegneria idraulica per la progettazione di canali di irrigazioni (Kennedy, 1895; Lacey, 1930; Lane, 1955). Leopold and Maddock (1953) introdussero il concetto di geometria idraulica nella geomorfologia fluviale e dimostrarono che i corsi'acqua modificano la pendenza nonché la sezione trasversale per raggiungere lo stato di equilibrio per una portata rappresentativa. I primi studi sono stati empirici, quindi un intenso lavoro teorico è stato svolto ai fini di spiegare le equazioni di regime. Parker (1978) dimostrò l'importanza di considerare la resistenza delle sponde nelle formulazioni nonché di usare modelli idraulici sofisticati per calcolare correttamente la distribuzione dello sforzo di taglio sul letto dell'alveo.

Una strategia alternativa è stata applicata per esplorare le proprietà geometriche dei canali. Langbein e Leopold (1962) considerarono i principi della termodinamica e suggerirono che la distribuzione dell'energia in un fiume tendeva verso lo stato piu probabile. Questo lavoro aprì un cammino teorico e poi altre teorie, chiamate "extremal hypothesis", sono state proposte: minima potenzia unitaria della corrente (Yang e Song, 1979), minima potenza della corrente (Chang, 1980), minima dissipazione di energia (Brebner and Wilson, 1967; Yang et al., 1981), massimo trasporto di sedimenti (White et al., 1982), massimo fattore di frizione (Davies e Sutherland, 1983) e massima resistenza al flusso (Eaton et al., 2004). Millar e Quick (1993) e piu recentemente Millar (2005) hanno proposto modelli che prendono in considerazione la resistenza delle sponde, un aspetto che non era stato incorporato nei precedenti lavori. Le teorie "extremal hypothesis" sono state criticate per la loro mancanza di base fisica (Ferguson, 1986; Parker et al., 2007). Tra l'altro, i difensori asseriscono la loro validità sulla base del principio di minima azione (Nanson e Huang, 2008), oppure nella esistenza di due feedback opposti che agiscono ad una scala ridota, quella della sezione trasversale (Eaton et al., 2006). Le teorie di regime normalmente considerano tre gradi di libertà (larghezza, profondità e pendenza) e quattro controlli esterni (portata liquida, apporto di sedimenti, diametro dei sedimenti, e resistenza delle sponde). Tuttavia, i parametri geometrici riflettono anche processi che aggiscono ad scale spaziale e temporali differenti (Weichert et al. 2009), un aspetto che non è stato considerato nelle teorie di regime.

La prima parte della ricerca è stata orientata alla revisione e discussione dei problemi teorici connessi sia con la rappresentazione dei sistemi fluviali sia con le teorie di regime. Come risultato, ho proposto i seguenti aspetti: a) le leggi della fisica ed i vincoli invocati nelle teorie di regime descrivono il comportamento di una popolazione di fiumi invece di descrivere i processi precisi al interno di un singolo tratto fluviale; b) ogni singolo elemento della popolazione ha dei confini incerti (larghezza e

profondità) ed anche delle proprietà incerte (diametro medio delle particelle nell'alveo, pendenza e portata a piene rive). Le teorie di regime sono state classificate secondo il numero di dimensioni ed il modo in cui i fiumi sono modellati. La classificazione è stata applicata alle teorie di regime per comprendere il debattito in torno alla validità delle teorie "extremal hypothesis".

La seconda parte della ricerca è indirizzata verso lo studio delle popolazioni di fiumi. Si presenta un confronto fra fiumi in stato naturale dalla Patagonia Argentina con quelli relativi ai fiumi disturbati dalle attività antropiche localizzati nella regione nordest di Italia. Sono state effettuati rilevamenti intensivi di campo in Italia ed Argentina; cinque tratti sono stati rilevati in Italia (appartenenti ai fiumi Brenta, Piave e Cordevole, tutti localizzati nella Regione del Veneto) e dieci tratti in Argentina (nelle provincie di Chubut e Rio Negro).

I tratti scelti per l'indagine hanno omogeneità morfologica lungo tutto il tratto e le stazione di misure delle portate vicine hanno almeno registri di 20 anni di dati. In Argentina le misure sistematiche delle portate iniziarono verso la metà del secolo scorso e quindi ci sono circa tra 23 e 63 anni di datti nelle stazione selezionate. In Italia, le misurazioni per il fiume Brenta si trovano nella stazione di Barzizza vicina a Bassano del Grappa, che ha registri dall'anno 1924. Per quanto riguarda il fiume Piave, dati da tre stazioni sono state analizzati: Belluno, Segusino e Perarolo. I tratti selezionati sono alluviali ed al meno una delle sponde è libera di evolvere. In certi casi la vegetazione copriva una delle sponde e in pochi tratti c'èrano opere di difesa spondale. Tutti i tratti iniziano in un raschio ("riffle") e finiscono anche in un'altro raschio, estendendosi lungo almeno una lunghezza di onda.

La informazione di campo, essendo estesa e dettagliata, è stata utilizzata ai fini di confrontare i corsi naturali e disturbati. Il confronto ha permesso di valutare la stabilità raggiunta dai corsi d'acqua italiani, considerando i fiumi patagonici come riferimento dello stato di equilibrio. Inoltre, seguendo il concetto di rapporto fra scale spaziali e risposta del canale proposta dai ricercatori Weirchert et al. (2009), si valutarono le previsioni delle teorie di regime quando si considera la pendenza come una variabile indipendente. Tre modelli, che incorporano un criterio di stabilità delle sponde, sono stati considerati. Ai fini di valutare la loro performance quando la pendenza è un controllo esterno, due modificazioni a questi modelli sono state proposte. Lo studio utilizza i dati dei fiumi rilevati nonché un database pubblicato composto da 92 tratti fluviali e 36 studi di caso di laboratorio. Alla fine, il modello di Millar (2005) è stato utilizzato per spiegare i cambiamenti recenti nei fiumi Brenta e Piave ed anche per valutare la loro possibile tendenza evolutiva.

L'ultima parte della tesi è stata indirizzata allo sviluppo, validazione ed implementazione di un modello bidimensionale basato sui processi, che è stato chiamato LICAN-LEUFU 2D. Questa parte del lavoro si basa sull'ipotesi che "*la morfologia del canale è non solo una conseguenza dei processi che aggiscono sul canale ma anche guidata da questi processi; inoltre, due dimensioni spaziali insieme ad un modello "depth-average" permettono di descrivere meglio la morfologia del canale*". La prima parte afferma che i processi sono i responsabili delle forme osservate nel canale, affermazione che costituisce il punto di vista assunto in questo studio per quanto riguarda il dibattito intorno alle teorie di regime. Tuttavia, non deve interpretarsi come un'opposizione alle teorie di "extremal hypothesis", oppure che non siano utile per prevedere la forma dei canali. Al contrario, come verrà dimostrato nella revisione dello stato dell'arte, le extremalhypotesis esprimono il comportamento del fiume alla scala di tratto, mentre in questo studio, le caratteristiche osservate alla scala di tratto verranno spiegate dai processi che aggiscono ad scale minori. La seconda parte dell'ipotesi significa che un modello bidimensionale

dovrebbe prevedere in miglior modo la morfologia di un canale da quanto si ottiene applicando un modello aggregato o unidimensionale, es.., il modello deve essere in grado di prevedere la geometria a scala di tratto (larghezza e profondità) nonchè la morfologia all'interno del tratto (pozze e raschi), che eccedono le capacità dei modelli essistenti.

Il modello è stato testato in tre differenti condizioni. Il primo test è stato realizzato sulla base delle misure di canaletta condotte presso l'Università di Hull. Il modello doveva prevedere la risposta di una canaletta di laboratorio, con fondo sabbioso-ghiaioso, che sviluppava una corazza statica in una situazione di apporto nullo di sedimenti. Nel secondo test il modello è stato utilizzato in una simulazione di medio-termine per estimare la forma del Fiume Azul quando vengono fornite come dati di input, le portate, il materiale di fondo ed il apporto de sedimenti. In questo modo, il test costituisce un'applicazione di un modello 2D nel campo delle teorie di regime. L'ultimo test riguarda l'applicazione del modello per lo studio di un caso: il Fiume Brenta. Il modello è stato caricato con una morfologia iniziale dell'alveo corrispondente all'anno 2010, e la granulometria superficiale. Il modello ha simulato il passaggio di tre piene straordinarie che si susseguirono nel periodo 2010-2011. Le previsioni del modello sono state confrontate con il DTM (modello digitale del terreno) che è stato rilevato alla fine del periodo. Inoltre, il modello è stato utilizzato per valutare la possibile tendenza evolutiva del tratto a medio termine.

SUMMARY

The present research studies fluvial processes –water and sediment flows – that define the shape of an alluvial channel. The relationship between forms and processes is complex because they are interrelated: the channel shape influences the water flow which drives the sediments movement on the channel bed that modifies the channel form, closing a circle. Although, the objective of the work is a very old question in fluvial studies, to explain the shape of rivers in terms of external controls and internal processes, the problem has not been solved yet and this study provies new elements for its solution.

The start of the quest for linking process and forms can be found in the development of regime theories which consists of a set of equations to estimate the width, depth and slope of a stable channel if liquid discharge and sediment supply are known. Regime theories were created in the XIX century within the context of hydraulic engineering in order to design stable irrigation canals (e.g. Kennedy, 1895; Lacey, 1930; Lane, 1955). Leopold and Maddock (1953) introduced the quantitative concept of hydraulic geometry into the context of fluvial geomorphology and showed that alluvial rivers adjust both their slope and channel in order to be in equilibrium for a certain representative discharge. The first studies were eminently empiric, hence there has also been an intense theoretical work focused on explaining regime relations. Parker (1978) demonstrated the importance of bank erodibility, and the need of using improved hydraulic models to calculate the shear stress distribution on irregular cross-sections.

Alternative conceptual approaches have been used to explore geometrical channel properties. Langbein & Leopold (1962) took advantage of thermodynamic principles to suggest that the distribution of energy in a river system tends towards the most probable state. After this first pioneering work, further so-called “extremal” hypotheses were proposed such as: minimum unit stream power (Yang and Song, 1979), minimum stream power (Chang, 1980), minimum energy dissipation rate (Brebner and Wilson, 1967; Yang et al., 1981), maximum sediment transport rate (White et al., 1982), maximum friction factor (Davies and Sutherland, 1983) and maximum resistance to flow (Eaton et al, 2004). Millar & Quick (1993) and Millar (2005) proposed models that take into account the bank strength, a distinctive condition not considered in previous works. Because of their lack of physical-based principles, extremal hypothesis approaches have been extensively criticized (Ferguson, 1986; Parker et al., 2007). Defenders claimed their validity based on the principle of least action (Nanson and Huang, 2008) or on the opposed feedback processes acting at the cross-section scale (Eaton et al., 2006). Regime models usually consider three degrees of freedom (width, depth, and slope) and four external control variables (liquid discharge, sediment supply, bed grain size, and bank strength). However, these variables reflect geomorphic processes acting at different temporal and spatial scales (Weichert et al. 2009) a crucial aspect not considered in regime models.

The first part of the research was then dedicated to review and discuss theoretical issues inherent to the representation of fluvial systems and to regime theories. As a result, I proposed that *a) physical laws and constrains describe the behaviour of a population of river reaches, instead of describing the exact processes within a single river reach; and b) each object contained in the population has uncertain boundaries (width, depth) and uncertain properties (median grain size, slope, bankfull discharge)*. Regime theories were classified according to the number of dimensions and the way of modeling the

fluvial system. In this way, light was shed on the current debate about the validity of extremal hypothesis theories.

The second part of the research focus on the study of the river-populations, consisting on the comparison of natural river reaches in Patagonia Region (Argentina) and river reaches disturbed due to human activities in Northern Italy. Extensive field measurements were conducted in Italy and Argentina; five river reaches were surveyed in Italy (belonging to Brenta, Piave and Cordevole rivers, in the Veneto Region) and ten river reaches in Argentina (in the mountain range of Central Patagonia).

River reaches were chosen for their morphological homogeneity and for having at least 20 years of continuous flow record. In Argentina systematic measurements began by the middle of twentieth century. For the selected gauge stations records covered a time span ranging from 25 to 63 years. in Italy, water discharge has been measured at the Brenta River since 1924 at the Barzizza station and for the Piave River, flow records are derived from three gauging stations at Segusino, Belluno y Perarolo. Reaches were selected for being completely alluvial and having at least one bank free to evolve. In some cases a thick vegetation was growing in the banks, and in few cases one of the banks was protected with groynes. All selected reaches started and finish at riffles and extended along a whole wave length comprising three riffles and two pools.

Then extensive and detailed field information was used to compare natural rivers in Patagonia and disturbed in Italy. The comparison was aimed to assess the stability state of Italian rivers, considering the properties of rivers in Patagonia as a reference of stable state. Then, following the concept of spatial scales and channel response proposed by Weichert et al. (2009), the consequences in regime models of considering the hypothesis that, while channel width and depth adjust quickly to changes in water and sediment supply, reach slope requires longer time spans, was explored. Three models, all of them incorporating a bank stability criterion, were considered in this study. In order to evaluate the performance of models introducing the slope as an independent variable, two modifications to previous models were proposed. The study also used published hydraulic geometry of gravel-bed rivers in other geographical regions (92 streams reaches) and laboratory data (36 small stream). Finally, Millar's (2005) regime model was used to explain recent morphological changes and potential recovery in the Piave and Brenta rivers.

The third and last part of the thesis was dedicated to the development and test of a 2D fully processes-based model, which was named LICAN-LEUFU. This part of the study was based on the assumption that "*the channel morphology is driven by and is a consequence of within-channel processes; and a two-spatial-dimensions and depth-averaged model describes best the morphology of the channel"*. The first part states that processes are the responsible of observed forms, which is the position hold in this study with regards to the debate on regime models. However, it should not be interpreted that extremal hypotheses are not necessary for predicting the channel shape. Extremal hypotheses express the behaviour at the reach scale while here, reach-scale features are explained by processes acting at a lower spatial scale. The second part means that the 2D model should do better in predicting channel morphology than 1D or aggregated models, i.e, the model is capable of predicting the reach-average form (width and depth) and also within channel morphology (pools and riffles) that are not within the capabilities of 1D or aggregated models.

The model was tested in three different ways. The first test was based on flume measurements conducted at the facilities of the University of Hull. The model was used to predict the response of a

laboratory flume that developed a static armour under conditions of sediment starvation. The observational consequences consisted on the bed change, surface grain size distribution change, outgoing sediment transport (bulk and grain size distribution). The second test was a middle-term simulation in which the model had to predict the shape of Azul River providing the actual water discharges, bed material, and estimated sediment supply, i.e., it was an application of the 2D model in the context of regime theories. The last test concerned the application of the model to a field case study: the Brenta River. The model was loaded with the initial morphology and surface grain size distribution and a series of runs were performed imposing the recorded discharges. Model predictions were compared against the final DTM (digital terrain model) and then used for assessing the possible evolution of the reach.

Section One

State of the Art

“Intuitivamente il concetto di sistema è strettamente legato al pricipium individuationis, cioè alla logica ordinatrice del soggetto che, dopo l’identità, pone l’unità nell’oggetto della sua esperienza, ovvero individua come uno un insieme di senzazioni connesse ad una percezione.”

Ludwig von Bertalanffy
Teoria generale dei sistema

“… elegir un conjunto acabado y relativamente limitado de rasgos, en los que se estudiará, en todos los individuos que se presenten, las constantes y las variaciones. Este último procedimiento es lo que se llamó el Sistema.”

Michel Foucault
Las palabras y las cosas

1 MULTIPLE VIEWS OF THE RIVER

At the beginning of the study of a new field it may be necessary to have a fuzzy definition of the study object in order to make possible research endeavor, but after a return to the foundations is crucial. The river, as a study object, has received much attention from the scientific community. Nowadays there are many issues concerning how to describe a river: the degrees of freedom, external controls, fundamental physical principles etc. All these topics emerged while answering the question about the channel stability, which can be tracked to the end of XIX century with the development of regime theories. Therefore I shall start this review with a brief history of regimen theories pointing out those aspects related with fluvial theories. Then, I'll present the current debate on regimen theories, mainly the controversies involving the theories based on extremal hypothesis. This will guide us to a review of basic concept such as the fluvial system and its boundaries, processes and structures, equilibrium in geomorphology, complexity and scales in the fluvial system. This review will constitute the theoretical framework of the research.

1.1 Brief history of regimen theories

A regimen theory consists on a set of equations that can be manipulated in order to provide the width, depth and slope of a stable channel if water discharge and sediment supply are known. In this brief summary the key contributions to the development of regimen theories and its application to gravel bed rivers will be presented. Special attention will be given to the identification of the specific issues that each investigator has worked on and the solutions proposed. These works, themselves, extend along time like a chain starting by the end of XIX century and continuing nowadays. Although present problems involved under "regimen theory" are not the same of those posed at the beginning, there are still conceptual issues that can be related to inherited manners of thinking that problems. This sections is aim to shed light on this aspects.

Regimen theories were created within the context of hydraulic engineering in order to solve a very pragmatical problem: the design of stable irrigation canals in India. By the end of the XIX century Kennedy (1885) published one of the earliest and most widely known works on the topic[1]. The aim of Kennedy was to provide a set of equations to be used in the design and construction of an irrigation canal with the condition that no silting would take place in it. Kennedy studied the Bari-Doad canal system in India. After many years of operation, these canals had attained equilibrium, as Kennedy said "*no silt was ever cleared away from these reaches*, *and therefore*, *for a considerable time the silt-transporting power in each has been just sufficient to carry all the sediment brought down*" (p. 281). Kennedy observed that discharge was constant and farther reaches were about equally turbid all the year round, i.e., control variables had constant intensity. On the other hand, the canal could adjust its width, depth and mean velocity. The canal was said to be in a state of "*permanent regime*" after slope and shape have attained constant values (there was no more siltation). Kennedy believed that sediment

[1] This moment was very intensive and important in the development of hydraulics because Reynolds was working on turbulence and published his famous contribution about the criterion to distinguish between laminar and turbulent flows (Reynolds, 1883) and the statistical approach introduced in the Navier-Stokes equations to describe turbulence flows (Reynolds, 1895). Furthermore, in Ireland, Manning was publishing his work on open channel flow (Manning, 1889).

transport, in suspension, was controlled by the vertical components of eddies directly related to depth. Sides had little effect and hence, were not further considered. That's why Kennedy proposed a design equation that related the critical velocity, for which silting was just prevented, in terms of flow depth; and introducing Kutter's resistance formula, he gave a criterion to calculate channel's slope.

Although Kennedy's work was soon taken as a reference, some aspects required for revision: it did not include width as a design parameter and it was only valid for the type of sediments carried by those studied canals. Instead, Kennedy gave empirical rules for the shape relation width-to-depth in later communications, as extended by Woods's work (1917). The problem of defining the right number of variables was stated and clarified by Lindley (1919) who affirmed that "*the dimensions, width, depth and gradient of a channel to carry a given supply loaded with a given silt charge, were all fixed by nature*". By that time his work received little attention and was much later recovered by Lacey, in 1930. Lacey took the problems left by Kennedy's work and made a notorious contribution recognizing the importance of Lindley "theorem", as he named it. Firstly, he demonstrated that channel width had an effect on critical velocity and replaced the depth by the hydraulic radius in Kennedy's formula; besides, he introduced a "silt factor" in order to take into account different types of sediments. Then, he derived a second relation for the width correlating flow area and critical velocity. Combining these two laws, he obtained an important relation between wetted perimeter and discharge:

$$P = 2{,}67Q^{0{,}5} \qquad 1.1$$

Wherein, P is the wetted perimeter (in feet) and Q, the discharge (in cubic feet per second). Finally, applying Manning's formula Lacey derived a third equation to calculate channel's slope and, in this manner, he demonstrated Lindley's theorem.

Lacey was not only interested in the construction of stable irrigation channels but also in other engineering problems, such as railway-bridge calculations. This is the first application of regimen theories to the context of fluvial systems. Reasoning that in large rivers the wetted perimeter can be closely approximated by the width at water-surface level, he derived the width (B, in feet) of alluvial channels:

$$B = 2{,}67Q^{0{,}5} \qquad 1.2$$

Therefore, the width of a stable alluvial river changes with the square root of the discharge and is independent of the type of sediments transported. There is not any clear definition in Lacey's work about the discharge to be used with this formula. He only refers a "maximum flood discharge" in the comments of a graphic (Lacey, p.276). The discharge would remain as a controversial point in later researches.

An inflection point in the study of rivers and regimen theories came out by the middle of XX century when Leopold and Maddock (1953) presented the concept of hydraulic geometry. Leopold and Maddock were working in the context of geology and geomorphology, within the conceptual framework of geographic cycle and the different stages in the development of landforms through the cycle as proposed by Davis (1899, 1902). At that moment the discussion was centered in identifying which variables the channel adjusted for attaining equilibrium. Mackin (1948) had argued that "*a graded stream is one in which, over a period of years, slope delicately adjusted to provide, with available discharge, just the velocity required for the transportation of the load supplied from the drainage basin*"

(cited by Leopold and Maddock, p.51). Leopold and Maddock revised this concept with the aid of quantitative analysis, something new in geomorphology[2]. At that moment, all the hydraulic information had been collected for engineering purposes and consisted on width, area and discharge for a range of stages at specific locations (gauging stations). With this information they applied the new concept of hydraulic geometry. "At-a-station hydraulic geometry" is the relation of velocity, mean depth and width of flowing water with the discharge at a particular cross section of a river. The relations are expressed by means of potential formulas, i.e., $Y = a X^b$.

$$B = aQ^b \tag{1.3}$$

$$H = cQ^f \tag{1.4}$$

$$U = kQ^m \tag{1.5}$$

Wherein, B is the water-surface width, H is the mean depth, U is the cross-section mean velocity, for a specific discharge Q.

These relations can also been used to study changes in the cross sections along the length of a river, and are known as "downstream hydraulic geometry". Different cross-sections in the hydrographic network are compared under the condition of constant frequency of discharge. Leopold and Maddock chose the mean annual discharge, that had approximately the same duration in all the streams they studied. They found that "… *in a downstream direction the rates of increase in width, depth and velocity relative to discharge are of the same order of magnitude for rivers of different sized drainage basins and of widely different physiographic setting*" (Leopold and Maddock, p.14). The resulting exponents in the power laws for downstream hydraulic geometry relations are:

$$b = 0{,}5 \qquad f = 0{,}4 \qquad m = 0{,}1 \tag{1.6}$$

Comparing these results with Lacey's equations, it follows that width in alluvial channels increase with the same rate as in irrigations canals. There is a discrepancy for the mean depth but it was attributed to a difference in sediment concentration. While irrigation channels must keep a constant concentration, rivers showed a slightly decrease in the downstream direction, a discrepancy that Leopold and Maddock's model was capable to explain (p.45). Moreover, other similarities were found such as the concavity of downstream bed profile that supported the analogy between alluvial channels and irrigation canals.

As a result, Leopold and Maddock showed that graded streams adjusted both slope and channel characteristics, enlarging the number of possible degrees of freedom stated by Mackin; and alluvial rivers were analogous to canals at regimen in the sense that channel characteristics followed the same rate of increase with discharge. Finally, it is worth underlining that the analogy was only valid considering constant frequency of discharge.

[2] It is interesting to note that Leopold first graduated in civil engineering, then he worked on meteorology and later he obtained a PH.D. in geology. He got a broad view combining the naturalistic approach of geology with the application of exacts sciences in engineering. His seminal paper with Maddock is considered as the introduction of quantitatively observations in the context of geomorphology. They concluded in this paper that: "*Geomorphology cannot move ahead if we remain content to describe processes of land sculpture only in qualitative terms. When viewed quantitatively, the interactions of various hydraulic factors are found to be more complex than the qualitative analysis have led us to believe, but the unraveling of their complexities constitutes advance of knowledge*" (Leopold and Maddock, 1953, p.52)

The hydraulic geometry concept was soon applied by other workers in different geographical settings. Although the mathematical formalism was kept, there was not agreement with regards to the discharge to be used. It was a critical point because the choice of discharge influenced the value of the exponents. Bray (1982) studied rivers in Alberta (Canada) and adopted the discharge that resulted in the "*highest coefficient of determination and lowest standard error*". The discharge that fulfilled this criterion resulted to be the 2 years flood flow. Hey and Thorne (1986), measured rivers in the United Kingdom considering the bankfull stage. They supported this selection with previous field evidence on the relation of dominant and bankfull discharge. The dominant discharge is a concept introduced to assimilate natural streams with irrigation canals, i.e., "*the steady flow that would produce the same average bankfull dimensions as the natural range of flows*" (Hey and Thorne, 1986, p.672)[3].

All the studies aforementioned followed an empirical approach, and the derived set of equations was descriptive in essence but did not explain the relation between variables. There has been a huge work to accomplish this scope.

A definitive step towards a rational explanation of hydraulic geometry was done by Lane with the recognition of shear stress as a key concept in channel stability. Lane worked for the US Bureau of Reclamation in an investigation with the scope of improving the design of irrigation canals. In order to establish the stability of sediments along the cross section, he considered that it was not feasible to study the interaction between flow and bed particles in terms of flow velocity. Instead, he focused on the analysis of forces. He distinguished two forces acting on particles, namely, due to water flow and also to gravity which tends to make particles roll or slide down the slope. In his article of 1955 Lane made important contributions to hydraulic engineering such as the maximum shear stress on bed and banks, the angle of repose of coarse and noncohesive material, and the formula to calculate the effect of bank slope in the stability of particles.

The concept of tractive force (or shear stress) was then applied to derive a theoretical cross section of a stable canal, named the "threshold canal" (see Li et al., 1976 for a complete exposition). A threshold canal is one in which all the particles, both on the slopes as well as on the bottom bed, are subject to the force just sufficient for entrainment, that is, the threshold shear stress. Considering that shear stress was proportional to water depth, Li et al. (1976) derived a roughly parabolic cross section. When this theory was applied to natural streams resulted in a paradox: the "stable channel paradox", as named by Parker (1978, 1979). Parker demonstrated that it was not possible for a channel with stable banks to convey sediments at the same time. Bed load was observed in gravel bed rivers for conditions near bankfull, i.e., shear stress above threshold on the bed, while for the channel to be stable shear stress should remain below the critical value along banks. Then, Parker showed that the simple relation between depth and shear stress was wrong, and it was necessary to investigate more deeply in the mechanisms involved in shear stress distribution. A solution was found with the aid of the work of Lundgren & Jonsson (1964), who presented a model for shear stress distribution based on lateral turbulent diffusion. Finally, Paker derived a new theoretical expression for the cross section that combined a central region with active bed, and lateral stable banks.

[3] More recently, Emmet and Wolman (2001) presented field evidence that the effective discharge, i.e., the discharge that transport most of the annual sediment bulk, is near or equal to the bankfull discharge in gravel bed rivers.

Parker's work received great attention and was extended by several investigators: Ikeda and coworkers (1988) improved the stability criterion considering that banks were composed of graduated material; later, Ikeda with Izumi (1990) modified the shear stress model adding the influence of bank vegetation; and Pizzuto (1984, 1990) worked on the stability criterion and applied a lateral sediment transport model in order to simulate channel widening processes.

The aforementioned theories predict channel width and depth at bankfull stage when slope, discharge and sediment caliber are known. However, other investigators considered that the channel had more degrees of freedom, such as roughness, even the slope, and velocity. It was soon recognized that the available principles (mass conservation and energy conservation) were not sufficient when applied to the river reach. As a solution, several investigators proposed an extra condition, named the "extremal hypothesis". The first one is owed to Langbein and Leopold (1962). They conceived the river reach to be analogous to an open system in thermodynamics, interpreting entropy in terms of probability: "*the distribution of energy in a river system tends toward the most probable state*" (p.2). This condition was achieved when the combination of exponents in the hydraulic geometry relations attained a minimum variance. As a result, they were able to explain the features of longitudinal profiles, the hydraulic geometry and drainage networks.

After Langbein and Leopold's pioneer work a huge number of extremal hypotheses were developed, always proposing some kind of optimization criterion, such as: minimum unit stream power (Yang and Song, 1979), minimum stream power (Chang, 1980), minimum energy dissipation rate (Brebner and Wilson, 1967; Yang et al, 1981), maximum sediment transport rate (White et al., 1982), maximum friction factor (Davies and Sutherland, 1983), maximum resistance to flow in the system (Eaton et al, 2004). Recently, Millar & Quick (1993) and Millar (2005) have proposed models that incorporate bank strength, a distinctive condition not considered in previous works. It is worth to mention that Cao & Knight (1997, 1998) also solved the stable-channel paradox, but within the context of extremal hypothesis, combining the entropy-based bank profile equations and the depth-mean-averaged momentum equation by Shiono and Knight (1991).

Although the astonishing quantity of extremal hypothesis, it has been demonstrated that most of them are equivalent (see Knighton, 1998, p.161). These models have got good success in explaining hydraulic geometry exponents but a debate has emerged due to their probably lack of physical base. Is it then possible to explain hydraulic geometry thoroughly in terms of mechanics, and in this manner, avoiding the extra condition? Or instead we have to admit, as Knighton affirms, that "*there is an element of indeterminacy in the behaviour of streams with mobile beds*" (1998, p.161), and hence, the additional hypothesis is indispensable.

1.2 The debate on regimen theories

Since their appearance, extremal hypothesis have been criticized and the main objections have been focused in their unjustified propositions. Recently, Parkers and coworkers (2007) have claimed that they found the "*missing information*" needed to solve the set of equations for stable rivers. Their proposal consists on an empirical "*relation that expresses how a catchment organizes itself to deliver gravel downstream*" (p.18). In summary, it is a power law relating sediment supply at bankfull stage and bankfull discharge. Because water discharge increases with basin area in the downstream direction it seems reasonable that the sediment supply will also vary against the drainage area. It follows that both

variables could be related. Although very interesting, it must be said that the relation proposed is not exactly a "solution for the problem" because if sediment supply was already known, then their set of equations would provide a solution anyway. That is, their model was sufficient under the condition that the discharge and bed load were provided. However, their claim of solution was directed to the extremal hypothesis school. In fact, they criticized particularly Millar's (2005) model stating that "*the extremal condition in question must be accepted a priori*" (p.18). This means that while the "valid and empirical" supply-relation proposed by Parker et al, would describe "the organization of the basin", on the other hand there would be doubts on Millar's proposal, that in the end as will be shown later, can be interpreted as an organization at the reach-scale. Shall thus we accept "a priori" Parker et al.'s sediment supply relationship?

It is worth to comment here some aspects of Millar's model (it will be treated in detail below). Millar extended the optimal theory, that had been previously developed by other investigators (see summary provided by Millar, 2005), incorporating the analysis of bank stability. His model had four unknowns: bottom width, central depth, downstream slope and bank angle, and almost the same constrains used by Parker and coworkers: a sediment transport relations, resistance to flow and bank stability. However, they were insufficient in Millar's model because he added the bank angle and besides, he enabled the bank angle to be lower than the critical slope (that corresponds to the condition of shear stress due to water flow equal the threshold value for initiation of motion). Therefore, a forth relation must be written in order to solve the set of equations. What would the result had been if Millar had imposed the threshold condition along the banks? Would the extra condition still be necessary?

Millar proposed a mechanism to support the optimal theory. He stated that "*Channel configurations that are steeper than the minimum slope can be considered to possess excess stream power, beyond the minimum required to transport the imposed sediment load*" (p.210). We will discuss this proposition with the aid of Figure 1.1 that reproduces Figure 1 in Millar's publication. This figure illustrates the slope neede to carry a given sediment load for different channels configurations. A wide channel needs a high slope because depth is low. On the other hand, a narrow channel needs also a high slope because most of the resistance is produced along the banks. In the middle of these two extremes there is a configuration with minimum slope. Are these configurations equivalent? Are the wide and narrow channels stable? If the channel is too narrow shear stress will erode banks enlarging the channel. On the contrary, a too large channel will promote sedimentation within the channel changing to a braided configuration or later to a narrower single-thread channel with erodible banks (threshold condition). This reasoning hints a drawback in Millar's model regarding the bank stability analysis. Figure 1, should not be interpreted as an expression of "indeterminacy", i.e., for a given discharge and sediment supply there are infinite configurations, because the lateral stability is not the same in all the situations.

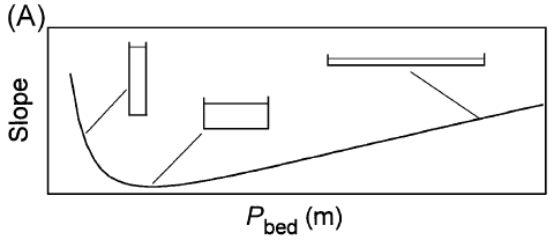

Figure 1.1 This graph has been proposed by Millar (2005) to show the needed slope for different channel widths (P_{bed}) in order to carry an imposed sediment load.

Ferguson (1986) also raised critics to extremal hypothesis arguing that they had never been justified physically. With regards to Langbein and Leopold's theory of minimum variance he affirmed that it *"is unhelpful because it cannot predict the actual width, depth and velocity variables that are of interest but only their relative rates of change, it is unjustified because it has no rational physical basis, and it is unnecessary because there is no shortage of deterministic approaches that give qualitatively and quantitatively reasonable predictions*" (p.25). In spite of the aforementioned drawbacks, Knighton (1994) added that "*it does provides one rationale for river channel adjustment which combines deductive methodology with the probabilistic viewpoint that only average or most probable states can be defined*" (p.160). At this point of the presentation, it should be clear that the indeterminacy problem always arises when the river is treated at the reach scale. We can situate Ferguson position in the rational approach that seeks the explanation to river reach behaviour in terms of mechanical interactions, and in fact he states that "*…the outstanding problem is to explain just how within-reach differences in hydraulic geometry are involved in the development and maintenance of equilibrium channel patterns that involve non-uniform flow through pools and riffles and over and around bars*" (p.26).

Recently, Nanson and Huang (2008) have presented a new justification for extremal hypothesis based on the principle of least action. Firstly, we have to mention, from what is expressed in their publication, that their position is wholly against Newtonian mechanical explanations, and instead they are in favor of more general principles. Newtonian approach is criticized due to its complexity, simplifications and idealizations, and its impossibility to explain the remarkable consistency of river forms an styles globally (including specially the cases with riparian vegetation) (p.926-927). Appling the least action principle Nanson and Huang concludes that the stable state corresponds to a "*minimum level energy demanded by the flow for carrying its water and sediments loads*" (p.938).

One objection may be stated against the applicability of the least action principle to fluvial systems. The action is defined as the temporal integration for the kinetic energy minus the potential energy at any time. Applying the variational technique in order to solve the simplest system, constituted by one particle in a gravitational field, it is possible to demonstrate that it reduces to Newton's law. In fact, every *"fundamental law can be put in the form of a principle of least action"* (Feynmann, 1964, p.19-7). Therefore, we see that both Newton's laws and the principle of least action are equivalent. However, there is a fundamental difference, as clearly stated by Feynmann: *"the principle of least action only works for conservative systems – where all forces can be gotten from a potential function. You know, however, that on a microscopic level –on the deepest level of physics- there are no nonconservatives forces. Nonconservative forces, like friction, appear only because we neglect microscopic complications – there are just too many particles to analyze"* (p.19-7) and the fluvial system is very far from been a conservative and microscopic system.

At this point of the discussion we shall formulate some questions:

> Is indeterminacy a property of the system or a feature belonging to the specific model elaborated by scientists?
>
> Shall we recognize the presence of different levels of organizations and hence different behaviours? In this sense, does the extremal hypothesis express reach-scale organizations and are mechanical interactions valid at smaller scales?

Is the bankfull discharge an upstream imposition or the result of within-reach geometry? If the latter option was right, all the models aforementioned would have incorrectly considered a system's output as an input.

In order to give an answer to these questions it is necessary to reformulate our concept of river and the manner to describe it. This will help us to clarify the conflicts between theories and to formulate the hypothesis of this study.

1.3 System, structure and processes

The concept of system is at the base of every research because each study must define its object cutting it from the universe, as Borges explains, *"un sistema no es más que la subordinación de todos los aspectos del universo a uno cualquiera de sus aspectos"*[4] (cited by Cereijido, 2009, p.33). With regards to fluvial systems we found useful remembering the definitions proposed by Chow et al. (1994) in their classical textbook on hydrology: *"a hydrological system is defined as a structure or volume in space, surrounded by a boundary, that accepts water and other inputs, it internally operates on them and produces some outputs"*. Their definition specifies a region in space, assumes an structure and observes the existence of fluxes. Taking all this elements, we define the fluvial system *as a region in space subject to the flow of water and sediments; it receives an amount of water and sediments, conveys them through the system operating mutually and produces an output.* This definition stresses the concept of processes above the structure. The river is, above all, a flow, the flow of water and sediments.

The system has a structure that consists on the particular arrangement of matter in space. The arrangement is measured by means of a quantity and the structure or organization is the variation of this quantity against a certain criterion. For instance, let us consider the median grain size of a unit volume, and the criterion of observation is the vertical direction. Then, a river with a vertical variation of grain size, from coarse grains on the surface to fine grains in the substrate is said to have developed an armour layer. Another unique feature of gravel-bed rivers is the presence of bed forms with shallow sectors (riffle) and deep regions (pools). The structure is described by means of bed elevation in the downstream direction. Each structure can be accounted with a proper parameter. Commonly, the ratio of surface median grain size to substrate median grain size is employed for the armour structure (absolute armouring index) or an index taking into account the sediment transport (Dietrich et al. 1989). With regards to riffle-pool sequences the ratio of riffle-spacing to channel width has been invocated (Hey and Church, 1986) or the bar steepness ratio (Millar, 1999).

Processes and fluxes will be used as synonyms. We are used to see forms and to deduce processes from the change in the forms. Form and processes are interrelated like each side of a coin, while processes are the diachronic aspect of the system form and structure represent its synchronic aspect. In fluvial systems there are two interacting processes: the flow of water and sediments. The flow of sediments is commonly named as "process of erosion", comprising the entrainment of particles (erosion), their transport and siltation. Each of these stages has to be adequately described in order to explain the whole flow of sediments.

[4] *"a system is nothing else than the subordination of all the aspects of the universe to only one, anyone, of its aspects"*

Form, water flow and sediment transport interact continuously. The shape of the channel defines the features of water flow, such as its velocity and shear stress on the bed, that in turn will drive the movement of particles, and finally, erosion and siltation will modify the channel shape and hence the circle is closed. Figure 1.2 illustrates the interrelationship and feedbacks between the three actors. This will be the object of an intensive review in the following chapters because is a key aspect of fluvial dynamics.

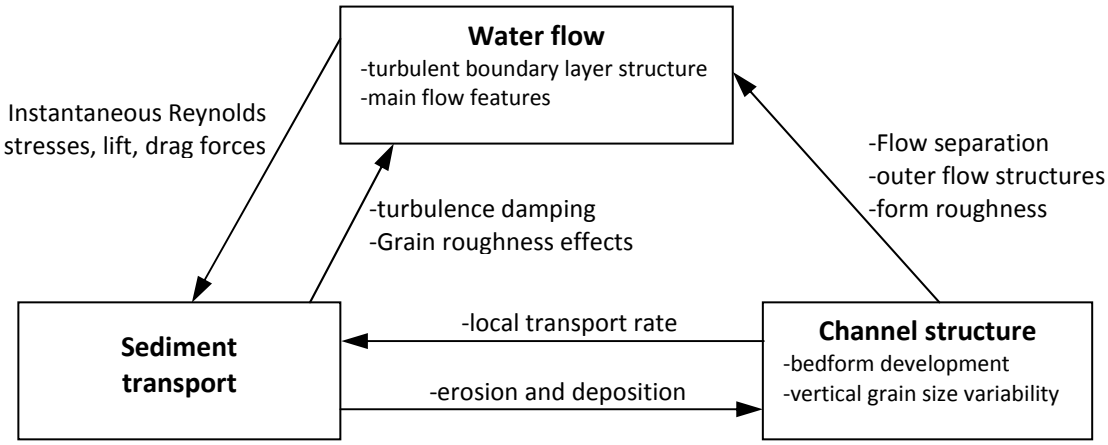

Figure 1.2. Interactions between water flow, sediment transport and channel structure (modified from Best, 1993)

The picture aforementioned shows processes at the very small scale, as follows from the inclusion of the boundary layer concept. In general, there has been a continuous reduction in the time- and space-scale of research, with an emphasis on explaining the dynamics of small site-specific river reaches. Furthermore, Lane and Richards (1997) affirm that *"short time-scale and small space-scale processes influence processes over longer time-scales and larger space-scales"*. Regimen theories have treated the river reach as a whole entity, however, these researchers point out the need of analyzing within reach processes. Viewing the system as a set of interacting elements, we can differentiate several levels of organization. The most elementary level comprises individual pebbles. An arbitrary upper level would be composed of a volume of material, and defined by an Areal element. The sum of areal elements can define specific larger elements such as pool-sectors, riffles or bars (morphological units). At each level corresponds a structure and characteristic parameter. Table 1.1 shows an example of this kind of hierarchical organization for a fluvial system.

Width, depth and slope are aggregated parameters that summarize the form of the channel at the system level, but they do not take into account the structure. It is necessary to pass to the next level. An area element can be considered as a system, with its own inner laws and interacting with surrounding parcels. In this case, the state of an element is described with its elevation, slope and grain size distribution. The structure at this level consists on the vertical variability of grain sizes. With the increase of calculus power of computers research has moved to model processes at the area level. The pebble level has been mention just for the sake of conceptual purposes but it is beyond the boundaries of regimen theories.

Table 1.1 Hierarchical levels of organization in the fluvial systems

Level	Structure	Parameters	Hydraulic models
Fluvial system	Channel pattern, and grain size variability (vertical and planimetric).	Aggregated variables: width, depth, slope, mean diameter	Empirical energy dissipation formulas for grain and form roughness.
Areal element	Vertical grain size variability. Pebbles arrangements	Elevation, local slope, grain size distribution, specific threshold of motion.	Empirical energy dissipation formulas due to grain roughness. Reynolds equations.
Pebble	Contact with surrounding pebbles	Size, weight, roundness	Navier-Stokes equations

Another point that deserves our attention regards the description of processes and its relation to the system levels. Flow resistance formulas, such as the Manning-Stricker relations, model water flow at the reach level connecting mean flow properties (shear stress, velocity) with mean bed surface properties (for instance, reach-averaged median grain size). Another example is the case of sediment transport formulas which are derived from field observations or laboratory measurements. In the first case bed load is the sum of individual measurements at different points over a period of time (see for instance, Milhous, 1979; and Powell et al., 2003). Then it constitutes an integrated mean value. Furthermore, surface-based models consider a mean grain size distribution for the surface material (see Parker, 1990). Recently, Chen and Stone (2008) have analyzed the sensitivity of Wilcock and Crowe (2003) sediment transport model with different grain size distributions and concluded that a "*global grain size distribution is not adequate for predicting the fractional bedload transport rate*". Then, the sediment transport formula relates the mean process intensity with average features of the bed. Our models simulate average processes over wide extensions and hence it limits their application to progressive smaller space scales.

1.4 The problem of defining the boundaries

Defining the boundaries of a fluvial system is not an easy task because there is a continuum from the channel to the adjacent floodplain. Even in the case we can recognize the presence of a "river" in the landscape and bring it from the background to the foreground, the action of "cutting" the object from the landscape needs methodological criteria. Leopold and Maddock (1953) proposed the concept of at-a-station hydraulic geometry that describes the geometric properties of the channel cross-section as a power function of discharge. Then each cross section has a characteristic set of exponents, one for each relation width-discharge, depth-discharge. Their approach recognizes the problem of lack of precise boundaries in fluvial systems and hence a continuous function is invocated. Many objects in nature have this feature. For instance, while it is easy to say how many waves are approaching the cost line, which is the line that defines the starting and ending point of an individual wave?

This problem is not exclusive of geomorphology, instead it has been studied in other areas such as pattern recognition and information processing. A pioneer work is that of Zadeh (1965) who proposed the concept of fuzzy sets.

A fuzzy set is a class of object with a continuum of grade of membership. In a traditional way of thinking about sets there are only two possibilities: an object belongs or not to the set. Instead, Zadeh proposes the membership function that takes values between 0 and 1. This function is applied to each object and gives the grade of membership to the particular set. If the function is near unity, it is said that the object has a high grade of membership. This concept is particularly useful for defining the fluvial system domain.

We have mentioned that the river can be defined as that region in space subject to the flow of water and sediment. Therefore, one way of "recognizing" a river is by means of the shear stress on the bed due to water flow. This parameter gives the intensity of water flow and besides is directly related to sediment transport. A procedure for recognizing a "river" from the landscape could be the following: a) define the limits of the studying area, b) divide this area into small parcels, b) measure the shear stress at each parcel during a whole year and take its average, c) define the membership function as the ratio of the mean shear stress and a reference shear stress (for instance, the maximum value), and d) apply the membership function to each parcel. The result will be a grayscale picture with low values, white parcels meaning "landscape" and dark cells or high values meaning "river". A possible picture could be as shown in figure 1.3.

Figure 1.3 portraying the channel area resembles longevity chart developed by Lane and Richards (1997). These researchers performed detailed topographical surveys in a small stream during a month. Channel dynamics was then evidenced by means of the longevity chart, in which the age of the cell increased when there was neither erosion nor deposition between consecutive DTMs. Figure 1.4, reproduces the result with "dark" cells representing zones of intense channel change that correspond to intense processes as employed in figure 1.3, and "soft" cells are not subject to changes and therefore a low value of membership function applies to them. Note that this map is equivalent to the fuzzy concept.

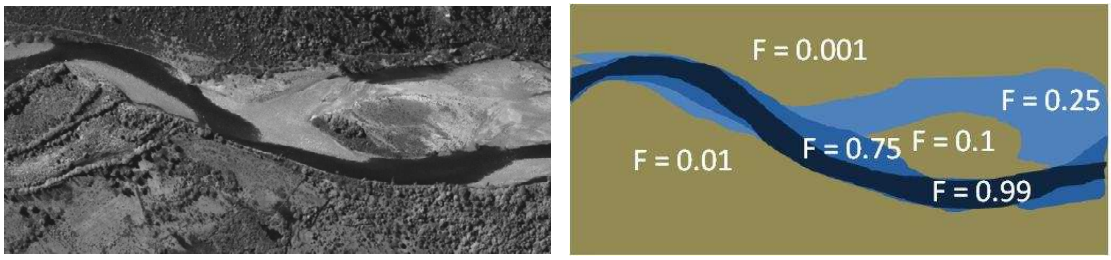

Figure 1.3. Fuzzy set concept applied to the river system for identifying its extension. On the left an aerial image of Azul River in Patagonia, Argentina; on the right, a possible representation of the river area according fuzzy logic.

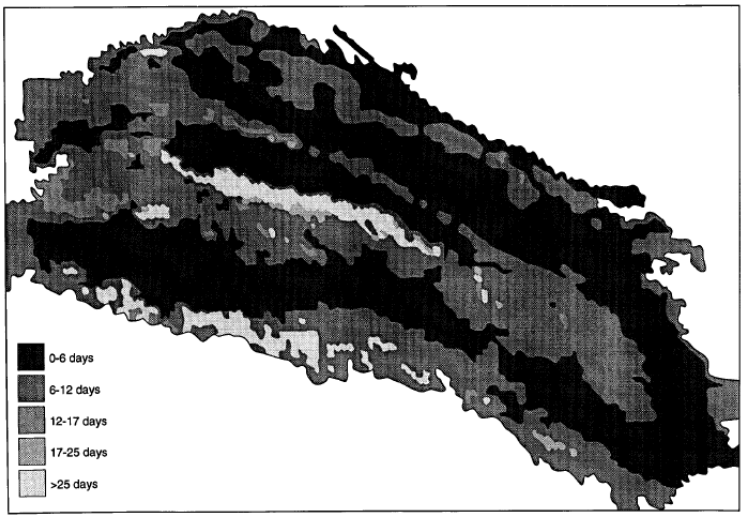

Figure 1.4. Map of channel longevity defined as the accumulated time for which there has not been erosion or deposition (Lane and Richards, 1997).

1.5 Regimen theories according to the number of dimensions

Every model starts defining its object, and in particular, the number of dimensions needed to describe it. The dimensions can be any variable that we choose to track the system evolution. For instance, dealing with a gas the variables used are its pressure, temperature and volume. There is an equivalent in fluvial systems as proposed by Eaton et al. (2004). These authors affirm that the alluvial channel state is defined by, again, three variables in an equilibrium state diagram: the aspect ratio (width/depth), the relative roughness (depth/grain size) and the dimensionless shear stress. In this study, we will use "dimension" as a space direction and by number of dimensions, the quantity of directions in space the researcher has chosen in order to develop his model. Once this choice has been made, the problem is how to describe the object with its structured, how to describe processes within the system, and finally, how to describe the relation of the system with the surroundings.

Considering the number of dimensions as a classifying criterion, three types of models can be recognized, namely: aggregated (or zero-dimension), one-dimensional (or cross-section) and two-dimensional (or distributed). This way of classifying is not rather new, and has already been used by Chow et al. (1994) in their textbook of hydrology. From them I borrowed the term "***aggregated***" and its definition: in an aggregated model the system is averaged in space or considered as a point without dimensions in space. The system is described by a set of aggregated parameters and variables, all of them calculated as an averaged in space. Some variables commonly used are the reach averaged width, mean depth, grain size and slope.

Distributed models consider that fluvial processes happen at different points in space and the system variables are functions of the spatial dimensions. When only one dimension is adopted it means that processes vary mainly along one direction, i.e., there is a preferential direction in space. In open channel flow one-dimensional models extend along the cross section because flow characteristics are constant in the downstream direction, i.e., there is a uniform flow.

Two-dimensional models are distributed models that consider processes as functions of space in both directions: across the section and streamwise. In spite of processes being distributed in space, the

system can still be described by means of aggregated variables. Therefore, we recognize that there are two aspects where the classification can be applied: form and processes. However, when analyzing form, it is clear that if the model aggregates processes then form must also be defined aggregately. Distributed model also accept a distributed way of describing forms. For instance, from a one-dimensional model the bankfull width can be calculated but also the cross section shape. And even, a two-dimensional model enables the study of formation and evolution of structures such as riffle-pool sequences.

1.6 Regimen theories and the way of modeling

Once the system has been defined, the number of dimensions have been chosen and the principal set of variables describing the system have been identified, the next step consists of specifying how the system works, i.e., the way it operates on the material it receives and produces some outputs. Researchers have followed different approaches that can be grouped into three classes: behaviorism, constrains-based, and processes-based.

Behaviorism in the context of fluvial dynamics means that the observer has identified a distinctive feature of the system as a whole. This kind of theory is commonly known as extremal hypothesis. I use the word behaviorism because it refers to something observed from the "outside"[5]. The extremal hypothesis expresses a feature that belongs to the system level and it does not exist at a lower level (subsystem or elemental level). However, the behaviour is related to complex stochastic interactions at the lower level. Recently, Eaton et al. (2006) proposed this picture in order to give a "physical base" to extremal hypothesis. Their qualitative model consists of a couple of feedback processes at a local scale (the cross section). On the one side, cross section variability results in an uneven distribution of shear stress that, by means of the positive feedback, increases that asymmetry. On the other side, it also promotes bank erosion and lateral migration of channel, with the corresponding increase in sinuosity and decrease in slope, all of them reducing shear stress, i.e., it is a negative feedback. These processes that take place within the system are at the base of at-the-system level behaviour, such as the slope-minimizing behavior proposed by Eaton and Church (2004). Behaviour is usually expressed as an optimization constrain and there is a huge variety of variables that researchers have used to describe that behavior, as has been exposed in section 1.1.

Another kind of approach consists on specifying a set of conditions that the system is compelled to achieve, i.e., the ***constrain-based models***. Three conditions have commonly been applied to fluvial systems: a) the system must convey a given water discharge, b) it must also convey an amount of sediments, and c) the shear stress is below a threshold value. These conditions can be related, in some cases, to basic physical principles. For instance, the second condition is a consequence of the application of mass conservation to a fluvial system at grade. If there is neither net erosion nor deposition within the system then its transport capacity must equal the sediment supply that is also equal to the system output. The third condition is a stability criterion. In a stable channel the shear stress must be higher than a threshold value in order to carry sediments but be lower in the bank regions. In the next chapter I will discuss the different criterion that researchers have proposed for a channel to be consider stable. On the contrary, the first condition has a weaker status because the amount of water a channel can carry without flooding the surrounding floodplain depends on the channel geometry. And the latter

[5] It can also be referred as a phenomenological law.

depends on several factors such as the flow regimen, sediment supply, bank strength, ecc. Therefore, the imposed condition relates several dependents variables instead of linking a control with a degree of freedom (or system variable). I will continue this topic in the next chapter where I will discuss about degrees of freedom in fluvial systems.

The third approach consists on establishing the rules of the game, i.e., the so-called **processes-based models**. In this case no mention is done, a priori, about the system's behaviour and any condition is imposed to the system. The rules, or the laws of physics, say how intense a flux of matter is (water or sediment) and they establish the dependence with local features such as bed roughness, grain size distribution, slope, ecc. Considering the flux of sediment, we have to distinguish a) the bed load comprising erosion, transport and deposition, that are described by means of the continuity equation and a transport formula, and b) bank processes where the list of proposed models is quite extensive (see the review by Pizzuto and the ASCE Task Committee, 2008).

1.7 The concepts of equilibrium

Equilibrium is an ambiguous concept in geomorphology, because it lacks for a precise definition, or has been used in different ways by many researcher. Philips (1992) even suggested its abandonment in the context of geomorphology. It is not the aim of this study to track the history of this concept. The interested reader can find a complete review in Thorn and Welford's work (1994). Instead, this concept will be defined in the context of dynamic systems. For this study, three concepts must be distinguished: equilibrium, steady state or statistically stable state, and mass-balance.

A system is said to be in equilibrium when its characteristic parameters remain constant over a period of observation, and there is not sediment flux. The river channel resembles an irrigation canal in the sense that it conveys water keeping its form with no sediment transport. This kind of state is achieved both in natural channels and laboratory flume under conditions of sediment starvation. When a dam is constructed there is a reduction in sediment supply to the downstream reach. Immediately, the system evolves changing its slope and armouring if gravels are available in the substrate material. When the erosion process stops, the system attains equilibrium. At this state, forces acting on each particle balance each other and there is no more sediment transport. This trend is also observed in laboratory flumes under the condition of sediment starvation. Firstly there is a phase of slope reduction followed by a second phase of surface armouring, until bed stabilizes. There is a huge literature about effects downstream of dams (see for instance, Garret and Wolman, 1984), and flume experiences (Proffitt, 1980). The key concept here is that the system has attained a static equilibrium and there is not sediment transport.

When the mean values of the variables that describe the system do not change with time the system is said to be in steady state or has attained a statistically stable state. The major difference with an equilibrium state is that in a steady state there are fluxes. The system not only transport water and sediments but also keeps its form. Furthermore, the form and structure is the consequence of the existence of processes. Most of natural rivers belong to this group. The shape of the alluvial channel is the result of erosion at one side and siltation on the opposite bank promoting channel migration. In order to maintain this morphology the channel must consume energy in doing processes. Figure 1.5 shows an example of a river reach at a steady state (Leopold et al. 1964, p.325). During 6 years topographic surveys were carried on at the same cross section. Although there was erosion at the left

bank and deposition in the opposite bank, the cross section remained with the same bankfull stage, bottom level and bankfull width.

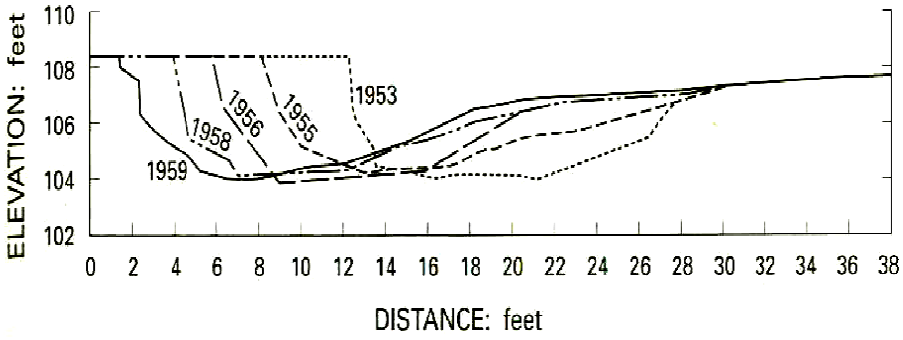

Figure 1.5. Example of a channel at steady state (picture from Leopold et al, 1964) with migration of the channel due to bank erosion and siltation in the opposite bank. Although there are processes acting in the channel, the cross sections conserves its shape.

Mass-balance means that all the volume of sediment that enters the system is conveyed downstream and exits the system. A channel in this condition is said to be "at grade". Conversely, if sediment supply excess outputs then the system aggrades and if there is a deficit, it degrades. Here, an adequate time span is also needed in order to quantify inputs and outputs.

The combination of steady state and mass-balance has commonly been named as "dynamic equilibrium". However, I preferred to keep the aforementioned definitions because it shows that structures are also possible out of equilibrium, and they are possible only in states far away from "equilibrium".

Regimen theories have made use of these concepts and it is important to recognize which state has been invocated as "equilibrium". Mass-balance has been widely assumed, i.e., the river reach is constrained to be at grade. However, the application of the other two concepts is not so clear. Commonly, an equilibrium state has been imposed to banks when defining that the shear stress is equal to or lower than the threshold of particles motion, but the channel is constrained to convey the sediment supply in the bed region. In other cases, Parker (1978) has affirmed that the alluvial channel, in steady state, is characterized by critical shear stress on the banks. This supposition has been posed in the context of aggregated models, and cannot be right in distributed models because conditions of lateral sedimentation and erosion require lower and higher shear stresses, respectively.

1.8 Complexity in natural systems and the debate revisited

When describing the behaviour of flocks, herds and schools, Reynolds (1987) cites this interesting anonymous observation from the XVII century: *"… and the thousands of fishes moved as a huge beast, piercing the water. They appeared united, inexorably bound to a common fate. How comes this unity?"* This expression evidences two aspects of natural systems: a large-scale whole view of aggregated particles as been one object with apparent own behaviour, and the presence of that individual objects. Reynolds was working in problems of computer representation and animations. In order to make an animation of a flock of birds he postulated three simple rules concerning the behaviour of individual

birds/fishes and then he let the set to evolve freely. The amazing result was that the simulations showed the observed cluster characteristics although the simple rules said nothing about the group behaviour.

The tendency to explain long-term and large-scale aspects of fluvial morphology in terms of short time-scale and small space-scale has been also a topic of debate. By the end of his life, Leopold presented a summary of his view of fluvial systems in an attempt to give a philosophical framework to fluvial geomorphology (Leopold 1994, 1997). In his article of 1994, he explained some aspects of fluvial systems by means of an analogy with biology, in particular, with Darwin's theory of Natural Selection. Leopold was facing the problem aforementioned, the large system scale and the small particle scale. He identified some features common to fluvial and biological systems, such as, uniqueness of each individual despite general similarities (been a river reach analogous to a population and a cross section, to an individual); some tendencies regarding group behaviour and the importance of history as a condition for future evolution.

Leopold (1994, p. 43) said that the most general physical laws (matter and energy conservation) were *"… insufficient to explain either path of particles or the interrelation of paths. Thus, they [were] insufficient to treat the surface form of the landscape or its change of form with time"*. As a consequence, he postulated the concept of entropy in order to explain rivers behaviour. He used the definition of entropy as the logarithm of the ratio of the probability of a given physical state to the probability of all other possible alternative states. And then he concluded that fluvial systems evolved between two opposing tendencies, minimization of energy expenditure and uniformity in energy expenditure.

In the light of concepts proposed in this work, we can see that Leopold was working at the system level, because when he introduced the concept of entropy he was comparing one system state against many possible. Furthermore, he stated that conservation laws were insufficient to explain the river evolution. However, it should be recognized that they are sufficient at a lower organization level, but they are not at the system level. In order to explain the river reach features in an aggregated model some other constrain must be invocated.

Recently, Eaton et al. (2006) have proposed a link between small-scale processes and reach-scale behaviour. Their purpose was to find a physical base for the slope-minimization behaviour described by Eaton and Church (2004) and several analogues optimization criteria. The large-scale trend and the local-scale processes interact by means of two feedbacks. At the local-scale an initial small asymmetrical shear stress distribution will produce a local higher sediment transport capacity and erode the channel bed. Assuming that shear stress is proportional to water depth, there will be a positive feedback because as bed lowers the erosion rate will increase. On the other hand, local erosion will promote bank failure, flow divergence and downstream sedimentation in the same bank side. As a result, the erosion process starts at a different location and propagates downstream. However, bank retraction will increase sinuosity and at the reach scale, channel slope will reduce, i.e., a negative feedback. The model is further developed with a consideration on sediment transport diffusion, characteristic of bedforms development downstream a perturbation and its relation with meanders length wave.

In this way, Eaton and coworkers showed that, at the reach-scale, channels exhibit self-organized behaviour that is the result of processes occurring at local-scale. That means that actual morphology is the result of active processes and not a matter of "*survival of the most stable*" configuration as suggested by Nanson and Huang (2008).

Finally, recalling the concepts presented in this chapter, it is possible to affirm that Nanson and Huang justification of extremal hypothesis based on the Least Action Principle implies a confusion of scales. Extremal hypotheses represent the behaviour of the system at the reach scale, and on the other hand, the least action principle is applicable at the very small spatial scale (scale that is far beyond the scope of any gemorphological study).

Besides the problem of scales aforementioned, there is another aspect of regime theories not well recognized among researchers: all the regime models deal with populations. There is a tension between the individual point of view and the study of population. This is central in Leopold analogy with biological systems, i.e, species: "*… river basins may be considered different species owing to the uniqueness of individual locations along the channel system, but at the same time each exhibits an orderly progression distinct from other river basins*" (Leopold, 1994, p.36). This "orderly progression" regards the relationship between hydraulic parameters against discharge. If in biology the study object is found in the species, in the fluvial context, the *whole* of individual locations along the channel system, must be adopted. Therefore, a regime models describe the relationships of certain parameters within the context of a population. Taking about the width of an individual river has no sense. It is the same problem afford by the science of statistic, where description and inference is applicable to the population and it is not valid to be apply in the single case. This is another distinction between models in the preceding classification: constrains and behaviors are applicable at the population scale, while processes have sense at the individual case: physical laws and constrains describe the behaviour of a population of river reaches, instead of describing the exact processes within a single river reach.

1.9 Deconstructing and integrating the fluvial system

When seen from outside a river is perceived as a unit, a wholeness or gestalt. This is the way the system is defined in the context of aggregated models (both constrain-based or behaviour-based). This kind or representation stressed the spatial aspect of the system because the "river reach" is identified as a "figure" standing in the foreground and separated from the "background". The figure is characterized by a quality that serves as a common reference for all the points in the interior. This quality is different in the background and this contrast defines the outline of the figure. These concepts, namely figure, background, outline, contrast, have been taken from the Gestalt psychology of perception, and they will prove to be useful to manage some aspects of the fluvial system.

In order to reformulate the problem raised in the debate on regimen theories I presented some concepts that mined the view of the river as a unit. The recognition of different spatial scales stressed the presence of phenomenological laws at each level, such as the Newton's hypothesis about the relationship between shear stress and velocity gradient at the very small scale, the empirical Manning's formula at the areal level or the extremal hypothesis behaviour at the reach scale. Furthermore, it has been affirmed that micro-scale events can alter or modified the evolution of the macro-scale system. The introduction of fuzzy sets shows that objects in nature have fuzzy boundaries and it is better to speak about a continuum variation from floodplain to active channel, instead of a sharp distinction between them. And finally, the proposition of a distributed model is based on the conception of the river system as composed by many areal-elements that interacts with each other. This completes the fragmentation of the river. At this point macro properties have vanished (width, depth, slope) and bankfull discharge is not an imposed condition but the result of the combination of hydrologic history and the system evolution.

Now, it is necessary to compound the pieces into a unique object again. Let us consider a two-dimensional region in space defined by the domain Ω. For each point within this region it is possible to give a number, "the degree of membership", that qualifies the point and its relationship to the set "river". The degree of membership function is defined in the following way:

$$\phi(x,y) = \frac{\tau_T(x,y)}{\tau_{ref}} \quad 1.7$$

Wherein τ_T is the average shear stress considering a time span of observation T. The reference shear stress τ_{ref} is the maximum value of τ_T over Ω.

The object "river" comprises a subdomain Γ that belongs to Ω. It is defined considering an arbitrary reference value for ϕ, let it be ϕ_0:

$$\Gamma = \{(x,y)/\phi(x,y) \geq \phi_0\} \quad 1.8$$

And its boundary, ρ:

$$\rho = \{(x,y)/\phi(x,y) = \phi_0\} \quad 1.9$$

Now, it is possible to define some basic geometric properties of the set "river", such as its area, volume, width and depth.

Area:

$$A = \int_\Gamma \phi da \quad 1.10$$

Volume:

$$V = \int_\Gamma h\phi da \quad 1.11$$

Mean width:

$$B = \frac{A}{L} \quad 1.12$$

Mean depth:

$$H = \frac{V}{A} \quad 1.13$$

Wherein, h is the depth considering the bankfull stage, i.e., the maximum water level before inundating the surrounding plain, and L is the length of the reach.

The reader may note that these definitions stress the process intensity. Therefore, the width evaluated in this way may be different to that calculated in the traditional way that assigns equal weight everywhere.

1.10 Hypothesis and methodology

The stability of gravel bed rivers will be studied in two different and complementing ways. One of them comprises the study of a population of river reaches and the other, the analysis of three case studies.

The first approach focuses on the overall behaviour of gravel bed rivers. It is based on the general assumption that ***physical laws and constrains describe the behaviour of a population of river reaches, instead of describing the exact processes within a single river reach***. Furthermore, each object contained in the population ***has uncertain boundaries (width, depth) and uncertain properties (median grain size, slope, bankfull discharge).*** The study of the population is mainly focused on the comparison of natural river reaches in Patagonia Region (Argentina) and river reaches disturbed due to human activities in Northern Italy.

In order to test this view the following methodology is proposed:

- Several river reaches will be selected in contrasting geographical settings: disturbed environment in Northern Italian Alps and natural environment in Patagonia.
- Each alluvial reach will be near a gauging station with available 20 years of records (daily mean discharge).
- Five cross sections will be measured covering the bankfull width and extending into the floodplain.
- Samples of material will be collected in order to characterized surface and substrate.
- Bankfull variables and confidence levels will be calculated (for width, depth, slope, bankfull discharge, reach average median grain size).
- Disturbed and natural gravel bed rivers will be compared in terms of morphological and sedimentological aspects.
- New hydraulic data will be added to published hydraulic data to evaluate the performance of regime models in describing the population.

Case studies are focused on a single individual case (not a population) and analyze the system response considering processes acting within the reach over a reduced time span. This study is based on the assumption that ***the channel morphology is driven by and is a consequence of active processes; and a 2D-depth-averaged model describes best both morphology and processes.*** In order to test this view the following methodology is proposed:

- The fluvial space is divided into a finite number of two-dimension parcels. Each parcel has properties, namely: elevation, slope, surface grain size distribution and substrate grain size distribution.
- The flow of water (velocity components) is described by means of two-dimensional depth-average flow equations, i.e., Reynolds model with the inclusion of a turbulence closure model (the standard k-e model). The principal forces acting on the water flow are due to bottom friction and turbulence. Secondary forces are negligible in wide and shallow gravel-bed rivers.
- Sediment processes consist of sediment transport, erosion and deposition, and bank stability. Sediment transport will be described with Wilcock & Crowe's (2003) model for mixtures and based on surface material. Erosion and deposition, i.e., bed elevation change is modeled with

Exner's equation extended for mixtures (considering an equilibrium sediment transport model). Bank processes consist on a simple sliding model for incoherent material.

- The model is applied to trhee different scenarios: a) a **flume experiment, where t**he model has to predict the response of a laboratory flume that develops a static armour under conditions of sediment starvation; b) a **middle-term simulation in which t**he model has to predict the shape and bed structure of Azul River providing the actual water discharges, bed material, and an estimated sediment supply; and c) a **field experiment wherein** the model has to predict the change in bed elevation in the Brenta River (Nove reach) after the passage of several floods during the period 23/8/2010 – 24/4/2011.

2 REVIEW OF REGIME THEORIES

2.1 Degrees of freedom and external controls

A graded stream has four independent variables, two of them belong to the basin scale (upstream conditions): discharge and sediment supply (caliber and load); and the others two refer to within-reach conditions: the valley slope and bank resistance. Differentiating independent and dependent variables is not a trivial problem because, as it will be explained later, it depends on the study scale. But in a preliminary stage these four variables can be chosen as external controls.

The reach develops a dynamic equilibrium adjusting its shape (width, mean depth, channel slope and bed forms) and its surface grain-size distribution. Width and depth are defined at bankfull stage; channel slope generally replaces the energy grade line slope; and bed forms with lateral bars, riffles and pools could be represented by the friction factor associate with bed forms (f"). In this list averaged values are proposed; for example, width is the mean value of the free surface width at bankfull discharge along the study reach.

It has always been recognized that fluvial systems have several degrees of freedom. Hey and Thorne (1986) have suggested that there are nine: width, mean depth, maximum depth, slope, velocity, sinuosity, riffle spacing, riffle width and depth. However, when developing regimen models researches have chosen some of them, not only as degrees of freedom, but also considering some as independent variable. For example, width, depth and channel slope are usually considered as degrees of freedom, while the surface diameter is taken as an independent variable. Surface diameter has been assumed as a dependent variable when studying downstream fining processes and armoring layer development (Parker and Sutherland, 1990; Hoey and Ferguson, 1994). It is not exactly wrong to define the surface diameter as an independent diameter in the context of aggregated models, because usually the substrate material is not considered. On the contrary, if substrate or sediment supply caliber were imposed, then the surface grain size should be treated as a dependent variable.

Energy or channel slope has also been treated as a degree of freedom since the pioneer work of Mackin (1948). According to Mackin a channel at grade has adjusted its slope in response to the sediment supply and fluid flow. When performing comparison between observed and predicted values, regimen models show better results in the case of width and depth, while slope shows considerable scatter. It has been attributed to a longer time for slope adjustment. So, which is the spatial scale and time scale within which a variable can be considered a degree of freedom or an independent variable? Recently, Weichert et al. (2009) have proposed three spatial scales with their own degrees of freedom: the micro-scale, the macro-scale and the reach-scale (Table 2.1). Stream response at the micro-scale occurs modifying the surface roughness developing an armour layer. At the macro-scale the stream can adjust its shape (planimetry and altimetry); while at the reach-scale the stream reaction is accomplished by a change in slope. If the study is focused in the micro-sale then the surface material is the only degree of freedom while the others work as external controls. At the macro scale, only the slope can be adopted as independent variable while in the largest scale, all variables are degrees of freedom.

Table 2.1. Dependent and independent variables according to the scale of analysis.

	Surface material	Width	Depth	Bed forms	Slope
Micro-scale	D	I	I	I	I
Macro-scale	D	D	D	D	I
Reach-scale	D	D	D	D	D

D: dependant variable; I: independent variable.

Bed forms and surface armour layer are the result of the interaction between many particles driven by water flow. This interaction, at least up to our knowledge, is random. But from this randomness coherent structures can emerge, that is, the system is able to organize itself. At the micro-scale, Church et al. (1998) have shown that the bed is able to organize itself by the development of bed structures such as grain nets that result in a higher resistance (critical shear stress for initiation of motion) and therefore, higher stability of the bed. At the macro-scale bed form development is the result of an initial disturbance (Venditti et al, 2005) and a characteristic transport length of individual particles (Pyrce and Ashmore, 2003).

Discharge has been treated as an external control. At first it seems a contradiction with what affirmed in the previous chapter, that bankfull discharge is a property of the system. The discharge, with its temporal variability, is actually imposed to the system and depends on climate and basin characteristics (geology, physiology, land use, etc.). However, the bankfull discharge is defined at the reach-scale as the maximum discharge the channel can convey without inundating the adjacent floodplain. From this definition derives the field procedure proposed by Leopold (see Chapter 6 for details) that considers bankfull levels and a local discharge rating curve to traduce levels into discharges[6]. According to this definition it is plain the consequence of assuming bankfull discharge as a dependent variable. However, the election of bankfull discharge as a summary quantity of the whole discharge range has been supported with its similarity with the effective discharge. The effective discharge concept was proposed by Wolman and Millar (1960) and is the discharge that transports most of the annual sediment load, and hence, it is responsible for most of the morphological work. Much recently, Emmett and Wolman (2001) showed that the bankfull discharge and the effective discharge were almost equal in gravel bed rivers.

The bankfull discharge as a valid external control has received justification from the frequency analysis of floods. In fact, it is said that bankfull discharge is a frequent flood that has, in mean, a return interval between 1,5 and 2 years, and thence, it has to be seen as basin property independent of the channel state. This affirmation is only valid in the context of "populations", but not in the individual case. Works of Williams (1978) and Petit and Pauquet (1997) conclude that the 1.5-year discharge may not represent the bankfull discharge in many rivers.

Finally, it seems that bankfull discharge, while been adopted as an external control by many scientists when developing regimen theories, has different interpretations according each model. Let us consider Millar's (2005) extremal-hypothesis-based model. Millar worked at the reach scale level and proposed a principle of reach organization, the so-called maximization of sediment transport efficiency. In this case

[6] The status of bankfull discharge as dependent variables has also been pointed out by Ferguson (1986, p.12): "*bankfull discharge is commonly used but is not really imposed from upstream since it depends on channel width and depth, with a tradeoff between its magnitude and its frequency*".

the system has the extension of the river reach and bankfull discharge is imposed from outside the system. When the Parker et al.'s (2007) model is considers the picture changes. They proposed a different organization principle that comprehends the whole basin: "*the catchment organizes itself to deliver gravel downstream*", and the amount of sediment is proposed to be related with the bankfull discharge. Therefore both sediment supply and bankfull discharge are features that belong to the basin-scale. Finally, in a processes-based model, where the areal element is the reference spatial scales, the bankfull discharge concept has no sense. At that scale there are just elementary fluxes transferring matter and momentum between adjacent cells. The bankfull discharge is an aggregated property at the reach scale.

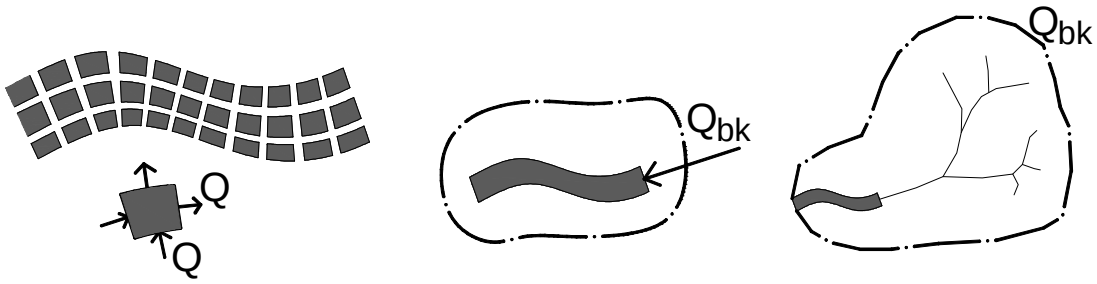

Figure 2.1. Three different interpretations for the bankfull discharge according the spatial scale of references. A) In a distributed models the bankfull discharge is an aggregated parameter at the system scale while there are just fluxes between areal elements; B) Millar's (2005) model representation where bankfull discharge is imposed form outside; and C) in Parker et al.'s (2007) model bankfull discharge and sediment supply can be considered the result of the basin organization to deliver sediments.

2.2 Aggregated models

The above distinction between dependent and independent variables is straightly related to aggregated models. Furthermore it is possible to track its origins in former regimen theories applied to irrigation channels, as has been explained in the preceding chapter. Traditionally river systems have been described by a handful of variables: the bankfull width, the mean bankfull depth, the channel slope, all of them considered as dependant variables, and the bankfull discharge, median surface diameter and sometimes the sediment transport was also considered, as external controls. In order to link dependant variables and external controls two basic conditions (constrains) have been imposed to the system: the channel must convey the bankfull discharge and silt supplied from upstream. The conditions are formalized with a resistance law and a sediment transport model. However, as there are three degrees of freedom, another condition is needed. At this point, each author has presented its own answer, as will be presented below. In this section, selected aggregated models that incorporate some kind of bank stability criterion are described underlining its most important features and issues.

In 1995 Julien and Wargadalam presented a model that considered secondary flow for the third condition aforementioned. Using Rozovskii's (1961) results, namely an expression that relates grain size, depth and curvature radius with the flow direction, they developed a set of four power expressions that were subsequently calibrated. When deriving the expression they assumed that the curvature radius was proportional to width, as has effectively been verified with field evidence (Leopold et al, 1964). However, Julien and Wargadalam calibrated their model with not only meandering rivers, but also

considering other morphologies like straight and braided rivers, that is, patterns where Rozovskii theory is not applicable. Therefore, doubts arise about the consistency of Julien and Wargadalam's model.

More recently, Millar (2005) has presented an extremal-hypothesis formulation. He considered a trapezoidal channel for which the bank slope was another independent variable. So, four relations were needed. The first relation is a flow resistance formula, namely, Keulegan's (1938) equation with Bray's (1979) calibration for roughness height, as used by Millar (2005):

$$\frac{\mathrm{U}}{\sqrt{\mathrm{gHS}}} = 2.5\ln\left(12.2\frac{\mathrm{H}}{\mathrm{k_s}}\right) \quad 2.1$$

and

$$\mathrm{k_s} = 6.8\mathrm{D_{50}} \quad 2.2$$

Wherein, U is the mean flow speed, h is the mean flow depth, S is the slope, k_s is the bed roughness related to the median grain size D_{50}.

The second relation is a sediment transport model, for which Millar chose Parker's (1990) model (see Chapter 4 for details). Shear stress is evaluated for bank and bed separately. Millar used experimental results performed in trapezoidal channels (Flintham and Carling, 1988; Knight, 1981):

$$SF_{bank} = 1.78\left(\frac{P_{bed}}{P_{bank}} + 1.5\right)^{1.4} \quad 2.3$$

$$\frac{\tau_{bank}}{\rho g H_0 S} = SF_{bank}\left(\frac{B+P_{bed}}{4H_0} sin\theta\right) \quad 2.4$$

$$\frac{\tau_{bed}}{\rho g H_0 S} = (1 - SF_{bank})\left(\frac{B}{2P_{bed}} + 0.5\right) \quad 2.5$$

Where P_{bed} and P_{bank} are wetted perimeters for bed and bank regions, respectively; B is the surface channel width, H_0 is the maximum water depth and θ is the bank angle.

The third relation establishes that bank shear stress must be lower than the threshold value for particle entrainment.

$$\tau_{bank} \leq \tau_c \quad 2.6$$

It follows that the sediment transport formula is needed to evaluate slope, the flow resistance to evaluate depth and the bank stability criterion completes the scheme evaluating the width. But, it is crucial the way in which this last criterion is posed. In fact, Millar assumes that the bank is stable when the shear stress is equal to or lower than the critical shear stress. So, the problem hasn`t a unique solution and another condition must be formulated: the extremal condition (maximum sediment transport efficiency).

$$\eta(W, H, S) = maximum \quad 2.7$$

With

$$\eta = \frac{G_b}{\rho Q S} \quad 2.8$$

wherein G_b is the bed-material transport rate at formative discharge.

The last selected model was proposed by Parker and coworkers (2007). Again B, H and S are the dependent variables; sediment supply and bankfull discharge are external controls, however, the researchers proposed that sediment supply can be evaluated from the bankfull discharge. Therefore, four relations must be established. The first relation is a flow resistance formula expressed in a power-type formula:

$$\frac{U}{\sqrt{gHS}} = a\left(\frac{H}{D}\right)^n \tag{2.9}$$

Where, a and n are coefficients to be calibrated against observations and D is adopted reference grain size (median grain size for this study). The second relations is the sediment transport formula proposed by Parker (1978):

$$q_b^* = 11{,}2(\tau^*)^{3/2}\left(1-\frac{\tau_c^*}{\tau^*}\right)^{4{,}5} \tag{2.10}$$

Wherein q_b^* is the dimensionless bed load; τ^* and τ_c^* are the dimensionless mean shear stress and critical shear stress. The last relation is a stability criterion which states that the average cross section shear stress is related to the critical shear stress for onset of motion:

$$\tau^* = r\tau_c^* \tag{2.11}$$

Where r is a constant. Note that there is not distinction between bank and bed shear stress as done by Millar. Instead, the mean value is used for both the stability criterion and the evaluation of sediment transport.

At this point three relations are sufficient for evaluating B, H and S, given the flow discharge and the sediment supply. However, Parker and coworkers postulated that the sediment supply was also related to the flow discharge:

$$q_b^*\frac{B}{D} = a_q\left(\frac{Q}{g^{1/2}D^{5/2}}\right)^{n_q} \tag{2.12}$$

Where a_q and n_q are coefficients to be calibrated. With this last expression the model depends only on the discharge and grain size D as independent variables. All the coefficients a, n, r, a_q and n_q are calibrated using data of B, H , S, D and Q: $a = 3{,}71$; $n = 0{,}263$; $r = 1{,}63$; $a_q = 0{,}00330$ and $n_q = 0{,}551$.

Parker et al.'s model predicts an increase in sediment supply with bankfull discharge to about a half power. Mueller and Pitlick (2005) studied sediment transport at headwater streams and found a linear relation, and Parker and coworkers attribute this discrepancy to the specific environment studied by Mueller and Pitlick, i.e., small streams (in fact, the drainage area was in all the cases smaller than 100 km^2). Emmett and Wolman (2001) studied gravel bed streams in a wider range, comprising basin areas from 55 to 4950 km^2. Later, King et al. (2004) published sediment transport data of many streams in Idaho state (U.S.A.) including those previously analyzed by Emmett and Wolman. The information avails to test Parker et al.'s "gravel-yield" hypothesis. Figure 2.2 shows the sediment transport at bankfull discharge calculated with the half power formula calibrated by Parker et al., using hydraulic geometry data and equation 2.10. Measurements exposed from aforementioned published data lays below the

Parker et al.'s model. It may indicate that the sediment transport formula (eq, 2.10) does not accurately quantify the actual sediment transport. However, data seems to follow the same trend, i.e., a half power relation as suggested by the dashed line. This relation is only valid for medium to large size streams while small streams exhibit a higher exponent (in figure, the dash line for lower discharges has an exponent of 2). The latter is in contradiction with conclusions from Mueller and Pitlick study. Their data has not been included in figure 2.2 because sediment transport was actually modeled instead of been measured.

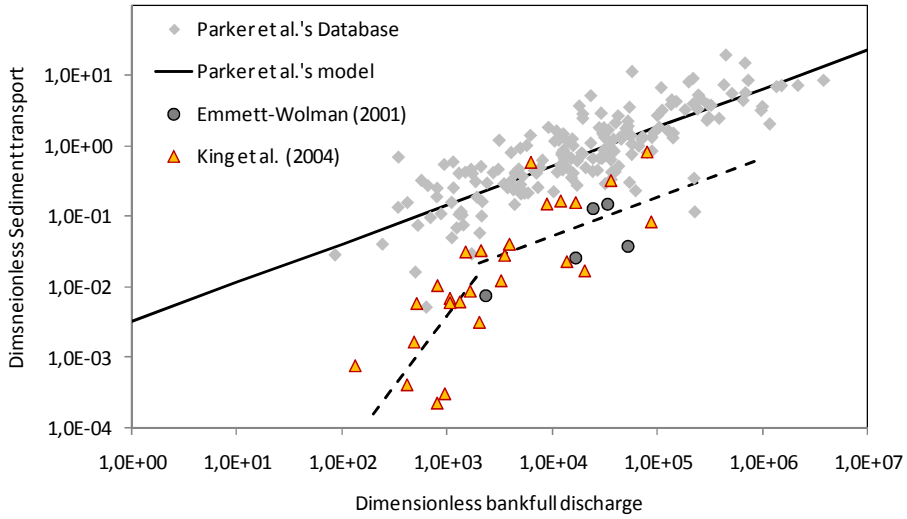

Figure 2.2. Comparison between the basin organization model proposed by Parker et al. (2007) against field data published by Emmett and Wolman (2001) and King et al. (2004). Grey dots represent calculated values using a sediment transport formula and the continuous line is the calibrated model.

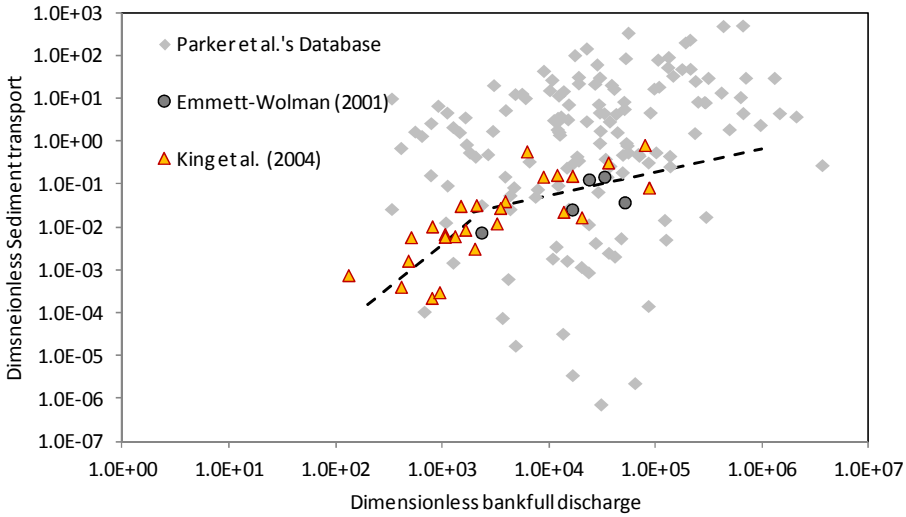

Figure 2.3. This graph has been produced using the same model for Figure 2.2 but calculating bed shear stress with hydraulic parameters instead of using the mean ratio r = 1.63. In this case, scatter is much wider and the relationship is weaker (r^2 = 0.072). The catchment organization is less evident.

There is a discrepancy between the cloud of data corresponding to measurements and that from calculus. This difference can be partially ascribed to the evaluation of the shear stress used by Parker et al. In fact, they do not discriminate between bed and bank resistance, and assume that the mean shear stress is 1,63 times the critical shields value for onset. Besides, if the mean shear stress is used in the transport equation, it means that the bed shear stress is assumed to be 63% higher than the threshold value for all the reaches. On the other hand, one can use actual values of mean shear stress derived from hydraulic geometry parameters ($\tau^* = HS/R_s D_{50}$). In this case (Figure 2.3) scatter is much considerable than using a unique value of r (Figure 2.2) and the relationships is weaker (r^2 = 0,072).

Parker and coworkers claimed that their model was fully physically based and critized Millar's model because its extremal hypothesis lacked for physical base and hence has to be accepted a priori. This situation can be questioned in the light of the concepts presented in this and the preceding chapter. Both models, been aggregated models, simplify the river system and a handful of variables are chosen as representative of the system state (B, H, S). Three conditions are stated: bank or cross section stability, a flow discharge that has to be conveyed and a sediment load to be transported downstream.

Millar postulates that the system (the river reaches) organizes itself in order to maximize the sediment transport efficiency. It means that for an imposed supply of water and sediments, slope must be minimum. In the case of Parker et al.'s model, the river reach must also convey the imposed discharges of water and sediment but in this case the basin, organizing itself, defines the respective amounts. The organization is transferred from the river reach (Millar case) to the basin scale (Parker et al.'s model). Direct field evidence supports a half power relationship between dimensionless bed load and bankfull discharge in Parker et al.'s model, but when a sediment transport model is used with actual mean shear stress values, this relation is weaker. Therefore, the "gravel-yield organization principle" should be reviewed considering actual field data.

2.3 One-dimensional models

A one-dimensional model consists of a cylindrical channel with permanent and uniform flow. Attention is focused on the cross section where velocity and shear stress distribution are usually calculated using the Lundgren and Jonsson's (1964) model or the Shiono and Knight (1991) model. The channel is divided in two regions: the central region and the bank region. In the central region the bed is flat and the shear stress is above the threshold value, a necessary condition for the existence of sediment transport. On the other hand, along the bank region the slope varies from zero (in the conjunction point with the central region) to a maximum value, the repose angle, at the top of the bank. It is possible to determine the shape of the bank defining a bank stability criterion and calculating the shear stress distribution. From the bank stability analysis it results an inverse relationship between channel depth and slope. If slope is known, the depth calculus is straightforward. Then width can be derived applying a flow resistance formula. Otherwise, the slope can be calculated using a sediment transport model if sediment supply is known.

Since Lundgren and Jonsson presented their model in the early '60, it has been widely used to develop one-dimensional regime models. The first to use it was Parker in 1978. He assumed that in an alluvial river the bank region would attain a critical state at bankfull discharge. Otherwise, the stream would not be able to shape the channel. He verified the model against laboratory and field data getting good agreement. His model was further developed to incorporate heterogeneous mixtures (Ikeda et al, 1988)

and the influence of bank vegetation (Ikeda and Izumi, 1990). Pizzuto (1990) used the same hydraulic model and considered lateral sediment transport and a bank failure model in order to simulate the bank retreat process. With the aid of numerical methods he solved the differential equations arriving to the same analytic results previously obtained by Parker (1978). Besides, his model was in good agreement with laboratory experiment results on widening in sand channels (Ikeda, 1981). The importance of Pizzuto's contribution relays on the fact that his model is fully processes-based, i.e., there is not any stability criterion specified a priori. However, the unsteady state modeled by Pizzuto has a final state defined by the same criterion used by Parker, i.e., critical shear stress along the bank region. In this way both approaches are equivalents.

Because Ikeda et al.'s model (1988) will be used extensively in Chapter 8 when analyzing natural and disturbed streams, it is described in detailed below. Ikeda and coworkers took Parker 's (1978) work as an starting point and extended it for banks composed of heregoneous mixtures. The hydraulic analysis performed by Parker gives the shear stress for each point along the cross section. In particular, its value for point A (see Figure 2.4), the limit of the central region is:

$$\frac{gH_cS}{R_sgD_i} \cong 1{,}23\tau^*_{thr} \qquad 2.13$$

Wherein, H_c is the water depth at the channel center, S is the channel slope, R_s is the submerged specific weight of the bed material (usually adopted to be 1.65), D_i is the reference grain size, and τ^*_{thr} is the threshold dimensionless shear stress for onset of motion. This equation states that shear stress in the channel is only 23% higher than the threshold value. Then a channel at bankfull stage has just the shear stress needed for sediment transport. In order to apply this relation as a stability constrain, grain size and threshold shear stress must be specified. The researchers considered that a static armour develops on the bank slope, so D_{90} is adopted as a reference grain size. Shear stress is evaluated using a modified expression of Egianzaroff's relation:

$$\tau^*_{thr} = \frac{0.05}{\left[log\left(19\frac{D_{90}}{D_{50}}\right)\right]^2} \qquad 2.14$$

Combining equations 2.13 and 2.14, an expression for water depth is derived.

Width is evaluated using a Keulegan's flow resistance formula. The bed roughness is related to the grain size with the relation: $k_s = 1{,}5D_{90}$.

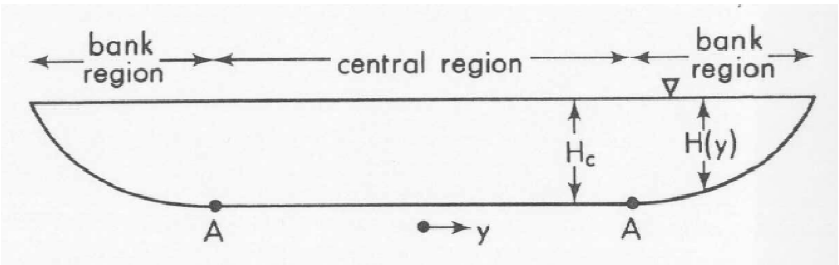

Figure 2.4. Idealized cross section of a natural stream. It is divided into two regions corresponding one to a central region with an active bed, and a bank region where shear stress equals the critical value for initiation of motion (after Parker, 1978).

In Lundgren and Jonsson's (1964) model a logarithmic distribution is assumed for the vertical velocity profile. Diplas (1990) performed laboratory experiments and proved this assumption. He also showed that the bank profile could be described by an exponential function.

Cao and Knight (1998) applied the hydraulic model developed by Shiono and Knight (1991) based on secondary currents (see Chapter 3 for details). The difference with respect to the others approaches relays in the assumption concerning bank stability. Cao and Knight proposed that bank profile results from the maximization of entropy that gives a parabolic curve. They also found an inverse relationship between depth and slope.

The key difference between the models aforementioned is how bank stability is defined: critical condition in Parker's model, zero lateral sediment transport in Pizzuto's model or maximum entropy in Cao and Knight's model.

2.4 Two-dimensional models

Truly two-dimensional hydrodynamic models have not been used as regimen models yet. The reason may relay on the extensive time spans needed for computation. Instead, 2D models have been applied to specific studies with reduced spatial scales and small time spans (for example, comprising a river reach and a flood event). Computational technology has enable the application of 2D and 3D models to river studies and a new branch, the computational river dynamics, has emerged from the computational fluid dynamics[7].

2d models are used for studying the horizontal distribution of flow and sediment parameters. The vertical variation of these parameters is not considered, and instead depth-average values are adopted. A fully physically-based model has to describe the flow of water, the flow of sediment and bed changes.

The flow of water is described by means of the depth-average version of the Reynolds equations. The Reynolds equations are derived from the general Navier-Stokes equations introducing a statistical model to represent velocity variability due to turbulence. The Reynolds equation deals with time average values of velocity and pressure. The fluctuating velocity component originates new terms known as Reynolds stresses that have to be determined by a turbulence model. Turbulence is also described by time-averaged quantities and therefore its laws do not simulate the real behaviour but instead it is intended to quantify the incidence of turbulence on mean flow. Most of 2D models used in computational river dynamics employ a depth-average k-e turbulence model. In this case the eddy viscosity depends on the turbulence kinematic energy (k) and its dissipation rate (e). For each or these variable there is a transport equation with production, diffusion, advection and dissipation terms (for details see Rodi, 1993; a review will be presented in the next chapter).

Sediment transport has received different treatments. Some researches consider uniform bed material i.e., it is represented by a single size class. Natural gravel bed river exhibit wide granulometric grain size distributions that extend from sand to cobbles. Sediment mixtures are represented by multiple size classes, requiring the study of the behaviour of each class. Just recently, Li and Millar (2007) extended the mobile-bed model developed by the Danish Hydraulic Institute (DHI MIKE21C) including the

[7] It is worth to comment that Wu (2007) has recently published a book synthesizing the knowledge of this new and growing science that had been sparse in literature up to now.

transport of heterogeneous mixtures. They apply the model to a reach of the lower Fraser River in Canada. Model results were confronted with field data and good agreement was found for water parameters (stages) and sediment transport. When multiple-size classes are used like in this application, the Exner's equation must be resolved for each grain size fraction and not only bed intensity is important but also its direction. In general, these models take into account the effect of bed slope and secondary currents to evaluate the sediment transport direction. In fact, grains follow the same direction that the main flow when the bed is flat. Any other slope produces a lateral flux due to the gravitational force. Besides, a curvature in flow trajectories induces secondary currents that produce lateral sediment flux, as well.

A very important aspect for modeling the river evolution is the possibility of lateral displacement. Bank erosion and deposition in the opposite channel bank is the main process associated with flood plain genesis and channel width adjustment. Bank retreat has been extensively studied and a complete review has been prepared by Pizzuto and the ASCE Task Committee (2008). Because gravel bed rivers have noncohesive banks an heuristic mechanism has been adopted (Pizzuto, 1990; Nagata et al., 2000, Schmautz and Aufleger, 2002; Wu, 2007). When bank slope angle is above the frictional angle of repose there is an instantaneous slide that restitutes the critical angle.

2D hydrological and sedimentological models have been applied in different morphological context. Lane and Richards (1998) apply STREMR[8] in order to explore the capabilities of this 2D hydraulic model in braided stream where bed roughness dominated flow pattern. Later, Abad and collaborators (2008) extended STREMR adding a sedimentological module to study water and sediment flow in meandering rivers. 2D models have also been applied to simulate channel evolution both in high gradient streams with braided pattern (see Nagata et al., 2000; Jang and Shimizu, 2005) and low energy, meandering streams (see Duan and Julien, 2005). Figure 2.5 shows different stages in the evolution of a braided and a meandering stream with the models aforementioned.

Long computation spans have been the major obstacle to apply 2D models in regime studies. There are three possible solutions to this problem. One of them is the use of powerful computers to resolve the differential equations for flow and sediments. But other more intelligent strategies focus the attention on improving the numerical methods and using standard nowadays technology. For example, implicit schemes enable wider time steps (see Wu, 2007), or higher order explicit schemes (Nagata et al., 2000; Jia and Wang, 1999; Jang and Shimizu, 2005). Garcia-Martinez and coworkers (2006) simplified the governing equations neglecting the turbulence model and applied an explicit scheme in four steps. In this way they were able to simulate the evolution of a 5-km reach of the Apure River (Venezuela) for 20 difference 1-year long scenarios and a 5-year simulation. Using a standard computer (Pentium IV, 3GHz), the 5-year scenario simulation took 6 days.

[8] STREMR is a 2D hydraulic model developed by Robert Bernard (2003). This model will be explained in detailed later because it was extended in the present study.

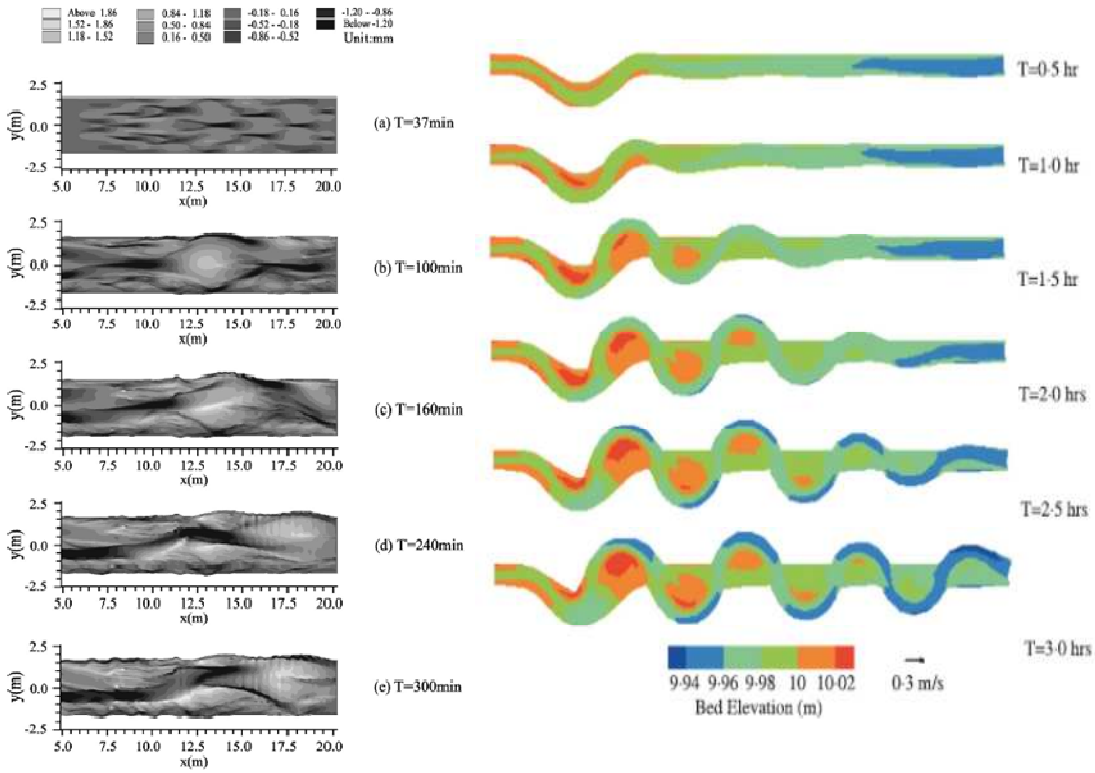

Figure 2.5. Examples of 2D processes based models to very different morphological patterns, a braided stream (on the Left, from Jang and Shimuzi, 2005) and a meandering stream (on the right, from Duan and Julien, 2005).

The third strategy consists on relaxing the physics of the problem. This approach states that it is not necessary to have the "exact" solution of the problem when long simulations are considered, such as 1000 years or more. Murray and Paola (1994, 1997) proposed one of the first cellular models to study braided streams. The cellular automaton model is based on the idea that complex and apparently stochastic behaviour can be produced from simple interactions. The domain is divided with a spatial grid (defining cells) and the interactions between adjacent cells are specified. In Murray and Paola's model water is distributed between three neighbor cells according to the slope. This distribution represents a rough approximation to the momentum conservation. The model also incorporates rules for sediment transport and bed elevation change. Although the model was very simple and with crude approximations for the physical laws it was able to reproduce the dynamic behaviour of braided channels: downstream and lateral migration of bars and channel. Murray and Paolas's work was the base for a series of cellular models that were, after that, created for the study of fluvial morphology. It is worth to mention Coulthard's CAESAR model (see Coulthard et al. 1997) that was developed firstly to study the evolution of both catchment and river reaches along wide periods of time (Coulthard et al. 1997, Coulthard et al, 2005), and then improved to model channel processes such as meanders development (Coulthard and Van De Viel, 2006).

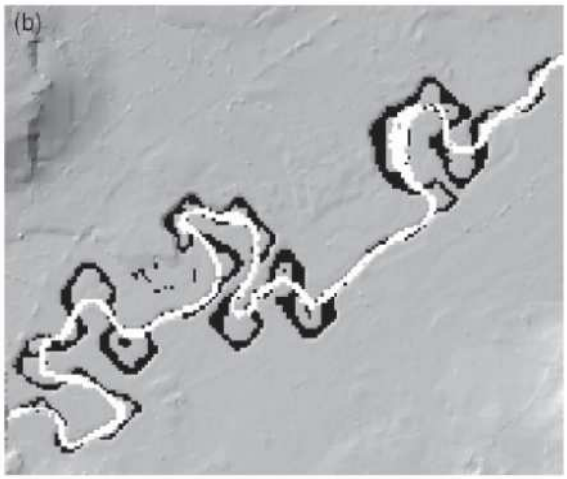

Figure 2.6. Example of the application of a cellular model to the development of a meandering stream (after Coulthard and Van de Viel, 2006)

Table 2.2. Aggregated models of regime theory

Researchers	Dependent variables	Independent variables	Equations	Methodology – Observations
Julien & Wargadalam (1995)	H – mean depth W – width U – mean velocity S – slope	Q – discharge Ds – surface diameter τ^* - mean boundary shear stress	- Continuity - Flow resistance (Darcy-Weissbach's equation and Keulegan's formula) - Particle mobility (Shields' criterion) - Secondary flow: relationship between W-H	Exponents and factor have been calibrated with a dataset of 382 observations (field and laboratory). Then verification and validation used and independent dataset composed of 382 records.
Millar (2005)	H – mean depth W – width S – slope θ – bank slope	Q – discharge D_{50} – surface diameter Gb – sediment supply ϕ' – bank strength	- Flow resistance (Darcy-Weissbach's equation and Keulegan's formula, applying Bray's (1979) results) - Shear stress on bed and banks according to experimental results from Knight (1981) - Sediment transport formula (Parker, 1990) - Maximization of sediment transport - Stability criterion for bank slopes	Regimen equations are derived from numeric calculus considering 1000 synthetic reaches. The proposed regimen equations are compared against field data.
Parker et al. (2007)	H – mean depth W – width S – slope Qb – sediment transport at bankfull discharge	Q – discharge D_{50} – surface diameter r – ratio between mean boundary shear stress (τ_0) and critic shear stress (τ_C).	-Flow resistance (Manning) -Sediment transport (Parker, 1978) -Stability criterion (relationship between τ_0 and τ_C. - Empirical relationship between Q and Qb.	Field data (72) is used to calibrate: r, relationship Q-Qb, resistance factor (Manning`s N). The proposed model is verified against another field data set (97).

Table 2.3. One-dimensional models of regime theory

Researcher	Hydraulic model	Sediment transport model	Bank stability criterion	Test
Parker (1978)	Lundgren & Jonsson's (1964) model: longitudinal momentum balance equation integrated along a normal to the bed; Keulegan`s equation and eddy viscosity model for turbulent closure.	Sediment transport equation for gravel bed rivers: Parker (1978)	Critical shear stress along the bank region	Field data of straight channels
Ikeda et al (1988)	Lundgren & Jonsson's (1964) model.	Approximation of Einstein's bed load formula for gravel mixtures using the surface D_{50}.	Consideration of heterogeneous mixtures. The reference grain size is D_{90} for the criterion of bank stability (static armour development)	Field and laboratory data of straight channels.
Pizzuto (1990)	Lundgren & Jonsson's (1964) model.	Parker's (1983) sediment transport equation, using a reference grain size (Ds)	The lateral sediment transport equals zero at equilibrium. The model considers a bank failure when bank slope is above the angle of repose	Test against laboratory data, considering the time evolution of the cross section.
Ikeda & Izumi (1990)	Applies the Lundgren & Jonsson's (1964) model in the central region. On the banks they consider the resistance due to vegetation	No sediment transport model. The slope must be specified.	Vegetation on banks modifies the local flow resistance coefficient but not the strength of banks. The stability criterion is similar to Ikeda et al (1988)	Comparison with field data that describes the presence of vegetation.
Cao & Knight (1998)	Shiono & Knight (1991) model: depth-mean averaged momentum equation; mean eddy viscosity; Darcy-Weissbach's equation, secondary currents contribution to the lateral transfer of downstream momentum	No sediment transport model. The slope must be specified	Entropy maximization principle: critical shear stress along the bank that results in a parabolic profile. Non uniform material is considered	Comparison with field and laboratory data.
Diplas (1990)	Lundgren & Jonsson's (1964) model. Laboratory measurements support the logarithmic velocity profile assumption	No sediment transport model. The slope must be specified	Balance of forces along the bank profile results in an exponential function	Laboratory and field data.

Table 2.4. Two-Dimensional models for morphological studies.

Researcher	Hydraulic model	Sediment transport model	Bank erosion model	Numeric method	Boundary conditions	Applications
Nagata et al. (2000)	Depth average shallow water equations. Secondary flow and k-e model for turbulent closure.	-Probabilistic approach of pick up rate of sediment and deposition. Uniform sand. The direction of sediment flow depends on bed topography and secondary flow.	Bank failure model	Moving boundary fitted-coordinates system. Finite volume method. Time integration with Adams-Bashforth method (2^{nd} order)	Not specified	Comparison against flume experiments with sand channels.
Jang & Shimizu (2005)	Depth average shallow water equation. Secondary flow. Manning roughness. Zero-equation model as a turbulence closure scheme.	-Meyer-Peter & Müller's equation with uniform material. The direction of sediment flow depends on bed topography and secondary flow.	Bank failure model	-finite difference method. Moving boundary-fitted coordinate system.	-fixed-bed at the upstream end. -U for upstream and H for downstream conditions. No "slip" condition for bars and banks	Comparison against two laboratory experiments (braided channels)
Garcia-Martinez et al (2005)	Depth average shallow water equation. Secondary flow. Manning roughness. No turbulence considerations.	-Meyer-Peter & Müller's equation with uniform material (gravels)	Not considered	-Finite element discretization (triangular elements) -Galerkin weighted residual method. Explicit method in four steps for time integration.	-dry-wet region model -upstream condition: discharge. -downstream condition: U, H or H-Q relationship. Slip condition	-Comparison with analytical solution. -Case study: Apure river, a 6km reach and a 5-year scenario.
Li-Millar (2007)	Model Mike 21C Saint Venant equations with secondary flow, Manning roughness coefficient, Zero-equation model as a turbulence closure scheme.	Parker's (1990) model for sediment mixtures	Not considered	-Finite difference method of 2^{nd} order accuracy in space and time. Curvilinear staggered grid	-upstream: discharge and bedload. -downstream: zero bed load flux	Case study: Frazer river in Canada

3 THE FLOW OF WATER

The flow of water and sediments are the governing processes that define channel morphology and structure. The attention in this chapter is directed towards the description of water flow in shallow water environments, such us gravel bed rivers. These environments have own features that differentiate them from deeper channels (lower width/depth ratio) as can be found in low relief regions. The review covers the physics for 2D depth-average models: the Reynolds equations and the closure turbulence models. Besides, issues regarding aggregated and 1D models are exposed, such as the problem of quantifying flow resistance in gravel bed rivers with complex topography and the evaluation and distribution of shear stress along the boundaries.

3.1 Governing equations of water flow

The fluid flow can be described in all details by means of the Navier-Stokes's equations and the continuity equation. The Navier-Stokes's equations relate flow properties (acceleration) with forces such as gravity, pressure and those due to viscosity. The set of equations describe the fluid motion considering the turbulent fluctuating motion and hence the result is the velocity and pressure field for each instant. The momentum and continuity equations can be written briefly using compact tensor notation:

$$\frac{\partial u_j}{\partial t} + \frac{\partial u_j u_k}{\partial x_k} = f_j - \frac{1}{\rho}\frac{\partial p}{\partial x_j} + \frac{\mu}{\rho}\left(\frac{\partial^2 u_j}{\partial x_k \partial x_k}\right) \qquad 3.1$$

$$\frac{\partial u_j}{\partial x_j} = 0 \qquad 3.2$$

Wherein x_j is the j-coordinate in the Cartesian coordinate system, p is the pressure, f_j is the j-component of the external force (per mass unit, i.e. an acceleration like that due to gravity) and ρ is the water density and μ its dynamic viscosity. On the right side of the equation there are the local (first term) and convective components of acceleration (second term), while on the right side there are the forces due to external fields, pressure gradient and viscosity effects (from left to right).

The solution of the Navier-Stokes's equations can hardly be found, if not impossible, for practical problems because it should describe the instantaneous properties of the field (velocity and pressure). Instead of dealing with instantaneous variables, Osborne Reynolds (1895) suggested a statistical approach. The instantaneous velocity field is decomposed into a mean and a fluctuating component. The mean velocity refers to a time interval that is long relative to the scale of turbulent disturbances, but short compared with long-term variations which would not be regarded as part of the turbulent fluctuation of the flow (i.e., transient problems):

$$\begin{aligned} u &= \bar{u} + u' \\ v &= \bar{v} + v' \\ w &= \bar{w} + w' \end{aligned} \qquad 3.1$$

The primed variables (‘) represent the turbulent fluctuations and the dashed variables are the time-average component of the field.

Introducing this definition for the velocity field into the Navier-Stokes’s equations and averaging with respect to time results the Reynolds time-averaged equations.

$$\frac{\partial \overline{u_j}}{\partial t} + \frac{\partial \overline{u_j u_k}}{\partial x_k} = f_x - \frac{1}{\rho}\frac{\partial \bar{p}}{\partial x_k} + \frac{\mu}{\rho}\frac{\partial^2 \overline{u_j}}{\partial x_k \partial x_k} - \frac{\partial \overline{u_j' u_k'}}{\partial x_k} \qquad 3.2$$

Note that in this equation there are new terms on the right side that contains correlations between fluctuating components. The velocity correlations appear to act as stresses on the fluid and therefore they are called turbulent or Reynolds stresses (per unit mass). In practical problems viscous stresses are neglected because they are much smaller than their turbulent counterparts except in the viscous sublayer very near the walls. In fact, the apparent “eddy viscosity” (see later) may exceed the molecular viscosity by a factor of 10^3 or more (Clifford & French, 1993).

In the original instantaneous problem there were four variables (u, v, w, and p) and four equations (Navier-Stokes’ equations and the continuity equation) that enabled a closure of the problem. On the other hand, when the statistical approach is applied the number of variables rises to ten: the mean pressure, three velocity components, and six Reynolds stresses components. In order to solve the problem several “closure models” have been proposed. A thorough review has been elaborated by ASCE (1988) and Rodi (1993). Here, only two approaches that apply the eddy viscosity concept will be presented because they are necessary for the development of the 2D model in Chapter 10.

3.2 Closure turbulence models

The turbulent viscosity (or diffusivity) concept was introduced by Boussinesq (1877). It assumes that, in analogy to the viscous stresses in laminar flow, the turbulent stresses are proportional to the mean-velocity gradients. The eddy viscosity is, in contrast to the molecular viscosity, not a fluid property but depends strongly on the state of the turbulence and may vary considerable over the flow field. For example, the x-z component of the turbulent correlations can be written as:

$$-\overline{u'w'} = \upsilon_t \left(\frac{\partial \bar{u}}{\partial z} + \frac{\partial \bar{w}}{\partial x}\right) \qquad 3.3$$

Prandtl (1925) proposed a model to evaluate the eddy viscosity distribution in the flow field, the so called “mixing-length model”. Considering a steady parallel flow in the x direction, with a non-uniform velocity distribution, he postulated that the eddy viscosity was proportional to a mean representation of the fluctuating velocity (V) and a mixing-length, l_m. The fluctuating velocity was set equal to the velocity gradient in the normal direction:

$$\upsilon_t = l_m V = l_m^2 \frac{\partial \bar{u}}{\partial z} \qquad 3.4$$

The mixing-length represents the length of the path (orthogonal to the longitudinal flow direction) that the fluid particle has to make in order to equal the difference between the original and final velocity (at the new layer) and the fluctuating velocity in the longitudinal flow direction.

This model can be used to close the Reynolds's equations and to derive important relations. Let's consider the simple case of parallel steady and uniform flow in a wide rectangular channel. The flow has a depth h, the bed slope is S and only the streamwise velocity (u) must be consider (the other mean velocities are null). The flow is fully turbulent so viscous stresses are neglected. Furthermore, the mixing-length is proportional to the distance from the bed: $l_m = k \cdot z$, and k is the Von Karman constant (k = 0,40). Applying the eddy viscosity concept to the Reynolds' equation it is possible to arrive to the following conclusions (Basile, 2005):

- ✓ Linear shear stress variation: $\tau(z) = \tau_b \left(1 - \frac{z}{h}\right)$ 3.5
- ✓ Hydrostatic pressure distribution: $p(z) = \rho g(h - z)$ 3.6
- ✓ Bottom shear stress: $\tau_b = \rho g h S$ 3.7
- ✓ Logarithmic velocity distribution: $\frac{\overline{u}(z)}{u^*} = \frac{1}{k} ln\left(\frac{z}{z_0}\right)$ 3.8
- ✓ Parabolic eddy viscosity distribution: $v_t(z) = k u^* z \left(1 - \frac{z}{h}\right)$ 3.9

Where, z is the vertical distance from the bed, and z_0, a reference distance from the bed for which the velocity is zero.

The main problem with the mixing length model is that it implicitly assumes that turbulence is dissipated where it is generated (Rodi, 1993). Hence, points downstream are not influenced by the turbulence generated at points placed upstream because turbulence is not transported downstream by the mean flow. Besides it is difficult to specify the mixing length, and so the model is of little use in complex flows.

Two-equations models overcome these difficulties by solving additional transport differential equations. Nowadays the so called standard k-ε model has become popular and it is used in many hydraulic engineering problems. Velocity fluctuations are linked with the kinetic energy of turbulent motion (per unit mass: k) (Rodi, 1993) and another differential equation is added for the length scale which in combination with the velocity scale equation constitute a set of two-equation turbulence model. The length scale is replaced with the dissipation rate ε and the eddy viscosity assumes:

$$v_t = C_\mu \frac{k^2}{\varepsilon} \quad 3.10$$

Where c_μ is a coefficient. The transport equations for k and ε are:

$$\frac{\partial k}{\partial t} + \frac{\partial}{\partial x_j}\left(\overline{u_j} k\right) = \frac{\partial}{\partial x_j}\left(\frac{v_t}{\sigma_k}\frac{\partial k}{\partial x_j}\right) + P_k - \varepsilon \quad 3.11$$

$$\frac{\partial \varepsilon}{\partial t} + \frac{\partial}{\partial x_j}\left(\overline{u_j} \varepsilon\right) = \frac{\partial}{\partial x_j}\left(\frac{v_t}{\sigma_\varepsilon}\frac{\partial \varepsilon}{\partial x_j}\right) + \frac{\varepsilon}{k}\left(c_{\varepsilon 1} P_k - c_{\varepsilon 2}\varepsilon\right) \quad 3.12$$

Where $c_{\varepsilon 1}$, $c_{\varepsilon 2}$, σ_k, and σ_ε are coefficient. The transport equations contain, from left to right, a temporal variation of the magnitude, an advection term, a diffusion term, the production and dissipation terms.

In the standard model the constants assume the following values: c_μ = 0.09, $c_{\varepsilon 1}$ = 1.44, $c_{\varepsilon 2}$ = 1.92, σ_k = 1.0, σ_ε = 1.3. Although these values are based on extensive examination of free turbulent flow (Rodi,

1993) universality should not be expected. Several adjustments have been proposed modifying the values (see Wu 2007, p.27, for a summary) or replacing the constants by functions of flow parameters (see Rodi, 1993).

3.3 Boundary layer

In order to analyze the more complex flow in a gravel bed river with bed forms it is better to get started considering the simplest situation. The simplest geometry is that of a prismatic channel with constant cross section and no bed forms. The flow is steady and uniform. Furthermore, as the channel is sufficiently wide the velocity distribution will be only a function of z, the vertical distance from the bed. As the grain or skin friction is the primary source of resistance, this configuration can be treated with the law of the wall developed within the boundary layer theory in fluid mechanics.

According to the boundary theory, the velocity distribution (u) along the bed-normal direction (z) of steady flow over a flat wide bed (the wall) can be described by two universals law: the inner and the outer law (Yen, 2002). The inner form of the law of the wall relates the velocity distribution to the bed roughness:

$$\frac{\overline{u}}{u_*} = \frac{1}{k} ln\left(\frac{z}{z_0}\right) \qquad 3.13$$

Where z_0 is the bed roughness length defined as the distance above the bed where the flow velocity goes to zero; k is the Karmans's constant; and u* is the shear velocity. The inner law applies within a partial region of the entire depth of flow. According to Garcia (2008) it holds for a thin layer z/H < 0,20, where H is the mean depth. Bathurst (2002) suggests a similar value for the layer (z/H < 0,15) where the law is valid and extends it to other types of flows beyond the uniform one: flows with adverse and zero pressure gradients an flows with secondary circulation. Although its straight domain of applicability the law has been used as a reasonable approximation throughout most of the flow depth in many streams and rivers:

The outer law, also known as the velocity defect law, introduces the mean depth H as the relevant length scale. Assuming that the maximum velocity u_{max} takes place at the water surface (z = H), the outer law can be written as.

$$\frac{u_{max}-\overline{u}}{u_*} = -\frac{1}{k} ln\left(\frac{z}{H}\right) \qquad 3.14$$

The domains of the inner and the outer law are not mutually exclusive. There is an overlapping region between the lower limit of the outer law and the upper limit of the inner law. If the bed is sufficiently smooth it will develop a thin layer where viscous effects dominate and turbulence is suppressed, the so called viscous sublayer. While this circumstance can appear in smooth pipes it is rarely satisfied in natural gravel bed rivers. In fact, most boundaries in alluvial rivers are hydraulically rough. Consequently, the viscous sublayer doesn't exist and will be disregarded for the subsequent analysis. In a hydraulically rough boundary the velocity distribution and the flow resistance depend exclusively on the relative roughness. Flow resistance is independent of the Reynolds number since viscosity doesn't play a determinant role. In this case the bed roughness length (z_0) is k_s / 30, where k_s is the effective roughness length. So, the inner law can be rewritten:

$$\frac{\bar{u}}{u_*} = \frac{1}{k} ln\left(30\frac{z}{k_s}\right) = \frac{1}{k} ln\left(\frac{z}{k_s}\right) + 8{,}5 \qquad 3.15$$

This expression will be used for deriving flow resistance formulas for gravel bed rivers. Because flow patter is modified by bed form it is necessary to analyze first, in a qualitative way, the link between channel morphology and flow pattern.

3.4 Channel morphology and hydraulics

Scientists have made a great effort to classify gravel bed rivers. According to their planform features gravel-bed rivers can be classified in straight, wandering and braided streams (Leopold et al, 1964). Other classification systems focus on bed form as a distinctive feature, that is the system proposed by Montgomery and Buffington's (1997). The latter will be considered because it will be clearer the relation between bed form and flow pattern. The system is especially adapted to mountain environments. Originally developed in the Pacific Northwest of U.S.A., it has also been applied with success in the Italian Alps (Lenzi et al, 2000). Rivers are classified into five categories; two of them apply to gravel-bed rivers, the so called plane-bed and pool-riffle.

A plane-bed reach can be recognized in the field due to its lack of bed forms. Usually, they consist of straight reaches, with no bars so the longitudinal profile is also a straight line (see figures 3.1 and 3.2). The cross section has a low with/depth ratio and the presence of large gravels and cobbles in the bottom gives low values of relative submergence (bankfull depth to grain size ratio). This geometric and sediment size characteristics are related to a specific flow pattern. The flow is uniform with a lack of convergent – divergent lateral flow sequences. The low aspect ratio and greater relative roughness may decompose lateral flow into smaller circulation cells (Montgomery and Buffington, 1997). When roughness is sufficient small a logarithmic law can be considered for the velocity vertical distribution. Instead, when roughness is very large this law doesn`t apply because the distribution is greatly disturbed by the presence of large particles. Nonetheless, in both cases the grain roughness is the primary source of flow resistance. A typical feature of plane-bed channels is the presence of a mobile armored bed surface at near bankfull discharge (Buffington, 1995). Parker (1990) has shown that a mobile armor layer indicates a balance between mean annual sediment supply and transport capacity for gravel bed rivers where the bankfull shear stress just exceeds the threshold value.

Riffle-pool reaches have a rhythmically sequence of lateral bars and an undulating bed with shallow and deep sectors (see figures 3.1 and 3.2). At low flow bars emerge and the bed pattern can be recognized. Lateral bars alternate making the low flow to describe a sinuous trajectory (sinuosity between 1.3 and 1.5). The highest point in the bar corresponds to the maximum depression in the channel, which is the pool. At the head of the bar the flow passes from one side to the other. This sector with a low water depth is called a riffle. Field observations evidence that these features are spaced evenly along the channel with a separation about five to seven channels width (Leopold et al, 1964; Hey and Thorne, 1986). The alluvial bar development requires a sufficiently large width to depth ratio and small grain sizes that are easily mobilized and stacked by the flow (Church and Jones, 1982). Surface grain size is variable with the courser sizes in riffles and finer sizes in pools. Substrate size in riffle-pool streams varies from sand to cobble, but typically is gravel sized. It is common to observe an armor layer with finer size in the substrate and coarser size in the surface (see Chapter Nº4).

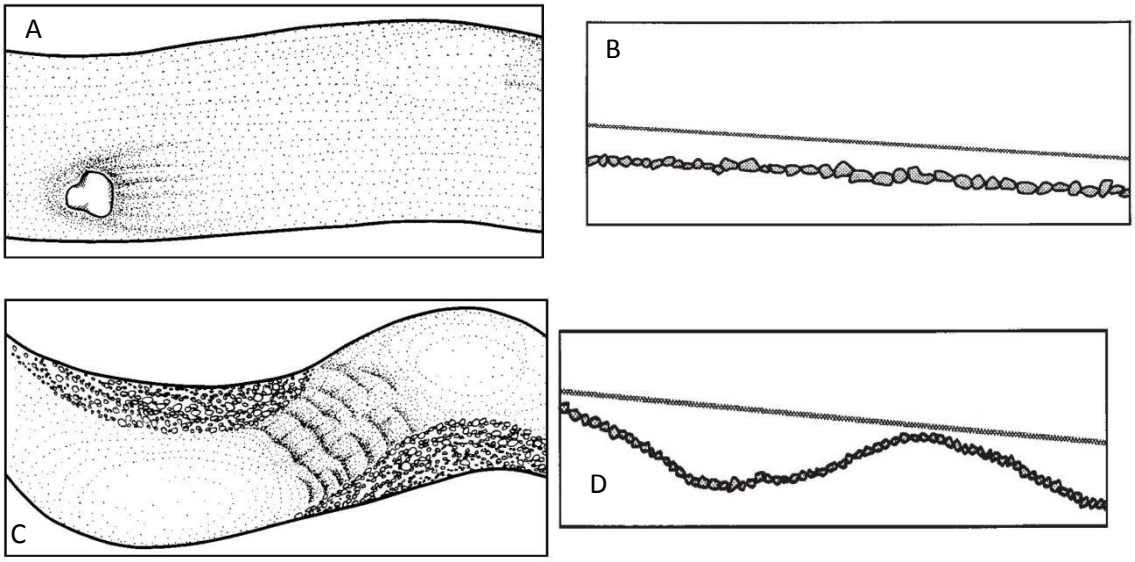

Figure 3.1. A, B) Plain pattern and bed profile of a plane-bed channel. C, D) Plain pattern and bed profile of a riffle-pool channel (modified from Montgomery and Buffington, 1997).

Figure 3.2. Left: Example of a plane-bed reach (Epuyén River in Chubut Province, Argentina); right: example of a riffle-pool reach (Brenta River in Veneto Region, Italy)

Due to this undulating bed the flow can`t be uniform. Thompson (1986) has presented a description of the flow along a riffle-pool sequence. At the upstream riffle surface current passes obliquely and is directed towards the outer bank (figure 3.3). At the outer bank there is a zone of upwelling and a strong inward movement of surface water towards a zone of convergence over the deepest part of the pool. Near the bed the current diverges and divides making two opposite secondary flow cells. The helix flow decays as the depth decreases downstream. At the crest of the depositional front, on the riffle, the flow diverges passing obliquely to the other bank starting the sequence again. The presence of secondary flow is not exclusively associated to the presence of alternating bars. They have also been observed in straight reaches (Leopold, 1982) suggesting that they could be a consequence of the instability in turbulent flow. In fact, Einstein and Shen (1964) demonstrated that a meandering thalweg could be produced on the bed of a straight laboratory channel by the action of twin surface-convergent cells of secondary flow induced purely by wall turbulence. Although secondary currents are present in both straight channels and sinuous channels, the intensity and origin in each case are different. In a straight channel the secondary flow is due to instabilities in turbulent flow and has a very low intensity (2% of

the principal current). On the other hand, a change in direction can create a secondary current, but this time with a higher intensity. That is the case of the riffle-pool reach.

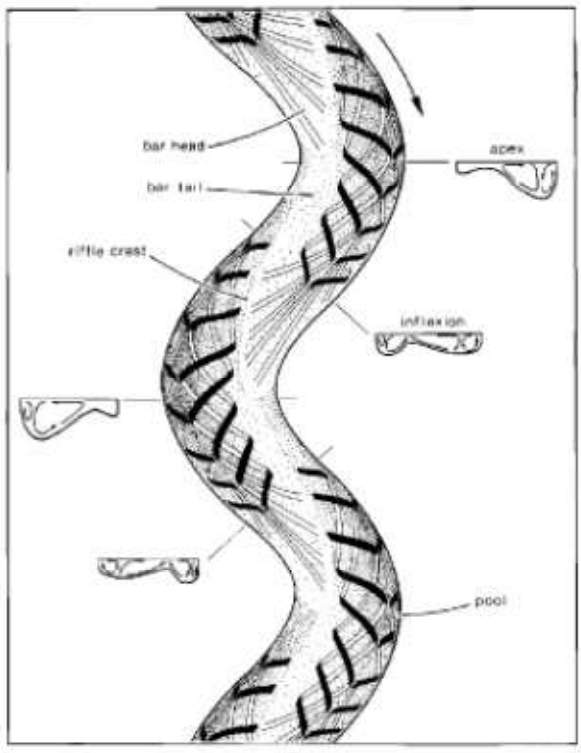

Figure 3.3. Flow model over a riffle-pool sequence developed by Thompson (1986). Black lines indicate surface currents and white lines near-bed currents.

Several theories have been proposed to explain the development of riffle-pool sequences. Langbein and Leopold (1968) proposed the kinematic waves theory that gives the interesting result of a static plan form for the maximum transport rate capacity. According to Yang (1971) riffle formation is the result of the combination of two processes: dispersion stresses acts over the potential riffle resulting in the sorting of the bed material. Keller and Melhorn (1973) invoked the alternating divergent-convergent flow with secondary flow pattern (as described later by Thompson, 1986) as the main mechanism for the development of scour and depositional patterns.

3.5 Flow resistance

The governing equations aforementioned, i.e. the continuity equation and the Reynolds time-averaged equations require the specification of the interaction between the flow and the boundary for their solution. A key issue in hydraulics is the quantifications of flow resistance due to rough boundaries.

The inner law can be used as an approximation of the velocity distribution in the vertical and then integrated in the whole flow depth, giving as a result the mean velocity of the flow:

$$\frac{U}{u_*} = \frac{1}{k} ln\left(11\frac{H}{k_s}\right) \qquad 3.16$$

Wherein U is the depth-average velocity and H is the flow depth. This relation is known as the Keulegan's resistance law for hydraulically rough boundaries (Keulegan, 1938).

Several relations have been proposed to quantify the mean velocity in an open channel flow. All these relationships introduce an adequate resistance coefficient. The most frequently used formulas are those developed by Manning, Darcy-Weisbach and Chezy:

$$U = \frac{1}{n} R^{2/3} S^{1/2} \quad \text{(Manning)} \quad 3.17$$

$$U = \sqrt{\frac{8g}{f}} \sqrt{RS} \quad \text{(Darcy-Weissbach)} \quad 3.18$$

$$U = C\sqrt{RS} \quad \text{(Chezy)} \quad 3.19$$

In witch n, f and C are the Manning, Darcy-Weissbach and Chezy resistance coefficients, respectively; R is the hydraulic radius and S is the slope. It is convenient to underline the difference between a resistance coefficient and the roughness factor. A roughness factor is a geometry measurement reflecting the actual effective unevenness of the boundary, while a resistance coefficient is a measure reflecting the dynamic behavior, in terms of momentum or energy, of the boundary in resisting the flow of the fluid (Yen, 2002). It is also necessary to say that not all the formulas are dimensionally homogeneous. In the Darcy-Weissbach formula the resistance coefficient (f) is dimensionless as it can be easily verified. Instead, manning's n and Chezy's C have dimensions. Manning's formula has been widely used because n remains almost constant for all flow depth. Besides, there are many publications suggesting values of n for different conditions (see Chow, 1994 and Barnes, 1967). Yen (1992, 2002) provided a modified Manning equation to the following forms:

$$U = M \left(\frac{R}{k_s}\right)^{1/6} \sqrt{gRS} \quad 3.20$$

$$U = \frac{\sqrt{g}}{n_g} R^{2/3} S^{1/2} \quad 3.21$$

In the first expression the dimensionless coefficient M is introduced, which can easily been related to n in the original Manning's formula. In the second formula, Yen (2002) retains the physical meaning of gravity and introduces a new factor to make dimensionally homogeneous the formula (n_g has the dimension of $L^{1/6}$).

In the uniform flow the shear stress on the boundary (τ_b) can be determined from the momentum balance for the reach and is expressed as:

$$\tau_b = \rho g H S \quad 3.22$$

Where ρ is the water density and S the bottom slope (equal to the water surface slope and the energy grade line slope). Taking into account the definition of shear velocity,

$$u_* = \sqrt{\tau_b / \rho} \quad 3.23$$

The resistance coefficients can be related to each other.

$$\frac{U}{u_*} = \sqrt{\frac{8}{f}} = \frac{R^{1/6}}{n\sqrt{g}} = \frac{C}{\sqrt{g}} = \frac{1}{k} ln\left(11\frac{H}{k_s}\right) \quad 3.24$$

Sometimes the logarithmic law has been approximated by power laws as the Manning-Strickler form. Parker (1990) proposed the following power expressions that is easier to manipulate and gives a good approximation for the Keulegan's resistance law:

$$\frac{U}{u_*} \cong 8{,}1\left(\frac{H}{k_s}\right)^{1/6} \quad 3.25$$

3.5.1 Skin roughness and the plane bed reach

A plane-bed reach is similar to a plane rigid-wall channel in that the source of resistance is grain roughness. However, there are two major differences between these situations: a) for a rigid impervious boundary, no water will penetrate the boundary, whereas for the sediment bed, water moves through the voids between the bed particles, and b) for a sediment plan bed some energy and momentum are spent on picking up, transporting and depositing the bed sediment (Yen, 2002).

Karman-Prandtl logarithmic velocity distribution and Nikuradse`s equivalent grain roughness concept have been extended to natural rivers although the sediment size distribution is not as uniform as the material used in the original pipe experiments. Following the Nikuradse equivalent grain roughness concept, ks is assumed to be proportional to a representative sediment size, D_x.

$$k_s = \alpha_x D_x \quad 3.26$$

In table 3.1 there is a list of values of α_x for the selected sediment percentile x. When possible it has been differentiated the type of resistance the researcher has measured. As it can be noted several sediment sizes have been suggested. Statistically, D_{50} (the grain size for which 50% of the bed material is finer) is most readily available. Physically, a representative size larger than D_{50} is more meaningful to estimate flow resistance because of the dominant effect of large sediment particles (Garcia, 2008).

Results exposed in table 3.1 deserve some comments. The first six rows apply to grain roughness in plane bed channels or flume experiments. There are methodological differences between the researchers. For example, both Stricker (1932) and Kamphuis (1974) derived their relations from flume measurements, Millar (1999) applied a lower bound criterion using field data, while Pitlick (1992) compared the velocity distribution measured infield and the one calculated with the logarithmic law. The lower limit of the equivalent grain roughness (k_s) is given by Millar: $k_s = D_{50}$; while the upper limit corresponds to Pitlick's results: $k_s = 3\ D_{84}$, that is almost 6 times the lower limit if we consider a typical value of 2 for the relation D_{84}/D_{50}. This upper limit seems too high if compared with other results for total roughness in gravel-bed rivers. In fact, the reported averaged value of α_{84} for gravel bed rivers is similar 3,21, indicating some kind of bed form resistance.

The problem emerges when applying these formulas to separate grain and form resistance. Kamphuis`s (1974) results have been used to quantify the grain resistance in order to determine the bed form resistance (Parker & Peterson, 1980), giving very low or negligible values; it has also been considered to determine the bed shear stress due to skin friction in downstream fining analysis (Parker, 1991a and 1991b), and to analyze sediment transport laboratory data (Wong and Parker, 2006). According to

Prestegaard (1983) k_s was calculated from measurements of velocity and calculation of shear velocity based on slope and depth instead of hydraulic radius. As depth values were higher than hydraulic radius it follows that k_s was overestimated. Therefore Prestegaard (1983) suggested a value of equivalent grain roughness equal to D_{84} (similar to the Nikuradse's assumption for pipe flow: $k_s = D_{90}$). However, much recently, Wong and Parker (2006) successfully used a Manning form equation proposed by Parker (1991) that approximate the Keulegan's equation imposing $k_s = 2\ D_{90}$ (Kamphuis, 1974). They reanalyzed the Meyer-Peter and Muller (1948) original data, accomplished a sidewall correction and, finally, achieved and excellent concordance with experimental data. Furthermore, they showed that the Nikuradse assumption underestimate the skin roughness. Another favorable result was obtained by Diplas (1990) who found $k_s = 2\ D_{90}$ measuring the flow resistance in self-formed sand bed channels in laboratory. On the other hand, considering field data, Millar (1999) suggested that roughness measures such as $3\ D_{84}$ or $2\ D_{90}$ overestimate the grain roughness and inherently included a component of the form roughness. Figure 3.4 illustrates this point. Field data of total resistance ($1/\sqrt{f}$) from gravel bed rivers is compared with skin resistance calculated with Millar (1999) and Kamphuis (1974) equation, that is, $k_{s'} = D_{50}$, $k_{s'} = 2 \cdot D_{90}$, respectively. Almost all the observed data (total resistance) is above the Millar criterion, with only 7 of 168 points falling under the perfect agreement line for skin resistance. Instead, for the Kamphuis's criterion the 27% of data is below this line, indicating that the skin resistance contains other factors, such as bed form, as suggested by Millar (1999). It follows that much research is needed to clarify this difference between skin roughness derived from field data and laboratory data.

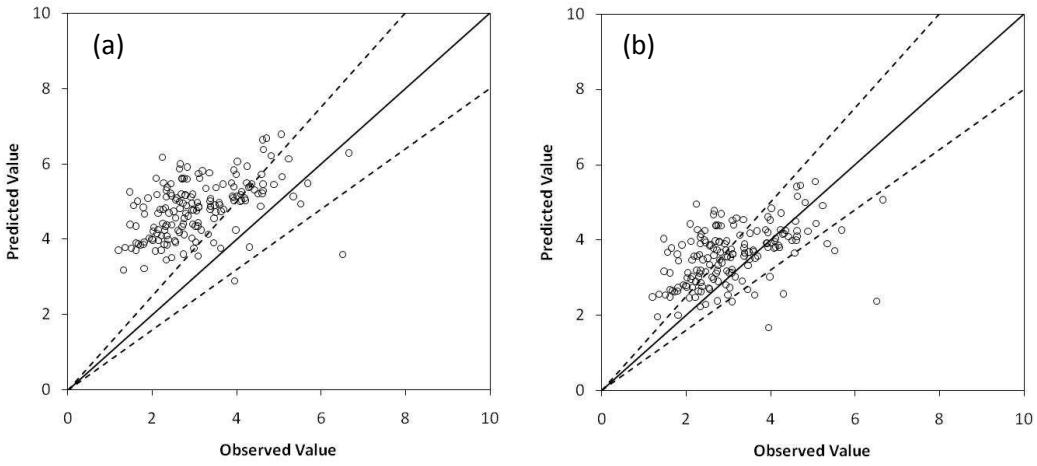

Figure 3.4. Comparison of predicted skin resistance and observed total resistance values of $1/\sqrt{f}$ using published data set. Dashed lines delimit errors of 25% or less. (a) Skin roughness $ks' = D_{50}$ according to Millar (1999); and (b) Skin roughness $ks' = 2\ D_{90}$ according to Kamphuis (1974), assuming the ratio $D_{90}/D_{50} = 2$.

Table 3.1. Values of equivalent roughness height according to several researches. The table shows values from flume experiments and field measurements.

Researcher	Sediment Size D_x	$\alpha_x = k_s / D_x$	Observations
Strickler (1923)	D_{50}	3,3	Applies for gravel beds without significant bed forms (Yen, 2002)
Kamphuis (1974)	D_{90}	2	Laboratory experiments with heterogeneous material
Diplas (1990)	D_{90}	2	Laboratory experiments with self-formed sand bed channels
Wong & Parker (2006)	D_{90}	2	Reanalysis of Meyer-Peter and Muller laboratory data: skin roughness
Millar (1999)	D_{50}	1	Grain resistance defined with the lower bound of observed resistances
Prestegaard (1983)	D_{84}	1	Assumed to calculate the energy slope due to grain resistance
Pitlick (1992)	D_{84}	3	Vertical velocity profile in a plane gravel bed stream near the threshold of motion
Meyer-Peter Muller (1948)	D_{90}	1	Grain roughness in laboratory flumes with plane bed.
Leopold et al (1964)	D_{84}	3,9	Total resistance measured in Brandywine Creek
Limerinos (1970)	D_{84}	3,2	Natural streams with gravels and cobbles.
Bray (1982)	D_{50} D_{84} D_{90}	6,8 3,5 3,1	Total resistance in gravel bed rivers
Whiting & Dietrich (1990)	D_{84}	2,95	Best fit for shear stress prediction for sediment transport calculations in a sand bed and a gravel bed stream.
Millar (1999)	D_{50} D_{84}	5,9 2,9	Best fit flow resistance equation for gravel bed rivers
Parker et al. (2007)	D_{50}	8,9	Best fit flow resistance equation for gravel bed rivers (see comparison below)
Lopez & Barragan (2008)	D_{50} D_{84} D_{90}	6,1 2,8 2,4	Analysis of published field data and direct measurement in mountain and gravel bed rivers in Spanish Pyrenees.

3.5.2 Bed form roughness and the riffle pool reach

The simplest attempt to quantify the total roughness in natural gravel-bed rivers consists of the application of the Keulegan's equation calibrating the equivalent grain roughness with direct field data. Several issues arise such as the definition of the geometric parameters and because Keulegan's equation applies to uniform flow been the actual flow in natural riffle-pool channels far from uniform. This topic will be treated in detail below.

Although all the values of α_x reported in Table 3.1 seem to correspond well between the researchers, the scatter presented in the original studies is considerable (see Fig 3.5). When bed forms are present, a single value such as k_s, alone, to represent all the effects of the size, shape, and spatial distribution of the roughness elements, is questionable. If the channel is sufficiently wide and the sediment transport is

in equilibrium, Yen (2002) proposes a minimum of three independent variables to describe the resistance coefficient.

$$f = F(Re; F; k_s/H) \qquad 3.27$$

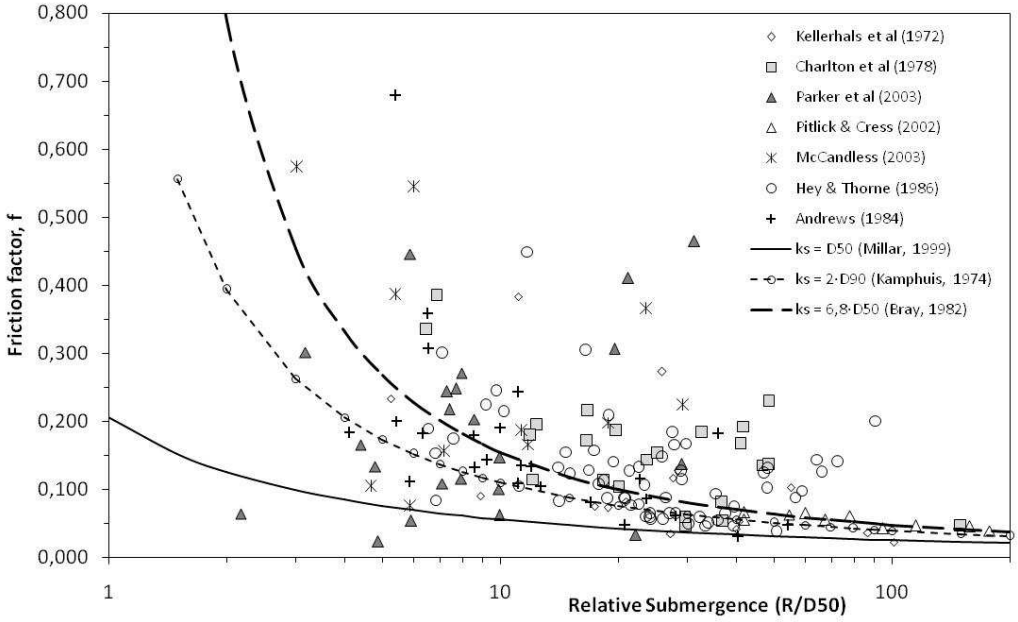

Figure 3.5. Variation of observed f with relative submergence. It has been assumed a representative ratio D_{90}/D_{50} =2 in order to compare Millar (1999), Kamphuis (1974) and Bray (1982) equations.

Where Re is the Reynolds number and F is the Froude number. Following this idea several researchers have proposed new formulas for gravel bed rivers that incorporate new variables. One of the first researchers that worked on this topic were Parker and Peterson. Their work is mentioned here because it introduces the pioneer idea of considering more variables, in this case, the shear stress straightly related with sediment transport.

Parker and Peterson (1980) analyzed field data of gravel bed rivers published by Kellerhals et al (1972). They divided the total resistance in grain and bed form resistance applying the criterion of energy slope division. The grain slope was calculated using laboratory results from Kamphuis (1974). Then they derived the bed form resistance formula.

$$C_b = 2{,}33 \cdot 10^{-6} \tau_G^{*\,-1{,}744} \qquad 3.28$$

In which C_b is the bar resistance coefficient (which is equal to one-eighth of the Darcy-Weisbach resistance coefficient), and τ_G^* is the grain Shields stress, $\tau_G^* = R_H S_G / R$; R_H is the hydraulic radius, S_G is the grain slope and R is the submerged specific gravity of sediment (equal to 1,65, generally).

In the conclusions, the authors note that the difference between the Kamphuis's (flume experiments with plane bed) and Limerino's (gravel bed rivers) relations is small, been less than 10% in terms of $C_G^{-1/2}$ for values of R/D_{90} as low as 2,6.

Jaeggi (1984) studied the formation of alternate bars in channelized rivers in Europe. He compared field data with flume experiments and developed a criterion for the bar formation. Besides, he also developed a resistance formula for the intermediate roughness range because, according to the results, the form roughness is negligible at bar forming flows.

$$\frac{U}{u_*} = 2{,}5\left(1 - e^{-\frac{\alpha Z_{90}}{S^{0,5}}}\right)^{0,5} ln\left(12{,}3\frac{Z_{90}}{\beta}\right) \quad 3.29$$

In which Z_{90} is the relative roughness (H/D_{90}); S is the slope; and from laboratory test with material similar to gravel the coefficient α and β have the values 0,02 and 2 respectively. Note that equation 3.29 is a modified version of Keulegan's formula, been 1/k = 2.5, the second factor a correction introduced and the last factor the logarithmic law with $k_s = 2\ D_{90}$.

Miller and Wenzel (1985) proposed a different approach that resembles the established solution for energy losses calculation in pipes. The friction loss is evaluated considering the Keulegan's equation with a grain roughness length equal to D_{90}. Local losses are calculated applying the known expansion/contraction expression for pipe:

$$S_L = C\frac{U^2}{2gL} \quad 3.30$$

Where S_L is the energy loss due to expansion and contractions of the flow, C is a coefficient (C_e for expansions and C_c for contractions), U is the mean velocity (equal to the downstream cross section velocity in a contraction or the upstream cross section velocity in an expansion), and L is the distance between two cross sections.

The authors applied this methodology to a case study in the field and in two laboratory tests. In both cases they applied the Bernoulli's equation to a reach considering several cross sections in a sequence of riffle-pool. As a result, they concluded that the flow resistance coefficient showed a marker decrease in value with increasing discharge and that local losses appeared to contribute significantly to total energy loss trough pool-riffle sequences under low flow conditions.

Hey (1988) states that uniform flow is applicable at the riffle cross section, and hypothesizes that the total roughness (D_t) for equivalent uniform flow through the pool-riffle sequence can be calculated from the average values of velocity, depth and slope. He also presents a cross section coefficient factor that takes into account the irregularities of the section. Field data comes from 62 gravel bed rivers in the United Kingdom.

$$\frac{1}{\sqrt{f}} = 2{,}03log\left(\frac{aH}{D_t}\right) \quad 3.31$$

Where H is the reach average depth; and D_t is the total roughness for the reach that is calculated with the following formula:

$$D_t = aH\left(\frac{D_g}{a_r H_r}\right)^{\sqrt{\frac{fr}{f}}} \quad 3.32$$

In which a and a_r are coefficients representing the effect of the cross-section shape on flow resistance for reach and riffle, respectively; and f_r is the friction factor at the riffle section. The grain roughness is $D_g = 3,5\ D_{84}$.

$$a = 11,1\left(\frac{R_H}{H_{max}}\right)^{-0,314} \quad 3.33$$

$$\frac{f_r}{f} = \frac{H_r^3 B_r^2 S_r}{H^3 B^2 S} \quad 3.34$$

Where H_{max}, the maximum flow depth; H_r the mean depth, B_r, the width and S_r the slope at the riffle section; H, B, and S are the corresponding average values for the reach.

Colosimo et al. (1988) developed a resistance equation that takes into account the Froude number and the sediment mobility parameter. They measured 43 reaches in Calabria (Southern Italy), with reasonably uniform and relatively low flow, friction slope greater than 0,2%, small and intermediate scale roughness (H/D_{84} between 2,25 and 12), mobility parameter greater than the critical value in more than 50% of the cases, and a Froude number between 0,20 and 1,30. Their proposed resistance equations is:

$$\frac{1}{\sqrt{f}} = 2,03log\left(\frac{\alpha H}{MD_{84}}\right) + (2,54F - 1,65) + \left(0,75 - 0,68\frac{\tau_{50}^*}{\tau_c^*}\right) \quad 3.35$$

In which, α is the shape factor defined as:

$$\alpha = 10e^{\left(\frac{8,5-2,5(1-C)}{5,75}\right)} \quad 3.36$$

$$C = ln\left(1 + \frac{2H}{B}\right) - \frac{H}{B} \quad 3.37$$

In which H is the mean flow depth and B is the width of the cross section. The dimensionless critical shear stress (τ_c^*) is 0,029, and the bottom dimensionless shear stress $\tau_{50}^* = H\ S/R\ D_{50}$. M is equal to $(A_1 + A_2) / A_2$ where A_1 and A_2 are defined in the same way as the Kramer parameter for grain size analysis, A_2 for the finer size and A_1 for the coarser size.

Afzalimehr & Anctil (1998) proposed a semilogarithmic formulation following the idea of Colosino et al (1988). The formula considers the influence of the relative roughness, the Froude number, the sediment mobility parameter, and a cross-sectional form factor. It is based on a broad field data set consisting of 280 gravel bed rivers located in Canada, United Sates, United Kingdom, New Zealand, Ireland and Italy. The data used for calibration has the following characteristic: slope between 0,0001 and 0,052; mean grain size from 2,7 mm to 180 mm; hydraulic radius from 0,2 m to 2,0 m ; and mean velocity between 0,25 m/s and 3,8 m/s.

$$\frac{1}{\sqrt{f}} = 2,03log\left(\frac{\Psi h}{D_{50}}\right) + 2,96F - 0,18\frac{\tau_{50}^*}{\tau_c^*} - 0,83 \quad 3.38$$

Where, Ψ is the cross-sectional form factor equals to $(p / w)^{0,5}$, in which p is the wetted perimeter (B + 2h), and B is the channel with; F is the Froude number; D_{50} is the median grain size; and τ_{50}^*/τ_c^* is the

sediment mobility parameter (the same defined by Colosino et al. 1988). The dimensionless critical shear stress (τ_c^*) is 0,03.

Millar (1999) compiled several published data for gravel bed rivers and suggested an original criterion for the definition of grain resistance in gravel bed rivers. He analyzed data and considered a lower bound to the observed resistance rather than attempting to derive a best-fit value for ks (like Bray 1982). He obtained a value of ks = D_{50} which is the lowest value indicated in table 3.1. Then he applied this criterion to Prestegaard's (1983) data, who had completed a detailed research on gravel bed topography. He calculate the bar resistance applying the new criterion (ks' = D_{50}) and found a good correlation between the bar resistance slope (S'') and the bar steepness ratio (A/L where A is the bar amplitude and L is the riffle spacing).

$$S'' = 0{,}95\frac{A}{L} \tag{3.39}$$

$$S = S' + S'' \tag{3.40}$$

$$S' = \frac{f'}{8}F_r^2 \tag{3.41}$$

Where F_r is the Froude number ($F_r = U/\sqrt{gH}$), f' is the grain friction factor calculated with the Keulegan's equation using ks' = D_{50}. He also compared S'' with others values of ks' commonly used (ks' = 3 D_{84} or 2 D_{90}, assumed by Parker and Peterson, 1980; Hey, 1988; Whiting and Dietrich, 1990). His results indicate that such roughness measurements overestimate the grain roughness and inherently include a component of form roughness.

Parker et al. (2007) analyzed published data of hydraulic geometry for bankfull discharge and compiled a data set with 180 reaches. The data set exhibits a wide range of streams: the slope varies from 0,0003 to 0,031; the relative submergence, from 2,2 to 177; and discharges from 0,7 m^3/s to 5440 m^3/s. The resistance equation has a power form where the coefficient and exponent were calculated by least squares regressions.

$$\frac{U}{u_*} = 3{,}71\left(\frac{H_{bf}}{D_{50}}\right)^{0{,}263} \tag{3.42}$$

In which H_{bf} is the cross section mean depth at bankfull stage. This power form can be converted to a semilogarithmic form applying a least square regression.

$$\frac{U}{u_*} = 2{,}55ln\left(11\frac{H_{bf}}{k_s}\right) \tag{3.43}$$

Where k_s = 8,94 D_{50}.

In order to compare the available resistance equations, a data set comprising 168 reaches has been compiled from literature. The data has been collected by Parker et al (2007) and contains data of gravel bed rivers published by Kellerhals et al (1972), Charlton et al (1978), Parker et al (2003), Pitlick and Cress (2002), McCandless (2003), Hey Thorne (1986), and Andrews (1984). Table 3.2 gives some illustrative information about the variation range for some parameters of the data set. Three criteria are used for the comparison: a) a visual criterion consisting in plotting observed and calculated values for $1/\sqrt{f}$; b)

evaluating the root-mean-square deviations (RMD); c) evaluation of the absolute average deviation (AAD).

$$RMD = \sqrt{\frac{1}{N}\sum_{j=1}^{N}\left(x_{calc_j} - x_{obs_j}\right)^2} \quad 3.44$$

$$AAD = \frac{1}{N}\left|\sum_{j=1}^{N}\frac{x_{calc_j} - x_{obs_j}}{x_{obs_j}}\right| \quad 3.45$$

Where x stands for $1/\sqrt{f}$, the subscript "calc" indicate the predicted value with a resistance equation and "obs" is the friction factor calculated from field data; N is the number of data.

Table 3.2. Range of selected parameters for the data set.

Parameters	Min	Mean	Max
Slope	0,03%	0,57%	2,80%
Relative submergence	2,2	27,6	177,5
Aspect ratio (B/H)	5,8	22,8	65,9
Froude Number	0,1	0,7	2,4
τ/τc	0,2	1,7	5,5

Using the same data of Parker et al (2007) it is not surprising that their formula gives the smallest deviations indexes (see table 3.3).

Table 3.3. Comparison of total resistance formulas. RMD means root-mean-square deviation and AAD, absolute average deviation.

Formulas	RMD	AAD
Bray (1982)	0,941	0,090
Jaeggi (1984)	1,145	0,058
Afzalimehr & Anctil (1998)	1,328	0,134
Parker et al (2007)	0,924	0,025

Bray's formula has also a good performance. Instead, Afzalimehr and Anctil's formula has the largest deviation indexes. It is a curios result because these authors showed that taking into account more variables it was possible to make better predictions for the friction factor. Graphically, both Azalimer/Anctil and Jaeggi formulas exhibit considerable scatter (see figure 3.6).

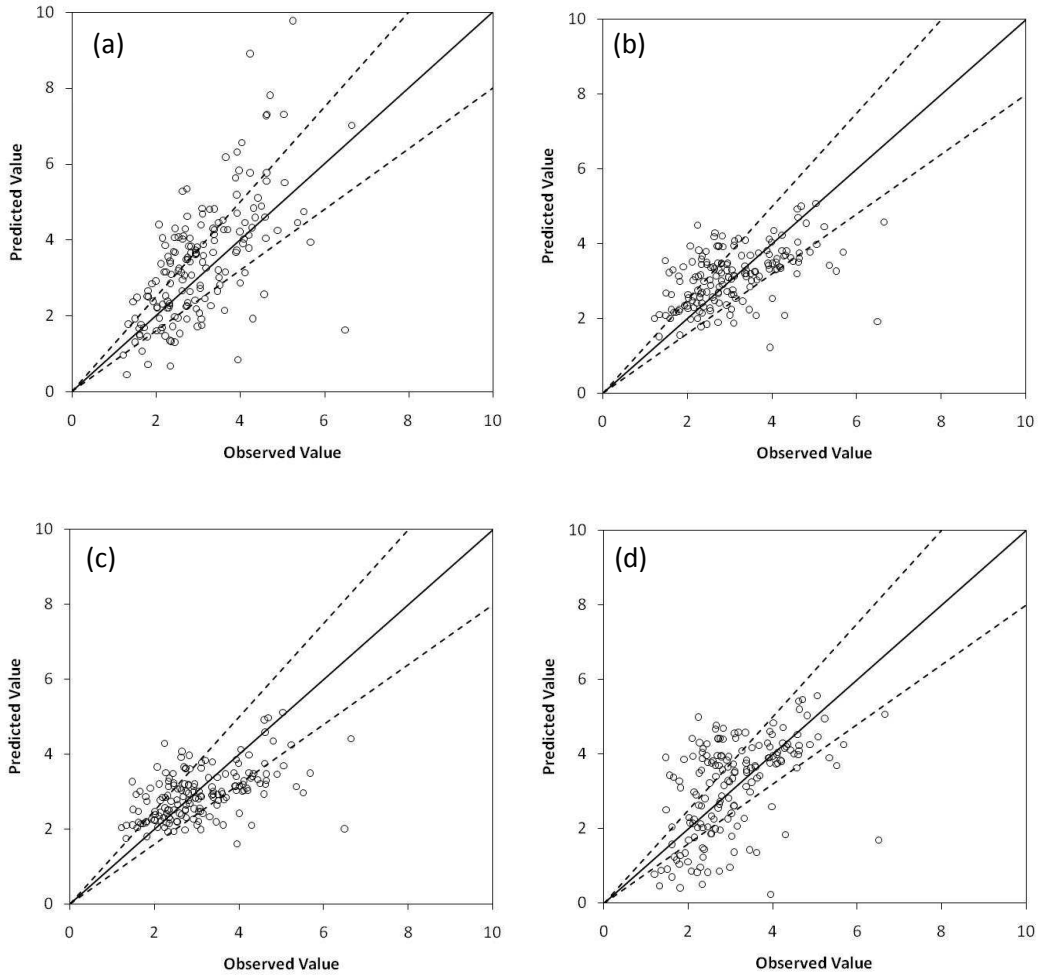

Figure. 3.6. Comparison of predicted and observed values of $1/\sqrt{f}$ using published data set and formulations proposed by: (a) Afzalimehr and Anctil (1998); (b) Bray (1982); (c) Parker et al, (2007); (d) Jaeggi (1984). Dashed lines delimit errors of 25% or less.

3.5.3 The point, cross-section and reach scale

Open channel computations or measurements are often made reach by reach or cross-section to cross-section, and the resistance coefficient should be determined accordingly. Yen (2002) analyzed this problem and concluded that there are 18 different ways to compute the average Manning n or the Darcy-Weissbach f for the reach. From equation 3.24 resistance coefficients are related to mean velocity and shear velocity. At the point scale, there are three possibilities for U/u*: a) measuring τ_0 and evaluating u*; b) to calculate it assuming a velocity distribution; c) considering the local depth h ($\tau_0 = \gamma hS$). For the cross-section scale, there are also three possibilities for U/u* according to the criterion for averaging τ: a) the shear stress along the cross section is the average of the point shear stress τ_0; b) it is taken the average on the shear velocity; c) mean shear stress considering the momentum equation for the whole cross section. Finally, the computation of U/u* for the reach presents the major quantity of possibilities because of the ways of computing and combing the average values of u* and U.

3.5.4 Skin and form resistance partition

The major scope in distinguishing the skin and form components in total resistance is for evaluating correctly the sediment transport intensity. The form drag results from the net pressure distribution over

an entire bed form. At any point along the surface of the bed form, the pressure force acts normal to the body. For this reason, form drag is not effective in moving sediment as bed load or in entraining sediment. Therefore, the part of the effective shear stress that governs sediment transport is the skin friction (Garcia, 2008).

Let's consider again a uniform flow over a mobile bed. The shear stress on the bed is thought to be composed of two parts, the skin friction and form drag. From the direct interaction between flow and particles comes the grain shear stress (τ_0') , and the bed form drag effect on flow is quantify by increasing the total shear stress (τ_0), this differences is the shear stress due to form drag (τ_0'').

$$\tau_0 = \tau_0' + \tau_0'' \quad 3.46$$

Considering the relationship between shear stress, shear velocity and cancelling the mean velocity, it is possible to work the previous relation to arrive to:

$$(HS_e) = (HS_e)' + (HS_e)'' \quad 3.47$$

Where H is the mean depth (that can be replaced by the hydraulic radius); and S_e is the energy slope.

There are two ways to further formulate the partition. Meyer-Peter Müller (1948) proposed to divide the total slope into a grain resistance slope S' and a bed form resistance S'', considering H constant.

$$S_e = S' + S'' \quad 3.48$$

Applying this partition to the Darcy-Weisbach expression, it follows that also the friction factor is linearly divided.

$$f = f' + f'' \quad 3.49$$

In which f' is the skin friction factor and f'' is due to bed form resistance. The skin friction factor is evaluated with the Keulegan's equation using the hydraulic parameters (H and U) from the whole flow.

In the second method the linear division is accomplished on the mean depth (or hydraulic radius) while the slope is retained constant. This method was first proposed by Einstein (1950).

$$H = H' + H'' \quad 3.50$$

And hence

$$\tau_0 = \gamma H' S + \gamma H'' S \quad 3.51$$

Where H' denotes the mean depth that would result in absence of bedforms but with U been held constant. H' can be calculated applying the Keulegan's equation:

$$H' = \frac{U^2}{8gS}\left[\frac{1}{k} ln\left(11\frac{H'}{k_s}\right)\right]^{-2} \quad 3.52$$

For given values of U, ks and S (reach average), H' is solved iteratively.

3.6 Shear stress distribution

Bed shear stress is the main flow parameter that governs sediment transport. This was first recognized by Lane (1955) who discarded the use of critical velocities in favor of the shear stress (see Chapter 1, section 1.1). This section presents several methods used by researchers when developing regime models: the area method used by Parker (1978), the depth average model used by Cao and Knight (1998) and the empirical formulas used by Millar (2005).

3.6.1 The Area method

Lundgren and Jonsson (1964) developed a method to determine the distribution of bottom shear stresses in shallow, symmetrical channels with rough bottom and gently varying bottom curvature. Their model is an extension of Prandtl's turbulent theory, taking into account the transfer of momentum across normals to the bottom. The assumptions adopted by Lundgren and Jonsson are: a) rough boundary that produces a logarithmic distribution of velocity along the normals to the bed, b) the channel profile is sufficiently "smooth" to render secondary currents negligible, c) the shear distribution is best described by the area method.

Considering a steady uniform flow, the Reynolds momentum equation is integrated along the bottom normal giving the streamwise momentum equation:

$$\tau_0 = \rho g S \frac{dA}{dP} + \frac{d}{dP}\int_0^{D_N} \tau_{\varsigma x} d\eta \qquad 3.52$$

Where, τ_0 is the local boundary shear stress, S is the water surface slope, dA is the differential area between normals to the bed, dP is the wetted perimeter below dA, D_N is the distance along a normal from the bed to the water surface, $\tau_{\zeta x}$ is the downstream-directed shear stress induced by turbulence which acts on the normals, x is the downstream axes, ζ is the cross-section axis tangent to the bottom, and η is the cross-section axis normal to the bottom.

Applying the eddy viscosity concept with a parabolic distribution along the depth and assuming a logarithmic distribution for velocity (see section 3.2) it is possible to arrive to the following expression for the cross-channel bed shear stress distribution:

$$\tau_0 = \rho g S \frac{dA}{dP} + \frac{d}{dP}\left(\alpha \frac{d\tau_0}{dP}\right) \qquad 3.53$$

Where α is given by

$$\alpha = \int_{K_s}^{D_N} \frac{1}{2}(\eta - K_s)\left(1 - \frac{\eta - K_s}{D_N - K_s}\right) ln\left(\frac{\eta}{K_s}\right) d\eta \qquad 3.54$$

The appropriate boundary conditions for solving this equation in a symmetrical channel are

$$\tau_0 = 0 \qquad \text{y = B/2 (on the banks)} \qquad 3.55$$

$$\frac{d\tau_0}{dP} = 0 \qquad \text{y = 0 (at the channel centre)} \qquad 3.56$$

The Lundgren and Jonsson's model has been largely used to predict the bottom shear stress distribution with the aim to elaborate regime models. Parker (1978) solved the differential equation using singular perturbation techniques and obtained reasonable agreement with field data. Pizzuto (1990) performed a numerical simulation adding a downslope transport model. He obtained good results with experiments data (Ikeda, 1981; Diplas, 1990). Also Diplas and Vigilar (1992) developed a hydraulic geometry model for threshold channels obtaining good results with laboratory data (Diplas, 1990) and field data. More recently, Kovacs and Parker (1994) developed a vectorial beadload formulation for the sediment transport along banks and valid to slopes up to the angle of repose. They developed a model coupling the sediment transport-model and a similar hydraulic model (neglecting secondary flow effects). The results were in good agreement with Ikeda's (1981) laboratory experiments.

Finally, it is worth to note that Diplas (1990) performed flume experiments and concluded that the rough-wall log law was a valid first-degree approximation of the actual velocity profile along normals to the boundary for the whole channel depth, even in the presence of bed-load movement on the bed. He also concluded that the turbulent-diffusion model was a more realistic approach to the flow in a straight channel, resulting in good agreement between shear-stress distributions predicted from this model with measured values.

3.6.2 The depth average model

Shiono and Knight (1991) developed a hydraulic model to solve the problem of the flow of water in straight open channels with prismatic complex cross-sections. Their objective was to determine the conveyance capacity, velocity distribution and boundary shear stress distribution in two-stage channels. This is the situation of most natural rivers that have flood plains that extend laterally away from the main channel with a gentle slope or are confined by terraces. Determination of hydraulic parameter is not easy by the presence of lateral exchange of momentum between the fast flow in the main channel and the slower moving water on the flood plain. In order to solve the problem they developed an analytical model that includes the effects of bed-generated turbulence, lateral shear turbulence and secondary flows.

Let's consider a steady uniform flow. The longitudinal streamwise component of momentum on a fluid element is integrated over the water depth in order to obtain a depth-mean-averaged momentum equation:

$$\frac{dH(\rho UV)_d}{dy} = \rho g H S + \frac{dH\bar{\tau}_{yx}}{dy} - \tau_b\sqrt{1+\frac{1}{s^2}} \qquad 3.55$$

Where τ_b is the bed shear stress, s is the side slope (1 : s, vertical : horizontal), S is de bed slope gradient, and the subscript "d" indicates that it is a depth-average quantity:

$$(\rho UV)_d = \frac{1}{H}\int_0^H \rho\bar{u}\bar{v}dz \qquad \text{and} \qquad \bar{\tau}_{yx} = \frac{1}{H}\int_0^H\left(-\rho\overline{u'v'}\right)dz \qquad 3.56$$

On the left side of equation 3.55 is the effect of secondary flows, while on the right side there are (from left to right): the force due to gravity, the variation of the transverse shear stress (due to turbulence) and the boundary shear stress (also due to turbulence). The solution is completed applying the eddy viscosity concept, but considering a depth-average value for the viscosity:

$$\bar{\tau}_{yx} = \rho \bar{\epsilon}_{yx} \frac{\partial U}{\partial y} \quad 3.57$$

$$\bar{\epsilon}_{yx} = \lambda U^* H \quad 3.58$$

Where U* is the local shear velocity ($U^* = \sqrt{\tau_b/\rho}$), H is the depth and λ, the dimensionless eddy viscosity coefficient. According to this definition the local shear velocity U* is affected by secondary flow, however the authors, looking for simplicity in the model, retained this expressions and considering that λ described various three-dimensional effects.

Finally, considering the Darcy-Weissbach resistance equation the streamwise momentum equation can be written with the depth-average velocity U as the dependent variable:

$$\rho g H S - \frac{1}{8}\rho f U^2 \left(1 + \frac{1}{s^2}\right)^{\frac{1}{2}} + \frac{d}{dy}\left[\rho \lambda H^2 \left(\frac{f}{8}\right)^{\frac{1}{2}} U \frac{dU}{dy}\right] = \frac{d}{dy}\{H(\rho UV)_d\} \quad 3.59$$

Shiono and Knight (1991) performed laboratory experiments with two-stage channels and observed that the shear stress due to secondary flow $(\rho UV)_d$ decreased approximately linearly either side of a maximum value which occurred at the edge of the flood plain and the main channel. It allowed them to take, at least as a first approximation, a constant value for the gradient of the secondary flow force:

$$\frac{d}{dy}\{H(\rho UV)_d\} = \Gamma \quad 3.60$$

With this approximation it was possible for the authors to complete an analytical solution of the momentum equation.

Abril (1995) performed a numerical simulation applying the finite element method and was able to describe with success the velocity and shear distribution obtained in laboratory experiments of two-stage channels. It is worth to present here the Abril's formulation with the purpose to evidence the differences with the Lundgren and Jonsson's approach. Abril considered a change in variables to simplify the differential equation. He proposed to use the square velocity as the dependant variable: $\omega = U^2$. Furthermore, expressing the channel side slope in general terms as $1/s = dz_b/dy$, and introducing the following substitutions:

$$\alpha = \frac{\rho}{2}\lambda H^2 \sqrt{\frac{f}{8}}$$

$$\beta = -\rho \frac{f}{8}\sqrt{1 + \left(\frac{\partial z_b}{\partial y}\right)^2} \quad 3.61$$

$$q = \Gamma - \rho g H S$$

Equation 3.59 is thus reduced to

$$\frac{d}{dy}\left(\alpha \frac{d\omega}{dy}\right) + \beta\omega = q \quad 3.62$$

The boundary conditions for this equation are: a) zero value of ω at the bank edge (y=B/2) and b) zero value for $d\omega/dy$ at the center for a symmetrical channel. This equation is essentially the same as the one proposed by Lundgren and Jonsson (see equation 3.53) if we consider the relationship between ω and τ_0 established by the Darcy-Weissbach equation and the shear velocity definition. However, there are some important differences: a) the function q incorporates the effect of secondary currents, b) this model considerate vertical depth H while Lundgren and Jonsson considerer normal area (dA/dP) in the q function, c) there is a mean value for the eddy viscosity (λ) while Lundgren an Jonsson considered a parabolic distribution.

Since its publication, the Shiono and Knigth model has been applied to laboratory channel and natural rivers in order to compare theory with measurements. Abril and Knight (2004) calibrated the Shiono-Knight model with measurements from natural streams and applied the model to determine the stage-discharge relationship. More recently, Liao and Kinght (2007) proposed analytical solutions for simple geometries such as rectangular channels and two-stage rectangular channels. Finally, Knight et al (2007) developed a simple model that divides the flow area into several panels with constant value and sign for Γ. The area division is based on the Tominaga et al. (1989) observations of the presence of three secondary currents cells near the bank: two strong cells directed toward the corner along an inclined plane, and a third cell near the free surface and side wall.

The Shiono-Knight hydraulic model has also been used to elaborate regime models. Knight and Yu (1995) considerer the special case of self-formed channels in uniform sand and obtained good results when testing the model against experimental data of Ikeda (1981). In this case Knight and Yu neglected the secondary current effect (Γ=0). Cao and Knight (1997) derived analytically the cross-section shape equation of threshold channels applying an entropy-based criterion. They obtained reasonable agreement with experimental data (Ikeda, 1981) and gravel bed rivers data (Hey and Thorne, 1986; Kellerhals, 1967; Bray, 1979; and Lane and Carlson, 1953).

3.6.3 Empirical approaches

Many researchers have attempted either to predict or to measure the lateral distribution of time-averaged boundary shear stress along the wetted perimeter of channels with regular shapes (rectangular, trapezoidal, etc.). Most of these studies have been conducted in laboratory and just a few have been undertaken in the field. Here some results are presented with their range of applicability.

Knight (1981) performed laboratory experiments with flumes. He used a rectangular channel with a fixed slope (0,1% aprox.). The channel had smooth walls and rough bed. The bed roughness could be increases covering a range for k_b/k_w from 1 to 10^4, where k_b and k_w are the bed and wall Nikurade equivalent sand roughness, respectively. The experiments covered a range for the aspect ratio B/H between 1,5 and 15.

Flintham and Carling (1988) also performed laboratory tests with open channels, but in this case with a trapezoidal geometry. The roughness was uniform along bed and banks.

Previous tests employed open channels. Subsequently researches used wind tunnel that enable them to explore a wide range of aspects ratio. Despite the fact that the flow in a closed conduct was different to the flow in an open channel, this approach proved to give good results (small differences according to Knight and Patel, 1985) and provided an easier way of experimentation.

Knight and Patel (1985) proved the wind tunnel technique and measured the boundary shear stress distribution in fully developed turbulent flows in smooth rectangular ducts with aspect ratios between 0,1 and 10. They found that the shear stress on the bed was about 13% higher than the mean bed shear stress, or 18% higher than the section mean shear stress.

Later, Knight and Patel's (1985) work was extended by Rhodes and Knight (1994) to the range of 0,025 – 50 for the aspect ratio B/H. They also employed a rectangular conduct with smooth walls. The extended formula for the shear force (see table 3.4) is intended to be valid for the range $0 \leq B/H \leq \infty$.

Recently, the ASCE Task Committee (ASCE, 1998) performed experiments with trapezoidal open channels with different bank angle (45°, 68° and 90°). They used homogeneous roughness in bank and bed for both situations: smooth and rough channels. The shapes analyzed were compressed in the range $0,1 < Pb/Pw < 5$, where Pb is the wetted perimeter of bed and Pw is the wetted perimeter of both walls. The results show that the bed and bank shear stresses are function of the ratio Pb/Pw, and can be fitted by a simple exponential equation.

Table 3.4. Summary of empirical formulae for shear stress on bed and wall.

Researchers	Formula	Observations
Knight (1981)	$\beta = e^{\alpha}[tanh\lambda - 0{,}5(tanh\pi\lambda - \lambda)^2]$ $\alpha = -3{,}264log\left(\frac{B}{h} + 3\right) + 6{,}211$ $\lambda = 1 - \frac{1}{5}log\left(\frac{K_{sb}}{K_{sw}}\right)$ $\frac{\tau_{wall}}{\gamma hS} = \beta\left(\frac{B}{2h}\right)$ $\frac{\tau_{bed}}{\gamma hS} = 1 - \beta$	Rectangular open channels $1{,}5 < B/h < 15$
Flintham & Carling (1988)	$log\beta = -1{,}4026log\left(\frac{P_{bed}}{P_{bank}} + 1{,}5\right) + 0{,}247$ $\frac{\tau_{bank}}{\gamma Y_0 S} = \beta\left[\frac{(W + P_{bed})sen\theta}{4Y_0}\right]$ $\frac{\tau_{bed}}{\gamma Y_0 S} = (1 - \beta)\left[\frac{W}{2P_{bed}} + 0{,}5\right]$	Trapezoidal channels
Knight & Patel (1985)	$\beta = e^{\alpha}$ $\alpha = -3{,}253log\left(\frac{2B}{h} + 3\right) + 1{,}584$ $\frac{\tau_{wall}}{\gamma hS} = \beta\left(\frac{B}{h}\right)$ $\frac{\tau_{bed}}{\gamma hS} = 1 - \beta$	Measurements in wind tunnel $0{,}1 < B/h < 10$
Rhodes and Knight (1994)	$\beta = \frac{1}{1 + \left(\frac{1 + 1{,}345x}{1 + 1{,}345/x}\right)^{-1{,}057}}$ $x = B/h$ $\frac{\tau_{wall}}{\gamma hS} = \beta\left(\frac{B}{h}\right)$ $\frac{\tau_{bed}}{\gamma hS} = 1 - \beta$	Smooth straight rectangular ducts (wind tunnel) $0 < B/h < \infty$

Direct shear stress measurement in field is a great challenge due to complex topography and velocity fluctuations that requires long time measurements. Whiting and Dietrich (1990) proposed an indirect method that combines field measurement and some pre-established equations. Their methodology consists of measuring the near-bed flow velocity at a known height close to the bed surface, and simultaneously the sediment transport is measured at the same place. Then, applying a sediment transport formula the shear stress is estimated. Applying the law of the wall they were also able to calculate the roughness height and relate it to a characteristic diameter.

More recently, Lisle et al (2000) applied a similar methodology. They used a quasi-three-dimensional flow model to estimate the bed shear stress. The model was previously solved and the calculated mean-depth-velocity distribution was compared against field data. Finally, Sime et al (2007) proposed a technique to estimate shear stress from a moving boat with an Acoustic-Doppler-Velocimeter. The method uses the vertically averaged velocity and a fixed roughness height and seems to give good results.

3.6.4 Comparison of different methods

The Lundgren and Jonsson's (1964) area method, the Shiono and Knight's (1990) depth average method and the empirical Flintham and Carling's (1988) formula will be compared. For the first comparison a trapezoidal channel has been selected with velocity and shear stress distribution measured in laboratory (Abril and Knight, 2004). The channel has a bottom with of 1,50m, and bank angle equal to 45°. Table 3.5 presents other geometric parameters. The researchers employed varying parameters (f and λ) over the bank. However, for this comparison, constant values have been adopted. Figure 3.6 presents the results for the velocity and shear distribution. Considering constant parameters, results are in good correspondence with the Abril and Knight's solution, especially in the channel region, while in the bank region there is some difference. However, the overall comparison against measurements is very good. With regards to Flintham and Carling's formula, it is observed an underestimation at the channel centre (-8%), and a lower underestimation if mean value is considered (-4%). In the bank region the empirical formula gives similar results with the shear near the toe of the bank.

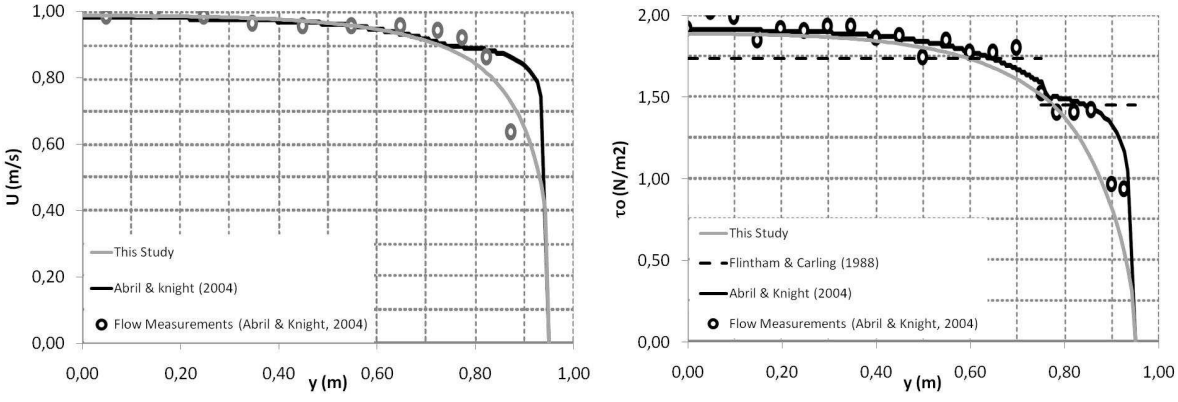

Figure 3.6. Comparison between laboratory data and different analytical methods and empirical formulas.

For the second comparison a hypothetical gravel bed river is proposed. Lundgren's and Knight`s model requires a smooth profile, so the exponential profile suggested by Diplas (1990) is considered. On the other hand, the Flintham and Carling's formula applies to trapezoidal channels. In this case an

equivalent trapezoidal channel has been calculated considering equal area and wetted perimeter (and therefore equal hydraulic radius). This equivalent trapezoidal channel has a bottom with of 47,4 m bank slope 2,46 H : 1 V, longitudinal slope 0,25% and depth of 2,56 m (see figure 3.7). Table 3.5 presents a compilation of calibrated parameters (Γ, λ, and f) obtained from laboratory conditions and natural channels. For this comparison, the following values have been chosen: $\Gamma/\gamma HS = 0,05$ and $\lambda = 0,07$ in the whole section, and f = 0,0421, evaluated with the Keulegan's equation with $k_s = 0,10$ m.

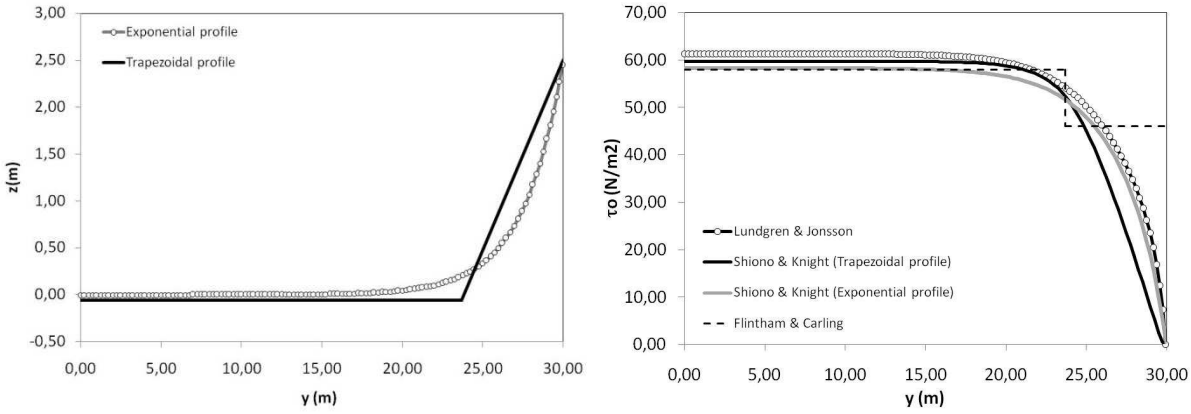

Figure 3.7. Right, the exponential and trapezoidal cross-section used for the comparative analysis. Left, results from the application of different analytical methods and empirical formula.

For the exponential profile, both analytical method give similar results in the bank region (see figure 3.7) but the shear stress calculated with the Shiono-Knight model are lower in the channel region, due to secondary flow effects. For the trapezoidal profile, there is a notable variation in the bank region because of the change in geometry. The empirical formula gives similar results for the main channel region but higher values with regards to the mean values from analytical models in the bank region.

Furthermore, it is observed that the shear stress at the channel centre is 14% higher than the shear stress at the lower end of the bank (y = 23,7m). This is in good agreement with field observation that hint that at bankfull stage the channel shear stress is approximately 20% above the critical reference value, while in the bank has attained the critical value.

Table 3.5. Hydraulic parameters calibrated in laboratory channels and natural mountain streams.

Case	H	S	W	$\Gamma_c/\gamma HS$	$\Gamma_s/\gamma HS$	λ_c	λ_s	f or n	Reference
Inbank flow Lab. channel	0,2m	0,103%	1,9m	0.057	-0.079	0.07	0.07	f=0.0153	Abril & Knight (2004)
Two Stage flow. Lab. channel	H=0.2m Hf=0.05m	0.103%	1.9m	0.15	0	0.07	0.16	f=0.016	Shiono & Knight (1990)
Tomebamba River	R=0,91m	1,76%	26m	0.05	--	0.07	--	n=0.103	Abril & Knight (2004)
Cuenca River	R=1,52m	1,5%	40m	0.05	---	0.07	--	n=0.07	Abril & Knight (2004)

Reference: H is the maximum depth, and Hf the flood plain depth, Γ_c and Γ_s are the secondary flow for gradients in the main channel and over de bank slope, respectively; λ_c and λ_s are the depth-averaged eddy viscosity for the main channel and the bank slope.

3.7 Modeling 2D open channel flow

2-D models are the result of integrating Reynolds's equations over the flow depth. The exposition of 2D-depth averaged models is based on Bernard's (1993) STREMR model which will be adapted later for modeling gravel bed rivers (see chapters 9 and 10).

Let's consider a three-dimensional quantity ϕ; its depth-average value Φ is defined by:

$$\Phi = \frac{1}{h}\int_0^h \phi \, dh \tag{3.63}$$

Wherein h is the flow depth. Applying this rule to the continuity equation, its 2-D depth-integrated is as follows (for a complete derivation see Wu, 2007):

$$\frac{\partial z_{ws}}{\partial t} + \frac{\partial (hU)}{\partial x} + \frac{\partial (hV)}{\partial y} = 0 \tag{3.64}$$

Where U and V are the depth-average quantities of local velocities u and v. When a fixed water surface is imposed, as in the original Bernard's (1993) model, the time derivative is null, and the continuity equations serves as a constrain: the divergence of the water flux must be zero.

The momentum equations are derived following a similar procedure. They can be written in the following form:

$$\frac{\partial U}{\partial t} + \mathrm{U}\frac{\partial U}{\partial x} + \mathrm{V}\frac{\partial U}{\partial y} = -\frac{1}{\rho}\frac{\partial P}{\partial x} + T_x - F_x + S_\mathrm{x} \tag{3.65}$$

$$\frac{\partial V}{\partial t} + \mathrm{U}\frac{\partial V}{\partial x} + \mathrm{V}\frac{\partial V}{\partial y} = -\frac{1}{\rho}\frac{\partial P}{\partial y} + T_y - F_y + S_\mathrm{y} \tag{3.66}$$

In a free surface flow the pressure gradient can be replaced by the water surface slope, assuming a linear pressure distribution ($\nabla P = \gamma \nabla z_{ws}$). T is the force due to viscous effects, F is the force due to bottom friction and S is the force due to secondary flow.

The friction force (per unit mass) is evaluated by the following expression:

$$F_x = Ch^{-1}\mathrm{U}|\mathbf{U}| \tag{3.67}$$

$$\mathrm{F}_y = Ch^{-1}\mathrm{V}|\mathbf{U}| \tag{3.68}$$

Where C is the bottom friction factor and $|\mathbf{U}|$ is the modulus of the depth-averaged velocity vector. Bernard (1993) approximates C with the Manning's equation. It can also be related to the roughness height using Keulegan equation. In this way friction forces depend on the degree of bed armouring.

$$C^{-2} = 2.5ln\left(11\frac{h}{k_s}\right) \tag{3.69}$$

Where α and n are coefficients, ks is the roughness height that is evaluated with the diameter D_{90}: ks = 2 D_{90}.

Viscous forces are the result of turbulent flow. Turbulence effect on mean flow is included by means of a viscous force T that is parameterized as follows:

$$T_{\mathrm{x}} = h^{-1}\nu_t \nabla \cdot (h\nabla \mathrm{U}) + 2\frac{\partial \nu_t}{\partial x}\frac{\partial U}{\partial x} + \frac{\partial \nu_t}{\partial y}\left(\frac{\partial U}{\partial y} + \frac{\partial V}{\partial x}\right) \quad 3.70$$

$$T_{\mathrm{y}} = h^{-1}\nu_t \nabla \cdot (h\nabla \mathrm{V}) + 2\frac{\partial \nu_t}{\partial y}\frac{\partial V}{\partial y} + \frac{\partial \nu_t}{\partial x}\left(\frac{\partial U}{\partial y} + \frac{\partial V}{\partial x}\right) \quad 3.71$$

Where in this case v_t represents the depth-averaged kinematic eddy viscosity

Finally, for depth-average models it is necessary to include a secondary flow force induced by channels change of direction. When streamlines are curved there is an acceleration of the depth-average flow that can be approximated by

$$S_x \approx \frac{1}{\rho}\frac{\mathrm{U}}{|\mathbf{U}|}\left[h^{-1}\mathbf{n} \cdot \nabla(h\tau_s) + 2\frac{\tau_s}{r}\right] \quad 3.72$$

$$S_{\mathrm{y}} \approx \frac{1}{\rho}\frac{\mathrm{V}}{|\mathbf{U}|}\left[h^{-1}\mathbf{n} \cdot \nabla(h\tau_s) + 2\frac{\tau_s}{r}\right] \quad 3.73$$

Where $\mathbf{n}$ is the unit vector normal to the velocity vector, τs is the secondary shear stress produced by helical flow and r is the local streamlines curvature radius.

$$r = \frac{|\mathbf{U}|^3}{\mathrm{UV}\left(\frac{\partial V}{\partial y} - \frac{\partial U}{\partial x}\right) + \mathrm{U}^2\frac{\partial V}{\partial x} - \mathrm{V}^2\frac{\partial U}{\partial y}} \quad 3.78$$

The depth-averaged shear stress produced by the secondary circulation is related to a vorticity-type variable, Ω.

$$\tau_s = \rho h \Omega \sqrt{C}|\mathbf{U}| \quad 3.80$$

The governing equation for Ω has the structure of a transport formula: Advection = Production – Dissipation + Diffusion, which will be presented later.

STREMR incorporates the standard k-ε model to evaluate the kinematic eddy viscosity. The depth-average eddy viscosity is defined in the same way as equation 3.10. Depth-average turbulence kinetic energy (k) and dissipation rate (ε) are calculated with transport equations that results from integrating equations 3.11 and 3.12 over the flow depth. Table 3.6 reports the production (P), dissipation (D), advection (A) and diffusion (D_f) terms to be use in the governing equations for k, ε and Ω. For a general variable F, the transport equation has the form:

$$\frac{\partial F}{\partial t} = P - D - A + Df \quad 3.81$$

This equation expresses the rate of change of the variable F due to: A, the convective transport owing to mean motion; D_f, the diffusive transport due to turbulent velocity and pressure fluctuations; P, the production term, in case of k means the transfer of kinetic energy from the mean flow to the turbulent motion and D, its dissipation, i.e., the transfer of kinetic energy into the internal energy of the fluid through viscous dissipation.

Table 3.6. Production, dissipation, advection and diffusion terms for the transport equations of k, ε and Ω

Term	k	ε	Ω
Production	$\nu_t\,\Gamma$	$\frac{C_{\varepsilon 1}\nu_t}{k}\,\Gamma$	$\frac{A_s C^{1/2}\lvert\mathbf{U}\rvert^2}{rh\left(1+9\,{h^2}/{r^2}\right)}$
Dissipation	ε	$C_{\varepsilon 2}\frac{\varepsilon^2}{k}$	$\frac{D_s C^{1/2}\Omega\lvert\mathbf{U}\rvert}{h}$
Advection	$\mathrm{U}_j\frac{\partial k}{\partial x_j}$	$\mathrm{U}_j\frac{\partial \varepsilon}{\partial x_j}$	$\mathrm{U}_j\frac{\partial \Omega}{\partial x_j}$
Diffusion	$\sigma_k^{-1}\left[\frac{\nu_t}{h}\nabla(h\nabla \mathrm{k})+\nabla\nu_t\cdot\nabla \mathrm{k}\right]$	$\sigma_\varepsilon^{-1}\left[\frac{\nu_t}{h}\nabla(h\nabla\varepsilon)+\nabla\nu_t\cdot\nabla\varepsilon\right]$	$\frac{\nu_t}{h}\nabla(h\nabla\Omega)+\nabla\nu_t\cdot\nabla\Omega$

In table 3.6 the production term is defined with

$$\Gamma = 2\left[\left(\frac{\partial \bar{u}}{\partial x}\right)^2+\left(\frac{\partial \bar{v}}{\partial y}\right)^2\right]+\left(\frac{\partial \bar{u}}{\partial y}+\frac{\partial \bar{v}}{\partial x}\right)^2 \qquad 3.82$$

and As and Ds are empirical coefficients. The standard k-ε model provides the coefficients that appear in table 3.6.

In the vicinity of sidewalls the gradient in turbulence and mean flow velocity is large. This situation requires an adjustment of the model. Considering only the case of turbulent flow, Bernard (2003) proposed a resisting shear stress related with the tangential velocity u_B:

$$\tau_B \approx \frac{C_D\nu_t(\delta)u_B(\delta)}{7\delta} \qquad 3.83$$

Where C_D is a drag coefficient, δ the distance normal to the wall.

Bernard (1993) presented a comparison of laboratory measurements and model predictions for a double bendway trapezoidal channel. He compared the depth-average velocity finding a very good agreement. The model has been applied to natural meandering rivers, as well. Rodriguez et al (2004) compared the results from STREMR and a full 3D model when applied to the Embarras River, a highly sinuous small river flowing along a low-relief landscape in Illinois (U.S.A.). They concluded that STREMR accurately predicted the main characteristics of the measured velocity field. In these cases the secondary flow correction was important because it redistributed the momentum in the transversal direction. More recently, Abad et al. (2008) also applied STREMR to meandering rivers but they extended the model to perform sedimentological simulations (STREMR HySed). They showed that the correction due to secondary flow was capable of capturing the location of erosion and deposition areas.

As the reader may have noted, all these examples refer to meandering rivers where it is expected an important role of the secondary circulation. But gravel bed rivers have low sinuosity and therefore it poses the question if it is also necessary a sophisticated model. Lane and Richards (1998) studied in details the flow properties in a small braided stream in a proglacial area of Switzerland. They performed a detailed topographic survey, velocity measurements and also studied the surface grain size distribution. Then, they evaluated the performance of STREMR by activating and deactivating the corrections due to turbulence k-ε model and the secondary flow. They arrived to the interesting conclusion that the secondary circulation correction had little effect upon velocity predictions. The same followed for the turbulence model. But in this case it doesn`t mean that turbulence is not important in the momentum transfer process, instead it suggest a lack of the model to represent actual processes. Furthermore, Lane and Richards underlined the importance of roughness specification as a source of error for velocity prediction. So, it was more important to improve the roughness characterization than the refinement of turbulence models. Finally, the effect of sidewall correction was small. It can be explain by the fact that gravel bed rivers have gentle bank slopes.

With regards to viscous forces, although they may not play a crucial role in describing physics they are important for maintaining numerical stability. In principle, the MacCormack scheme, a numerical method used in STREMR for solving the momentum equation, is unconditionally stable for appropriately small time-steps; but in practice, it usually requires some viscosity to remain stable (Bernard, 2010).

To sum up, friction forces are important and they will be related to the surface roughness; viscous forces will be kept in order to assure numerical stability; sidewall effects and secondary forces will be disregarded because they have a minor role in shallow and nearly straight channels.

In 2D models shear stress due to bottom roughness appears explicitly as a friction force (named F in 3.65). Usually the friction force is related to the square of the velocity, like in Chezy's equation (see eq. 3.20). Multiplying the force per unit mass (F) by the depth and water density gives the bottom shear stress. The direction of the shear stress are assumed equal to the main flow direction if secondary currents are negligible.

$$\tau_x = \rho C \mathrm{U} |\mathbf{U}| \qquad 3.84$$

$$\tau_y = \rho C \mathrm{V} |\mathbf{U}| \qquad 3.85$$

Where the friction factor C is evaluated using equation 3.69 or any of the expressions in equation 3.24.

4 THE FLOW OF SEDIMENTS

The aim of this chapter is to show the complexity of gravel bed rivers inherent to sedimentological structures and sediment flow, and the difficulty to model sediment processes. The armour layer is described first as the paradigm of bed structure in gravel bed rivers. Attention is paid on the research conducted to explain its origin, regulation function in bed load transport and field evidence of its persistence during flood events. After, that attention relays on grain organization and its consequences for the entrainment of particle. Following these qualitative sections there is an exposition of governing equations for bed evolution and surface grain size distribution. Finally, recent sediment transport models for gravel mixtures are reviewed, focusing in surface-based models.

4.1 Bed structure and the armour layer

Gravel-bed rivers have a particular feature that distinguishes them from sand-bed rivers: a bed surface that is coarser than the sub-surface and the material transported during floods. This coarse surface layer is often called the "armour layer". This phenomenon is related to the presence of mixture of sand, gravel and cobbles in bed transport, also the nature of hydrograph and especially to the intensity of shear stress. In fact, some gravel bed streams show a lack of an armour layer, that is the case of ephemeral streams subject to flash floods (Powell et al., 2001; Hassan et al., 2006).

The bed surface can exhibit three situations: a static armour layer, a mobile armour layer and the absences of armour layer. The static armour layer has been observed downstream of dams as a result of a deficit in sediment supply and the removal of the fine fractions. The mobile armour is present when there is sediment supply and can be analyzed as a general case between two extremes: the static armour and the absence of armour, as will be shown later. The presence of a mobile armour layer was first explained by Parker and Klingeman (1982). Gravel bed rivers transport mixtures composed by sand and gravel. If the reach is at grade the coarser fraction must be transported at the same rate that the finer fraction. Because coarse grains are intrinsically less mobile than the finer grains and in order to achieve equal transport of all sizes there must be an overpresence of coarse material on the bed surface.

The existence of this coarser layer was first reproduced in laboratory by Parker et al. (1982b). They demonstrated that the formation of an armour layer can coexist with the motion of all available grain sizes, because motion is sporadic. They modeled typical field transport during floods and concluded that particles in the subpavement were only occasionally disturbed. Parker et al. (1982b) experiment suggests that it is possible the coexistence of a mobile layer and its persistence during floods that are capable of moving all grain sizes. Subsequently, a great effort was afforded to demonstrate it with field measurements. Andrews and Erman (1986) provided such first evidence. They studied the Sagehem Creek, a small gravel-bed stream in the Sierra Nevada, California (bankfull discharge of $2m^3/s$). They performed measurement of bed load transport with a Helley-Smith bed load sampler, and 150 painted rocks were placed on a riffle in order to observe the persistence of vertical sorting in the bed material. They also measured the surface bed material (pebble count) during low flow and at high flow. Analyzing all this information they concluded that the coarse layer was present during small discharges and

remained unchanged during very large discharges. Besides, only few particles were entrained at any instant by even the peak flood flows.

A much direct evidence of persistence of the armour layer has been recently presented by Clayton and Pitlick (2008). They studied the Colorado River in the Rocky Mountain National Park, an alluvial meandering stream with bed material composed of gravel and coarse sand. The drainage area above the study reach wa 150 km^2 and the mean annual flood was 16,1 m^3/s. In 2002 the authors performed detailed topographic and granulometric surveys: 15 cross-sections, surface sediment samples (pebble count) and subsurface sediment samples (bulk samples). In 2003 there was an intensive flood and the river avulsed upstream of the study reach abandoning it nearly at the peak discharge. This left the bed texture essentially as it was at the peak of the flow and allowed them to re-survey it soon after the event. They could verify that the coarse bed surface texture persisted despite shear stress was above the critical entrainment value.

Another kind of approach followed by researchers to verify the formation and persistence of the mobile armour layer considers the use of sediment transport formulas and numeric methods. Wilcock and DeTemple (2005) considered the bed load sediment transport data from the Oak Creek (Milhous, 1973) and Goodwin Creek (Kuhnle, 1992). For both cases available data consisted on: surface and subsurface grain size distributions, and bed load transport with its grain size distribution for each event. Wilcock and DeTemple applied the Wilcock and Crowe (2003) sediment transport formula based on surface grain size. Using sediment transport data they could back-calculate the surface grain size necessary to produce the same sediment transport rate and grain size distribution. They found a remarkable coincidence between measured at-low-flow and calculated surface grain size distribution for the Oak Creek at high water stage. It was remarkable because different floods were considered and besides, the Oak Creek data had not been used in developing the transport model. Instead, for the Goodwin Creek the predicted surface grain size was somewhat coarser than the observed one. However, the researchers could prove that the surface grain size persisted over all transport rates observed for both streams and suggested that low-flow armour layers persist over typical floods.

Parker et al. (2008) investigated the characteristics of the armour layer using a 1D model. The model simulated the condition in flumes with constant feed (bedload feed rate and grain size distribution of the feed material). The discharge was changed to produce a series of repeated cyclic hydrographs. As a result of the simulations, they found that at the upstream part of the flume there was a cyclic change in bed elevation following the hydrograph, but the remarkable result appeared in the downstream part. Over the great majority of the reach the bed elevation and surface size distribution became invariant in time. However, the bed transport rate and size distribution changed according to the hydrograph. Higher flows transported larger quantities of coarser material, and lower flows transported finer material. Therefore, the implications for gravel bed rivers were that they responded to changes in discharges by modifying the bed load transport while minimizing the response of the bed. This conclusion was also supported by a laboratory experiment performed by Wong and Parker (2006).

There are two main variables that govern the development of an armour layer: hydrograph shape and sediment supply. Dietrich et al. (1989) related the armour degree with the sediment supply. They proposed that surface coarsening occurs primarily where there is a transport supply imbalance. A deficit in sediment supply will produce a coarser layer. More recently, Hassan et al. (2006) studied this relationship and considered also various hydrograph shapes. They performed a set of flume experiments

over a range of hydrograph shapes under conditions of sediment starvation. Their results support the observations of Dietrich and collaborator's (1989) that the sediment supply dominates the development of bed armouring, and besides, hydrographs shape has a secondary role. With regards to this last point, they observed that most of the sediment sorting occurred during the falling limb of the hydrograph. During constant hydrographs, representing snow melt conditions, the bed developed a well-armoured surface; short asymmetrical hydrograph, representing conditions of flash flood in semiarid regions, did not result in substantial vertical sorting; and when symmetrical hydrograph were imposed the degree of sorting depended on the duration of the hydrograph.

As has just been noted, if the bed load characteristics are known it is possible to evaluate the granulometric characteristics of the surface layer. Parker and Sutherland (1990) presented a method to predict the armour grain size distribution. In their original publication they used the Oak Creek model, based on Parker's (1990) bed load transport formula, and the Canterbury model that uses the Paintal's (1971) transport relation. Most sediment transport relations can be written in this way:

$$\frac{R_s g q_i}{F_i u_*^3} = G\left(\tau_g^*; D_i\right) \tag{4.1}$$

Were R_s denotes the relative specific weight of sediments, q_i is the volumetric bed load of the i-th size fraction that in the surface layer has a frequency F_i, u^* is the shear velocity, τ_g^* is the dimensionless shear stress referred to some characteristic parameter of the surface (in this case, "g" denotes the geometric mean), and D_i is the mean grain diameter for the i-th size fraction.

From the fractional bed load q_i, the total bed load and its grain size distribution (f_{bi}) can be derived[9]:

$$q_T = \sum q_i \tag{4.2}$$

$$f_{bi} = \frac{q_i}{q_T} \tag{4.3}$$

With these expressions, it is possible to solve eq. 4.1 for F_i:

$$F_i = \frac{f_{bi}/G\left(\tau_{sg}^*;D_i\right)}{\sum f_{bi}/G\left(\tau_{sg}^*;D_i\right)} \tag{4.4}$$

This is the general equation that enables the calculus of the surface grain size distribution if the bed load grain size distribution and the shear stress intensity are known. Completes the solution the use of an appropriate bed load transport equation. The equation can be used to predict any of the three situations aforementioned: static armour, the mobile armour and no armour. The mobile armour is the general state while the other two are extreme situations. The static armour occurs when the sediment transport is reduced (low sediment supply), so its grain size distribution (F_{ai}) can be calculated as the limit of q_T towards zero:

$$F_{ai} = \lim_{q_T \to 0} F_i \tag{4.5}$$

[9] For the sake of simplicity the extremes in the sums have been omitted, however, it is easy to see that the sums are made over the entire grain size distribution, i.e., considering N factions, i = 1 … N.

Appling the Parker´s (1990) transport model, Parker and Sutherland (1990) solved the limit and obtained a simple result:

$$F_{sai} = \frac{f_{bi} D_i^{1,35}}{\sum f_{bi} D_i^{1,35}} \tag{4.6}$$

On the other hand, when a very high sediment transport is considered the surfaces grain size distribution tends to the bed load grain size distribution.

$$\lim_{q_T \to \infty} F_i = f_{bi} \tag{4.7}$$

In order to illustrate these situations I selected the Epuyén River, in Patagonia Argentina, a gravel bed river with a riffle-pool morphology. For this river there is sediment data on surface and subsurface material (see Chapter 7). At the selected reach, the bed presents a coarse layer with a median diameter of 43 mm while the substrate is finer with a median diameter of 23 mm, so the degree of armouring is 1,97 (ratio of surface and subsurface median diameter). The subsurface size distribution was determined by a bulk sample while for the surface material the pebble count method was applied. Figure 4.1 shows that in the subsurface material there is an absence of coarse fractions, situation that will condition the calculus for these fractions. I considered the gravel fraction (D ≥ 2mm) and assumed that the grain size distribution of the bed load was equal to the substrate for all the discharges. In addition, the Parker's (1990) bed load equation was applied to calculate the surface size distribution.

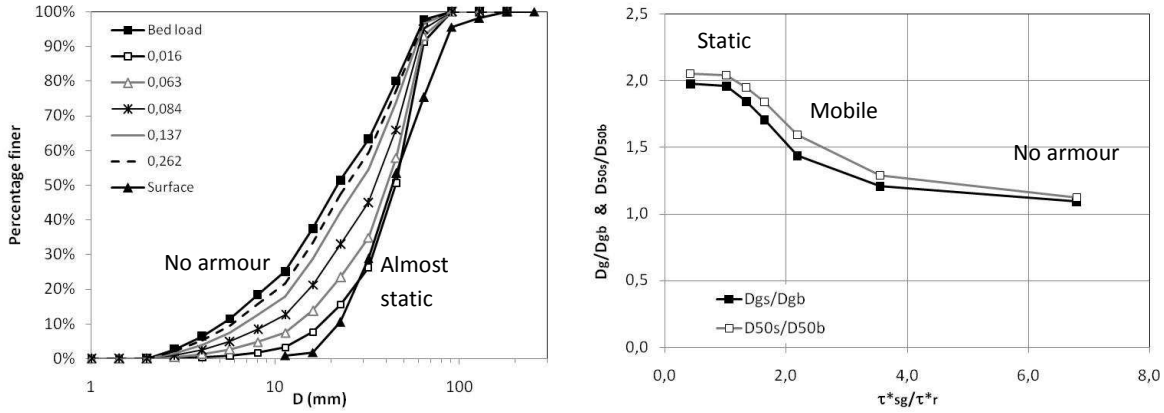

Figure 4.1. Variation of the surface grain size distribution with different shear stress intensities. Left: granulometric curves for different dimensionless bed shear stresses (τ_g^*). Right: variation of the median and geometric mean diameter for different shear stress ratio (the reference value is 0,0386).

There is a tendency for coarsening of the surface when the shear stress is low (low sediment supply). The observed armour degree (1.97) is reached for a dimensionless shear stress (τ^*_{50}) of 0,041. For very high sediment transports the armour layer tends to vanish and the degree of armouring approaches unity. The median diameter for the static armour evaluated with the Parker and Sutherland (1990) expression is 45mm, almost the same to the actual surface median diameter. Therefore, for the Epuyen River, it can be said that the surface has developed a static armour. In fact, this shear stress corresponds to a 5 years-period-return flood. A biannual flood produces a lower shear stress of 0,035. This can be explained considering that the study reach is not far downstream from Epuyén Lake, where it begins, and that in the mean way it receives sediment from only one tributary.

Several researchers have observed that gravel bed rivers in low to medium gradient ($S \leq 0{,}004$) present bankfull reach-averaged shield number (τ^*_{50}) in the order of 0,049-0,060 (Parker, 2007; Andrews, 1983; Andrews and Erman, 1986; Mueller et al., 2005). On the other hand, sand-bed rivers that clearly do not have an armour layer, show Shields number near 1.86. High values can also be attained in gravel bed rivers, especially in ephemeral streams with flash floods. Reid el al. (1995) studied the sediment transport of Nahal Yatir, an ephemeral stream in Israel (basin area of 18 km^2). The channel had a width of 3,5 m, a slope of 0,0088 and a depth of 0,90 m. The stream does not present an armour layer and the median size was 10mm. With this data the maximum Shields number is 0,30, and according to the previous calculus, the degree of armouring would be nearly 1.

Finally, it is worth to mention a recent laboratory experience directed by Luca Mao. The aim of Mao and collaborators' (2011) experiments was to compare the characteristics of mobile and static amour developed under controlled conditions. In order to develop a static armour a sediment starving (zero sediment feeding) condition was imposed, while the mobile armour was achieved by recirculating sediments. They used a 8 m long and 0,30 m wide titling flume. A sediment mixture composed the bed, with the following characteristics: 20% sand, 80 % gravel, and D_{50} = 6.2 mm. The armour layer was created under several discharges, in the range of 13,2 to 25,6 l/s. As a result they observed that in the case of zero sediment feeding highly structured and imbricate armour developed. On the other hand, mobile armour exhibited a poorer degree of organization. The static armour was coarser than the mobile armour. Besides, the mobile armour was insensitive to the imposed discharge while the static armour was coarser for higher discharges.

4.2 Sediment transport and sedimentological variability

The previous section has shown one of the most important structures of gravel bed rivers, i.e., the armour layer. There are other sedimentological features that influence sediment transport: patches, bed structure of grain organization. These topics will be discussed firstly and consequences for modeling will be shown later.

Non-uniformity of the sediment flux may be attributed to spatial distribution of grain size. Paola and Seal (1995) studied the special case of patches. A patch (also known as facie or textural unit) is a homogeneous streambed area with no systematic spatial variation of bed material size (Bunte and Abt, 2001). The variation in mean size is referred as "patchiness". Paola and Seal (1995) proposed a statistical model for taking account of the spatial variability of grain size distribution and shear stress, and found a notable enhancement of downstream fining in the North Fork Toutle River, a gravel bed river in Washington. They suggested that patchiness was a natural consequence of a tendency for equal mobility to break down for very poorly sorted and/or bimodal sediments and that the patches developed because local deviations from equal mobility tended to sort the sediment until a configuration that satisfied equal mobility locally.

The local critical shear stress can be modified by the presence of patches modifies or also by bed structures. A bed structure is an arrangement of grains in the channel bed which may influence the propensity of individual grains to be entrained by the flow (Church, 2006). Four kinds of arrangements are recognized (see figure 4.3).

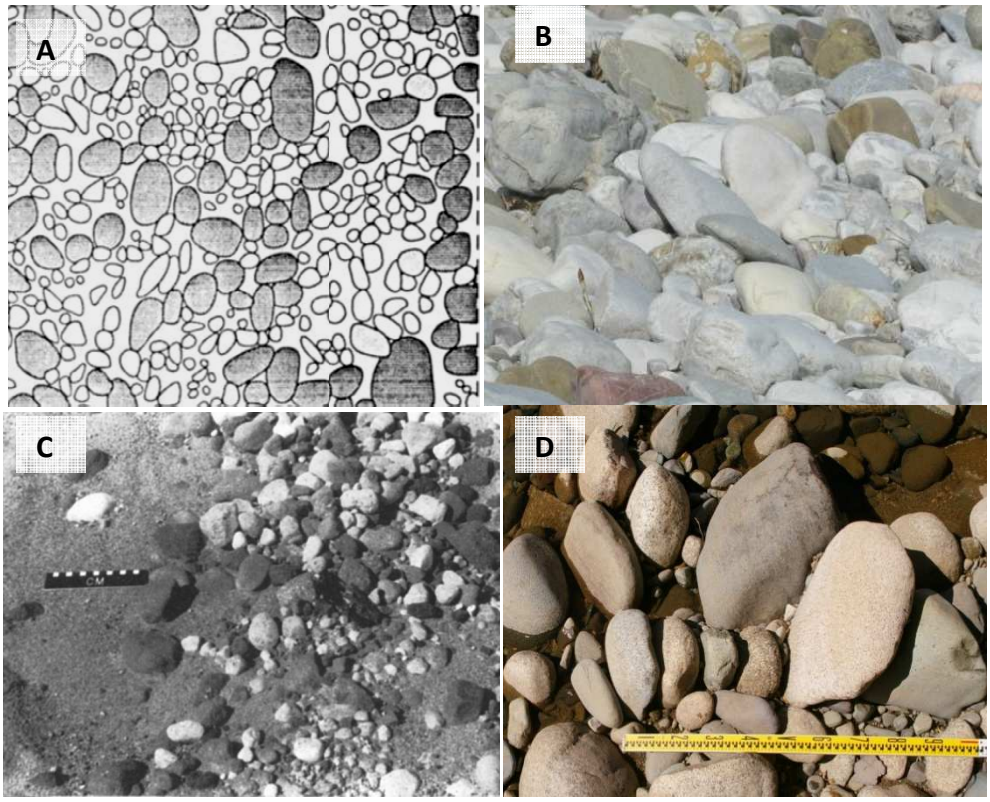

Figure 4.3. Examples of bed structures and variability: A) Grain net developed in laboratory test (Church et al., 1998); B) Grain imbrication in Piave River, Italy (photo courtesy Luca Mao); C) Grain size patches in North Fork Toutle River (Paola and Seal, 1995); D) Grain clusters on a lateral bar in Alto Chubut River, Patagonia (flow is from left to right).

- ✓ **Grain packing:** the arrangement of particle position with respect to each other which is influenced by shape and size of individual grains.
- ✓ **Grain imbrications:** consists on the overlapping of the downstream nearest particle that discourages its mobilization. It involves particles of similar size. When imbrications are along the b-axis, denotes a relatively low transport rate.
- ✓ **Grain cluster:** it is the accumulation of relatively large grains into compact groups upstream of a bigger particle.
- ✓ **Grain nets:** consist of an extension of clusters into irregular lines of cells-like arrangements.

In any of this ways the bed is able to resist higher shear stresses because the presence of a structure decreases particle mobility. Church et al. (1998) performed field observation and laboratory experiments and identified the development of reticulate stone cells in cobble-gravel streams. They demonstrated that these structures promoted streambed stability by dramatically reducing the sediment transport. Finally, for highly structured surfaces they measured an increase of 400% in critical Shields number (based on the transported material data).

Bed sorting is tightly related to bed forms in riffle-pool sequences. Field observations indicate that riffles surfaces are coarser and more structured than pool sectors (Sear, 1996). Riffles are subject to turbulent

flow during low-magnitude flow conditions that enhance grain structure through particle vibration. This difference in structure makes riffles more stable and contributes to the persistence of these units as topographical high points. On the other hand, pools have finer and looser material, with scarce stricter and hence lower threshold for initiation of motion. As a result of these sedimentological differences, Sear (1996) shows that sediment transport increases in pools more rapidly than in riffles when discharge increases and hence riffles can be characterized by net aggradation during near-bankfull flow conditions.

Table 4.1. Summary of sedimentological features of riffle and pools (after Sear, 1996)

Bedform	**Riffle**	**Mid-pool**	**Pool-tail**
Bed state	Congested	Smoothing	Smoothing
Sedimentary structure of surface	Tightly packed	Loosely packed	Loosely packed
Surface material	Coarser	Decreasing	Finer
Entrainment threshold	High	Decreasing	Low
Bedload balance	Aggrading	Degrading	Degrading

Sediment transport reveals hysteric effects due to the change in sediment supply and bed structure. A recent research carried on a flume laboratory has shed light on this topic. Mao (2012) has measured the sediment transport and bed structure with laser scanner so as to see the effect of different hydrographs. The results indicate that sediment transport during the falling limb is lower than during the rising limb; the surface grain size of the bed remains constant throughout the hydrographs but the grain size of transported sediment exhibit a counterclockwise hysteresis; bed is restructured during the falling limb.

Sediment transport is a complex process that results from the interaction of complex turbulent flow and also complex interactions between particles. There are many parameters that are involved. Recently Chen and Stone (2008) studied the uncertainty in predicting sediment transport using Wilcock-Crowe model, due to variations in mean grain size distributions. Wilcock and Crowe (2003) derived a surface-base sediment transport model using flume measurements. The key aspect is that they related sediment rates to global surface grain size distributions in the flume. Chen and Stone wondered if part of bedload variability could be explained by an actual variable surface material. In order to answer this question a Monte Carlo approach was used to simulate grain size distribution variability and uncertainties for each sediment transport prediction was assessed. They concluded that global grain size distributions are not adequate for predicting the fractional bedload transport rate; fractional transport rates can have significant uncertainty while total rates have much less uncertainty.

4.3 Modeling bed and sediment transport interactions

There are two approaches for modeling sediment transport and its interaction with bed properties (elevation and surface grain size distribution). The simplest approach assumes a state of local equilibrium in sediment transport. This is the case of flume experiments where bed load are correlated against flow parameters when bed load has attained a constant value, or the grain size is almost constant (Wilcock et al., 2001). The second approach recognizes that steady states are not achieved in natural streams. This approach is known as non-equilibrium (or unsaturated) sediment transport models.

Let us consider first the equilibrium sediment transport model. As aforementioned this approach assumes that local sediment transport has attained a condition of equilibrium. The Exner equation that relates changes in sediment transport with temporal variation of bed elevation is expressed in the following way:

$$\left(1-\lambda_p\right)\frac{\partial z_b}{\partial t} = -\sum \nabla \cdot \mathbf{q}_k \tag{4.8}$$

Where λ_p Is the material porosity, z_b is the bed elevation and $\mathbf{q}_k$ is the sediment transport vector for the k-th grain size class. In case of equilibrium $\mathbf{q}_k$ is evaluated with a sediment transport model (see next section), i.e., it depends only on flow properties (shear stress and flow direction) and bed properties (grain size distribution). The sum on the right side indicates that the divergences must be evaluated for all the grain size classes.

The second approach assumes that there is a temporal and spatial lag between flow variation and sediment transport adjustment. Bed change is evaluated considering a bed-load exchange model (Wu, 2007):

$$\left(1-\lambda_p\right)\frac{\partial z_b}{\partial t} = \frac{1}{L}\sum(q_k - q_k^*) \tag{4.9}$$

wherein q_k and q_k^* are the actual and equilibrium sediment transport rates of the k-th grain size class of bed load, respectively; and L is the adaptation length. Note that in this case an extra variable is introduced, this is the actual transport rate and an extra relationship is required (see Wu, 2007 for details):

$$\frac{\partial}{\partial t}\left(\frac{q_k}{u_{bk}}\right) + \frac{\partial(\alpha_x q_k)}{\partial x} + \frac{\partial(\alpha_y q_k)}{\partial y} = \frac{1}{L}(q_k - q_k^*) \tag{4.10}$$

In which u_{bk} is the bed-load velocity, and α_x and α_y are the direction cosines of bed-load movement. The length scale for sediment transport may be related to the length scale of the dominant bed form (Wu, 2004). In the case of gravel bed rivers with alternate bars this length is between five to seven times the channel width (see Hey and Thorne, 1982).

The above two approaches serve to define the temporal evolution of the bed elevation. With regards to the surface grain size distribution the active layer concept has been invocated. This model was first proposed by Hirano (1971) and then extended for gravel bed rivers by Parker and Southerland (1990). It recognizes that bed fluctuates during sediment transport. Moreover, fluctuation in sediment transport is linked to fluctuation in bed elevation. Surfer particles have a higher probability of entrainment into motion than buried material. The simplest model defines a surface layer with equal entrainment probability, the so called active layer, and a sublayer with zero probability. The mass balance is used to analyze interaction between sediment transport, active layer and sublayer. For an equilibrium model the expression is as follows:

$$\frac{\partial(L_a F_k)}{\partial t} = \frac{-\nabla\cdot\mathbf{q}_k}{(1-\lambda_p)} + f_{Ik}\left(\frac{\partial L_a}{\partial t} - \frac{\partial z_b}{\partial t}\right) \tag{4.11}$$

Wherein L_a is the height of the active layer, F_k and f_{Ik} are the surface and interface exchange grain size fractions, respectively. On the left side there is the temporal change of k^{th} size class material contained in the mixing layer, while on the right side, the first term is the exchange between moving sediment and

mixing layer and the last term is the exchange between the active and sublayer due to a change in bed elevation. When a non-equilibrium sediment model is employed, the term relative to the bed load interaction has to be changed:

$$\frac{\partial(L_a F_k)}{\partial t} = \frac{q_k - q_k^*}{(1-\lambda_p)L} + f_{Ik}\left(\frac{\partial L_a}{\partial t} - \frac{\partial z_b}{\partial t}\right) \quad 4.12$$

The active layer has a height of the same order that the largest particles: $L_a = nD_x$. Usually, n has been chosen as n = 2 and $D_x = D_{90}$. The interface grain size distribution f_{Ik} depends on whether the bed is degrading or aggrading. When the bed degrades it is evident that it is equal to the substrate grain size distribution. The problem arises when bed aggrades. In this case researchers have adopted a mixture between the bed load and the active layer material.

$$f_{Ik} = \begin{cases} f_{ssk} & when\ bed\ degrades \\ \alpha F_k + (1-\alpha) f_{bk} & when\ bed\ aggrades \end{cases} \quad 4.13$$

where f_{ssk} is the substrate kth grain size fraction. There is not a unique value for α and instead, as it varies α between 0 and 1, it is possible to make the exchange material been any proportion of mixing layer and bed load materials. For instance, Parker et al. (2006) adopted α = 0.5, while Wu (2004) adopts α = 1, that is, the exchange material is equal to the mixing layer material.

4.4 Sediment transport formulae

This section presents the latest bedload formulas that have been proposed by several researches analyzing field and flume data. There is not a general agreement regarding the formula structure, nor the basic physical phenomenon modeled. Some researchers consider that the instantaneous bed load depends directly on the surface material characteristics, such as Parker (1990), Wilcock and Crowe (2003), Hunziker and Jaeggi (2002), and Powell et al. (2003). Others, considers the subsurface material, like the classical Meyer-Peter and Müller bedload formula recently re-evaluated by Wong and Parker (2003). Another approach is considering bulk transport rather than fraction transport. Two new formulas have been presented recently by Barry et al. (2004, 2007) and Bathurst (2007). Both cases consider the degree of armouring.

Parker's (1990) model.

In 1990 Parker presented a new bedload transport equation reanalyzing the Oak Creek sediment transport data. Previously, he with Klingemann and McLean had derived a substrate-based relation (Parker et al., 1982a). In this case, the substrate-base relation was modified to consider exclusively the surface material properties, which is actually directly affected by flow and participates in the transport process. In both cases, the relations were derived from field data (Milhous, 1973). Milhous measured the sediment transport in Oak Creek, a small creek in Oregon, USA, with a width of 3,6 m and a slope of 1%. The channel consisted of a sequence of riffle and pools, although the study reach was majority riffle or transitional. The bed surface was composed of gravel, with an armour layer (mean diameter near 54 mm) and a finer substrate (median size near 20 mm). Milhous performed measurements and reported data for bed load and suspended sediment transport (winter of 1969-1970). He also reported grain size distributions of the transported sediment and the channel's surface layer. With the additional of surface and subsurface grain size distribution provided by Klingeman et al. (1979), Parker was able to develop

the surface-based relation for gravel mixtures. It is important to note that for the application of his relation the surface grain size distribution must be cut at 2mm, i.e., Parker only considers the gravel fraction as sand may be transported as suspended load with little interaction with the bed. Besides, when Parker refers to surface material he considers the armour layer that comprises not only the superficial material but also the subsurface material within a depth equal to the diameter of the largest stone (i.e. a bulk sample). Finally, the model uses a reference Shield stress for which the bed load is small but not zero.

Sun and Donahue's (2000) model.

Sun and Donahue (2000) followed an approach first proposed by Einstein in deriving his sediment transport equation, that is, an analysis of probability for the motion of particles. Sun and Donahue proposed their new formula on the bases of a theoretical study combining stochastic processes and mechanics. The model is intended to be applied to full motion conditions and non-uniform bed material. The theoretically derived equation was verified against experimental data with full motion transport (shear stress 3,5 - 9,8 times the critical value). In the experiments a natural non-uniform sediment was employed with continuous grading from sand to gravel (0,06 mm to 8 mm). Furthermore, analyzing field data, the authors proposed a modification in cases with partial transport in natural rivers. Habersack and Laronne (2002) applied this formula to the case of Drau River in Austria. They estimated the immobile fraction of the bed (P_m) with the relation proposed by Wilcock (1997):

$$Y_{ri} = 39{,}6R^{1/2}\frac{\tau_{ri}^*}{(\Delta_i)_r(D_i/D_{50})} \tag{64}$$

Where Y_{ri} is the entrained proportion of each fraction at the reference shear stress and therefore can be regarded as $Y_{ri} = 1 - P_m$; τ_{ri}^* is the reference dimensionless shear stress and $(\Delta_i)_r \approx 1$.

Wu, Wand and Jia's (2000) model.

The authors have studied the hiding and exposure effect in sediment transport of non-uniform material. They developed a probabilistic model for the hiding factor that considers the bed material grain size distribution. The sediment transport model assumes a small transport intensity (Wr* = 0,002) for a reference shear stress. The model's parameters were determined using published laboratory and field data: three sets of laboratory data for nonuniform bed-load transport (Lu, 1986; Kuhnle, 1993; and Wilcock and McArdell, 1993), and five natural gravel bed streams in the United State (Williams and Rosgen, 1989). The authors didn`t specify that the model is surface-based, they just refers to "bed material". As the probability analysis regarded the surface analysis, in my opinion, the grain size distribution needed to calculate the hiding factor should correspond to the surface material, i.e., the model should be applied as surface-based. Finally, the authors propose a way to remove the form drag effect on bottom shear stress. However, in Table 4.2 a simplified expression is presented where the shear stress corresponds to the fraction due to grain roughness.

Hunziker and Jaeggi's (2002) model.

Starting with a study of the development of the armour layer, Hunziker and Jaeggi elaborated a sediment transport formula for gravel mixtures. Considering a mobile armour bed, the authors calibrated the model verifying the equal mobility condition. Equal mobility means that subsurface bed material, supplied and moving sediment, are all the same. Secondly, following Parker and Wilcock, they

chose a surface-based model. Finally, they used the basic structure of the Meyer-Peter and Müller formula adding a hiding function. The model was calibrated using flume data from Meyer-Peter and Müller´s (1948) and Smart and Jaeggi´s (1983) experiments. Therefore, the model represents a generalization of previous formulas. Furthermore, the model used additional flume data form Guenter (1971); Suzuki and Kato (1991); Suzuki and Hano (1992) for the calibration of the hiding function.

Wilcock and Crowe's (2003) model.

Wilcock and Crowe analyzed the effect of sand in bed load transport and proposed a surface-based transport model for gravel mixtures. The researchers used a titling flume, 8 m long and 0,6 m wide. The gravel size ranged between 2 and 64 mm and sands were between 0,5 and 2 mm. The proportion of sand varied from 6,2 to 34,3%. They measured the sediment transport rate, the grain size distribution of transported material, flow characteristics and the grain size distribution of bed surface (grid-by-number method). The model has a similar structure to Parker's (1990) model. However, the exponent b (see table 4.2) of the hiding-exposure function depends on grain size; and the reference shear stress for the mean grain size depends on the sand content: when the sand content increases, the reference shear stress decreases and then there is a raise in the mobility for all fractions.

Powel, Reid and Laronne's (2003) model.

Powell, Laronne and Reid have studied the sedimentary dynamics of desert rivers. In 2003 they presented the results for four years of bedload measurements in Nahal Eshtemoa, an ephemeral stream located in the northern Negev Desert, Israel. The stream is subjected to flash floods with high rates of sediment transport, as high as 12,6 kg/m.s. During these floods shear stress can arrive to eight times the critical value for initiation of motion. At the study site, the reach is straight, 6 m wide, presents vertical banks of 1,2 m height and the mean bed slope is 0,0075 m/m. The channel is not armoured and the bed material has a median size of 17 mm. During the four-year study period, 19 events were monitored measuring flow depth and water surface slope (and then calculating the channel average shear stress), bed load transport rates using a Birkbeck-type bed slot sampler, bedload grain size distribution and bed material samples (areal surface sample and subsurface volumetric sample). As the channel does not have an armour it is not possible to define whether the model is surface-based or subsurface-based. However, the model has all the elements to be considered surfaced-based (Parker, 2008).

Meyer-Peter and Muller's model corrected by Wong and Parker (2006).

The Meyer-Peter and Muller's (1948) formula has been one of the most widely used to simulate bed-load transport in research activities and engineering applications. It was derived from experiments carried out in the Laboratory for Hydraulic Research and Soil Mechanics of the Swiss Federal Institute of Technology, at Zürich, Switzerland. They performed measurements of sediment transport with uniform bed material and mixtures. They reported that in most of the runs a plain bed persisted in flume, but in some runs bed forms were present. One important aspect of the original formula is the bed-form correction. The researchers introduced a factor that reduced the sediment transport when there were bed forms. This aspect was reanalyzed by Wong and Parker (2006). Firstly they performed a partition of the energy slope in order to remove the walls effects and could verify that the grain roughness was well described using a height equal to $2D_{90}$, a well known result supported by previous researches (Kamphuis, 1973, see previous chapter, section 3.5.1). Therefore, the bed-form correction was not necessary. They reanalyzed the runs for which bed forms were absents considering the sidewall

correction and not considering correction for bed forms. As a result they obtained an amended form of the Meyer-Peter and Müller relation for the case of lower-regimen plane-bed equilibrium transport conditions. The model is based on the shear stress excess; no sediment transport occurs when shear stress is below a threshold value.

Barry, Buffington and King's (2007) model.

Following a previous research performed by Whiting et al. (1999), Barry and collaborators applied the idea that the observed transport data could be best fitted by a simple power function of total discharge. In this way, they analyzed sediment transport data from 24 gravel bed streams in Idaho (King et al., 2004). In the original formulation (Barry et al., 2004) there was a dimensional inconsistency that was resolved later scaling the discharge with the 2-year flood (see table 4.2). The authors hypothesized that the exponent in the power function was related to the degree of channel armouring: a greater degree of channel armouring will delay mobilization of the armour layer and results in a steeper bed-load rating curve. They used the Dietrich et al. (1989) criterion to describe degree of armouring (see section 7.6). With regards to the coefficient α (table 4.2), they assumed that it represents the magnitude of bed load transport that is a function of basin sediment supply and discharge, both of them related to the drainage area. These are the characteristics of gravel bed streams considered for the formula derivation and test are: slope between 0,0007 and 0,051; surface median grain size between 5 and 204 mm; 2-year flood between 0,032 and 731 m^3/s.

Bathurst's (2007) model.

In the last years, sediment transport information from measurements in several natural gravel bed streams, mostly from the United State, has been published. With this available information, Bathurst performed a revision and actualization of Schoklitsch's (1962) equation. Bathurst distinguished two phases of sediment transport: phase 1, where the fine material moves over coarser fractions and the flow discharge is below the threshold for the break-up of the armour layer; phase 2, the current moves material from the armour layer that produces an increase in the rate bedload/discharge. At phase 2, the bed load discharge depends on water discharge and armour ratio. Therefore, he considered just phase 2 and incorporateed the armour ratio in the formulation. He combined flume and field data covering a wide range of slope (0,00275 - 0,2 in flume, and 0,00048 - 0,048 in rivers), and grain sizes (3,3 - 44,3 mm in flumes, and 6 – 146 mm in rivers). The new formula has the same structure that Schoklistsch's formula. Finally, it must be mention that the formula is applicable to determine mean rather than instantaneous transport rates, besides it determines bulk transport, not transport for size fraction.

Looking the plethora of bed-load formulas one wonders if there is one or several that quantify best sediment transport. First we must recognize that some formulas are based on field data and others used laboratory data in their derivation. This is an important point because in laboratory flumes it is possible to have uniform conditions: hydraulics, sedimentological and topographic. With regards to field-based models, bias can appear due to different geographic settings. Since the emblematic work of Gomez and Church (1989), there has been a great concern in verifying the models against field data. They compared 12 bed load formulae developed for use in gravel bed channels and concluded that no one performed consistently. However, they recommended stream power equations, in particular, Bagnold's equation. Some years later, Reid et al. (1996) compared several models with field data from Yatir, an ephemeral stream in Israel. They concluded that Meyer-Peter and Müller's (1948) equation fitted best within the limited scatter of the field data, and better than Bagnold (1980) and Parker's (1990) equations. They

attributed this success to the fact that sediment was not supply-limited by channel-bed armour development.

Lenzi et al. (1999) and D'Agostino and Lenzi (1999) tested several sediment transport models in the context of a headwater stream so as to see the incidence of sediment availability. The Rio Cordón is a small mountain stream (catchment area 5 km^2) placed in the Dolomities (Eastern Italian Alps). The flow regime is characterized by high discharges due to snow melt during spring (May and June) and by summer floods originated by cloudbursts. An automatic experimental station was constructed for measuring and automatically recording water discharge, fine sediment and coarse load. The variability of bedload rate and yield reflects the variability in flow discharge. Bedload and flow data for "ordinary" (low peak flow floods) and "exceptional" sediment transport events were used to test the range of applicability of the bedload equations proposed for high gradient streams. As a result, it was observed that such equations overestimated bedload rate for ordinary events (see Figure 4.4) while their reliability increased when used to predict high bedload transport rates like those recorded during the exceptional flood that affected the Rio Cordon in the summer of 1994 (T.R. between 30 and 50 years). The best agreement between computed and measured values of cumulated bedload volumes was found by using the Bagnold (1956), Smart and Jaeggi (1983) and Rickenmann (1991) formulas. The Schoklitsch (1962) equation also provided good estimations for instantaneous bedload rates at high-sediment transport intensity and unlimited sediment transport conditions. The analysis of critic conditions for initiation of motion also underlines the different between ordinary (with limited-sediment supply) and exceptional (with unlimited-sediment supply) events. Figure 4.4 also shows the relationship between discharges (ration between peak discharge and critical discharge) and degree of bed material moved by water flow. For low intensity events (peak discharge below 2,5-3,0 times the critical discharge) transported material is finer than bed material indicating the prevailing of selective processes. Instead, during the flashy event of 1994 most of the bed material was entrained, indicative of an equal mobility condition.

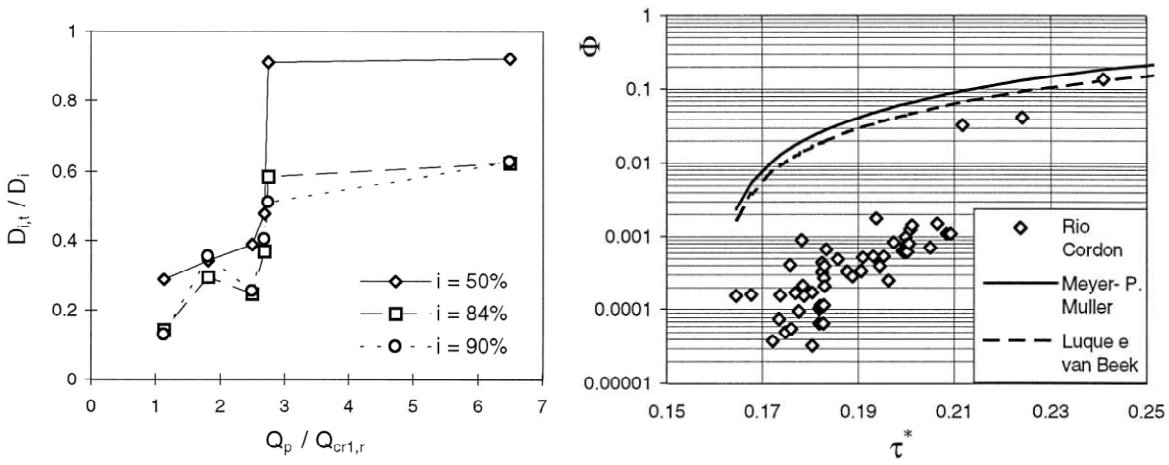

Figure 4.4. On the left: Selective transport and equal mobility in Rio Cordon; $D_{i,t}/D_i$ ratio between the characteristic diameters of transported sediment ($D_{i,t}$) and the corresponding bed diameters (D_i), as a function of peak discharge (Q_p) and critical discharge ($Q_{cr1,r}$) ratio (modified from Lenzi et al. 1999). On the right: Dimensionless transport intensity (Φ) vs. dimensionless shear stress τ^* for the data set recorded on the Rio Cordon with a comparison against selected sediment transport models (after D'Agostino and Lenzi, 1999).

More recently, Bravo-Espinosa et al. (2003) evaluated different conditions of bedload (transport-limited, partially transported limited and supply-limited). They concluded that equations proposed by Parker et al. (1982a), Schoklitsch (1962) and Meyer-Peter and Müller (1948) adequately predicted bedload transport in channels with a transport-limited condition. Overall, the best results were given by Schoklitsch and Bagnold's equations. In their study, Bravo-Espinosa et al. (2003) used reach averaged parameters; a different approach was followed by Habersack and Laronne (2002). They performed detailed measurements in Drau River, in Austria. They measured bedload with a large 6-inch Helley-Smith sampler and verified its efficiency with a Birkbeck-type slot sampler. They also performed detailed measurements on hydraulic, topography and sedimentological features. Then they were able to compare different formulas and recommended the use of fractional bed load equations, supplemented by limited bed load sampling. Besides, they concluded that shear stress-based formulas using single values for the threshold of motion did not perform as well as stream power equations; and formulas that incorporated stochastic concepts (such as Sun and Dunahue, 2000) were the most promising, at least, for Alpine gravel-bed rivers.

Finally, when deriving their own bedload equation, Barry et al. (2004, 2007) compared the performance of several previous models against a wide field dataset from gravel-bed streams in Idaho. They showed that at best, Ackers and White's (1973) and Parker et al.'s (1982a) equations presented median errors of less than 2 orders of magnitude; while at worst, median errors of more than 13 orders of magnitude were found for Meyer-Peter and Müller's (1948) and Bagnold's (1980) equations. Obviously, their fitted power function had the best performance.

Table 4.2 exposes the formulas, variable definitions and main features of the sediment transport models described above. It is worth to note some common mathematical structure that is important for processes description. The models developed by Meyer-Peter and Müller (corrected by Wong and Parker, 2006), Wu et al. (2000), Hunziker and Jaeggi (2002) express transport intensity in terms of an excess in shear stress, let it be: $\tau_b^* - \tau_{th}^*$ (been τ_b^* the bed dimensionless shear stress, and τ_{th}^* the threshold for initiation of motion). This particular formulation imposes a zero sediment transport when the bed shear stress is below the threshold value. A similar situation occurs in Bathurst (2007) model and in Powell, Laronne and Reid (2003). In the first one, there must be a positive excess of discharge, while in the second, there is a minimum value for the parameter ϕ. On the other hand models proposed by Parker (1990) and Wilcock and Crowe (2003) offer a continuous variation of sediment intensity.

As a concluding remark for this section I would like to present an example of the application of different bedload equations to a particular case. I considered surface and subsurface grain size data from Epuyén River, a gravel bed river in Patagonia, Argentina. For the selected reach, the channel has a slope of 0,46%, the surface median diameter is 43,1mm and the subsurface median diameter is 15,4mm. Figure 4.5 shows the bedload transport predicted by the analyzed formulae. Meyer-Peter and Müller's equation has been applied for the subsurface material. It has also been used for fractional transport introducing the Andrews (1983) hiding-exposure factor. It is remarkable the difference in bedload predicted between the formulae. For example, at the maximum shear stress considered (50 Pa), bedload varies between 0,27 and 4,75 kg s^{-1} m^{-1}, that is, the maximum value is 18 times the smaller. This is not surprising if we consider the scatter in the original derivation of each equation. Figure 4.5 illustrates the scatter in field data that Parker used for the derivation of his model. For any value of ϕ_{50}, between maximum and minimum value there is a near 6 fold difference.

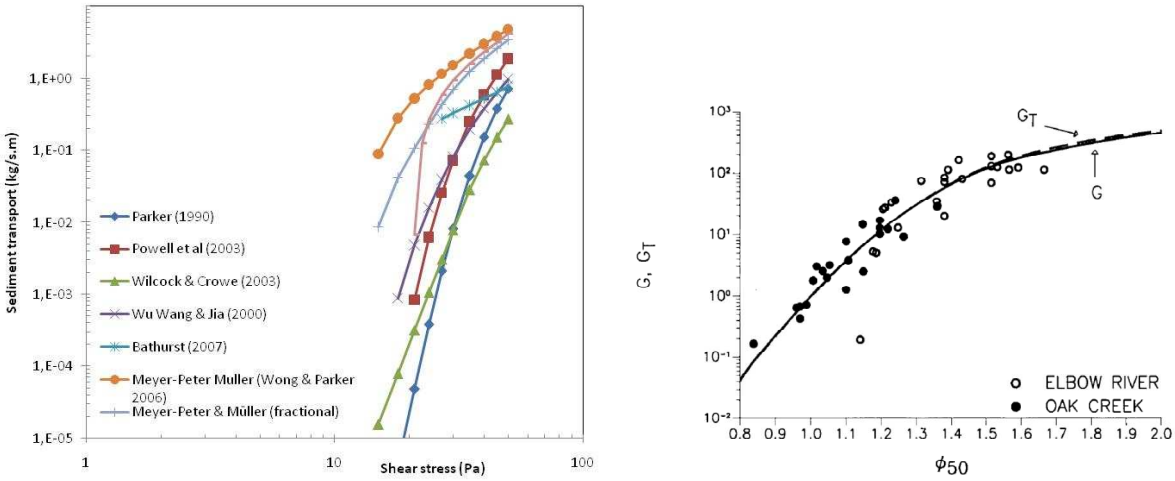

Figure 4.5. On the left: comparison of sediment transport rate predicted by different formulae for the Epuyén River. On the right: scatter in field data used for the derivation of Parker's (1990) model.

Variable definition used in table 4.2

q_i Bulk sediment transport per unit width, for i-th grain size class ($m^2 s^{-1}$).

q_b Total bulk sediment transport ($m^2 s^{-1}$).

q^* Dimensionless sediment transport.

g_s Mass sediment transport per unit width ($kg\ s^{-1}\ m^{-1}$)

τ^* Dimensionless shear stress. Subindex "c" and "r" refers to critic and reference values, respectively.

τ_b Bed shear stress ($kg\ m^{-1}\ s^{-2}$)

u^* Shear velocity ($m\ s^{-1}$)

D Grain size (m)

R_s Submerge relative specific weigh of sediments (normally assumed to be 1,65)

Fs Sand fraction content

Subindexes indicate the references grain size: "g" geometric grain size, "50" median grain size, "m" mean grain size, "i" mean value of the i-th class. If not indicated, the surface layer material is considered, instead when "ss" is added it refers to subsurface material.

Table 4.2. Selected bed-load formulas for mixture of sand and gravel.

Researcher / sediment transport formula	Variable definitions	Observations
Parker (1990) $$\frac{q_i g R_s}{F_i u_*^3} = G(\phi)$$ $$G(\phi) = \begin{cases} 11{,}93\left(1-\frac{0{,}853}{\phi}\right)^{4,5} & for\ \phi > 1{,}59 \\ 0{,}00218 e^{14{,}2(\phi-1)-9{,}28(\phi-1)^2} & for\ 1 \le \phi \le 1{,}59 \\ 0{,}00218\phi^{14{,}2} & \phi < 1 \end{cases}$$	$$\phi = \omega\phi_{sgo}\left(\frac{D_i}{D_g}\right)^{-0{,}0951} \quad \phi_{sgo} = \frac{\tau_g^*}{\tau_{ssrg}^*}$$ $$\tau_g^* = \frac{\tau_b}{\gamma R D_g} \quad \tau_{ssrg}^* = 0{,}0386$$ $$\omega = 1 + \frac{\sigma}{\sigma_0(\phi_{sgo})}\left[\omega_0\left(\phi_{sgo}\right) - 1\right]$$	Surface based model. Functions σ_0 ω_0 are given graphically (Parker, 1990) defined by table (Parker, 1990b). Model developed from field data (Oak Creek).
Sun and Donahue (2000) $$\frac{q_i}{F_i\sqrt{g R_s D_i^3}} = \frac{0{,}3 \cdot \alpha_i}{\Psi_i^{3/4}(1-\alpha_i)}$$	$$\Psi_i = \left[\tau_i^*\left(\frac{D_i}{D_m}\right)^{0.5}\sigma_g^{0.25}\right]^{-1}$$ $$\alpha_i = 1 - \frac{1}{\sqrt{2\pi}}\int_{-2.7(\sqrt{0.0822\Psi i}+1)}^{2.7(\sqrt{0.0822\Psi i}-1)} e^{-0.5x^2}dx$$	Surface based model. Full motion. In case of partial transport Ψ_i is replaced by $(1\text{-}P_m)^{3.75}\Psi_i$. Based on flume data and verified against field data.
Wu, Wang and Jia (2000) $$\frac{q_i g R_s}{F_i u_*^3} = 0{,}0053\frac{1}{(\tau_i^*)^{3/2}}\left(\frac{\tau_i^*}{\tau_{ri}^*} - 1\right)^{2,2}$$	$$\tau_{ri}^* = \tau_{r0}^*\left(\frac{p_{ei}}{p_{hi}}\right)^{-0,6} \quad \tau_{r0}^* = 0{,}03$$ $$p_{ei} = \sum_{k=1}^{N} F_k \frac{D_i}{D_i + D_k}$$ $$p_{hi} = \sum_{k=1}^{N} F_k \frac{D_k}{D_i + D_k}$$	Surface based model? The authors refer F_i as the grain size distribution of "bed material".

Table 4.2. Continue.

Researcher / sediment transport formula	Variable definitions	Observations
Hunziker & Jaeggi (2002) $\frac{q_i}{F_i\sqrt{gR_sD_m}D_m} = 5\left[\varphi_i(\tau_m^* - \tau_{cm}^*)\right]^{1.5}$	$\varphi_i = \left(\frac{D_i}{D_m}\right)^{-\alpha}$ $\alpha = 0{,}011(\tau_m^*)^{-1.5} - 0{,}3$ $\tau_{cms}^* = \tau_{cm0}^*\left(\frac{D_{mss}}{D_m}\right)^{0{,}33}$ $\tau_{cm0}^* = 0{,}05$	Surface based model. Model developed using flume data .
Powell, Laronne and Reid (2003) $\frac{q_i g R_s}{F_i u_*^3} = 11{,}2\left(1 - \frac{1}{\phi}\right)^{4{,}5}$	$\phi = \frac{\tau_{50}^*}{\tau_{c50}^*}\left(\frac{D_i}{D_{50}}\right)^{-0{,}26}$ $\tau_{c50}^* = 0{,}03$	Surface based model, developed exclusively with field data.
Wilcock and Crowe (2003) $\frac{q_i g R_s}{F_i u_*^3} = G(\phi)$ $G(\phi) = \begin{cases} 14\left(1 - \frac{0{,}894}{\phi^{0{,}5}}\right)^{4{,}5} & for\ \phi \geq 1{,}35 \\ 0{,}002\phi^{7{,}5} & for\ \phi < 1{,}35 \end{cases}$	$\phi = \frac{\tau_g^*}{\tau_{ssrg}^*}\left(\frac{D_i}{D_g}\right)^{-b}$ $\tau_{ssrg}^* = 0{,}021 + 0{,}015e^{-20Fs}$ $b = \frac{0{,}67}{1 + \exp(1{,}5 - D_i/D_g)}$	Surface-based model. Model based on flume data exclusively. Fs, sand content.
Meyer-Peter and Müller (correction by Wong and Parker, 2006) $q^* = \frac{q_b}{\sqrt{gR_sD_m}D_m}$ $q^* = 3{,}97(\tau_m^* - 0{,}0495)^{1{,}50}$	$\tau_m^* = \frac{\tau_b}{\gamma R D_m}$	Subsurface based model? Uniform sediment, plane-bed. Model based on flume data.

Table 4.2. Continue.

Researcher / sediment transport formula	Variable definitions	Observations
Bathurst (2007) $g_s = a\rho(q - q_{c2})$	$a = 29{,}2S^{1{,}5}(D_{50}/D_{50ss})^{-3{,}30}$ $q_{c2} = 0{,}0513g^{0{,}5}D_{50}^{1{,}5}S^{-1{,}20}$ $q_{c2} = 0{,}0133g^{0{,}5}D_{84}^{1{,}5}S^{-1{,}23}$	Bulk transport. Bathurst uses the mean of q_{c2}. Model based on flume and field data.
Barry, Buffington and King (2007) $g_s = \alpha\left(\frac{Q}{Q_2}\right)^{\beta}$	$\alpha = 8{,}13x10^{-7}A^{0{,}49}$ $\beta = -2{,}45\delta + 3{,}56$ $\delta = \left(\frac{\tau_{Q2} - \tau_{50}}{\tau_{Q2} - \tau_{50ss}}\right)^{1{,}5}$	Bulk transport. Model based on field data. Drainage area A in m^2.

Section Two

Field research and analysis

"In calling up images of the past, I find that the plains of Patagonia frequently cross before my eyes; yet these plains are pronounced by all wretched and useless. They can be described only by negative characters; without habitations, without water, without trees, without mountains, they support merely a few dwarf plants. Why, then, and the case is not peculiar to myself, have these arid wastes taken so firm a hold on my memory? Why have not the still more level, the greener and more fertile Pampas, which are serviceable to mankind, produced an equal impression? I can scarcely analyze these feelings: but it must be partly owing to the free scope given to the imagination."

Charles Darwin.
A Naturalist's Voyage Round the World.
The Voyage of The Beagle

5 STUDY RIVER BASINS

In order to test the hypothesis of this study a set of river reaches were surveyed in two different geographical contexts: Italy and Argentina. It is known that the rivers in Italy have been largely altered by human activities during the last 200 years. On the contrary, gravel bed rivers in the mountain range of The Andes, Argentina, are still in virtually unimppacted conditions. In particular, these rivers are located in the Patagonia region, a geographic region with unique characteristics in the southern corner of Argentina (it includes the provinces of Tierra del Fuego, Santa Cruz, Chubut, Rio Negro, Neuquén and part of La Pampa).

The first part of this chapter presents the criteria used for selecting the gauging stations, and main features are described. Afterwards, each basin is described considering climate, morphology, hydrographic features and land use. A brief account of the geological setting is also included so as to complete the background information for a later comparison in Chapter 7. Finally, a statistical test is applied to hydraulic geometry scatterplots of Argentinian rivers so as to verify their stability in the last 20 years.

Figure 5.1. Location of gauging stations and corresponding river reaches selected in Northern Italy. Circles indicate the location of gauging stations with its reference code (for instance, IT04, is the code of Brenta River Near Bassano, see table 5.1), and triangles indicate the main cities in the region.

5.1 Selection of river reaches

Fifteen river reaches have been selected, ten in Argentina and five in Italy. Figures 5.1 and 5.2 show the location of each river reach in Italy and Argentina, respectively, and tables 5.1 and 5.2 report the main characteristics of each site. In Argentina, most of the river reaches are located in the Northwestern corner of Chubut Province, and some in the Southwester side of Rio Negro Province

(central Patagonia). On the other hand, the river reaches selected in Italy are placed in the Alpine and Pre-alpine region, all of them in the Veneto Region[10].

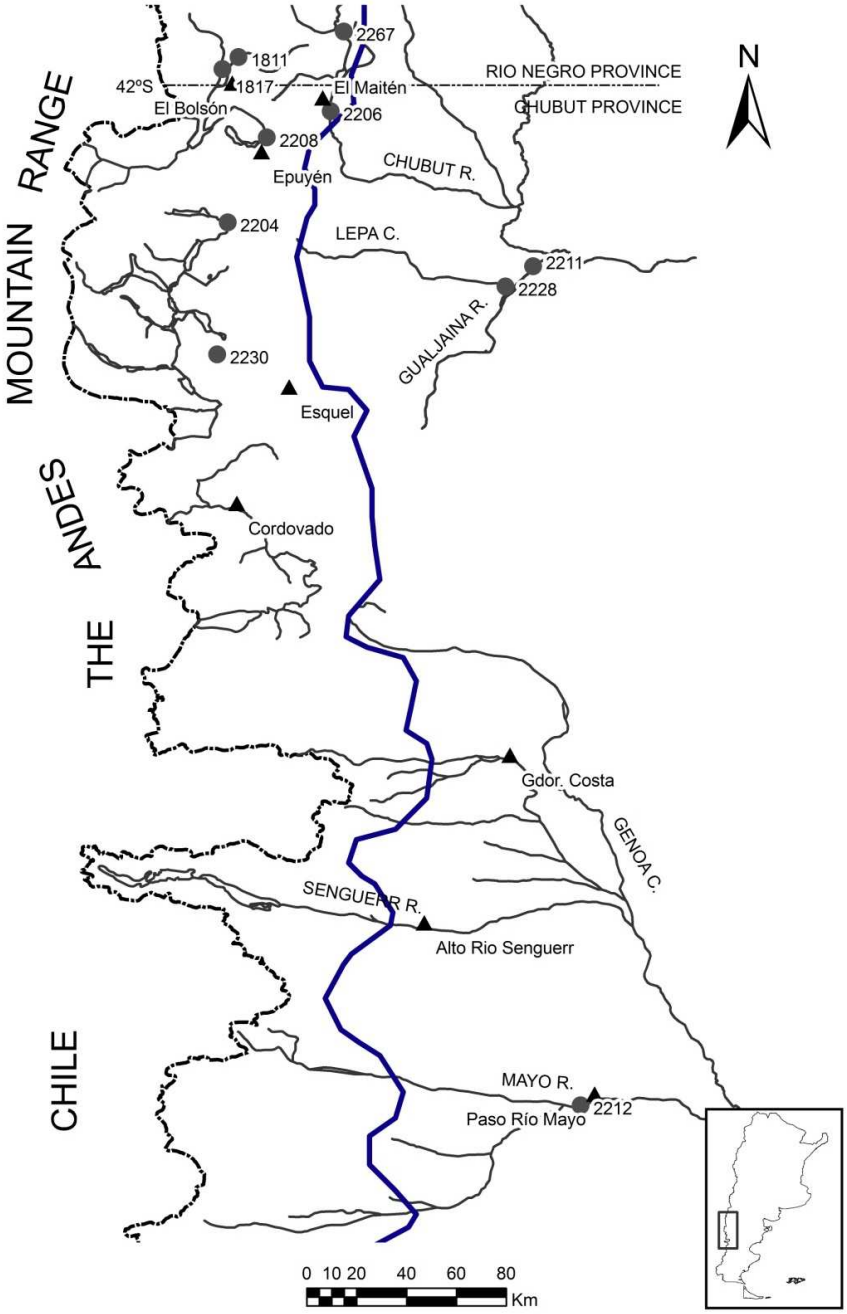

Figure 5.2. Location of gauging stations and corresponding river reaches selected for the study in central Patagonia, Argentina. Circles indicate the location of gauging stations with its reference code (for instance, 2208, is the code of Epuyén River in Argentina, see table 5.2), and triangles indicate the main cities in the region. The blue line indicates the approximate maximum extension of glaciers during the last glaciation (from Rabassa and Clapperton, 1990).

[10] Both, Argentinean and Italian territories are divided in smaller administrative states called Province in Argentina and Region in Italy. Moreover, in Italy a Region is divided in Provinces with its own administration, while in Argentina a Province is further divided in Departments, but due to the low population density, the next administration level are communities.

The study sites were selected near gauging stations with long records, at least with 20 years. In Patagonia station this requirement was easily verified, but for Italian streams a softer criterion was applied (see tables 5.1 and 5.2), because in many cases the record length was shorter. After analyzing the available information, a preliminary survey was conducted so as to verify that each reach was alluvial, the geological conditions remained constant, and there were not major human disturbances, such as bridges, weirs, bank protections or groynies. As a result, ten streams were selected in Patagonia and 5 river reaches belonging to 3 streams were chosen in Italy. In the case of Italian reaches, the location does not correspond to the gauging station because these sectors are highly disturbed. Therefore, I selected the nearest alluvial reach.

Table 5.1. Location and hydrological records available for gauging stations in Italy. Four river reaches are placed in the Piave River basin. A description of each basin is provided in section 5.2. Reaches are placed near gauging stations: 1) 7.1 km downstream near Ospitale di Cadore Town, 2) 1 km downstream, 3) 6,7 km upstream, near Santa Maria Town, 4) 4,6 km downstream near Cartigliano Town, and 5) 3,4 km upstream near Peron Town. See figure 5.1 for the geographical location of each reach.

Code	Stream	Gauging station Location	Drainage Area (km^2)	Discharge record (years)	Basin
IT101	Piave River (P)	Perarolo di Cadore[(1)]	1230	16	Piave River
IT102	Piave River (BL)	Belluno[(2)]	1965	14	Piave River
IT103	Piave River (S)	Segusino[(3)]	3464	18	Piave River
IT201	Brenta River	Bassano del Grappa[(4)]	1567	72	Brenta River
IT301	Cordevole River	Ponte Mas[(5)]	696	18	Piave River

Table 5.2. Location and hydrological records available for gauging stations in Argentina. Several rivers belong to a major basin (indicated in the last column) which are described in section 5.3). In some cases, the surveyed reach did not included the gauging station. References 1) the reach is 5,7km upstream the gauging station, near El Maiten Town; 2) the reach is placed 2,3 km downstream the gauging station, near “Los Alerces” Camping. Also see Figure 5.2 for the geographical location of each reach.

S.RR.HH. Code	Stream	Gauging station Location	Drainage Area (km^2)	Discharge record (years)	Basin
2211	Gualjaina River	Loc. Gualjaina	2800	48	Chubut River
2228	Lepà Creek	Loc. Gualjaina	1168	28	Chubut River
2206	Chubut River	Loc. El Maitèn[(1)]	1200	63	Chubut River
2204	Carrileufu River	Loc. Cholila	580	50	Chubut River
2230	Cohihues Creek	P.N. Los Alerces	24	35	Futaleufú River
2212	Mayo River	Loc. Río Mayo	5450	43	Senguerr River
2267	Alto Chubut River	Nacimiento	412	25	Chubut River
1811	Quemquemtreu River	Escuela Nº 139	650	49	Puelo River
1817	Azul River	El Azul[(2)]	395	39	Puelo River
2208	Epuyén River	La Angostura	500	52	Puelo River

Gauging stations in Argentina are managed by the *Subsecretaría de Recursos Hídricos de Nación*. This bureau has provided the hydrologic records consisting of mean daily discharges, maximum instantaneous discharges, measurements summaries (with information regarding width, area, wetted perimeter, etc, for each discharge measurement). In Italy the information has been provided by the *Azienda Regionale per la Protezione Ambientale*, from the Region of Veneto, which is in charge of the gauging stations operation. The information provided consists of mean daily discharges and stages. Mean hourly discharges were also available for selected flood events.

5.2 Characteristics of river basins in Italy

5.2.1 Piave River basin

The basin of Piave River extends over 4500 km^2 in the Veneto Region (Italy) territory. The main fluvial stem has a length of 220 km starting near Peralba Mount at an elevation of 2030 m a.s.l. (Belluno Province) and finishing in the Adriatic Sea (Venezia Province). The basin is placed mainly in the mountain region (3900 km^2) and less on the Venetian plain.

The hydrographic network is developed mainly along the right side of the river. There are three principal tributaries; two of them, the Boite River near Perarolo di Cadore and the Maè River near Longarone are placed at the northern side of basin, and the third, the Cordervole River, collects water from the western region.

The basin has a humid temperate-continental climate, which is common in the entire eastern Alps region. Precipitation has a wide spatial variability due to the complex topography. The mean precipitation is 1350 mm, with a minimum of 1000 mm in the north-western side (it includes the basin of Cordevole River) and higher values in the central-eastern corner (near the Vajont basin). Autumn is the rainiest season followed by the spring, been November and June the months that concentrate most of the annual rainfall. Summers are hot (frequent maximum temperatures of 33-35 °C) and humid, while winters are cold (mean temperature of 2-3 °C) and also humid.

At the headwater torrents have high slope and flow along very narrow valleys. At high elevations typical structures due to glacial processes can be identified, such as glacial circus and big pools, mainly in the high flat lands. Besides, valleys have the typical U-shape associated with glaciers erosion. The Valley of the upper Piave River is narrow and deep, and cuts the stratified rocks that constitute the basement of the region.

At Ponte nelle Alpi the characteristics of the landscape change dramatically. At this place the river arrives to a former synclinal that directs the flow towards Feltre. This reach is characterized by a wide valley with a flat bottom and gentle sides, the so-called “Vallone Bellunese” (Bellunese Valley, hereafter). Six levels of terraces have been recognized that are associated with the recent geological history (Late Pleistocene - Holocene). After Feltre, the river enters into a narrower valley that cuts the Grappa-Tomatico-Cesen-Visentin mountain range, which stratification constitutes a long anticline arc. Finally, the river flows through a zone with a syncline disposition arriving to the deep gorge at Nervesa. This point constitutes the end of the mountain basin, and following the river flows along the Venetian plain.

The mountain area of the basin is occupied by tows of median to small dimensions. The total population of Belluno Province, which holds the mountain basin, is 213.747 inhabitants. The economic activity of the population has been strongly diversified been present primary activities (traditional agriculture and mining) secondary and tertiary activities, as well. Recently, tourism has gain in importance (with Cortina, one of the European most important city in this field), but industries have also a discrete presence.

5.2.2 Brenta River basin

The basin of Brenta River has an extension of 2.280 km^2, divided 1.120 km^2 in Veneto Region and the remaining, in the Trentino-Alto Adige Region. The river has its origin in the Caldonazzo Lake (450 m a.s.l.) in Trento Province. It flows along the Valsugana Valley and after flowing through the wide Venetian Plain (crossing the Provinces of Vicenza, Padova and Venezia) it arrives to the Adriatic Sea. The length of the main stem is near 174 km. At Bassano del Grappa the river abandons the mountain valley and flows into the plain. Therefore, the course of the river can be divided into two reaches: an upper reach, 70 km long, within the mountain area, and a lower reach, 104 km long, in the Venetian Plain.

The principal valley divides the moutain basin in two unequal parts, been the biggest placed on the left side and hence, it contains most of the tributaries, such as, the Cismon Torrent the main one, and others smaller, the Ceggro Torrent, The Maso Torrent and Grigno Torrent. From the right side the Brenta River receives the discharges of Cesa Torrent.

The mountain basin has also a humid temperate-continental climate. The mean annual precipitation is 1313 mm but the runoff at the basin outlet is 105%. Such a high value of runoff is due to the contribution of karst springs which are located in the lower part of the drainage basin (Prealps). The rainy seasons have the maximum precipitations during the months of May-June and October-November.

The landscape is very different in the upper and lower part of the basin. In the upper part the river flows through a typical glacial-fluvial valley (U-shaped), the Valsugana Valley, from the Caldonazzo Plain up to the Primolano gorge. In the lower part, the Venetian Plain can be divided into an old deposition plain (alluvial fan of Bassano, Upper Pleistocene) placed on the left side of the Brenta River, and a more modern plain, the current Brenta River floodplain (Holocene).

Considering only the upper part of the basin (Communities of Valsugana and Primiero) the population is near 82,500 inhabitants.

5.2.3 Geological setting

There are two important topics relative to the characteristics of sediment load carried by rivers and the sediments that constitute the floodplain; they are the type of rock and its availability. The rock type is important because of its strength and hence its implication in fluvial phenomena such us downstream fining. On the other hand, a stream, in order to accomplish the processes of erosion and transport, must have near sources of sediment. The geological formations favorable for fluvial drawing are composed of loss material organized in different depositional structures: hillslopes, alluvial fans, landslide deposits, blankets from rock substrate weathering, ecc. The aim of this section

is to underline the main classes of rocks present in the study basin and the recent geological events that furnish sediments to the current fluvial system.

In the Piave River basin several and different rock types crop out with a variety of origin, composition and age:

- Schist-phyllite rocks (Paleozoic) are present in the eastern side of the basin,
- Sandstone, marlstone, argillite are found upstream Pieve di Cadore, in the Biois basin and also in the Bellunese Valley,
- Powerful series of sedimentary rocks: limestone and dolomite in the dolomite region, and limestone in the massif located in the Prealps.

The most diffused rocks within the Piave River basin are limestone and dolomite.

With regards to the Brenta River basin there is also a wide variety of rocks, but in this case metamorphic rocks are more frequent because they constitute the rock basement of the Southern Alps. The following types of rocks are recognized:

- A variety of rock outcrops: limestone, dolomite, gneiss, phyllite, granite and volcanic rocks (andesite, rhyolite, etc) are found in the upper part.
- Sedimentary rocks with a prevalence of limestone and dolomite but also marlstone and argillite are predominant, in the lower part of the basin and in the dolomites' massif of "Pale di San Martino".

The depositional structures that currently furnish sediments to the rivers have been created recently (Late Pleistocene – Holocene). In the Alps the last glaciations (Würm) took place between 24,000 and 16,000 BP, the maximum expansion of glaciers was likely between 20,000 and 18,000 BP, and deglaciation started 16,000-15,000 years BP. During the last glaciation the Piave River Basin and the Brenta River Basin were covered by huge glaciers, as the entire Alps range, that flew into the Venetian Plain. In particular, the Piave glacier flowed towards the Venetian Plain in two branches (Figure 5.3). The western branch built the Quero end moraine system, whereas the eastern one, passing through the Lapisina Valley, built the Gai and Vittorio Veneto systems (Surian and Pellegrini, 2000).

During and after the retreat of the Würmian glacier, slope processes were very active. Large landslides dammed the valley bottom at several places causing the formation of lakes and changing the course of the Piave River. For instance, during the first phase of deglaciation two big landslides occurred, the so called, Marziai and Collesei di Arzù landslides (Pellegrini et al., 2004). These slides have influenced dramatically the morphological evolution of Quero channel but also the Piave River along the Bellunese Valley. Upstream each landslide a lake was created and the base level was changed. But the life of these lakes was very short because they were soon filled by the sediments carried by the river. The lake of Marziai (which was 20km long) was probably filled in the period between 17,000 and 15,000 years BP (Pellegrini et al., 2004). The sedimentary fill indicates that after the retreat of the würmian glaciers an important phase of aggradation took place. This was due to the large amount of sediments available on the slopes during and after the deglaciation and the lack

of sufficient power in the streams for transporting the load. Today, a series of six terraces levels are observed in the Bellunese Valley. The highest terrace represents the end of the main filling of the valley floor (dated about 8000-9000 years BP). After this aggradation phase, streams were mainly subjected to degradation. The increase in slope stability caused a reduction of erosive processes in the drainage basin and a decrease of sediment load in the streams. Downcutting was also due to the tectonic uplift. Lower terraces are then associated with downcutting and lateral shift, processes which characterized the river for the rest of the Holocene (from 8,000-9,000 years BP to the present) (Surian, 1998).

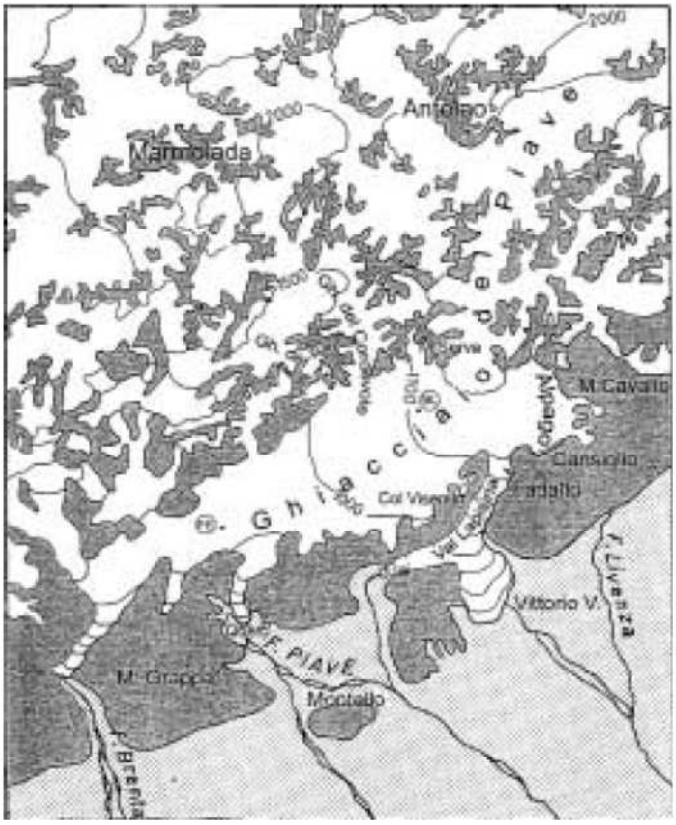

Figure 5.3. The maximum expansion of the Piave glacier during the last glaciation (from Pellegrini et al., 2004). The glaciations affected the entire Alp mountain range and glaciers flew into the Venetian Plain.

5.2.4 Chronology of human interventions in the basins of Piave and Brenta rivers

The chronology of human interventions is quite similar in both rivers. At the beginning of 19th century the entire zone suffered a deep structural and economic crisis originated in the way of use of the resources and a steady demographic growth. Woods extension experienced a dramatic decrease especially during the time of the Napoleonic wars. The aforestation was not uniform in the region, instead it assumed local features in different locations within the basin. These factors were related to climate (altitude), demography (raise in population), economy (main local activities) and social (relationship between the town and the surroundings). For instance, in the lower regions of the basin it was the pressure from the towns that made the woods to disappear. Instead, in certain upper regions, woods were used for producing fuel for the metal industry. At the same time, there was a remarkable land use change. Those lands previously covered by woods were transformed into crops and pastures. Erosion processes were then promoted because of high quantities of animals and a

lack of appropriate pasture maintenance (Da Canal, 2006). Natural reforestation has been taking place since World War I but most effectively after the '50s because of a rapid abandonment of traditional farming and cropping activities on the mountain slopes owing to the development of industry and tourism (Comiti et al., 2011).

During the first years of the 20th century it was evident the need of electric energy generation and the development of irrigation systems. Since the '30s until the '60s all the current dams were constructed. Tables 5.3 and 5.4 present a detailed chronology of dam construction in Brenta and River basins, with an indication of the drainage area upstream of the dams. Although the area subject to dam regulation is large, the storage capacity is rather low, only the 4% of the annual precipitation is storage in dams within Piave River basin. Then, dams have a scarce capacity for storing volumes during flood events and hence to reduce peak discharge. But, actually dams were not design with that scope; instead, the complex network of dams and conducts was thought looking for the optimization in the use of water for energy generation and irrigation scopes. On the contrary, the main effect of dams has been on the regime of sediment delivery. The presence of artificial reservoirs has stopped the natural sediment flow during floods affecting the sediment balance in the fluvial network placed downstream.

Table 5.3. Dams constructed in the Brenta River basin. The drainage area upstream the dam is indicated (Surian and Cisotto, 2007).

River	Dam	Drainage area upstream (km^2)	Year of construction
Cismon Torrent	Ponte Serra	497	1909
Costa Brunella Torrent	Costa Brunella	0.7	1941
Cismon Torrent	Corlo	628	1954
Senaiga Torrent	Senaiga	58	1954
Noana Torrent	Val Noana	8	1958
Cismon Torrent	Val Schener	204	1963

The decrease of sediment supply has also been a consequence of other human interventions: bank protection occurring mainly during the 19th century and the implementation of torrent control works from the 20s, both promoted channel stability due to the increase of bank strength and fixing the stream bottom bed.

More recently, another human activity has altered the dynamic of these fluvial systems. Between the '60s and '90s intense gravel mining was carried out in the main channel and its main tributaries. Official records, which are presumably underestimation of actual values, indicate that in Piave River 170,000 m^3 were excavated in the upper basin in 1973, 303,000 m^3 in 1993 and 348,000 m^3 in 1995 (Surian, 1999). However, a recent study based on detail topography of a long Piave River reach indicates that the total extracted volume may be in the order of 6 million cubic meters (Comiti et al., 2011). In the case of Brenta River, according to official data 8,6 million of cubic meters of sediments were supposed to have been mined between 1953 and 1977, but aerial photographs taken in those years indicates that the volume of sediments removed from the channel was much larger (Surian and Cisotto, 2007).

Table 5.4. Chronology of dams construction in the Piave River basin. The area indicates the basin drainage area upstream of the dam (Surian 1999).

River	Dam	Drainage area upstream (km^2)	Year of construction
Tesa Creek - Rai River	S.Croce	136	1929
Piave River	Soverzene	1690	1929
Ansiei Creek	S.Caterina	255	1931
Piave River	Comelico	362	1931
Cordevole Creek	Ghirlo	419	1939
Piave River	Piave di Cadore	818	1949
Boite Creek	Valle di Cadore	380	1950
Gallina Creek	Val Gallina	14	1951
Caorame Creek	La Stua	28	1954
Mae Creek	Pontesei	151	1955
Boite Creek	Vodo	323	1958
Vajont Creek	Vajont	62	1958
Piave River	Busche	3174	1960
Mis Creek	Mis	108	1964

5.2.5 Brief history of the evolution of Brenta and Piave rivers

The Brenta River has experienced a dramatic narrowing process in the last decades, been 442 m wide by the beginning of 20th century and arriving to 224 m in 2003 (see Figures 5.4 and 5.5). This process has been accompanied by incision along the reach. In same places it has been up to 2,5 m. Mean channel slope has increased only slightly, from 0,0033 m/m to 0,0036 m/m. This figures show that channel narrowing has been much more important than channel incision, i.e., while width has changed by -49%, slope has only change by an amount of 9%.

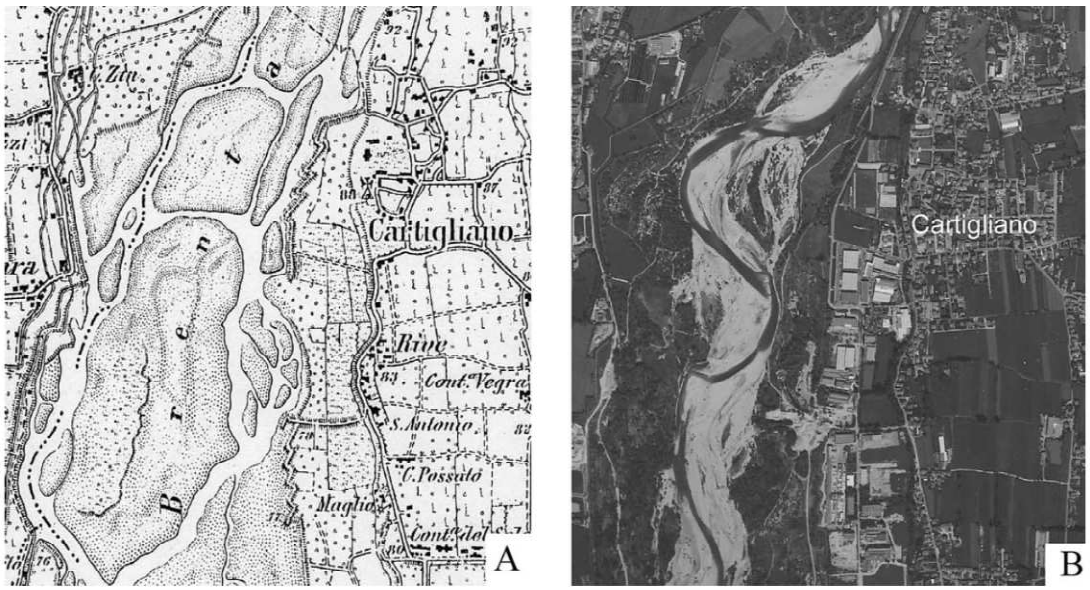

Figure 5.4. Channel narrowing along the Brenta River. A) topographic map of 1887: B) aerial photograph of 1999. Note that besides the narrowing process, there is also a change in channel pattern (from braided to wandering) with an increase in channel sinuosity (modified from Surian and Rinaldi, 2003). This reach of Brenta river was selected for this study.

The case of Piave is quite similar to the Brenta River (Surian et al., 2009; Comiti et al., 2011). During the 20th century, the active channel progressively narrowed, reaching in 1991 an extension of approximately one-third of its extent in at the beginning of 19th century. The active channel area reduced in two different stages (Figure 5.5). A first phase of adjustment took place during the first half of the twentieth century and was characterized by a loss of about 35% of the initial active channel area. This trend was interrupted by the high magnitude/low frequency (200 year recurrence interval) flood event that occurred in 1966, and the subsequent narrowing phase (from 1970 to 1991) was even more intense, occurring at a rate 10.6 m/year in terms of channel width. Interesting, during the following period (1991–2003), a reversal occurred with an evident sharp widening tendency that extended the active channel at a rate of 9 m/year. With regards to the long-term bed level changes, bed elevation in 1929 was about 1 m higher than present days, with a rather complex trend of bed level adjustment trends (Comiti et al., 2011). Like in Brenta River, channel narrowing has been the major channel reaction to changes in sediment supply while slope has slightly changed (0,0044 to 0.0045 m/m).

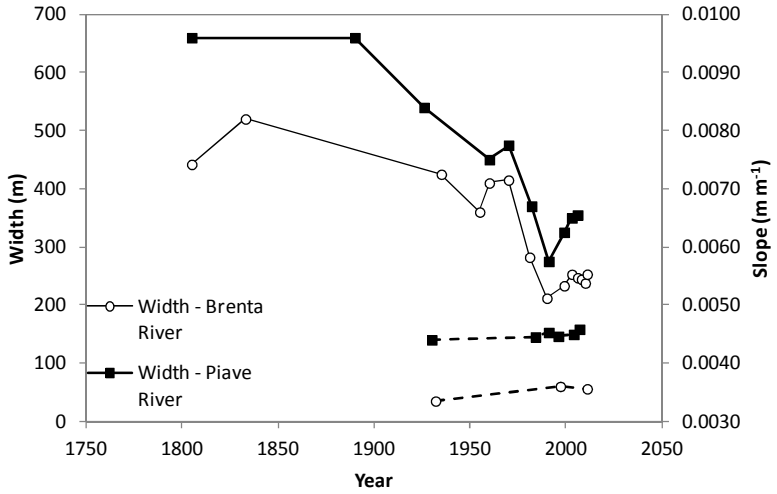

Figure 5.5. Morphological changes in Piave and Brenta River during the last 200 years (Surian et al., 2009; Comiti et al., 2011). Note that channels have adjusted mainly their width in response to sediment supply alterations while slope has remained almost insensitive.

5.3 Characteristics of river basins in Patagonia

5.3.1 Chubut River basin

The Chubut River has a wide catchment with its upper watershed in Rio Negro Province and its mouth in the Atlantic Ocean. The basin is mainly in Chubut Province and its total area is 53.234 km^2 (SsRrHh, 2002). However, for this study only the upper basin will be considered. It is closed at the confluence of Chubut and Gualjaina rivers where the drained area is 13.860 km^2.

At the western corner of the basin there are low mountains belonging to the eastern sector of the Andes mountain range (the peaks are nearly 2000 m a.s.l.). The headwater streams start at this mountains and flow down feeding the Chubut River. The streams flow through the “Patagonides” system with a North-South orientation. The landscape is composed of smooth hills and flat plains, the so-called “mesetas” (Figure 5.6 and 5.8).

The fluvial network is composed of Chubut River, Alto Chubut River, Chico River and Ñorquinco Creek in the northern part, and in the south, there are the Gualjaina River and Lepa Creek.

Figure 5.6. View of the Valley of Gualjaina River near its confluence with Chubut River (looking eastward). This is a typical landscape of the extra-andine region. On the background there is the Huancache mountain range composed of volcanic rocks. On the foreground a terraces is recognized on the left (composed of gravels, sand and silt transported by older streams) and on the right is the current floodplain.

The catchment is affected by the anticyclones from the South Pacific. The western side of the basin has a cold-humid climate with snowfall during winter. Annual precipitation is near 1000 mm but it decreases sharply towards east and south. Rains predominate during autumn and winter. Therefore, Chubut River presents floods during autumn and winter owing to rain events, while during spring they are due to snowmelt. The thermal amplitude is low owing to the high moisture content in air. The mean annual temperature is lower than 8ºC. The eastern side of the basin has a continental dry-semiarid climate. The precipitation is very scarce, only 200 mm. Because moisture is also scarce the thermal amplitude is high.

The predominant vegetation corresponds to the xerophilous steppe type and presents two classes: bushes, composed of neneo (Mulinum spinosum), jarilla (*Larrea tridentata*) and malaspina (trevoa patagonica); and a second class composed of herbs dominated by the coirón (festuca gracilina). In the flat plains (mesetas) bushes almost disappear. In the Alto Chubut River valley it is possible to find "mallines" (wetlands) with abundant arboreal vegetation.

The population is very scarce and is scattered in this region. The main towns are El Maitén (3,782 inhabitants[11]), Gualjaina (648 inhabitants), Cushamen (580 inhabitants) in Chubut Province and Ñorquinco (444 inhabitans) in Rio Negro Province.

5.3.2 Futaleufú River basin

The catchment is mainly placed in Argentina but the mouth of the river is in the Pacific Ocean (in Chile). The catchment covers an area of 7.630 km^2 in the North-western corner of Chubut Province.

[11] All statistical data has been provided by *"Dirección General de Estadística y Censo"* of Chubut Province and refers to the INDEC 2001 census.

The catchment watershed is defined by a mountain range along the western and northern limit with peaks as high as 2500 m a.s.l. The eastern side is defined by the pre-cordillera mountain ranges (Leleque and Esquel) that constitute the western border of Chubut River basin. Along the southern border there are the mountain ranges of Grasa and Kaquel and Barrancos Hills. The western side presents a rough relief shaped by the action of glaciers: discontinuous mountain ranges separated with deep valleys occupied by lakes. The eastern sector presents a gentle relief with hills and large plains.

The catchment mean annual precipitation is nearly 1300 mm, but there is a steep gradient oriented west-east. In the western mountain range precipitation can be above 2500 mm, while in the east it is 500 mm. The pacific anticyclone produces precipitations mainly during autumn (rain fall) and winter (mainly snowfall). Flood during spring are due to snowmelt. The basin has a complex drainage network composed by many lakes linked with deep incised rivers. This series of connected lakes regulated the fluvial regime. The Carrileufu River and the Cohihes Creek belong to this lacustrine-fluvial system.

The Los Alerces National Park is within the basin with an extension of 2630 km^2. It was created in 1937 and preserves the richest and most exuberant formation of the Andino-Patagonic wood, the so called “Selva Valdiviana”; which most outstanding component is the larch (Fitzroya cupressoides). The Andino-Patagonic wood covers most of the hillslopes arriving until the lake coasts and river banks. Besides the larch, woods are also composed of maiten (Maytenus boaria), cohihues (Nothofagus dombeyi) and lenga (Nothofagus pumilio). In the upland pastures predominate. On the other hand, where precipitation is low (eastern side) thin and sparse vegetation (xerophilous steppe) alternates with bare surfaces.

This catchment is the most populated been the population concentrated in few urban centers: Esquel city (28,089), Trevelin city (4,856 inhabitants) and Cholila town (1,981 inhabitants).

5.3.3 Puelo River basin

The basin of Puelo River (area 6.041 km^2) is another case of international catchment that has its headwater in Argentina (Rio Negro and Chubut provinces) crosses the international border and has its mouth in the Pacific Ocean. The origin of Puelo River is in the homonymous lake in Argentina. This lake has several tributaries: the Turbio River from the south, the Epuyén River from the east and the Azul River from the north that receives the flow of Quemquemtreu River.

At the western side of the catchment there is the sharpest and highest relief with mountain range separated by deep valleys that evidence the action of old glaciers. Towards the eastern corner the relief is gentler with lower and rounded hills, wide valleys and plains (see figure 5.7).

The climate is cold-temperate. The highest precipitations fall near the international border where the mountain range is highest, during autumn and winter, owing to the humid winters from the Pacific. There is a sharp gradient of precipitation from west to east. In the mountain range near Chile precipitations can be as high as 3000 mm; in the valleys of Azul and Quemquemtreu rivers it is 1000 mm while in the eastern watershed it has decreased to 500 mm.

The vegetation diversity is related to the climate and the relief. Woods of Nothofagus are very common within the basin especially in the middle-western sector that receives the most humid winds that enable the growth of many species typical of the “Selva Valdiviana”.

The population is concentrated in a few towns: El Bolson (13,560 inhabitants) in Rio Negro Province and Lago Puelo (2,090 inhabitants), Epuyén (534 inhabitants) and El Hoyo (955 inhabitants) in Chubut Province. Tourism is the main economical activity. The basin holds the Lago Puelo National Park with an extension of 240 km^2.

Figure 5.7. View of the Valley of Azul River, upstream the confluence with Quemquemtreu River (looking towards south). The landscape shown is an example of the mountain region. Mountains are composed of granitoids. On the bottom-left corner is the hillslopes of “Loma del Medio” a hill that separates the valleys of Azul and Quemqeumtreu rivers. The hill is composed of sedimentary rocks (tuff, sandstone, and marine sediments) and was covered by glaciers during the last glaciation. At the hillslopes and the bottom of the valley there are glacial deposits.

5.3.4 Senguer River basin

This is an extensive basin, one of the most important in Chubut Province. The total area is 61.131 km^2 distributed mainly in Chubut Province and a small part in Santa Cruz Province. The fluvial network has a very small density; the basin is crossed by the Senguerr River that has only two tributaries: the Mayo River and the Genoa Creek.

The western watershed is placed along the Andes mountain range with not very high mountains (below 2000 m a.s.l.). The watershed is irregular, with a north-south orientation, due to the presence of transversal mountain ranges and glacial lakes. The central part is dominated by flat surfaces (outwash terraces) interrupted by incised fluvial valleys (Figure 5.8). On the eastern side there is the Patagonoides system with low and gentle hills.

Like the Chubut basin, the catchment is also influenced by the Pacific anticyclone. Precipitation is most frequently during autumn and winter with its highest intensity in the western watershed (1200 mm) and the lowest on the eastern plains (between 100 and 200 mm). The annual mean temperature is near 8º C, with low amplitude in the western side due to the high moisture content, and increases eastward.

The western mountain range is covered by the Andino-patagonic wood composed mainly of Nothofagus such us the ñire (Nothofagus Antarctica), guindo (nothofagus betuloides) and lenga (Nothofagus pumilio). Towards the southern part of the mountain range woods are replaced by the xerophilous steppe because high mountains in the Chilean territory retain most of the moisture carried by winds from the Pacific. The steppe continues eastward with bushes species such as the neneo (Mulinum spinosum).

Figure 5.8. View of the Valley of Senguerr River at the crossing with National Route 40. This is a very common landscape at the south-western corner of Chubut Province. The morphology is quite simple, large plains cut by wide valleys (canyon-cutting during mid Pleistocene). The rock basement is composed of sedimentary rocks (tuff, sandstone, claystone) that are recognized in the hillslopes. Covering the latter formation there are the Patagonian Gravels, a stratum of cobles, gravels and sands transported and deposited by huge streams during glacial smelt (outwash). Tthe current floodplain of Senguerr River extends at the center of the picture.

The population of this large basin is really scarce. There are three main towns: Sarmiento (8.028 inhabitants), Paso Rio Mayo (2.939 inhabitants) and Alto Rio Senguerr (1.454 inhabitants). The main economic activity is cattle farming (cows and sheeps).

5.3.5 Geological setting

A description of the lithologies present within each catchment would not be useful, not only because of the large extensions involved but also because in all the extra-andine streams the current valley filling material (and hence involved in sediment transport) is not related to those in the surrounding. This lack of correspondence is due to the huge work done by glaciers during the Pleistocene that carried material from the cordillera into the pre-cordillera basins.

The Cenozoic sedimentation is tightly related to the interaction between glaciations and the Andine orogenesis, and it must also be added the sea transgression owing to the glacial-eustatism and to the movement of the continental plate. The huge volume of material transported and deposited by the action of glaciers was then reworked by rivers at different periods. The interglacial periods provided the water discharge needed for transporting sediment and hence to shape the valleys which now seem out-of-scale with regards to current streams (Figure 5.8). The Patagonian territory is crossed by these valleys from west to east with several terraces levels (with structural and fluvial origin). The Upper Cenozoic deposits cover an area of 600,000 km^2 aprox. although their thickness is not of relevance.

A good example of the aforementioned sedimentary discrepancy is observed in the valleys of Lepa and Gualjaina rivers, which are placed eastwards the Cordillera, in the so called Pre-cordillera region. The local basement is composed of Tertian material such as volcanic rocks (andesite, basalt, rhyolite, etc) and sedimentary rocks (tuff, claystone, siltstone and sandstone). However, the gravels and sands found in the valley are related to volcanic and plutonic rocks from the western basins.

Therefore, only general indications can be given for the lithologies found in the mountain basins. Within the Puelo River basin there are outcrops of granitoids, mesosiliceous vulcanite and some marine sediments. In the Futaleufú River basin predominates the granitoids and the mesosiliceous vulcanites. With regards to the Senguerr River basin, glacial deposits predominates all over the basin but at the headwater of Senguerr River (Fontana Lake) there are outcrops of sedimentary rocks (marine and continental) and vulcanite to a lesser extent.

Patagonian Gravels ("Rodados Patagonicos")

This formation occupies a wide area of more than 450,000 km^2, covering most of Patagonia Extrandina. Deposits are composed of cobbles, gravels and sand, generally known as "Patagonian Gravels". The oldest sediments are due to piedmont aggradations, but the younger are associated with glaciations mainly those of the Upper Tertian. The formation is recognized in the field as a wide fluvio-glacial plain (outwash) which extends from the mountain range up to the Atlantic Ocean. Because the distribution of glaciers was not uniform along the Patagonian Cordillera the origin of the formation has been linked to glaciations in the south and piedmont in the northern Patagonia.

It is necessary to differentiate between the Patagonian Gravels from those deposits clearly related to fluvial processes that constitute the terraces systems of most of the biggest rivers in Patagonia (Colorado and Negro rivers in Rio Negro Province; Chubut, Chico and Sengerr rivers in Chubut Province; and Deseado, Santa Cruz, Gallegos rivers in Santa Cruz Province), and the deposit of the floodplains. But, the fluvial deposits (post-glaciations) are tightly related to Patagonian Gravels because the latter has provided all the sediments that has been later reworked by rivers.

Chronology of glaciations

The southern Andes have been repeatedly glaciated during the Late Cenozoic times. The Patagonian Andes were glacier-covered sometimes ca. 4.6 Ma BP and icefields expanded repeatedly between 2,4 and 1,2 Ma BP. The greatest Patagonian glaciations developed during the Early Pleistocene, contrary to the global pattern. In the southern Patagonia, glaciers advanced up to 200 km east of the mountain front and reached the Atlantic continental shelf; they terminated also on the Pacific shelf south of latitude 43°S. The ice formed a continuous mountain ice cap all along the Andean crest south of the Chilean lakes region and discharged immense outlet gravels which had formed as the mountain became uplifted in the Late Tertiary (Rabassa and Clapperton, 1990).

The mid Pleistocene may have been characterized by a prolonged interglaciation or else by smaller scale glaciations, but this interval was apparently disturbed by a strong pulse of uplift which led to the canyon-cutting event. This led to the evolution of the modern landscape as the piedmont zone with its cover of Patagonian Gravels, and glacial deposits became deeply dissected. Subsequent glaciations, in the later Pleistocene, had to follow this new drainage network. The principal discharge of the icefields was now through a large number of outlet valley glaciers.

The last glaciations appear to be direct equivalents of the early Wisconsinan, Late Wisconsinan and late-glacial stades of the northern hemisphere and may date to the intervals ca. 70.000, 20.000 - 18.000 and 15.000 – 10.000 BP. This last glaciation has been named Nahuel Huapi in Argentina and Llanuinhue in Chile.

The early late-glacial interval is clearly represented by moraines throughout the southern Andes (15.000 – 14.000 BP). The subsequent advance which culminated elsewhere in the world's mountain regions at ca 11.005 – 10.000 BP may be absent around much of the Patagonian icefields if they had become severely reduced in size during the preceding interstadial.

Most glaciers in southern Andes fluctuated during the Holocene Neoglacial intervals and some of the large debris-covered glaciers and rock glaciers of the Mendoza Andes formed at this time. Three major fluctuations of Patagonian icefield glaciers in the last 5.000 years have been dated. Studies carried on in Northern Patagonia have established a precise chronology for the "Little ice age", the last fluctuation that took place during XVI and XIX centuries.

5.4 Verification of stability of natural rivers

Rivers in Patagonia were selected as a reference population of undisturbed streams. Because gauging stations are not placed near urban centers and besides there is almost no economic activities in the corresponding upstream basins, disturbances due to human interventions are virtually null. Therefore, the natural characteristic should be guaranteed. However, a verification of stability was performed. A stream has been considered stable if the selected morphologic parameter remained statistically constant during the observation period (see definition of steady state, section 1.7). Width was chosen as the morphologic parameter because the experience gained in Italian rivers indicates that width is a sensible feature in gravel bed rivers that adjusts quickly in response to disturbances in upstream sediment supply. The comparison consists of plotting the hydraulic geometry (width-discharge plot) for two different periods. Figure 5.9 shows the analysis performed for each Patagonian stream considering periods 1990-1999 and 2000-2007. Almost all the reaches exhibit a good superposition of data indicating that there have not been morphological changes during, at least, the last 20 years. However there are some cases that deserve further analysis.

Table 5.5, shows the result of the statistical analysis. It was tested the null hypothesis that the regression lines fitted to each period were identical, or there was no difference at all[12]. The p-value for Quemquemtreu, Chubut and Epuyen rivers is below 0,01 and hence there is significant difference between regression lines. In the three cases the most recent regression line is below the oldest line indicating that a channel narrowing has taken place at the gauging station. However, it seems not reasonable that the channel actually experienced a narrowing tendency, being this attributed to the growth of thick vegetation on the banks that has reduced the effective flow area and hence as the flowing width is actually measured, it seems as if the channel has got narrower. Figure 5.10 illustrated this point with two photographs of the current situation at Chubut River and Quemquemtreu River gauging stations.

[12] For a detailed exposition of the statistical procedure see section 7.2.

Cohihues Creeks exhibit wide scatter in the hydraulic geometry and a very low p-value. This situation is due to a strong morphological activity observed in this stream that changes channel regularly eroding banks and forming new deposits.

Table 5.5. Statistical test conducted for assessing the stability of gravel bed rivers in Patagonia. The p-values are the result of stating the null hypothesis that the regression models for each dataset (periods 1990-1999 and 2000-2007) are identical.

Stream	p-value	Stream	p-value
Azul River	0.29	Gualjaina River	0.614
Quemquemtreu River	$2.8 \cdot 10^{-30}$	Mayo River	0.361
Carrileufu River	0.052	Lepá Creek	0.194
Chubut River	0.001	Cohihues Creek	$1.6 \cdot 10^{-5}$
Epuyén River	$5.9 \cdot 10^{-6}$	Alto Chubut River	0.090

The hydraulic geometry of Alto Chubut River shows two different curves, although the p-value is not small (0,09). This change is due to the displacement of the cross section used to measure discharges because it was not possible the access to the previous location after a large flood

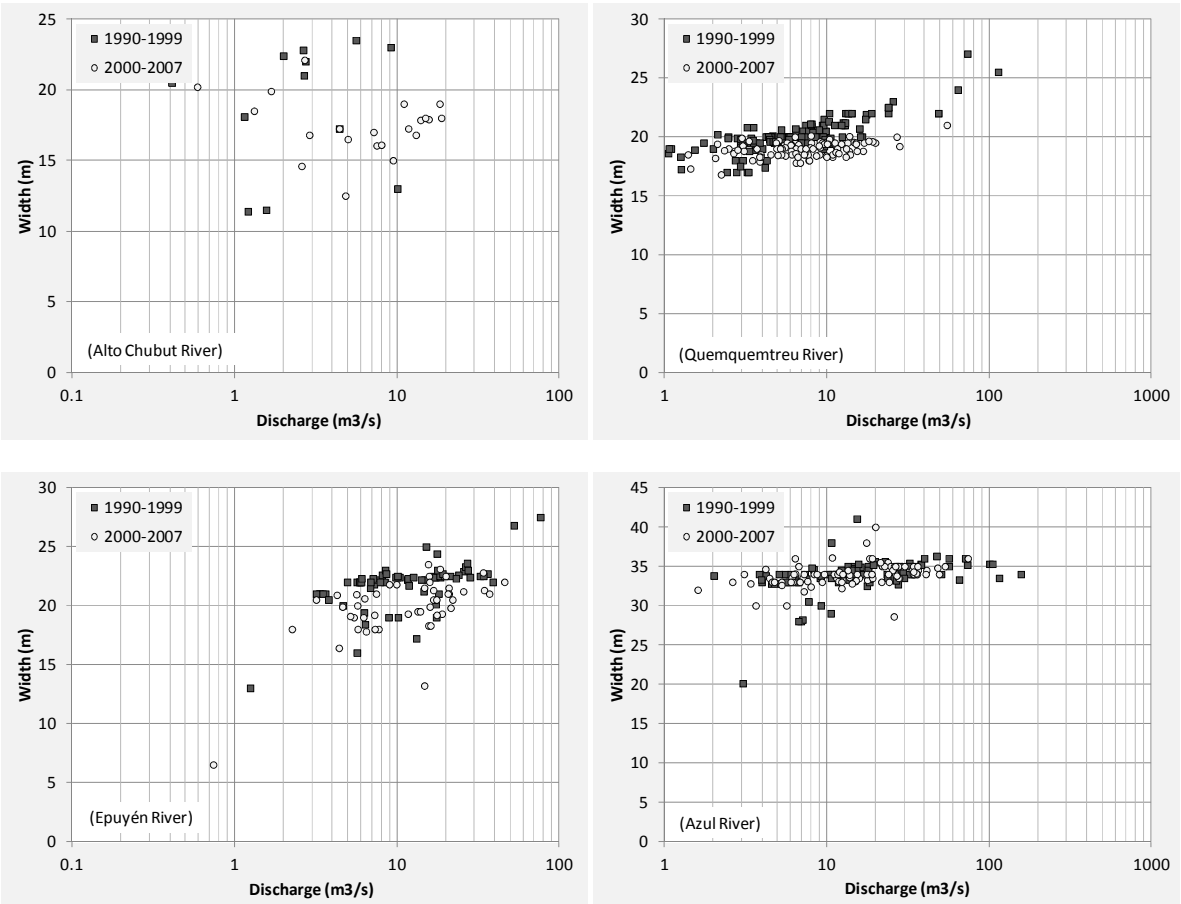

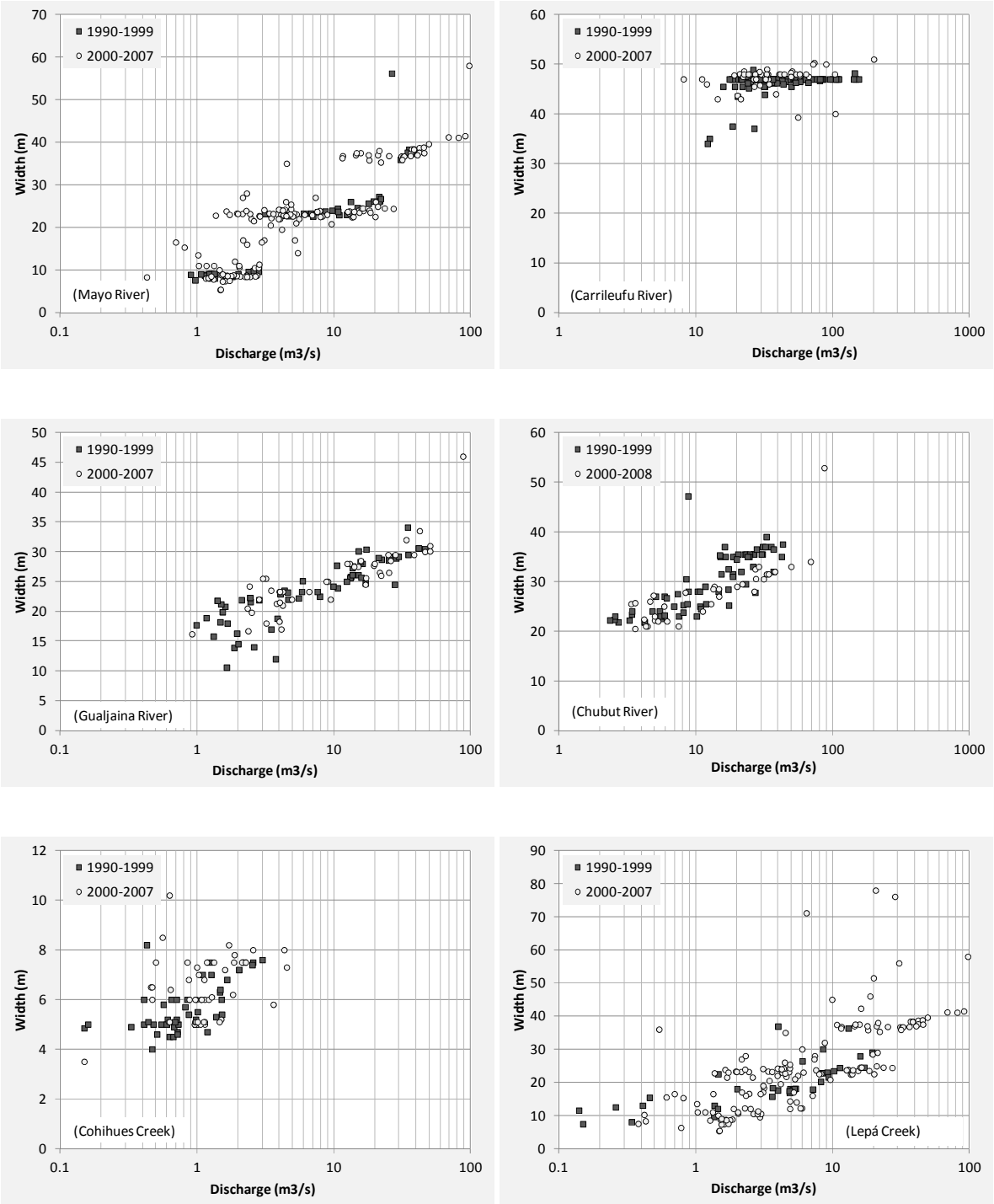

Figure 5.9. Verification of steady state condition in gravel bed rivers in Patagonia (Argentina). Plots show the hydraulic geometry using width-discharge relations for two time spans 1990-1999 and 2000-2007. The superposition of points of both periods indicates that there have not been morphological changes, at least in the cross section at the gauging station. It is worth to underline that all the gauging stations are placed in alluvial reaches.

Figure 5.10. The presence of trees along the reach where the gauging stations are placed (Left: Chubut River at El Maiten; right: Quemquemtreu River) may be the reason in the reduction of “effective width” as results from the records (see also Figure 5.9)

6 MATERIALS AND METHODS

One of the major sources of scatter in results comes from methodological differences. This noise makes difficult to compare data from different studies because it is not clear if scatter in hydraulic geometry plots has to be attributed to actual natural variability (within and between reaches) or not. Therefore, in this section I will present a detailed description of the methodology employed when surveying and computing geometric parameters. Another important aspect to take into account is the variability of each parameter. It is common that a parameter changes along the reach. For instance, the width is higher at riffles and lower at pools or mean cross section grain size distribution is coarser at riffles and finer at pools. Then, when computing reach-average parameters some information is lost; one single values stands for a continuous variation of the variable. One way to have an idea of this variation is computing the confidence interval for the variable or the extreme percentiles (let's say 2,5% and 97,5%). This section also contains the criteria assumed for evaluating the confidence intervals that have been specially adapted for each parameter.

6.1 Variable definitions and field methodologies

Each reach can be described with a minimum information consisting of width, mean depth, slope, surface median diameter, bankfull discharge and friction factor f. For this purpose five cross sections have been surveyed along a whole wave length comprising three riffles and two pools. The selected reach starts and finishes at a riffle and consequently it covers a sequence riffle-pool-riffle-pool-riffle (Figure 6.1). The pool cross sections have been placed at the deepest location when possible and riffle cross sections have been placed in the highest location, that is, at the riffle's head. This methodology has already been employed by Hey and Thorne (1986).

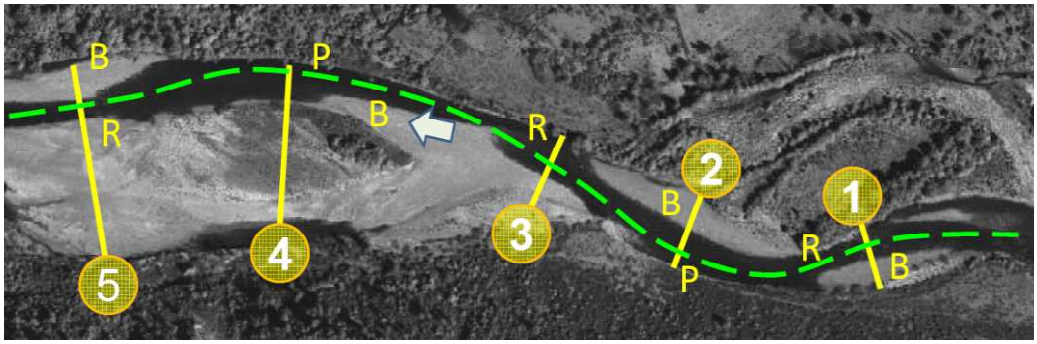

Figure 6.1. Example of cross section definition along a river reach (Azul River, Argentina). The location of each cross section corresponds to a morphological unit: (R) riffle; (P) pools. In the figure lateral bars are also indicated (B) and the water flow is from right to left.

6.1.1 At-a-station variables

For each cross section the width, mean depth and surface grain size have been measured. In the case of width and mean depth, it is necessary to recognize and measure the bankfull level. Then, with the aid of the cross section that has been surveyed, it is possible to evaluate all the geometric variables: width, area, mean depth equal to the ratio of area and width, and wetted perimeter.

Surface grain samples have been taken for each cross section in order to describe the riffle-pool variability and for evaluating after that the reach average distribution. Due to the presence of water a traditional grid sampling procedure would be cumbersome so, it was preferred to apply the random walk approach (Wolman, 1954). The sampling area comprises the cross section and the surrounding area some meters downstream and upstream, extending along the cross section up to the bankfull level. For each cross section a minimum sample of 120 gravels has been taken, summing a total sample of 600 gravels for the whole reach, that is above the minimum of 400 stones suggested by Rice and Church (1996). Special care was taken for covering all the bankfull area and to sample in a uniform manner all the sectors so as to ensure representativeness.

6.1.2 Reach average values

In order to have a mean value of the variable along the reach the weighted mean has been calculated from the at-a-station values. This is the case of geometric parameters and the mean velocity. The weighted mean has been derived from the general integral definition of mean value for continuous variables:

$$\bar{y} = \frac{1}{L}\int_0^L y \cdot dx \qquad 6.1$$

Where L is the reach length, x is the downstream distance and y, the variable to be evaluated. The simplest way to approximate the integral, when only discrete data is available, is applying the trapezoidal rule.

$$\bar{y} = \sum_{i=1}^{5} p_i y_i \qquad 6.2$$

Where p_i are the weight factors:

$$p_1 = \frac{x_2 - x_1}{2L} \qquad 6.3$$

$$p_k = \frac{x_{k+1} - x_{k-1}}{L} \qquad 6.4$$

For k = 2, 3, 4. Instead, for the last value it is:

$$p_5 = \frac{x_5 - x_4}{2L} \qquad 6.5$$

The general variable y stands for any of the cross section geometric parameters: width, depth, hydraulic radius, flow area, ecc. In the case of the grain size distribution a special care was taken for computing the reach average distribution. Firstly, partial frequencies were calculated for each cross section, and then, for each partial frequency the weight average was evaluated (in eq. 6.2, “y” stands for each partial frequency of each grain size class at a time).

The mean friction factor has been calculated considering reach average values. The average velocity is calculated considering the mean value of the inverse area because it usually differs from the inverse of the mean area. The hydraulic radius is calculated for each cross section and then the mean value is taken:

$$\bar{U} = Q\overline{A^{-1}} \qquad \overline{R_H} = \overline{\left(\frac{A}{P}\right)} \qquad 6.6$$

It is worth to note that these averages have to be evaluated following the weight rule (eq. 6.2 – 6.5).

The friction factor has been evaluated applying the Darcy-Weissbach formula:

$$f = \frac{8g\overline{R_H}S}{\bar{U}^2} \qquad 6.7$$

The reach slope deserves a special consideration. For this research I have also followed Hey and Thorne (1986) criterion that consists of evaluating the slope from the bankfull levels. In this case a lineal regression model is applied to the sample composed of downstream values (x) and corresponding bankfull levels (y). The slope of the water surface was chosen because it is meaningful for further hydraulic calculus (shear stress, stream power, ecc).

6.1.3 Bankfull discharge

The determination of the bankfull discharge requires a specific procedure. It has been standardized by Leopold (1994, p. 133) and here a summary is presented. First, the thalweg profile was surveyed in order to evaluate the downstream distance (x). The selected reaches were visited looking for bankfull levels indicators. Both banks were inspected and more than one indicator were applied when possible. Usually indicators were the maximum elevation at point bars, and the inflection point in banks. The bankfull level was measured and the presence of terraces was verified so as to avoid confusing them with the flood plain. When present, terraces were also surveyed. It was also necessary to measure the elevation of the zero reading of the gauging plate. Finally, the channel bottom with the bankfull and terraces levels were plotted in the longitudinal profile. A regression analysis was performed for bankfull levels data and then the bankfull level at the gauging station was estimated. Knowing the elevation of the zero plate the bankfull height was calculated and finally the bankfull discharge came from the relationship between height and discharge (rating curve).

With regards to Italian rivers, it was necessary to apply a different methodology. Gauging stations were placed in non alluvial river reaches or near barrages. Therefore, there were neither morphological indicators nor suitable conditions to apply Leopold's criterion. Instead, the bankfull discharge was estimated by direct observation. For Piave River photographs records of flood events near the gauging station at Belluno were studied. The bankfull discharge corresponded to the daily mean discharge of the selected day for which the bankfull stage was achieved. After that, its return period was calculated and assumed valid for the other reaches (within the basin). The corresponding bankfull discharge was evaluated from the frequency analysis at each gauging station. In the case of Brenta River measured levels during flood events were available (instead of photographic document). The same aforementioned procedure was applied

6.2 Characterization of variability

Mean values describe the main properties of the reach: width, depth, grain size distribution, etc, but it is also useful to know the variability of these parameters. There are two kinds of variability. There is a spatial variability due to the variable variation along the streamwise direction; this is the case of the width and depth. A second kind of variability regards bankfull discharge. It is not intended as the variability of discharges, but the uncertainty in its determination due to uncertainties in the identification of bankfull levels and the temporal variation in the rating curve. A special problem

arises for the surface grain size distribution. Here there is a spatial variability, as pools tend to have finer material than riffles and a statistical uncertainty in the reach-averaged grain size distribution due to a finite sample. Each situation will be analyzed in details in the following sections.

6.2.1 Confidence interval for geometric variables

Both mean depth and width vary from one section to another. Let's suppose that the cross-section location has been chosen randomly. There is a certain probability to measure a width B, which would be in the range B_{min} – B_{max}. This probability has been calculated as the division between the reach length for which $B_{min} < B < B_{max}$ and the total reach length. In a practical way, width values are sorted from lower to higher and then the accumulated frequency curve results from summing all the distances for which the width is equal to or smaller than a certain value B and dividing by the reach length. Then, this curve is used for calculating the percentiles $\alpha/2$ and $1-\alpha/2$ that define the confidence interval (with a confidence level α).

The confidence interval for the slope has been evaluated considering that this variable has been calculated by means of a regression model. The standard error of the regression coefficient b (the slope) is:

$$s_b = s_e \sqrt{\frac{1}{\sum_{i=1}^{N}(x_i - \bar{x})^2}} \qquad 6.8$$

where s_e is the standard error of the estimation that will be defined later (eq. 6.17). The parameter b follows a t-Student probability distribution, then, the confidence interval with a significance α is:

$$b \pm t_{\left(\frac{\alpha}{2}, N-2\right)} s_b \qquad 6.9$$

wherein t is the reduced variable with a t-student distribution and N-2 degress of freedom.

6.2.2 Confidence interval for bankfull discharge

Let's consider two populations: one for the independent variable x (the downstream distance) and the dependent variable y (bankfull elevation minus the zero reading elevation at the gauging plate). Y is a random variable, therefore, for each x there can be more than one possible y. Assuming that the variation in y can be explained by the variation in x with a linear model then for a particular value of x the mean value of y ($\mu_{y,x}$) can be expressed as:

$$\mu_{y,x} = \alpha + \beta \cdot x \qquad 6.10$$

where α and β are coefficients. But as the population is not known an inference from a sample has to been made. The regression model for the sample is:

$$y^* = a + b \cdot x \qquad 6.11$$

In this case, a and b are the best estimations for α and β. Both the mean value of y and a particular value of y for a given x are estimated with y*. Applying the minimum squared difference between true and estimated values of y, it is possible to arrive to the following expression for a and b:

$$b = \frac{s_{xy}}{s_x^2} \qquad a = \bar{y} - b\bar{x} \qquad 6.12$$

wherein s_{yx}^2 is the sample covariance and s_x^2 is the variance of x:

$$s_{xy}^2 = \frac{\sum_{i=1}^{N}(x_i-\bar{x})(y_i-\bar{y})}{N-1} \quad 6.13$$

$$s_x^2 = \frac{\sum_{i=1}^{N}(x_i-\bar{x})^2}{N-1} \quad 6.14$$

For a particular x, let's say the progressive at the gauging station x_g, it is possible to make a point prediction of y (let's call it y_g^*) using the lineal regression model:

$$y_g^* = a + b \cdot x_g \quad 6.15$$

Furthermore, it is also possible to make a prediction of the interval for y_g^* if it is assumed that y has a t-student probability distribution around the mean value. This distribution is used when the sample is small; otherwise the normal distribution is applied. Then, the standard error for the prediction of a particular value of y is:

$$s_{fy} = s_e \sqrt{1 + \frac{1}{N} + \frac{(x_g-\bar{x})^2}{(N-1)\cdot s_x^2}} \quad 6.16$$

where s_e is the standard error of estimation:

$$s_e = \sqrt{\frac{\sum(y_i-y_i^*)^2}{N-2}} \quad 6.17$$

It follows that the standard error of prediction will be greater if the gauging station is placed at the ends of the selected river reach. In order to minimize this error the river reach should be defined so as to leave the gauging station placed in the middle of the reach (that is near the mean value of x). Finally, the confidence interval for y is estimated considering confidence level α:

$$y_g^* \pm t_{\left(\frac{\alpha}{2};N-2\right)} s_{fy} \quad 6.18$$

Where t is the reduced variable with a t-student distribution and N-2 degrees of freedom.

The same analysis is applied to the next two populations: the elevations, y, and discharges, Q. In this case there are two problems, y is not an independent variable and the relationship is not lineal. The first step consists of transforming the non-lineal problem into a lineal one. Usually, Q is given in terms of a quadratic function of y. Considering a sample, the best estimation of the real Q and mean value of Q for a given "y" is:

$$Q^* = a + b \cdot y + c \cdot y^2 \quad 6.19$$

Defining the variable z as:

$$z = \left(y + \frac{b}{2c}\right)^2 \quad 6.20$$

The quadratic function reduces to a linear relationship:

$$Q^* = A + B \cdot z \qquad 6.21$$

Where

$$A = a - \frac{b^2}{4c} \quad \text{and} \quad B = c \qquad 6.22$$

In the same way as done previously, it is possible to calculate the standard error of estimation (s_e) and the standard error of prediction for Q (s_{fq}), and Q will have a probability distribution around the point estimation Q_g^* for a given y_g. In this way the best estimation of Q comes from the best estimation of y for x at the gauging station. But the calculus of the confidence interval for Q has to consider de variability of both y and Q, i.e., the composed probability of every y and Q. The probability that Q is between two arbitrary values Q_a and Q_b is:

$$P(Q_a \leq Q \leq Q_b) = \int_{t_a}^{t_b} \int_{-\infty}^{+\infty} f\left(t; N_y\right) \cdot f\left(w(s); N_Q\right) \cdot dt \cdot ds \qquad 6.23$$

Where f is the density function for the t-student probability distribution; N_y , N_Q are the degrees of freedom for y and Q (the size of each sample minus two) and the other terms are evaluated in the following way:

$$w(s) = \frac{Q_o - Q(s)}{s_{fQ}} \qquad 6.24$$

$$Q_o = Q_g^* + s_{fQ} \cdot s \qquad 6.25$$

$$y_s = y_g^* + s_{fy} \cdot s \qquad 6.26$$

Q(s) and Q_g^* are calculated from y_s and y_g^* using the quadratic regression model. In the same way, t_a and t_b can be back calculated from Q_a and Q_b . For example, in equation 6.25 Q_0 is replaced by Q_a and s by t_a .

The product inside the integral (eq. 6.23) is the composed probability: the product of the probability to find one y for a given x in a surrounding interval dy (dt in the reduced variable) and the probability that Q is in a surrounding interval dQ (ds in the reduced variable) considering the best estimate of Q from that y.

6.2.3 Confidence interval for surface grain size distribution

The grain size distribution of surface material changes along the stream. Usually riffles are coarser than pools, and hence a good representation would consist of showing mean distributions for each sector. Instead, in the case of the reach average percentiles, such as D_{50}, the problem is different. In this case it is necessary to calculate the uncertainty of this estimation and one way to do this is using the bootstrap method. This approach was developed by Efron (1979) and has the advantage that it does not assume any particular probability distribution for the parameter to be estimated.

The starting point is a sample with N numbers "x": Sn = {x_1, …, x_N}. Let's T be a statistic parameter of the sample. Then M samples are taken with replacement each one with size N from the original sample Sn. For each sample the statistic of interest (t) is calculated resulting in a set of M values: {t_1,

…, t_M}. The distribution of these values is called the "empirical bootstrap distribution". This distribution has two important properties: a) its standard deviation is the bootstrap estimation of the standard error of T; b) the percentiles $\alpha/2$ and $(1-\alpha/2)$ of this distribution are the limits of the bootstrap confidence interval for the parameter T, with a confidence level $1-\alpha$.

It follows that the bootstrap method can be applied to evaluate the confidence interval of each percentile D_x (for example, x = 16, 50 and 84).

6.3 Dimensionless parameters and spread of uncertainty

A normal practice in experimental research is the use of dimensionless parameters. Grouping several variables reduces the number of variables and the amount of work needed to explore their dependence. For the present study six variables has been considered: width (B), depth (H) slope (S) discharge (Q) acceleration due to gravity (g) and a representative grain diameter (D). Slope is already a dimensionless parameter so there remains 5 variables. As the number of dimensions is two (length and time), it is possible to define three independent dimensionless parameters. These parameters can be defined with two repetitive variables and one independent variable. Known dependent variables (H and B) should not be considered as repetitive variables. The choice of the repetitive variables has not always been the same. If two kinematic variables (g and Q) are chosen, the dimensionless parameters that results are:

$$\mathrm{H}' = Hg^{1/5}Q^{-2/5} \tag{6.27}$$

$$\mathrm{B}' = Bg^{1/5}Q^{-2/5} \tag{6.28}$$

$$\mathrm{Q}' = Qg^{-1/2}D^{-5/2} \tag{6.29}$$

These are the parameters employed by Parker et al. (2007). Another more widely used alternative consists of taking a geometric and a kinematic variable; let them be D and g (Millar, 2005). The corresponding dimensionless parameters are:

$$\mathrm{H}^* = HD^{-1} \tag{6.30}$$

$$\mathrm{B}^* = BD^{-1} \tag{6.31}$$

$$\mathrm{Q}^* = Qg^{-1/2}D^{-5/2} \tag{6.32}$$

In both cases one independent variable (D or Q) remains in all the parameters. In this study dimensionless parameters are used to compare data with different scales, that is, from large gravel bed rivers to small laboratory flumes. I preferred the second alternative because different types of variables, geometric and kinematic, are included (see also Shames, 1995, p.290).

Because variables involved in the definition of dimensionless parameters are subjected to natural variability, it is also possible to define their confidence range. Furthermore, the origin variables (H, B, D) do not have known theoretical probability distributions, but empirical distribution from field surveys. Therefore, a Monte Carlo approach is best suit for this problem: a large number (10.000) of random values for H, B, Q and D_{50} are generated following the empirical distributions and

dimensionless parameters are calculated. Their confidence interval is then evaluated from the corresponding cumulated frequency functions.

6.4 Calibration of friction factor

The friction factor can be estimated for the whole river reach by calibration using one-dimensional models, instead of using mean geometric values and assuming uniform flow (as has been presented in Section 3.5). The one-dimensional model assumes a steady state gradually varied flow. The governing principles are the energy conservation and the mass conservation (Figure 6.2). They can be stated in the following way:

$$y_1 + \frac{\alpha_1 U_1^2}{2g} = y_2 + \frac{\alpha_2 U_2^2}{2g} + S_{f1,2} L \qquad 6.33$$

$$Q_1 = Q_2 = Q \qquad 6.34$$

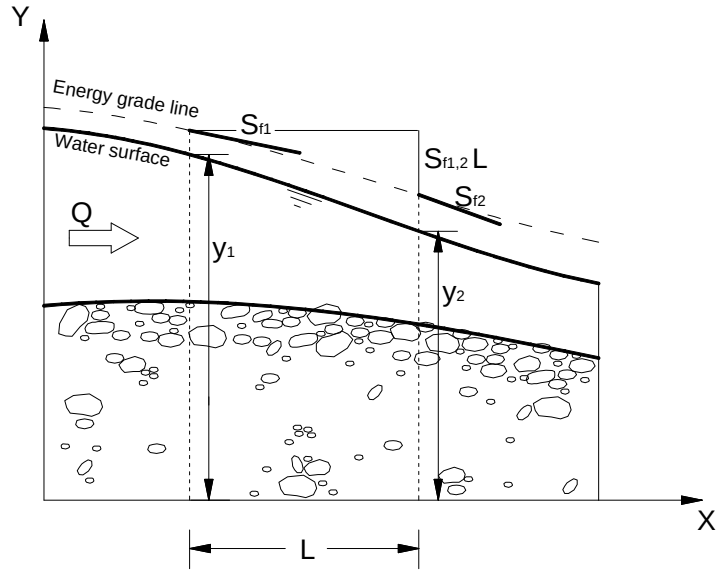

Figure 6.2. Open channel energy relationships for one-dimensional modeling.

Where α is the Coriollis coefficient, y is the water surface elevation, $S_{f1,2}$ is the unit length energy loss between sections 1 and 2, L is the distance between cross sections, and U is the mean velocity, and Q is the discharge. The first equation comes from the energy conservation principle, while the second one is the continuity equation which simply imposes the constancy of discharge along the reach. Equation 6.33 is solved for each cross section assuming a horizontal transversal water surface. The energy loss is evaluated using the Darcy-Weisbach formula.

$$S_f = f \frac{U^2}{8 g R_H} \qquad 6.35$$

Where S_f is the energy slope, $R_H$is the hydraulic radius and f is a friction factor. Because a mean energy slope between two cross sections is required, the geometric mean is taken:

$$S_f = \sqrt{S_{f1} S_{f2}} \qquad 6.36$$

The boundary condition is applied at the downstream where the measured bankfull stage is imposed. For the other four cross sections, water surface elevations are computed solving eq. 6.33 with eq. 6.36, and using a numerical method (such as Newton-Raphson).

The calibrated friction factor is the one that minimized the squared deviations (SD):

$$\mathrm{SD} = \sum_{i=1}^{4}\left(y_i^{calc} - y_i^{obs}\right)^2 \qquad 6.37$$

Figure 6.3 illustrate the calibration procedure with the case of the Azul River. It has to be underlined that the friction factor calibrated contains the effects owing to grain roughness and topography variability (bed form resistance). In particular, it is quite evident the location of riffle and pools in figure 6.3, and note that the water surface elevation is not linear but is affected by bed topography.

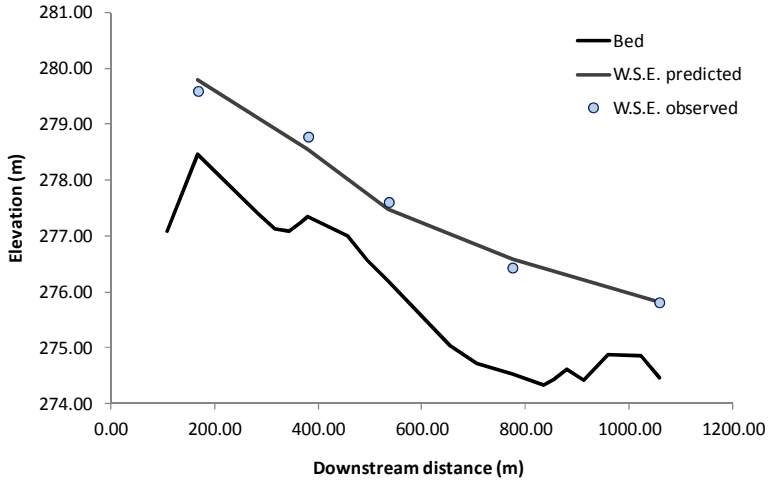

Figure 6.3. Example of calibration of the friction factor for a gravel bed river with a riffle-pool sequence.

7 COMPARISON BETWEEN NATURAL AND DISTURBED RIVERS

The aim of this chapter is to asses whether disturbed gravel bed rivers in Italy are significantly different than a set of river reaches in Patagonia that still preserve a pristine state (see Chapter 5). First of all, a brief comment on results regarding hydraulic variables is presented. Then, a comparison is made covering hydrological features (flow regime, bankfull events characteristics, the torrential nature and frequency analysis of extreme events), morphological features (shape factor and riffle-pool sequence) and sedimentological features (surface grain size spatial variability, degree of armouring and sediment supply). The reader is referred to tables A1, A2, A3 contained in Appendix A for further details of the mentioned parameters.

7.1 Hydraulic geometry variables

7.1.1 Bankfull discharge

There is a wide range of bankfull discharge in the selected streams. The lowest value is 19,5m^3/s (Cohihues Creek) and the highest is 350m^3/s (Brenta River). The amplitude of the confidence interval depends on the scatter in regression models: a) progressive-bankfull levels, and b) stage-discharge at the gauging section. Usually, the stage-discharge model had the largest scatter, and therefore its standard error was bigger. The best estimation, considering the narrowest confidence interval range, corresponds to Mayo River for which the extremes of the range are ±25% around the mean value, i.e., there is a 95% of probability that the bankfull discharge is between 31,9 and 51,2 m^3/s. The other gauging stations present wider ranges (see figure 7.2), for instance Chubut River at El Maitén (-76%, 334%) and Alto Chubut River (-60%; 192%). For these streams, Figure 7.1 illustrates the steps in the calculation of bankfull confidence interval showing a) the regression models for bankfull stages, b) the regression model for the rating curves and c) the probability density functions. With regards to Chubut River, it must be mentioned that the gauging station is placed 10 km downstream the study reach. At this place the river is confined by alluvial terraces and the banks are covered with thick vegetation (composed mainly of salix). Because good indicators of bankfull levels were not easily recognizable in the field, it is not surprising the low correlation coefficient obtained.

7.1.2 Bankfull width

At bankfull stage the narrowest stream is 8,0 m wide (Cohihues Creek) while the largest is 99,9 m (Piave River at Segusino). Mean width has a lower degree of variability. In general (Figure 7.2), there is a 27% variation around the mean value, with a minimum in Piave River at Perarolo (±11%). On the other hand, the largest variability is observed in Mayo River with a range: -46% + 99%.

7.1.3 Bankfull mean depth

This variable displays the same characteristics for the width. For the studied reaches the mean depth is between 0,27 m (Cohihues Creek) and 1,81 m (Carrifeufú River). In general, the confidence interval has the same range as the width; it is 30% around the mean value (Figure 7.2). The lowest variation is found in the Brenta River (-6% and 8%). Conversely, the Mayo river displays again the widest variation in depth (-49% to 91%).

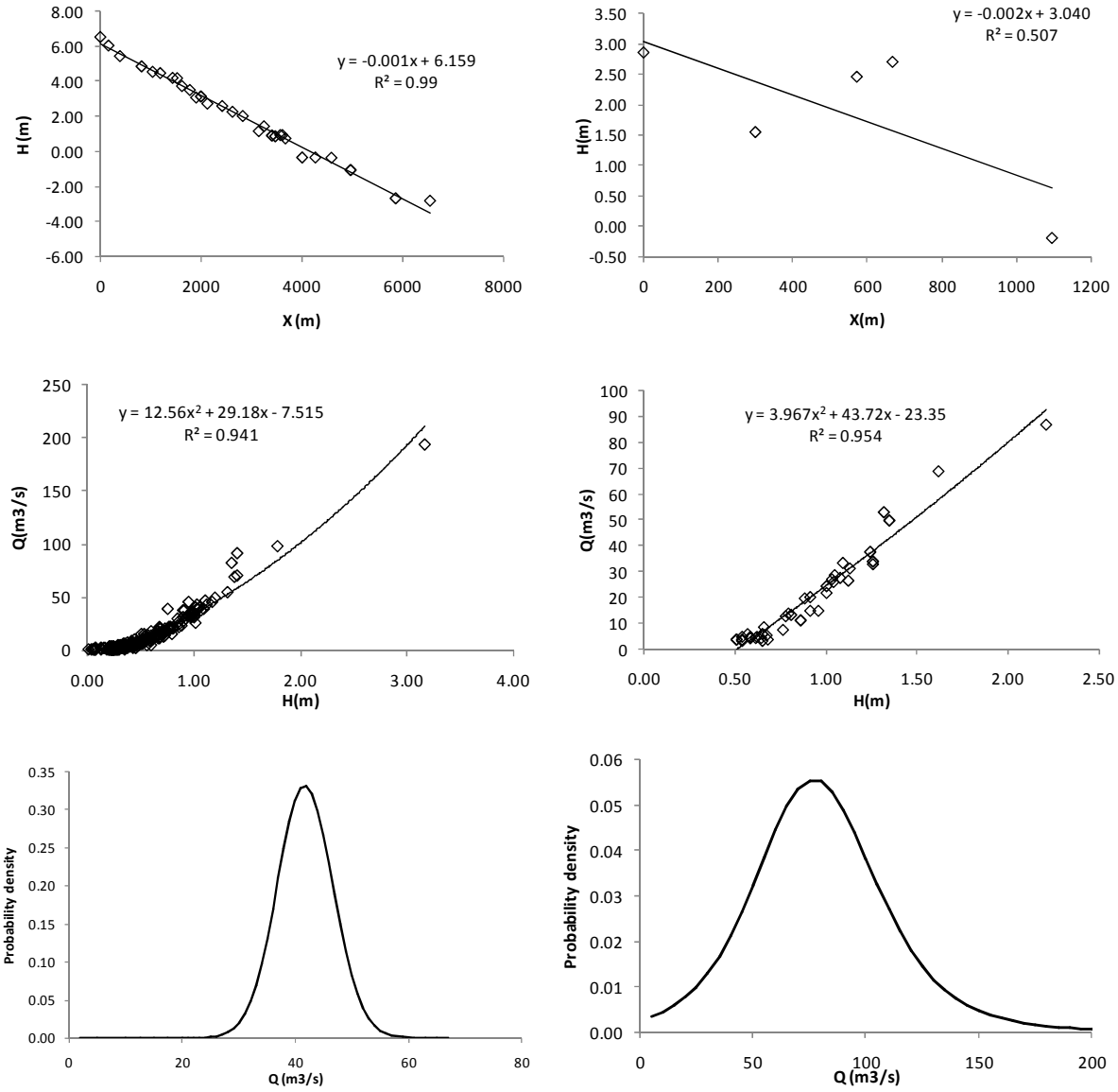

Figure 7.1. Calculation of bankfull discharge confidence interval, at Mayo River (left) and Chubut River at El Maitén (right). For each reach the bankfull stage-progressive regression model, the stage-discharge regression model, and the probability density curve are showed.

7.1.4 Slope

The error in this parameter is related to the uncertainty in bankfull level profile. The lowest confidence interval corresponds to Piave River (at Perarolo) with extremes ±4% around the mean value. On the other hand, the worst situation is found in Carrileufu River with ±44%. This wide range can be explained by the particular difficulties found in this reach for identifying the bankfull level due to the high density of vegetation cover (trees, bushes and grass). If this last case is excluded, it can be said that the mean range for the confidence interval is ±16%.

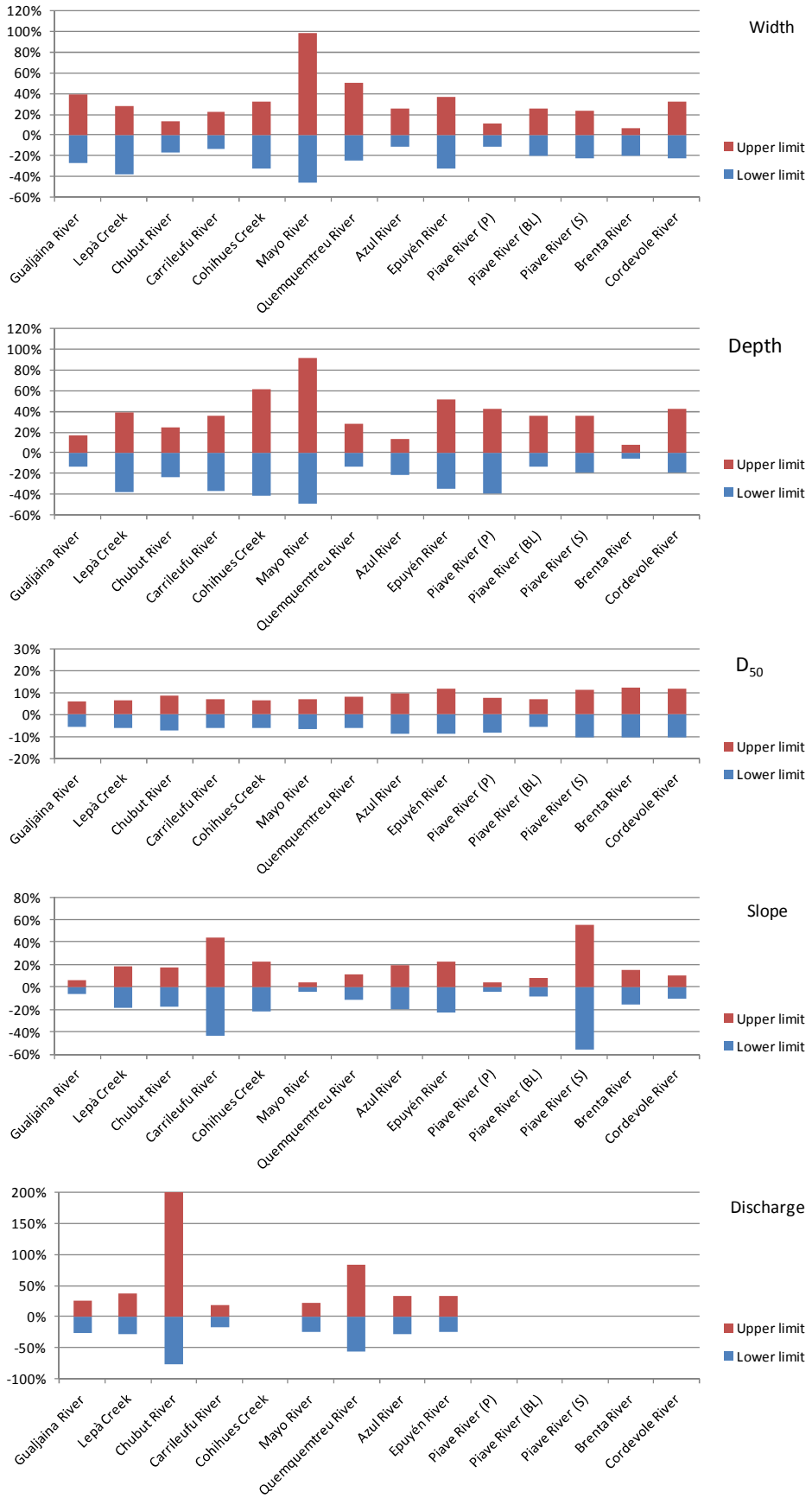

Figure 7.2. Confidence intervals (2,5% - 97,5%) for main stream parameters (width, depth, slope, median grain size and discharge). Confidence intervals are expressed relative to mean values.

7.1.5 Median surface grain size (D_{50})

The major source of surface grain size variability comes from the local sorting with fine material in pools and coarse material in riffles. Figure 7.3 shows the sedimentological data for Azul River, in Patagonia. The range is quite clear, the pool median diameter is 51mm (23% below the reach mean) and the riffle median diameter is 83 mm (24% above the reach mean). Now, considering the reach-averaged grain size distribution the confidence interval for the median diameter is lower, more or less 10% in Italian rivers and 7% for Patagonian rivers (Figure 7.2). An exception is represented by the Alto Chubut River that has a confidence interval with extremes -16% and +17%, because the sample is smaller (259 particles). The reach with the finest material is Gualjaina River with a median diameter 19,5 mm, while the coarsest reach surveyed is Alto Chubut River with a median diameter equal to 93,4 mm.

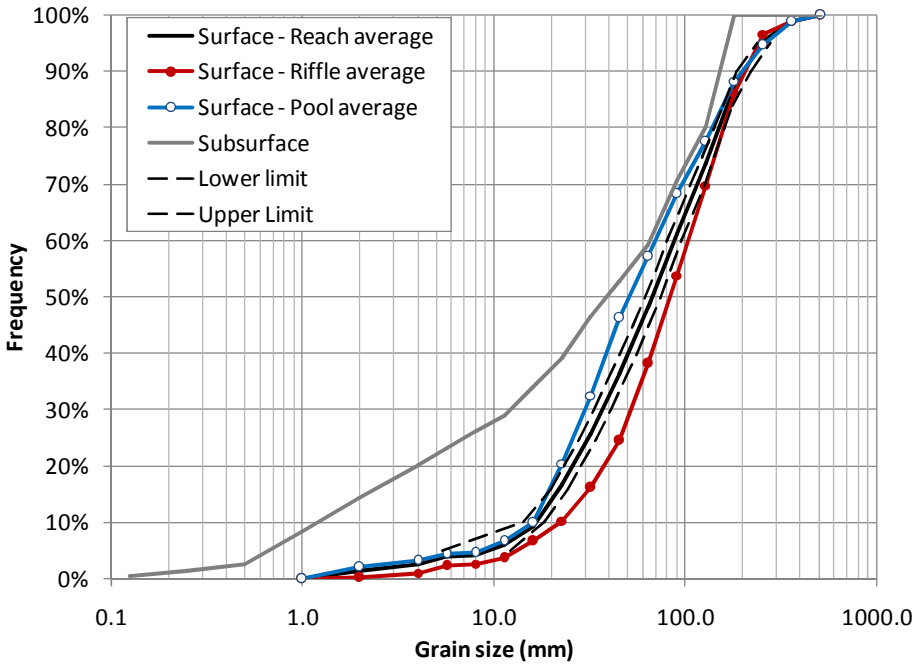

Figure 7.3. Example of grain size information of Azul River (Patagonia). For each studied river reach grain size distributions were evaluated for riffle areas, pools areas, reach-average with confidence intervals and subsurface material.

7.2 Dimensionless parameters

The scatterplots of hydraulic geometry parameters exhibit a wide spread of data even when parameters are transformed into logarithm units (Figure 7.4). Field evidence from this study indicates that variability in geometric parameters is not low and can be quantified by a confidence interval of ±30% around the mean (for a 95% of probability). Figure 7.4 also contains the confidence intervals for dimensionless parameters.

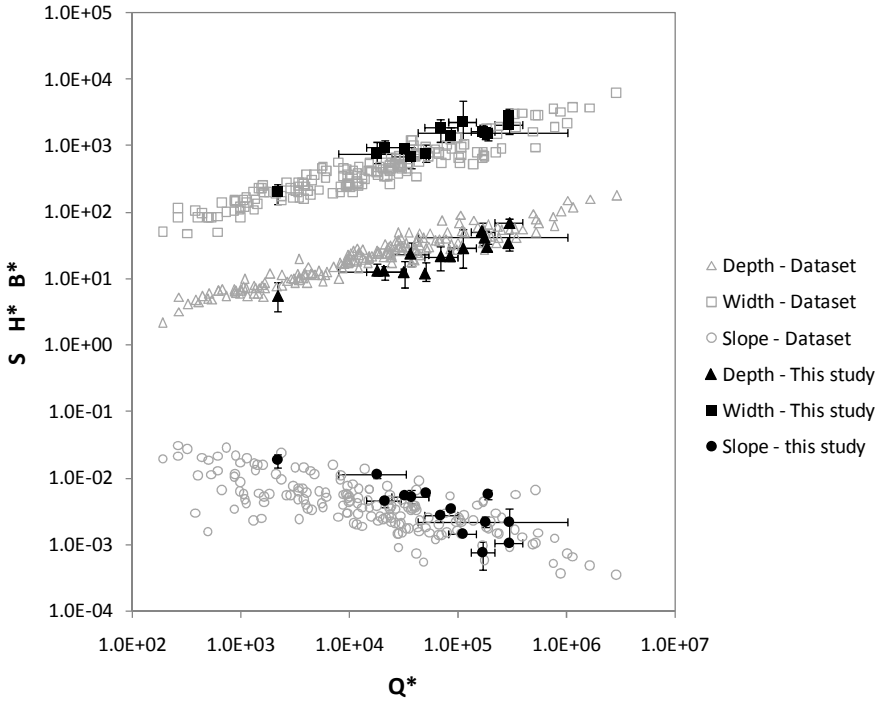

Figure 7.4. Scatterplot of dimensionless parameters for width B*, depth H* and slope S, against discharge Q*. The plot shows the dataset compiled by Parker et al. (2007) and from this study with indication of confidence intervals (95%).

Does the scatter in Figure 7.4 reflect the natural variability inside the river population or it is an uncertainty related to sampling methodology? In order to answer this question a simple t-test was performed with the new hydraulic geometry data. Considering the channel width, a regression model was applied so as to eliminate the dependence of width with dimensionless discharge. After that, for each reach there were 5 residuals and it was stated that their mean value was equal to zero (null hypothesis). As a result, 9 reaches out of 14 had mean values significantly different to zero (with $p<0.05$ but 12 out of 14 with $p<0.01$). Therefore, when considering 5 cross sections, the scatter seen in regime plots can be attributed to significant differences between river reaches.

It is quite evident in figure 7.4 that the width of the river reaches studied lie somewhat above the dataset compiled by Parker et al. (2007). On the contrary, the mean depth is below the aforementioned population. Considering the above result, that scatter is due to significant river reaches differences, it is necessary to test if the difference observed now between the populations is really significant. This verification is accomplished performing an analysis of covariance (ANCOVA). Firstly, a statistical model is constructed for the response variable (y), i.e., logarithm of width, depth and slope, in terms of the explanatory variables: the logarithm of dimensionless discharge (x) and a dummy variable (z).

$$y_i = \beta_0 + \beta_1 x_i + \beta_2 z_i + \beta_3 x_i \cdot z_i + \varepsilon_i \qquad 7.1$$

Wherein ε_i accounts for the random variation. The dummy variable takes a finite number of values (0, 1) such that each value represents a different group:

$$z = \begin{cases} 0 & for\ this\ study\ datset \\ 1 & for\ the\ reference\ datset \end{cases} \qquad 7.2$$

Two hypotheses are of interest the coincidence and parallelism of regression lines. The hypothesis of coincidence states that both slopes agree and also intercepts agree for the two regression lines of each population. Using model 7.1, the hypothesis is:

$$H_0 \ : \ \beta_2 = \beta_3 = 0 \qquad 7.3$$

If the hypothesis of coincidence is rejected, it is still interesting to test the hypothesis of parallelism that states that the slope parameters agree for the two populations, but the intercepts are allowed to differ. So, the null hypothesis is

$$H_0 \ : \ \beta_2 = 0 \qquad 7.4$$

Table 7.1 summarizes the results of each test performed for each hydraulic geometry parameter. Considering the width-discharge relation first, a very low p-value in the first test indicates that the null hypothesis is rejected and the two lines do not coincide. However, for the second test, the p-value is high and hence, lines are parallel (Figure 7.5). It means that width grows with the same rate in both populations, but the base-line is different for the two groups. A second model was fitted to the data: $y_i = \beta_0 + \beta_1 x_i + \beta_2 z_i + \varepsilon_i$. The result consist of two regression models (z=0 and z=1, respectively):

This study dataset: $B^* = 9{,}2Q^{*0{,}439}$ 7.5

Reference dataset: $B^* = 5{,}33Q^{*0{,}439}$ 7.6

The relation depth-discharge presents a similar situation (Figure 7.5). The null hypothesis about coincidence is rejected (p-value<0,01) but the hypothesis of parallelism is accepted. Again a second model can be fitted as has been done for the width:

This study dataset: $H^* = 0{,}28Q^{*0{,}394}$ 7.7

Reference dataset: $H^* = 0{,}41Q^{*0{,}394}$ 7.8

Finally, the slope-discharge relation has a p-value of 3,7% and hence, the null hypothesis cannot be rejected. Both populations are described by the same regression model.

$$S = 0{,}10Q^{*-0{,}331} \qquad 7.9$$

Table 7.1. P-value calculated for the different test performed. Hypotheses of coincidence and parallelism have been tested in all the relations: width-discharge, depth-discharge, slope-discharge, area-discharge, shape factor-discharge and depth-slope

	B* - Q*	**H* - Q***	**S - Q***	**Area* - Q***	**B/H - Q***	**H* - S**
H0 : Coincidence	8.9E-09	1.1E-06	0.037	0.052	1.2E-10	0.918
H0: Parallelism	0.760	0.149	0.071	0.088	0.838	0.942

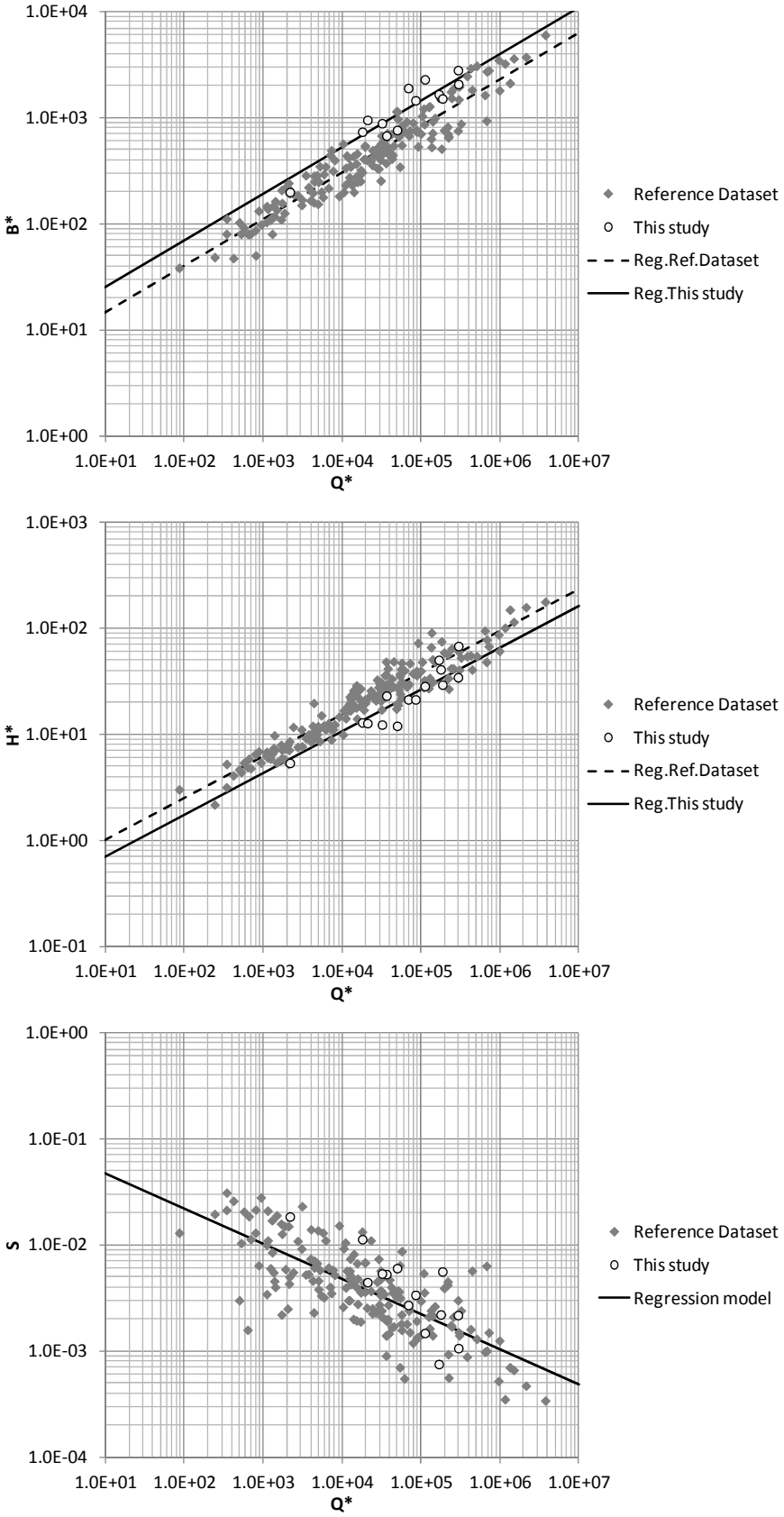

Figure 7.5. Comparison of regression models applied to the reference dataset (Parker et al. 2007) and that from this study.

As a final remark, table 7.1 also reports the analysis made for the dimensionless cross section area and the shape factor (width to depth ration). The analysis indicates that according to the methodology applied in this study, the studied river reaches tend to be wider and shallower ($p < 0,01$ for B/H relation) than the reference population. On the contrary, there are coincidences for the cross section area trend ($p > 0,01$) and also for the relation between dimensionless depth and slope ($p > 0,01$).

It is worth mentioning that methods other than used in this study have been used for assessing hydraulic geometry. With regards to those cited in this study, Hey and Thorne (1986) employed mean values from 5 cross sections, as has been used in this study; Andrews (1984) followed a similar criterion with 3 to 5 cross sections. The reaches selected from Mueller et al.'s (2005) work belongs to a previous study of King et al. (2004), who evaluated width and depth at bankfull stage from at-a-station relationships. However, it is not possible to state that differences relay on different protocols because subsequent analysis (see section 7.5.3) shows coherence between this study results and previous researches.

Because the aforementioned researches used the standard procedure for evaluation the bankfull discharge, it is reasonable to accept that reach average median grain size determination, and uncertainties in the bankfull level determination are most likely to be on the base of the discrepancy.

7.3 Hydrological characteristics

7.3.1 Annual distribution of discharges

Flow duration and magnitude are important in channel development. These hydrological characteristics are related to climate, basin geology, basin morphology and vegetation cover. The basin characteristics determine its capacity to storage water and the runoff production. On the other hand, climate defines the amount of water that the fluvial system has to convey downstream and its annual distribution. There are two principal hydrological regimes: snowmelt regime and pluvial regime. Figure 7.6, shows the mean monthly discharge relative to the mean annual discharge. Italian streams display two distinctive peaks. The first one is due to snowmelt rains in spring (May) and the second one is due to rains in autumn (October and November). During summer and winter this rivers have low discharges and the variation between seasons is quite sharp.

In Patagonia, rivers have a regimen composed of two peaks, again due to snowmelt and rains. They differ from their counterparts in Italy, in the occurrence of the rainy season. In Patagonia, most of the rain falls during winter (July and August). After that, begins the falling limb of the hydrographs but are soon interrupted by snowmelt floods (October and November). Streams placed in pre-cordillera are more influenced by the snowmelt regime; this is the case of Gualjaina River, Lepá Creek, Chubut River and Alto Chubut River. Conversely, streams which basins are within the cordillera, and so they are influenced by humid winds from Pacific Ocean, have a rain component more pronounced. For instances, it is quite evident in Azul River and Epuyén River.

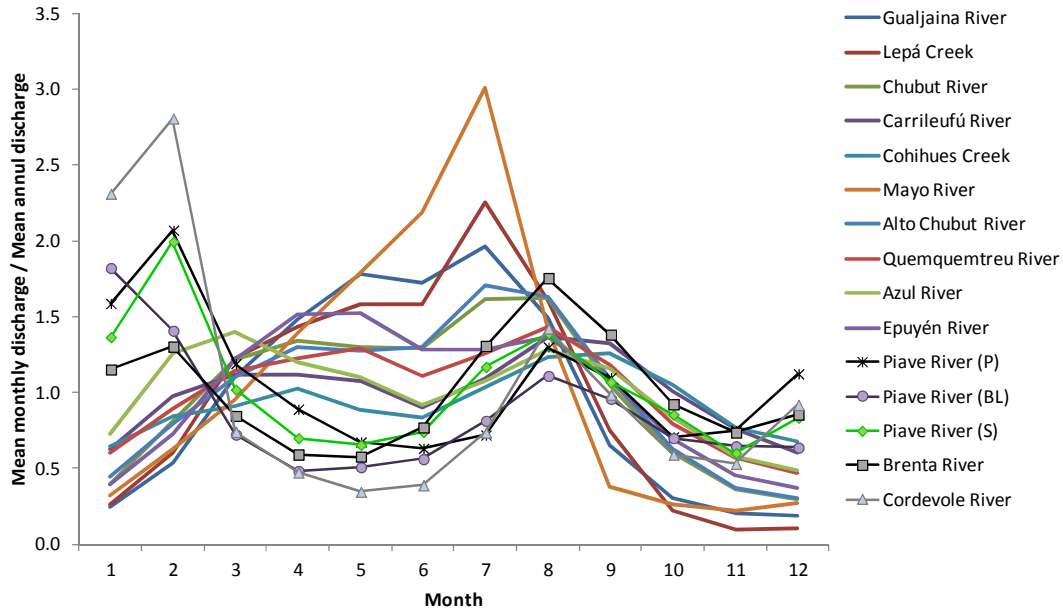

Figure 7.6. Annual distribution of discharges. Mean monthly discharge relative to mean annual discharge. For a seasonal comparison the first month indicates the beginning of autumn in both regions (month Nº 1 corresponds to April in Argentina and October in Italy).

7.3.2 Duration of discharges

An inspection of the duration curves (Fgure 7.7) reveals a wide range of discharges for the selected reaches. However, four characteristic curves can be recognized.

Because the plot is constructed with log-scale in ordinate axes and normal-distribution scale in abscissa, a line represents a log-normal distribution of discharges. This is the case of three Patagonian rivers: Carreleufú River, Cohihues Creek and Azul River. Their basins are located adjacent the international border Argentina-Chile, been highly influenced by humid winds from the Pacific Ocean.

A second type of curves consists on a bimodal log-normal distribution. It is recognized in Figure 7.7 as a line with a step, and is found in patagonian rivers: Chubut River, Gualjaina River, and Quemquemtreu River. This feature owes to the presence of different populations that are summed in the gauging station records. For instance, the gauging station at Gualjaina River is placed downstream of its confluence with Lepá Creek.

Another typical feature of some Patagonian rivers is the lack of water during summer. This situation is reflected by duration curves that drop sharply for low discharge, but evidence a log-normal tendency for higher discharges. This is the case of Lepá Creek, Alto Chubut River and Mayo River. All these streams are located in the Pre-cordillera region, and therefore, the summer discharge depends on the remaining snow in the upper basin.

Most Italian streams included in this research belong to a separate type. Their discharge-duration curves exhibit a lineal trend in the graph (log-normal distribution) for durations above 10%. Below this value discharges rise quickly following also a lineal trend. Therefore, the regime can be interpreted as a log-normal population of low discharges (stored in the basin or human reservoirs) interrupted by high discharges (flash flood events). For example, in the Cordevole River during 90%

of the year the discharge is equal to or lower than 12,6 m^3/s. For the remaining time, during 5% of the year the discharge is above 21,7 m^3/s and for 1% of the year it exceeds 94,7 m^3/s.

It has to be underlined that the duration curve of Brenta River resembles that of Patagonian rivers (log-normal distribution).

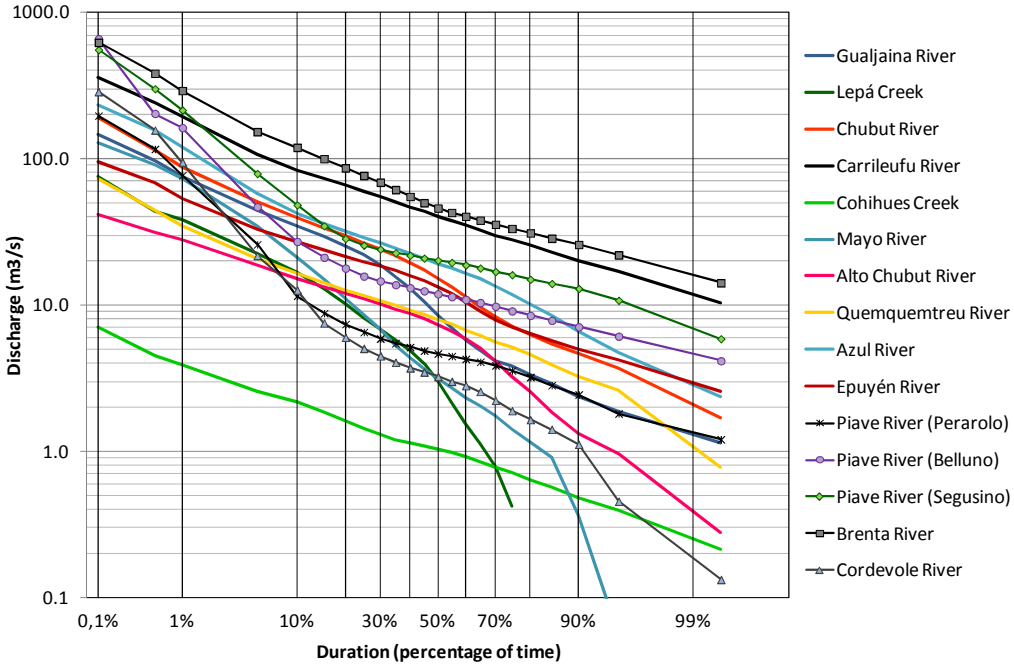

Figure 7.7. Flow duration curves for the studied reaches in Patagonia and Italy. Four typical regime are found: a) log-normal distributions (see Carrileufù River); b)bi-modal log-normal distributions (see Gualjaina River); c) regime with very low summer discharge (see Lepà Creek); and d) regime with flash floods (see Piave River).

7.3.3 Bankfull discharge

How many days in the year is the flow able to change the shape of the river channel? Most of the morphologic work is done by discharges close to the bankfull discharge, as verified by Emmet and Wolman (2001) in their study about gravel bed rivers. Because of that, the bankfull discharge is used as a reference parameter for plotting dimensionless discharge-duration curves (Figure 7.8). The surprising result is that, regardless the river size, all the curves are very similar for high discharges. The bankfull discharge has a duration in the range of 1% to 5%, i.e., there is a discharge equal to or larger than the bankfull discharge during just 3,5 to 18 days in a year. The unique exception is Quemquemtreu River with a particularly large bankfull discharge which duration is 0,37% (equal to 1,3 days).

It is also worth to note that with the use of dimensionless curves it is more evident the different behaviours aforementioned.

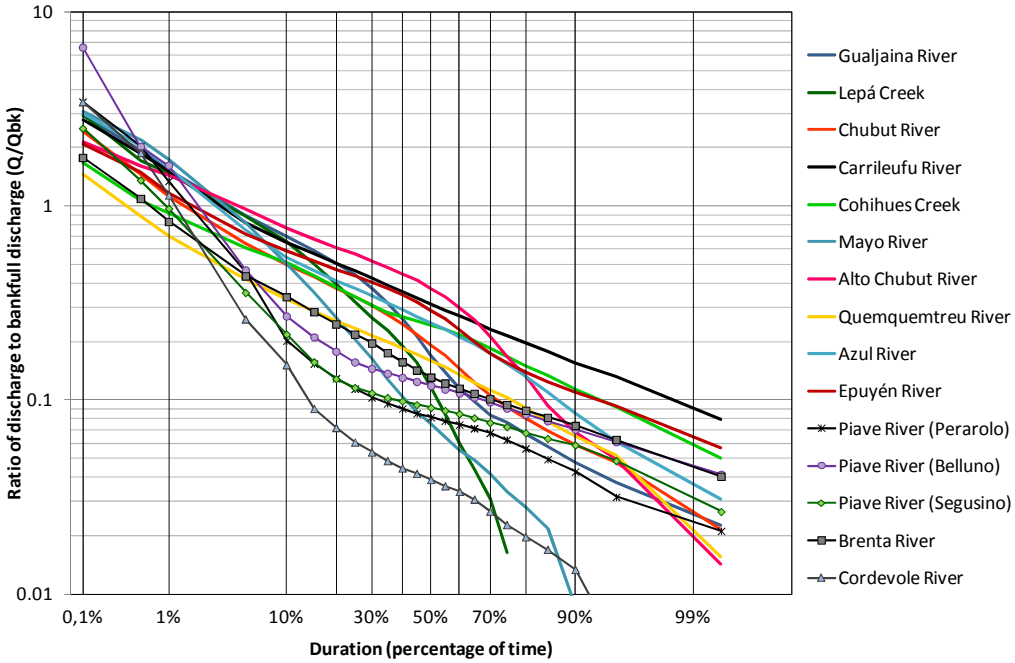

Figure 7.8. Dimensionless flow duration curves using the bankfull discharge. Although the wide range of discharges (almost 2 orders of magnitude) exposed in Figure 7.7, when discharges are got dimensionless all the curves get together for high discharges.

Bankfull discharge is a frequent flood that has a return period of 1,5 years in Patagonian rivers (Figure 7.9) which implies a mean occurrence of the bankfull discharge equal to two times every three years. However, the return period is not constant, and the range is between 1,11 and 2,40 years (see table A2, Appendix A). Furthermore, only 4 out of 10 cases lie in the range 1,3 to 1,7 years.

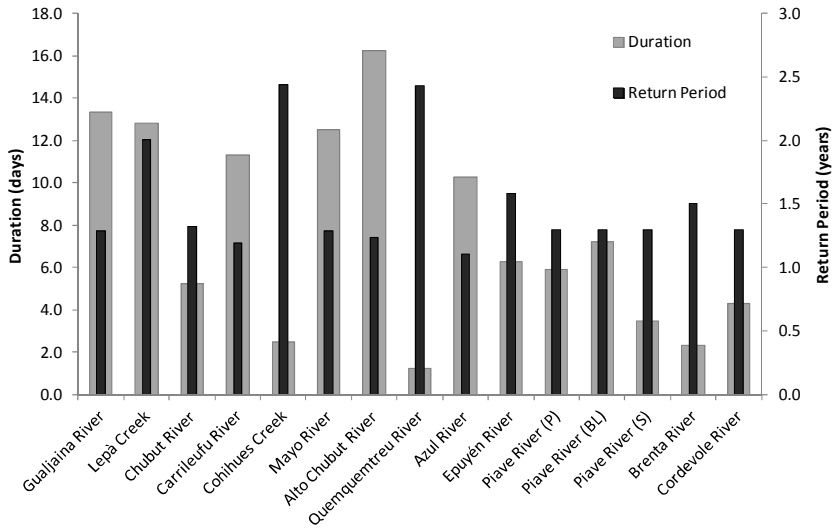

Figure 7.9. Comparison of duration and return interval of bankfull discharge.

In Italy, the return period has been estimated from direct observation. In the case of Piave River there are photographic documents available for the flood happened in 4 November 2008. Figure 7.10 shows the flood covering the whole channel and the surrounding flood plain in the left bank. But water did not arrive to the right bank that is actually a recent terrace due to an incision process under course in Piave River (Surian, 1998). This flood had a peak discharge of 97 m^3/s (daily mean value) that corresponds to a return period of 1,3 years. Despite the fact that there is evidence of no

constancy of bankfull discharge return period for river reaches placed within the same basin (Andrews, 1980)[13], in this study it was applied to all the streams within Piave River basin.

In the case of Brenta River, independent data was used consisting of field surveys of water surface stages in monitored cross sections, during different flood events. This gave a bankfull discharge of 350 m^3/s, that corresponds to a 1,5 years return period flood.

The results aforementioned are similar to others published in literature. For instance, Andrews (1980), Emmet and Wolman (2001), Leopold et al. (1964, p- 319) and Williams (1978) coincide that the bankfull discharge return period is near 1,5 years but there is not a common frequency of occurrence.

Figure 7.10. Flood in Piave River near Belluno (4 Novembre 2008) at bankfull level. Note that water reaches the floodplain level at the left bank (right in the photograph), but it is below the top of the right bank which is actually a terrace (photo courtesy Lorenzo Picco).

7.3.4 Frequency analysis

Much geomorphic work is accomplished by very frequent floods that are present 1 to 5% of the year, as recently mentioned. However large floods have also an important role because this pulse-type perturbation can disturb the system. This aspect is explored analyzing the flood frequency curves. Figure 7.11 exposes the relation between flood magnitude (mean daily peak discharge) and the annual-probability (expressed as return interval). Piave River (at Belluno) has a distinctive behavior, namely, its curve grows rapidly and an extraordinary flood (100 years return period) are as high as 20 times the bankfull discharge. The Piave River is placed in the Alps region, in Italy, and its rainy floods are pulse-type with quickly rising and falling limbs. Note that the Piave River has very low discharges for most of the year (less than 20% of the bankfull discharge during 90% of the year). In Patagonia a similar duration curve is found in the Lepá Creek, but extraordinary floods are not so intensive. In this case discharges are lower than 20% of bankfull flood during 60% of the year due to a lack of water storage capacity in the basin.

The other streams have curves that cover a wide range of flood intensities. The Carrileufú River, in Patagonia, exhibits the lowest flood magnitude. An extraordinary 100-years return period flood is

[13] Note also in table A2 (Apendix A) that the return period of Lepá Creek and Gualjaina River are different but the former is within the basin of the second.

just 2,93 times the bankfull discharge. It is not surprising because the gauging station is located some kilometers downstream the river beginning in the Cholila Lake. Therefore, the runoff is stored temporarily in the lake and floods downstream are milder. This is also the situation of Epuyén River, with a similar flood-magnitude behaviour and also with a lake upstream the gauging station that regulates the runoff of a large portion of the basin. Nevertheless, there are others streams that have a similar behaviour without the present of a regulating lake. This is the case of Quemquemtreu River, in Patagonia (Q_{100} = 3,49 Q_{bk}) and Brenta River (Q_{100} = 3,99 Q_{bk}), in Italy.

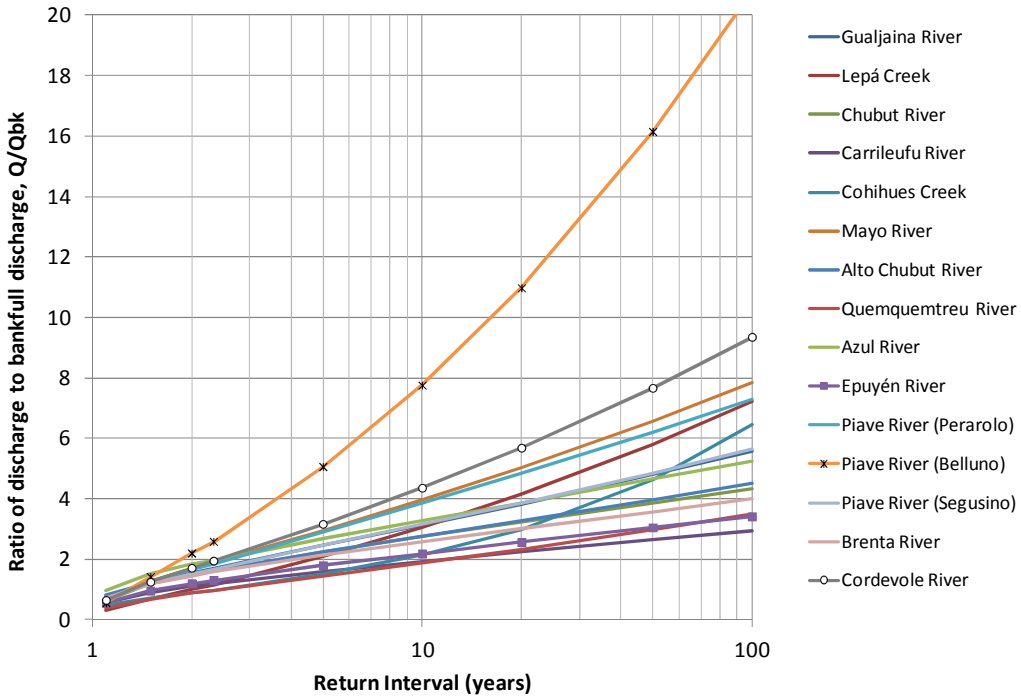

Figure 7.11. Flood magnitude relative to bankfull discharge against return period in Patagonian and Italian rivers.

It is also interesting to compare the studied rivers against other contrasting environment in the world. Figure 7.12 shows the regional discharge-frequency curves as the ration of food magnitude and mean annual flood (2,33-years return period). Again, the Piave River at Bellluno and also the Lepá Creek are near those curves belonging to streams in environments with intensive floods such as Sri Lanka (due to monsoonal rains) and the Southwest in U.S.A, a semiarid region with typical torrential floods. Some streams, with moderate flood intensity such as Gualjaina River, Mayo River and Quemquemtreu River (in Patagonia) and Cordevole River with Piave River at Perarolo (in Italy) follow tendencies similar to humid environments in East U.S.A., Japan and U.K. While the other streams that have a milder flood magnitude resemble the behavior of streams in humid regions of Canada and Italy. Finally, it is also worth to note that in all the cases the behaviour is far away from those belonging to tropical environments (Congo and Guyana).

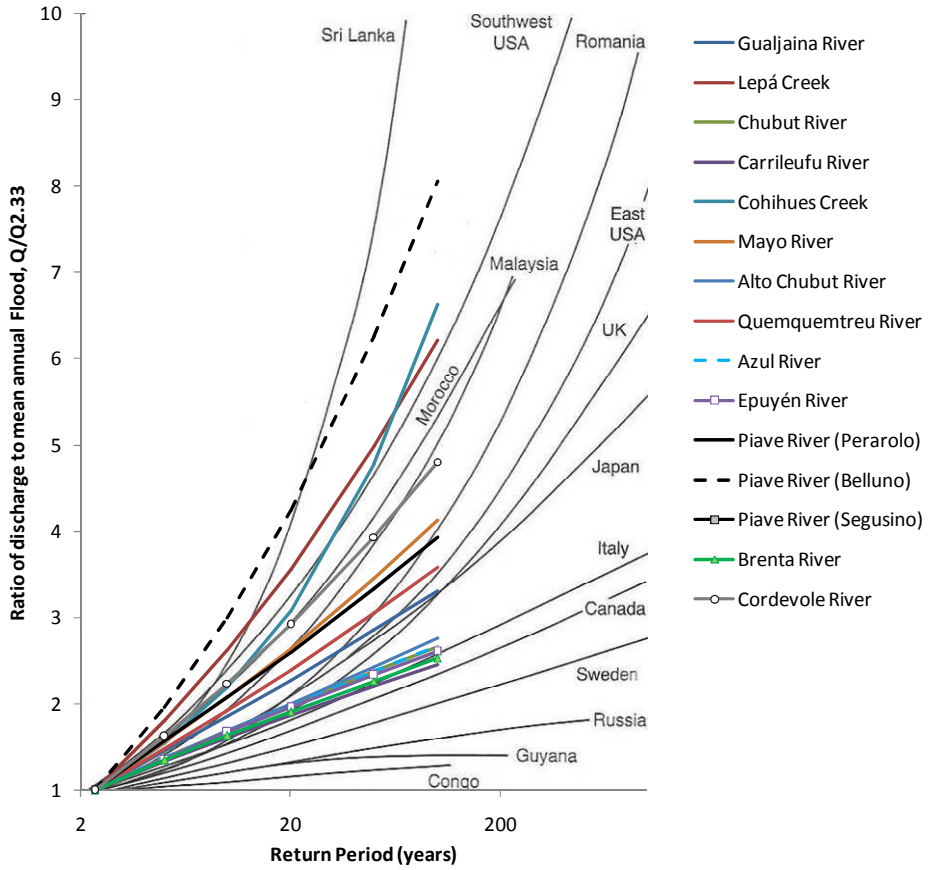

Figure 7.12. Regional grows curves showing flood magnitude relative to mean annual flood against return period from different regions in the world (modified from Knighton, 1998).

7.3.5 Torrential behaviour

In order to complete the hydrologic characteristics of the studied rivers and to further distinguish Italian and Patagonian rivers, a torrential index is defined. This index is intended to measure daily variability of the discharge during a flood event. It is defined as the ratio of the instantaneous peak discharge and the mean daily discharge for the same day. Table A2 (Appendix A) contains the numerical values of this index while Figure 7.13 shows a graphical representation. There is a remarkable difference between floods in Italy and Patagonia. In Patagonia, the instantaneous peak discharge is 7,5% higher than the mean daily discharge. The Azul River has the maximum index with a value of 13%. Nevertheless this value is still much lower than those in its alpine counterparts. The Italian rivers exhibit a mean torrential index equal to 1,55 with the lowest value in Brenta River (1,28), and the highest in Cordevole River (1,77).

As a concluding remark about hydrological characteristics it can be said that the major difference between regimes in alpine and Patagonian rivers relays in the hydrographs recession limb. Considering the flow duration curves and the torrential index it follows that alpine rivers experiment flash flood with very fast rising limb (high torrential index) but also very fast falling limb. This last aspect is recognized in the duration curve in the lack of moderate discharges. In Patagonia, flood events have similar intensities, as it can be seen in flood-frequency graphs (Figures 7.11 and 7.12), but the raising limb is slow (a low torrential index) and the falling limb is gentler (see the log-normal distribution in Figures 7.7 and 7.8).

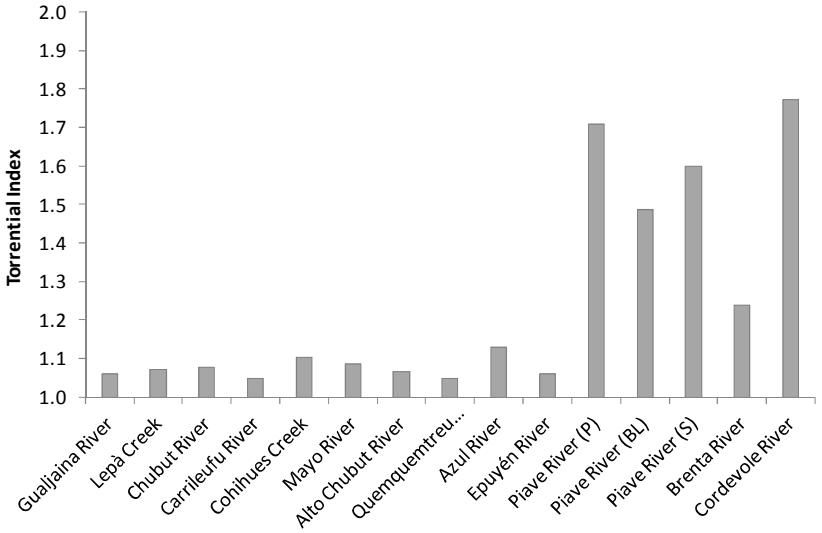

Figure 7.13. Torrential index defined as the ratio between the instantaneous peak discharge and the mean daily discharge.

An illustrative example is provided by two flood events with similar peak discharge, one happend in the Carrileufú River (Patagonia) and the other in the Brenta River (Italy). The mean daily peak discharge in Carrileufú River was 582 m^3/s while in Brenta River the mean daily discharge was 605m^3/s but the mean hourly discharge was 676 m^3/s (Figure 7.14). Although Brenta River has the lowest torrential index of all the alpine streams, it is still evident the high slope of the rising limb. But it is more interesting the falling limb. While for Carrileufú River it took more than a month and a half to recover the original discharge (near 75 m^3/s) , in the Brenta River the discharge reduced 82% of the effective discharge (measured as the difference between the peak discharge and the initial discharge) in just 3 days after the peak.

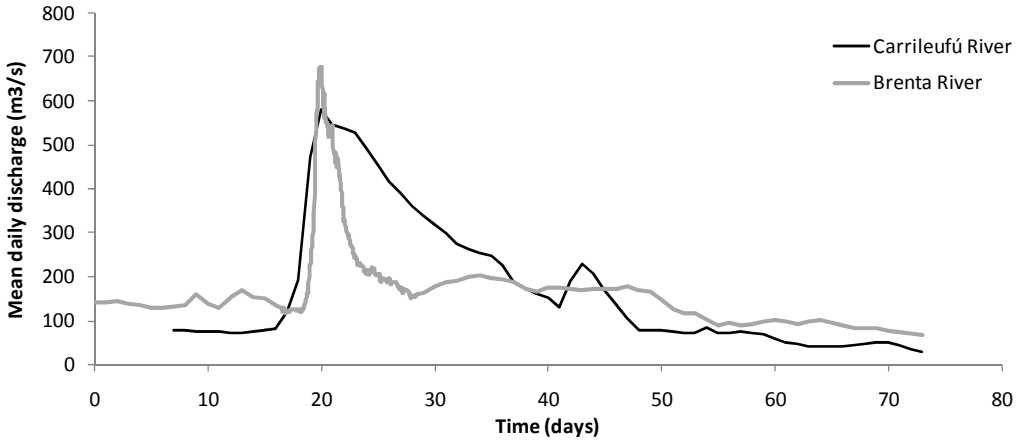

Figure 7.14. Example of two floods with similar peak discharge in an Alpine stream (Brenta River) and an Andine stream (Carrileufú River). For the Carrileufú River mean daily discharge is available while for Brenta River hourly discharges have been employed.

7.4 Bankfull shear stress

Shear stress at bankfull discharge is an important parameter that reflects the intensity of frequent floods and their capacity for doing morphologic work. Let us consider the dimensionless shear stress $\tau_{50}^{*} = H \cdot S / R_s D_{50}$, where R_s is the relative specific weight of sediments. In Patagonia, streams exhibit a wide range, from 0,023 to 0,092, with a mean value of 0,052. The lowest value corresponds to Carrileufú River, and it can be explained by a very low slope (0,00075). On the other hand, Cohihues Creek has the highest dimensionless shear stress, and again it can be related to its slope (0,02). These two streams are also good example of different behaviors. The first one is a very stable river. There are not bank erosion signs along the reach and its discharge rating curve is quite constant during the last 50 years. On the contrary, Cohihues Creek is very dynamic and its rating curve changes every year. Finally, it can be seen that the range and mean value for the dimensionless shear stress fits very well in the distribution for gravel bed rivers in the world. Figure 7.15 illustrates the distribution of dimensionless shear stress as results from the dataset published by Parker et al. (2007).

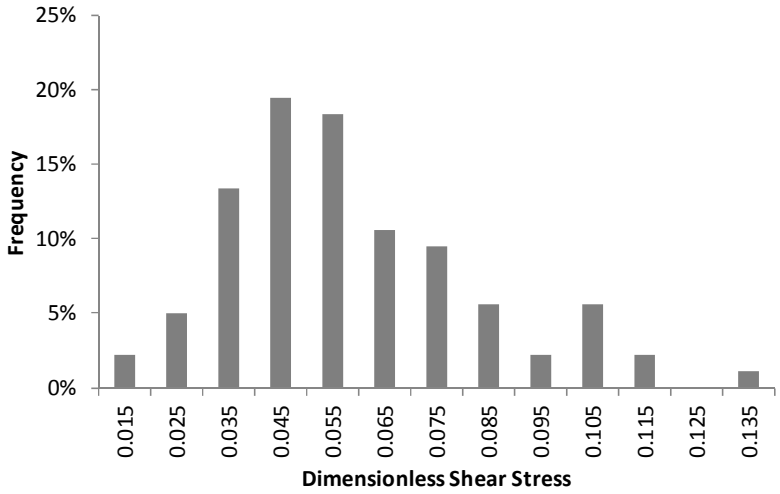

Figure 7.15. Frequency distribution of dimensionless shear stress for D_{50} in gravel bed rivers (dataset compiled by Parker et al. 2007).

With regards to Italian streams, the mean dimensionless shear stress is somewhat higher: 0,055. However, in this case the sample is composed of only five cases; four of them have a low dimensionless shear stress, near 0,040 (Piave River and Cordevole River) while one has a high value: 0,100 (Brenta River). Such high value is unusual in gravel bed rivers, when compared against observed values in other gravel bed rives (Figure 7.15).

It is also interesting to compare the dimensionless shear stresses against a reference value for sediment transport. For this purpose the value of 0,03 is adopted (Figure 7.16). Now, the mean of Patagonian rivers is 1,7 and 1,4 for rivers in Italy (excluding the Brenta River). These values indicate that bankfull discharge intensity is not very much higher than that needed for sediment transport, a result also found by Andrews (1984).

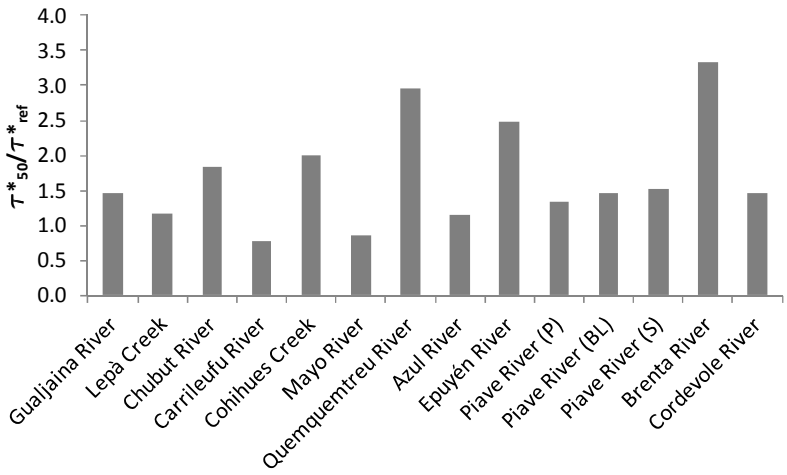

Figure 7.16. Dimensional shear stress intensity compared against the reference value ($\tau^*_{ref} = 0{,}03$).

7.5 Morphological characteristics

7.5.1 Qualitative comments

Piave River at Belluno can astonish its first time viewer. Its morphological and sedimentological characteristics were so different from those in its Patagonian counterparts that it is worth describing them. The following description is almost valid for all the Italian rivers analyzed in this study. The territory subject to floods is large and is made up of a principal channel, a secondary channel, and several levels of bars. The principal channel conveys water during most of the year but during a flood, near bankfull, flow divides and takes secondary channels. When the secondary flow is strong enough it makes of the secondary channel, the principal one. In Piave River two levels of bars are recognized (the lower and upper level). Another interesting feature is the wide diversity of surface sediment sizes. We recognized several sectors with uniform sediments (patches). For instance, in Piave River near Belluno there were sectors with cobles (mean diameter near 200 mm), and others with fine gravels (10 mm) near sectors with fine sediments (sand). It was also evident the presence of lob deposits tending to cover lateral channels but also the main channel, the latter due to returning flow from high bars. In this particular reach, there was (autumn 2009) a long central bar cut at several sectors due to a sinuous flow. It looked like a nested configuration: a straight channel with a central bar belonging to a large-scale morphology, may be related to large floods, and within this morphology there was another one, consisting in a sinuous channel due to low discharges.

All the features aforementioned are unusual in most, but not all, Patagonian rivers. They generally exhibit a regular pattern. The channel is straight for high discharges, but the flow follows a sinuous path for low discharges. The latter relates to the presence of alternating bars and the associated bed topography: riffles at crossovers and pools corresponding to bars. Furthermore, surface sediments follow well known spatial distributions, namely a gradual variation from coarse material at riffle to fine material at pools. On the contrary, one also finds in Patagonia some rivers similar to Italian one. This is the case of Lepá Creek, a wide gravel bed stream with evident secondary channels that change to principal channel from one year to the next one (but the whole morphology is mainly single-thread). It also has lob-deposits that fill the secondary channels (Figure 7.17).

These contrasting features suggest that the possible explanation could be found in different hydrological regimes. In fact, Italian river reaches resemble streams disturbed by large floods, rushing water that practically washes the surface and its morphology producing a new one. The inner morphology detected in the main channel could be the result of the hydrograph falling limb. But the lack of a clear form could be associated to a lack of moderate discharges after the peak discharge. The Lepá Creek case can support this hypothesis considering that it has also intensive floods (Figure 7.12) and a deficiency of low discharges (Figure 7.7).

Figure 7.17. Lob deposits of gavels tending to cover a lateral channel in Piave River (left) and Lepá Creek (right).

Figure 7.18. Confluences and defluences. (Above) A secondary channel -on the right- in Cordevole River; (below) a defluence in Lepá Creek; when the picture was taken the principal channel was the right one; instead, a year later the flow had switched to the left one.

7.5.2 Shape factor

Beyond the different contexts of Italian and Patagonian rivers, when reach-averaged parameters are analyzed the qualitative differences aforementioned vanish and they exhibit similar features. Let's consider the shape factor defined as the ratio of width to mean depth (Figure 7.18). Rivers in Patagonia cover a wide range, from 29,3 for the narrowest/deepest stream (Epuyén River) up to 89,0 for the widest/shallower stream, the Lepá Creek, while the overall mean value is 52,6 (St.dev. 23,7) . The small sample from Italy falls within this limits, with a mean value of 56,7 (St.dev. 10,9). The Brenta River is the narrowest/deeper stream (B/H = 51,6) and the Piave River at Segusino is the widest/shallower (B/H = 81,3).

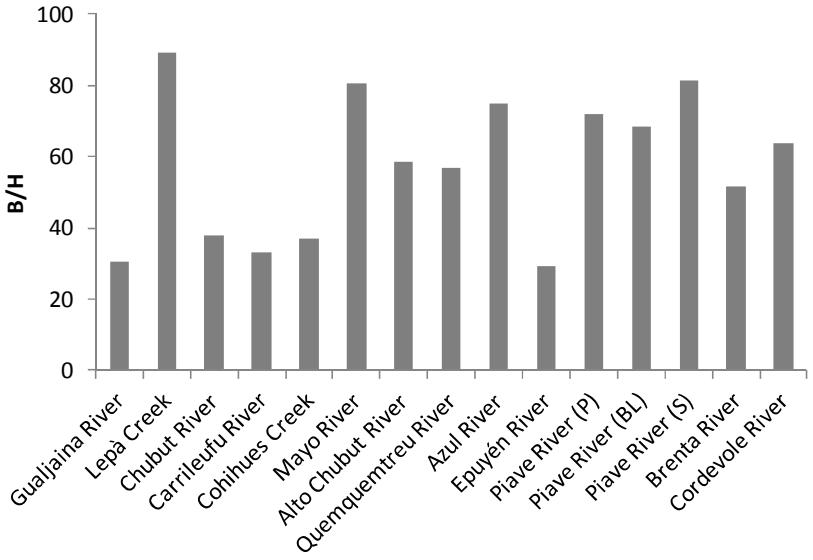

Figure 7.19. Shape factor for gravel bed rivers in Italy and Patagonia.

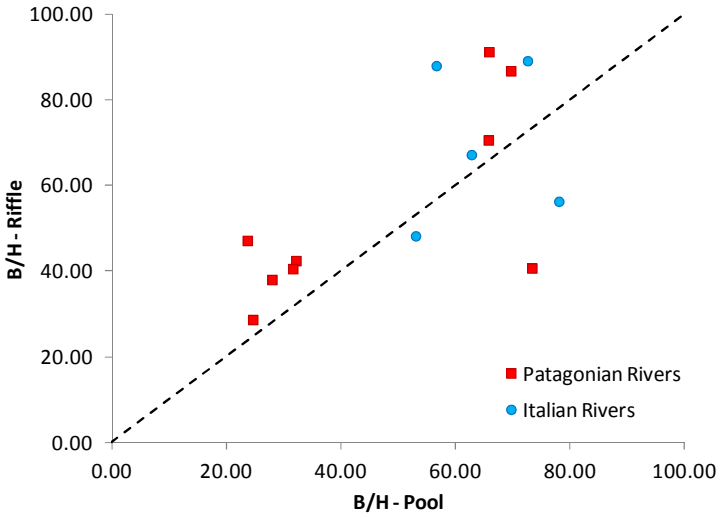

Figure 7.20. Shape factor calculated at riffle and pools cross sections. The dashed line indicate equal shape factor for both riffles and pools. In general riffles are wider and shallower than pools.

The shape factor depends on the local morphological units, i.e. riffles and pools. Because cross sections were surveyed along these units, it is possible to verify the spatial variability. Figure 7.20

shows the shape factor as calculated for riffle (considering the mean of three cross sections) and for pools (averaging two cross sections). In general, most of the streams have wider and shallower riffles (higher B/H) while deeper and narrower pools (lower B/H). It can be said that only one stream in Patagonia (Quemquemtre River) and one in Italy (Cordevole River) clearly do not verify this trend, been pools wider/shallower than riffles.

7.5.3 Riffle spacing

Gravel bed rivers have alternating bars and a bed topography with a rhythmic sequence of shallow sectors (riffles) and deep sectors (pools). The wave length of these features is proportional to the channel width. Hey and Thorne (1986) found that the riffle spacing (Z) was 6.3 times the channel width. In order to explore this relationship with natural and disturbed rivers, the new data is compared against Hey and Thorne's database from British rivers. As it can be appreciated in Figure 7.21, the new data from Patagonia and Italy follows very well the trend observed by the English researchers. Furthermore, the new data covers a sector with few information in their original work. It is also interesting to note that there is no difference between streams in Patagonia and Italia, and moreover, data from Alpine streams has less scatter than their Andine counterparts.

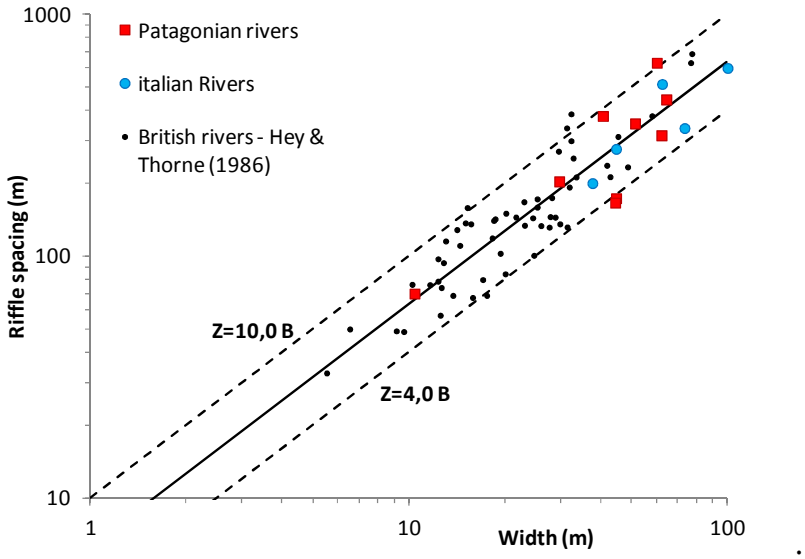

Figure 7.21. Riffle spacing in British, Patagonian and Italian rivers (modified from Hey and Thorne, 1986). Z is the riffle spacing and B is the channel width. The continues line represent the best fit: Z = 6,7 B.

The result that the riffle-spacing is similar in the three dataset (Patagonia, Italia and Britain) was also verified performing a statistical analysis (ANOVA). The null hypothesis states that the three regressions lines (one for each population) are identical. The result was a p-value p = 0.28, and hence the null hypothesis cannot be rejected: riffle spacing is the same for the three populations. For the overall data the best fitting line is Z = 6,7 B.

7.6 Sedimentological characteristics

It is well known that gravel bed rivers exhibit a positive relationship between bed topography and sediment characteristics. Riffles are coarser and sediments are tightly packed, while pools have finer and loosely packed sediments (Sear, 1996). Figure 7.22 shows the reach average median diameter

with the interval of spatial variation. The upper limit is the riffle's D_{50}, and the lower limit corresponds to the pool's D_{50}. The widest ranges are found in Italian rivers showing a high spatial variability of grain sizes. Taking mean values, we can say that grain size over riffles is 60% coarser than the reach mean, while in pools grain diameter is 25% below the reach average. The most notorious case is Piave River at Perarolo, where surface grain size varies from 31,3mm to 72,8mm. Conversely, streams in Patagonia have more uniform sediments. Again, considering mean values, riffles are just 18% coarser than the reach average and pools are 14% finer. Therefore, the amplitude of diameter variability in Patagonian Rivers is nearly one half the amplitude in Italian Rivers. Nevertheless, individual cases need attention. Carrifeufú River has almost a uniform surface material. It relates to the lack of well developed bed forms. Moreover, some rivers in Patagonia have high variability such as Epuyén River and Mayo River.

With regards to the vertical variation, all the streams have developed an armour layer, i.e., a surface layer composed of coarser material than the substrate material. One way of describing this feature is by means of the absolute armouring index defined as the ratio of surface median diameter to subsurface median diameter. Figure 7.23 shows the relative armour for the mean reach, pool sectors and riffles. Italian gravel bed rivers have the highest relative armour, with a mean value of 2,33. Only two steams in Patagonia have such a high value, Carrileufu River (2,79) and Mayo River (2,66), while the others have lower degree of armouring, with a mean of 1,61. It is worth to underline again the wide range of spatial variability of sizes in Italian Rivers. Relative armour is higher than 3 in riffles and below 1,5 in pools.

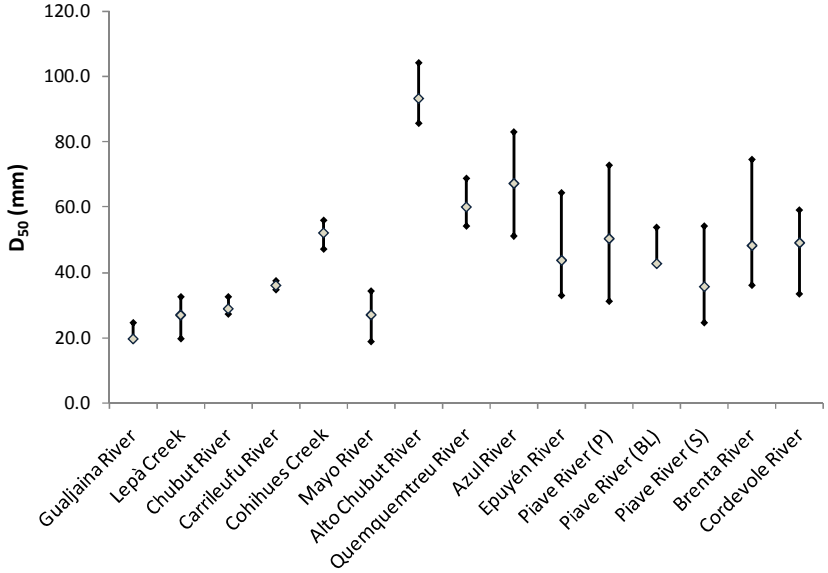

Figure 7.22. Spatial variability of surfaces grain sizes. The central box indicates the reach average median diameter. The upper and lower limits correspond to riffle's and pool's median diameter, respectively.

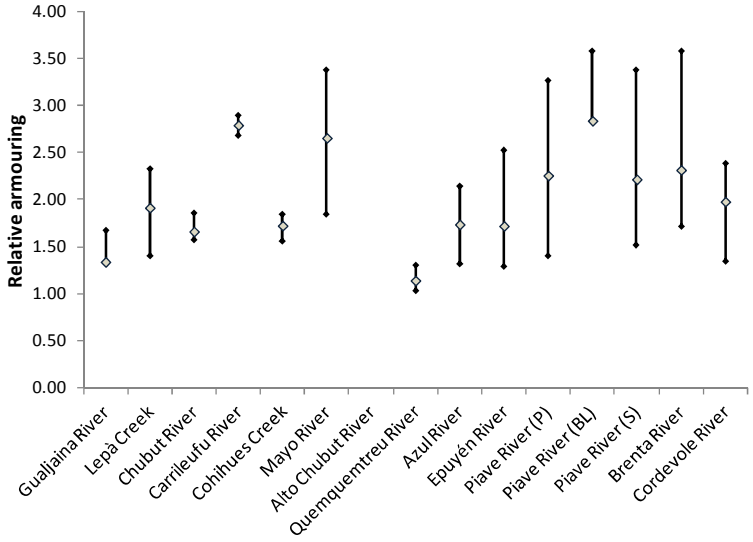

Figure 7.23. Relative armour (ratio of surface median diameter with subsurface median diameter). The central box indicates the reach averaged armour index while the bar indicates reach variability (upper limit at riffle and lower limit for pools)

A second way of describing the armour of a gravel bed river has been proposed by Dietrich et al. (1989). Armouring is described in terms of a dimensionless sediment transport ratio q^* which is the transport rate for the coarse surface normalized by the transport rate for a surface as fine as the substrate. The choice of the sub-surface as a reference is based on the observation that substrate and bedload have similar grain size distributions[14]. Dietrich and collaborators proposed that surface coarsening develops in gravel bed rivers when local bedload supply from upstream is less than the ability of the flow to transport the load. Then, q^* should be unity when sediment supply rate matches the river's ability to transport the load, and should decrease towards zero as the surface coarsens when supply is reduced. These researchers proposed an approximate equation for predicting sediment transport that employs a shear excess as formulated by Meyer-Peter Müller(1948) (see Chapter 4):

$$q^* = \left(\frac{\tau_{bk}-\tau_{cs}}{\tau_{bk}-\tau_{cl}}\right)^{1,5} \tag{7.1}$$

Wherein τ_{bk} is the shear stress at bankfull discharge, τ_{cs} and τ_{cl} are the critical boundary shear stresses for the surface material and bed load, respectively. The parameter q^* ranges from 0 for low sediment supply and well-armoured surfaces, to 1 for high bed load and unarmoured surfaces.

Dietrich and collaborators compared their hypothesis against flume and field evidences. Figure 7.24a reproduces their results. Boxes represent three experiments conducted in a small flume where sediment transport and surface armour where measured (refereed as 1,7; 6,1 and 17,4 that means the transport rate in g/min). Run 17,4 corresponds to a state of no armoured bed where all sediment

[14] Dietrich and collaborators have based this choice on a previous work owe to Parker et al. (1982). This topic is related to the hypothesis of equal mobility suggested by Paker and Klingeman (1982) which states that "*In a graded gravel bed stream, the grain size distribution of the average annual yield of transported gravel tends to be finer than that of the gravel contained in the armoured surface evident at low flow and similar to that of the gravel contained in the substrated below*". More recently favorable evidence supporting this hypothesis has been presented performing laboratory experiments (Parker and Toro-Escobar, 2002; Wilcock and Southard,1988) and field observations (Lisle, 1995)

supply was transported along the flume, hence $q^* = 1$. The other two experimental situations where obtained reducing the sediment supply and promoting surface coarsening. The figure also contains the results calculated for the river reaches studied in this work. The result is not plausible because it suggest that the rivers have a relative higher supply but at the same time have higher absolute armour indexes. It is a situation possible in Dietrich et al's. model only in those cases where there are intense shear stress (see curve $\tau_b/\tau_c = 4{,}24$ in Figure 7.24a) which is not the situation in these gravel bed rivers. In Section 7.4 it was shown that the mean dimensionless shear stress in Patagonian streams was 0,052 and 0,04 in most Italian rivers.

The Miller-Peter and Müller 's (1948) transport model is based on the shear stress excess concept, and uses only one parameter for the whole grain size distribution, the median grain size. Because for the present study sedimentological data is extensive, an alternative expression is proposed:

$$q^* = \frac{q(F,\tau_{bk})}{q(f_{ss},\tau_{bk})} \tag{7.2}$$

This expression retains the basic idea of Dietrich and collaborators but changes the way sediment transport rate are calculated. In this case, q is the transport model for gravel-sand mixtures developed by Wilcock and Crowe (2003), F is the surface grains size distribution, $f_{ss}$is the subsurface grain size distribution and $\tau_{bk}$is the bankfull shear stress. The Wilcock and Crowe`s model was selected because it takes into account the important influence of sand (present in bed surface) in sediment transport.

Figure 7.24b shows the new results. Dietrich et al.'s experiment results have also been calculated. Although the comparison is not so good for the experiments points, the new results for gravel-bed rivers is more plausible. Italian rivers seem to have extremely low sediment supply, been the sediment transported at bankfull stage below 5% the maximum possible. An exception is found in Brenta river where $q^* = 0{,}19$. This value is strange because the reach is placed at the beginning of the alluvial reach in the Veneto plain (see description in Chapter 5) and hence sediment supply from bank erosion is still negligible. The high value of sediment transport actually owes to extremely intensive bankfull shear stresses, as high as 78 Pa ($\tau_{50}^* = 0{,}1$).

River reaches in Patagonia exhibit a wider spread of supply conditions. It spans form nearly 0 at Carrileufu River, up to 0,31 in Chubut River. The case of Carrileufú river can be explained due to the lack of sediment supply because the studied reach is near Cholila Lake, the origin of the river as already mentioned.

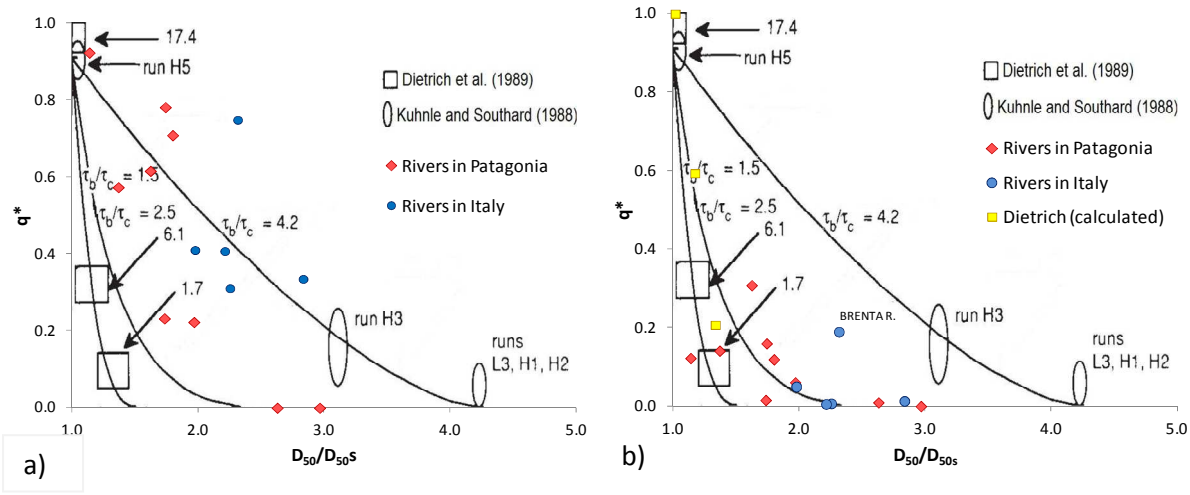

Figure 7.24. Comparison of absolute and relative armour indexes. The figure is based on Dietrich et al.'s (1989) work, exposing their experimental results, those of Kuhnle and Southerland (1988) and calculated values for Patagonian streams and Italian, based on field measurements of surface and subsurface material, and bankfull hydraulic conditions. Two different sediment transport models have been applied: a) Meyer-Peter and Müller (1948) as proposed by Dietrich et al. (1989), and b) Wilcock and Crowe (2003).

Finally, it can be said that for the same hydraulic conditions (shear stress), sediment supply is higher in Patagonian Rivers than in Italian Rivers. This conclusion, based on the analysis of amouring indexes, is congruent with Surian et al.'s (2009) study. These researchers analyzed the relationship between channel adjustment and sediment fluxes in five Italian Rivers using several techniches (analysis of historical maps, aerial photographs, topographic and geomorphological surveys). In the case of Piave and Brenta Rivers they indicate that the morphological adjustments, namely narrowing, incision and pattern changes, are the consequence of several human interventions: in-channel gravel mining, dams, and bank protections. All these interventions reduce dramatically the sediment supply for the river system.

7.7 Are disturbed Italian Rivers different to Patagonian at-natural-state rivers?

In this last section the comparison between disturbed grave bed rivers in Italy and those still in natural state in Argentina is revisited using statistical tools. Now the problem is formulated in terms of the following question: are mean value of representative parameters of disturbed rivers different to those from the reference set of natural rivers in Patagonia? In order to answer this question the null hypothesis that averages are actually identical (or that there is no difference at all) is proposed.

The populations will be described by the following list of parameters.

Hydrological and hydraulic parameters:

- Bankfull duration and return interval.
- Ratio of median discharge to bankfull discharge. This parameter describes the flow duration curve considering the half-time duration discharge.
- Torrential index.

- Intensity of floods measured as the ratio of the dimensionless shear stress to the reference shear stress (τ^*_{bk}/τ^*_{ref}).

Morphological features:

- Reach average Shape factor, and shape variability by means of the ratio B/H at riffles and B/H at pools.
- Riffle spacing.

Sedimentological features:

- Spatial surface grain size variability evaluated as $\left(D_{50riffle} - D_{50pool}\right)/D_{50}$
- Absolute armouring.
- Sand content in the substrate material.

Table 7.2 exposes information of mean values and standard deviations for each selected parameter. Before carrying out the test to compare the two sample means, it is necessary to test whether the sample variances are significantly different. For this purpose the Fisher's test is used assuming the null hypothesis that both variances are equal. Table 7.2 shows the F value calculated (column 5) and the critic value for a 5% significance level. In some cases the null hypothesis must be rejected and then mean comparison requires the use of Welch's test (unequal population variances); otherwise the usual t-test is applied. The last two columns have the calculated t values and the corresponding p-values. Considering a significance level of 5%, it can be said that Italian rivers are different to Patagonian rivers in terms of hydrological parameters: bankfull duration, the duration curve (ratio Q_{50}/Q_{bk}) and the torrential index. It means that floods affecting Italian rivers are more torrential and high discharges have lower durations (flash floods) than in Patagonia. On the contrary, the average frequencies of bankfull discharge (return interval) are identical and its intensity in terms of shear stress. Furthermore, during half of the year discharges are much lower (almost one-half) in Italian rivers than in Patagonia.

With regards to the morphology, it can be affirmed that the spatial variability of the shape factor is higher in Italian streams because the parameter B/H_{riffle} / B/H_{pool} is higher and the averages are significant different. Another significant differentiation is found for the surface grain size variability. Rivers in Italy exhibit a wider range of variability, i.e., riffles are much coarser than pools than what is observed in Patagonian rivers. Vertical sorting is also a factor of difference: the armour layer in Italian streams is much coarser than that in Patagonian rivers.

Both populations have similar rifle spacing, reach average shapt factor and bankfull dimensionless shear stress. Therefore, it can be said that Italian and Argentine rivers are similar when observed at the reach scale, but differences emerge at lower spatial scale. It is also worth to note that the substrate sand contents are also similar in both populations.

Table 7.2. Comparison of average values of selected parameters for Patagonian and Italian rivers. Figures in brackets represent the standard deviations. (*) the Carrileufú River has not been taken into consideration for the calculus of absolute armour because it is near a lake and its lack of sediment supply is not a common situation.

Parameters	Patagonia	Italy	Variance test		H0 test	
	Average (St.dev.)	**Average** (St.dev.)	**F**	**Fcritic**	**t**	**p-value**
Bankfull return interval	1.59 (0.51)	1.34 (0.09)	32.83	6.00	1.50	0.17
Bankfull duration	9.17 (5.04)	4.86 (1.64)	9.40	6.00	2.46	0.03
Duration curve Q_{50}/Q_{bk}	0.22 (0.09)	0.09 (0.04)	6.21	6.00	3.71	0.003
Torrential Index	1.08 (0.03)	1.56 (0.21)	67.17	6.00	5.15	0.007
τ^*_{bk}/τ^*_{ref}	1.99 (0.79)	1.86 (1.05)	1.79	6.00	0.27	0.79
B/H	52.76 (22.43)	67.35 (10.95)	4.20	6.00	1.36	0.20
B/H_{riffle} / B/H_{pool}	1.41 (0.33)	1.93 (0.44)	1.77	6.00	2.54	0.02
Riffle spacing Z/B	6.42 (2.29)	6.09 (1.37)	2.78	6.00	0.29	0.77
($D_{50riffle}$ - D_{50pool}) / D_{50}	0.34 (0.21)	0.65 (0.26)	1.57	6.00	2.46	0.03
Absolute armour (*)	1.74 (0.45)	2.32 (0.32)	2.00	6.10	2.54	0.03
Sand fraction in substrate	0.18 (0.07)	0.17 (0.02)	7.73	6.00	0.40	0.70

8 ANALYSIS

The energy dissipation due to the turbulence generated by bottom roughness and bed forms is still an obscured topic in natural channel hydrodynamics. Although a lot of effort has been dedicated to this topic our knowledge and predictive formulas are not good enough to represent accurately this phenomenon. Chapter 3 presented several issues have been presented regarding the applicability of mean friction factors at the reach scale. This topic is important for the development of regime theories where a resistance law is always invocated. Usually, the resistance law is used to derive an expression for the channel width, and hence, a bad representation of the processes of energy dissipation will induce poor width predictions later. The first part of this chapter is, then, dedicated to analyze the reach-averaged friction factor with new data from this study. Several methods for averaging hydraulic parameters will be compared.

Following, the performance of selected regime theories will be assessed. The chosen theories include some kind of bank resistance criterion. They are: Millar's (2005) extremal hypothesis-based model, Parker et al.'s (2007) model and Ikeda et al.'s (1988) model. The experience gained in Italian rivers indicates that width changes very quickly due to sediment supply alterations but channel slope takes a longer time span (see Chapter 5). Then, considering the spatial scale under study and following Weichert et al. (2009), the channel slope will be considered as an independent factor.

8.1 Bankfull friction factor

As has been introduced, several issues still remain regarding the predictability of friction factors. One issue concerns the way geometric parameters are averaged along the reach. Because the processes involved are not linear, the way mean parameters are evaluated can give different results. This is the first topic to be analyzed.

The friction factor accounts for the total energy dissipation due to the turbulence produced by grain protrusion (skin roughness) and flow separation, convergence and divergence associated with bed forms and downstream cross section variability. Because grain size and bed forms are two ways of channel organization the friction factor can be interpreted as a reach descriptor. There are several ways to evaluate it, as has already been presented in Chapter 3. Here, three procedures will be used:

1. The friction factor is evaluated considering reach-averaged values for depth (standing for the hydraulic radius) and mean velocity (discharge divided the mean area). The mean flow area is calculated as the product of the mean depth and width. Then, recalling the Darcy-Weissbach equation (3.18), the friction factor can be written as:

$$f = \frac{8gHS}{\left(QH^{-1}B^{-1}\right)^2} \qquad 8.1$$

2. The friction factor is also evaluated taking reach-averaged values but this time the hydraulic radius and the inverse of area are considered (see equation 6.6).

$$f = \frac{8gR_HS}{(QA^{-1})^2} \qquad 8.2$$

3. The third method consists on calibrating the friction factor using the whole topographic information and applying a 1D steady state gradually varied flow model (see Section 6.4 for details).

The first method is the only one that can be applied with the available published information because researches usually report mean values of depth and width. Instead, when information of each cross section is available, mean values for area and hydraulic radius can be calculated and the second method can be applied. Because more information is used this method is supposed to give better results. In order to have a reference value for the comparison, the third method is assumed to provide the most accurate value of friction factor, because cross sections are used instead of aggregated parameters.

Table 8.1 presents the friction factor calculated by means of the three methods for each river reach of this study. The Alto Chubut river has been excluded because it presents a friction factor value too high, which is out of the normal range (f calibrated is equal to 2.4). This anomaly could be attributed to a recent intensive flood[15] that has lowered the bottom channel. According to a dweller, previous to the flood it was possible to cross the river with a horse because the bed had gravels and sand. But after the flood it was not possible any more due to the presence of cobbles and blocks. A careful inspection of inflexions points in the cross sections has revealed a possible 0,40 m lowering in the bottom elevation that could explain the high value of f[16].

Table 8.1. Friction factor for gravel bed rivers in Patagonia and Italy. The equivalent Manning's n has been calculated using the calibrated friction factor.

Code	Stream	Location	Friction factor			Manning`s
			Method 1	Method 2	Calibrated	n
2211	Gualjaina River	Loc. Gualjaina	0.129	0.113	0.104	0.038
2228	Lepà Creek	Loc. Gualjaina	0.162	0.118	0.130	0.037
2206	Chubut River	Loc. El Maitèn	0.092	0.085	0.085	0.034
2204	Carrileufu River	Loc. Cholila	0.075	0.062	0.062	0.031
2230	Cohihues Creek	P.N. Los Alerces	0.192	0.135	0.149	0.035
2212	Mayo River	Loc. Río Mayo	0.116	0.078	0.078	0.030
1811	Quemquemtreu River	Escuela Nº 139	0.329	0.272	0.264	0.055
1817	Azul River	El Azul	0.152	0.143	0.140	0.041
2208	Epuyén River	La Angostura	0.181	0.139	0.126	0.040
IT101	Piave River (P)	Perarolo	0.062	0.049	0.049	0.023
IT102	Piave River (BL)	Belluno	0.073	0.065	0.095	0.034
IT103	Piave River (S)	Segusino	0.065	0.051	0.064	0.030
IT201	Brenta River	Bassano del Grappa	0.055	0.053	0.059	0.029
IT301	Cordevole River	Ponte Mas	0.020	0.017	0.017	0.013

[15] During the winter of 2009 there was a flood with peak discharge of 46m3/s (RI 6 years). The survey was carried on the next summer season (February, 2010).

[16] For instance, considering eq. 8.1, keeping S,Q and B constant but increasing H, It follows that f must also increase.

Another unexpected value is that of Cordervole River, but in this case it is somewhat low. In fact the calibrated friction factor f is 0.017, or its Manning's n equivalent value is 0.013[17]. A possible explanation is that the discharge considered is rather high and hence the friction factor must be low for enhancing conveyance. This hypothesis can be supported with the presence of a secondary channel (Figure 7.17) that may divert some discharge at bankfull stage, and hence, the actual discharge carried by the main channel would be lower and the friction factor, higher. A similar, but not so extreme situation is found in Piave River at Perarolo (Manning's n equal to 0.023).

For the rest of the dataset, the friction factor or its equivalent Mannings's coefficient are within expected values for gravel bed rivers (see Chow, 1994; Barnes, 1967).

8.1.1 Comparison of different methodologies

The first analysis consists of comparing method 1 and 2 against method 3. A graphical representation of table 3 is presented in Figure 8.1. It is evident that the second method gives the best result. Almost all the points that belong to the first method are above the line of perfect agreement, i.e., this method overestimates the friction factor. On the other hand, the points of method 2 are placed around the perfect agreement line. Performing a analysis of variance of the slope it can be said that the slope of the scatterplot from method 1 (which is 1,28) is significant different to 1 (p-value 0,005) and hence method 1 gives results significant overestimated according to method 3 (by calibration). Instead, the null hypothesis is accepted for method 2 (p value 0,516) and hence the slope is equal to 1, i.e, method 2 gives the same results that method 3.

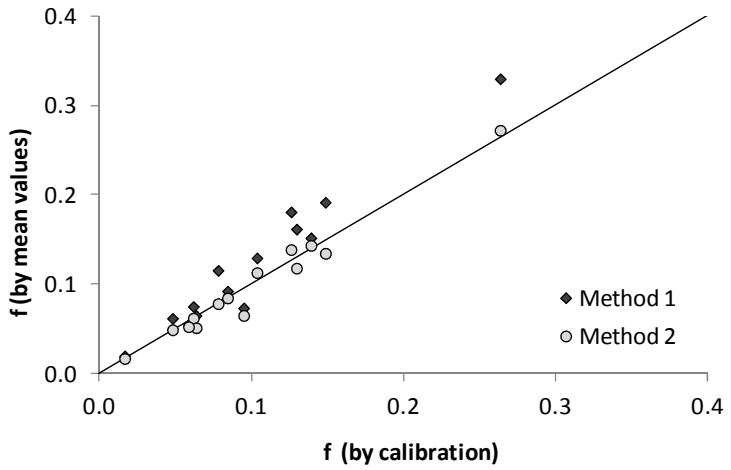

Figure 8.1. Comparison between two different methods for evaluating the friction factor from reach average values. The continuous line represent the perfect agreement (slope = 1). The dashed line is the regression model for method 1.

Inspecting eq. 8.1 it is seen that there are two possible sources of error which are related to the approximation of hydraulic radius and mean velocity. The first one consists on approximating the hydraulic radius with the mean depth. However, both parameters are almost equal for wide channels; in this study, the aspect ratio ranges from 29 to 89 and the error introduced when using the aforementioned approximation is less than 3%. Because this difference is small the second approximation should be the major source of error. It regards the use of reach-average velocity:

[17] Such a low Manning's n value is found in artificial channels with smooth concrete surfaces (Chow, 1994).

method 1 calculates U from the discharge and mean width and depth ($U = Q \cdot H^{-1}B^{-1}$) instead of taking the average of the velocity along the reach ($U = Q \cdot \overline{A^{-1}}$). In order to put in evidence this aspect equation 1 is divided by equation 2 and the following assumptions are considered: $R_H \cong H$ and $f_2 \cong f_3 \cong f$, i.e., the hydraulic radius is equal to the mean depth and the friction factor from method 2 is equal to that of method 3 which is considered to be indeed the true value.

$$\frac{f_1}{f} = \frac{\left(\overline{A^{-1}}\right)^2}{(H^{-1}B^{-1})^2} \qquad 8.3$$

Then, the relative errors are defined[18]:

$$\varepsilon_f = \frac{f_1}{f} - 1 \qquad 8.4$$

$$\varepsilon_A = \frac{\left(\overline{A^{-1}}\right)^2}{(H^{-1}B^{-1})^2} - 1 \qquad 8.5$$

The theoretical equation 8.3 indicates simply that relative errors are equal. Figure 8.2 exhibits a very good trend between the variables. Two points are considered outliers because they are far away from the main scatter[19]. Performing a regression model it is seen that almost 66% of the variation in f error is explained by the variation in the Area error. However, the regression line has a slope below 1 and an ordinate intercept different to zero. In order to test if the empirical model is different to equation 8.3, a test for the slope and intercept was performed. In the case of the slope, the null hypothesis states that the slope is equal to 1. It was accepted with a p-value 0.436. The null hypothesis for the intercept states that it is zero and was also accepted with a p-value 0.404. Therefore, the theoretical model is accepted and it can be affirm that the error in the determination of the friction factor according to method 1 is due to an incorrect evaluation of the reach-averaged flow velocity.

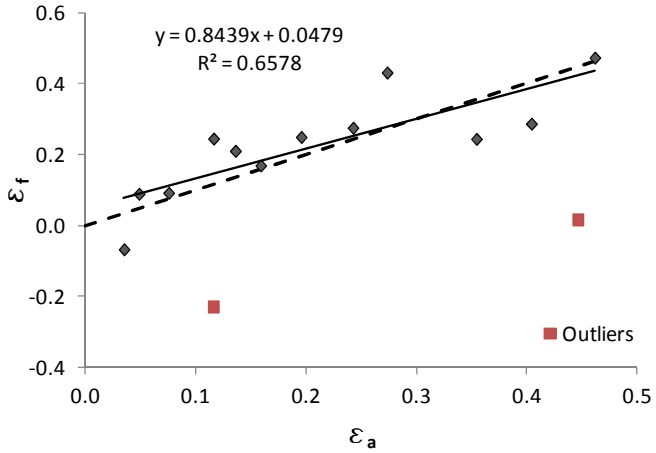

Figure 8.2. Relationship between the relative error in the determination of the friction factor and the way of evaluating the reach average mean velocity. The continuous line is the empirical model (linear regression) and the dashed line is the theoretical relation according to equation 8.3.

[18] The actual definition of the relative error of areas should not include the squares but they have been kept for performing later a liner regression, otherwise, a change of variables should have been done for linearization.
[19] The residual (observed value minus the predicted value with the regression model) is significant different to zero with a p-value below 0.001.

8.1.2 Performance of Kamphuis's model

In chapter 3, it was presented a detailed review of studies conducted to relate energy losses with bed roughness (see section 3.1.3 "Skin roughness and the plane bed reach"). It was underlined an inconsistency between results from flume experiments and those from field measurements. In short, experiments evidence suggested that the roughness height in a plane-bed channel was 2 D_{90}. On the contrary, analyzing field measurements Millar (1999) suggested that roughness measures such as 3 D_{84} or 2 D_{90} overestimated the grain roughness and inherently included a component of the form roughness; he proposed that $k_s = D_{50}$. Why does a gravel bed river, which also has a hydraulic rough boundary, has a roughness much lower than flumes in laboratory? This topic will be re-analyzed in the light of the findings of this study. First of all, it must be recognized that usual published data allows only the use of method 1 for calculating the friction factor and this is the data employed by Millar. In the previous section it has been shown that approximating the mean velocity with the expression $U = Q \cdot (H^{-1}B^{-1})$ produced overestimated values of friction factor. Therefore, the calibrated value will be used for this comparison.

The calibrated value of friction factor is used to back-calculate the roughness height by means of the Keulegan's equation:

$$\sqrt{\frac{8}{f}} = \frac{1}{k} ln\left(11 \frac{R_H}{k_s}\right) \qquad 8.6$$

Figure 8.3 shows the calculated roughness k_s/D_{90} and also includes flume experiment results from Kamphuis (1974) and Diplas (1990). Experimental data is located around $k_s/D_{90} = 2$ limited by a lower value of 1 and an upper value of 3. Field data seems also to fit within this range but there are some points that require a special inspection. Cordevole River and Piave River at Perarolo exhibit very low roughness values (points 3 and 4 in figure 8.3). This situation has already been detected previously and now it is translated into roughness calculus. With regards to Quemquemtreu River and Gualjaina River (points 1 and 2 in figure 8.3), the roughness is high but the reason is not clear.

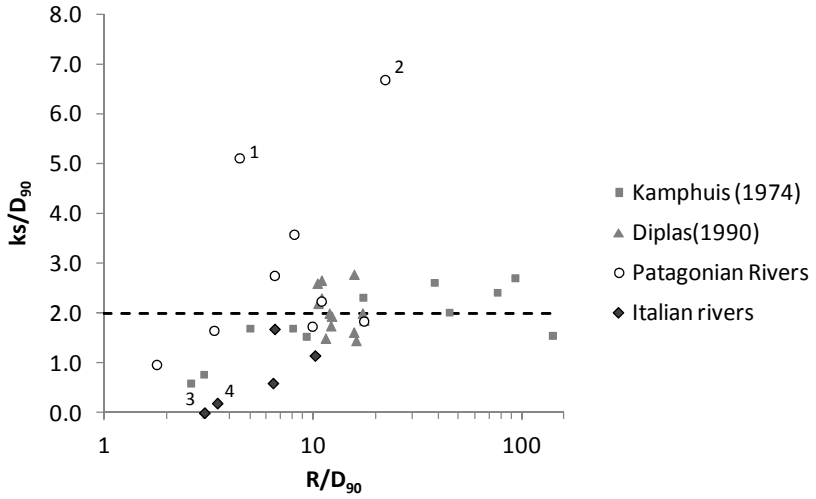

Figure 8.3. Roughness height comparison between gravel bed rivers and flume experiments. The dash line is the mean value proposed by Kamphuis (1974) and verified later by Diplas (1990) and Wong and Parker (2006). Numbers indicate: 1) Quemquemtreu River; 2) Gualjaina River; 3) Cordevole River; and 4) Piave River at Perarolo.

Excluding the outliers aforementioned, the mean of both populations (field and flume) are compared. Appling a t-test it is seen that both mean are equal with a p-value of 0,598. Then the comparison indicates that the roughness height evaluated as $k_s/D_{90} = 2$ is also applicable to gravel bed rivers, at least to those surveyed in this study, in contradiction with Millar's (1999) conclusions. Because laboratory results are based on plan-bed channels, it suggests that at bankfull stage, bed roughness is the major source of turbulence and energy dissipation in gravel bed rivers. Bed forms do have their contribution but should be more important at lower stages. This conclusion is coherent with previous studies like those of Parker and Peterson (1980), Jaeggi (1984) and Miller and Wenzel (1985) (see section 3.5.2 for details).

Finally, it is not clear why some gravel bed rivers have such low roughness values that have influenced Millar to proposed the envelope $k_s = D_{50}$ and to contradict laboratory evidence. However, it seems reasonable that mean hydraulic geometry data should be used with caution and care inspection of the local hydraulic conditions at each reach should be paid. For instance, some Italian river reaches may be interpreted to lie near Millar's envelope while actually the friction factor has some bias. Figure 8.4 shows the typical scatterplot using method 1.

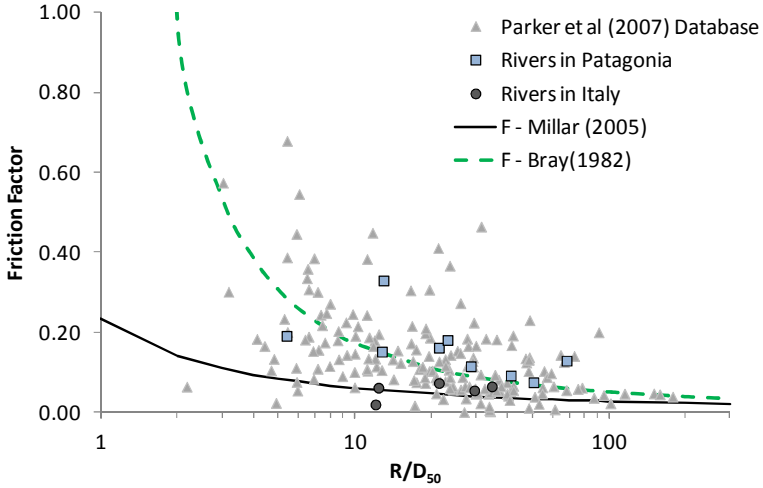

Figure 8.4. Relationship between the friction factor and the relative submergence for studied reaches and published data. Friction factor is evaluated with method 1 (see text).

8.2 Performance of regimen theories

In the first chapter it was stated that this study was based on the general assumption that ***physical laws and constrains described the behaviour of a population of river reaches, instead of describing the exact processes within a single river reach***. Furthermore, each object contained in the population ***had uncertain boundaries (width, depth) and uncertain properties (median grain size, slope, bankfull discharge).*** After, in Chapter two, a detailed review of regime theories put in evidence some issues concerning the definition of degrees of freedom. Following Weichert et al. (2009), the appropriate spatial scale for this kind of study is what they have named the macro-scale. At this spatial scale surface material and cross section are allowed to change but slope is considered as an independent variable.

On the other hand, the armour layer found at the bed surface is straightly related to the upstream sediment supply, as has been shown in Chapter 4. But, the sediment supply and a transport model are used in regime theories for deriving a third relation for the slope (that is considered a degree of freedom). Because sediment supply is very difficult to evaluate and it is not a usual data published with hydraulic geometry, researches have replaced it by a sediment transport relation using the slope as a known value (for instance, Millar, 2005). But the approach proposed here is conceptually different in two aspects. First, the slope is imposed (i.e., treated as an external control) because it takes a longer time span for the reach to adjust it and so, it is related to the river organization at a larger spatial scale. Secondly, the observed surface material is an indication of the sediment load that the river reach receives. If, for a specific studied reach, the supply was higher, then the observed grain size would be smaller (following Dietrich et al., 1989, see section 7.6). Then, imposing the observed surface grain size stands for the current sediment supply.

To sum up, for this study only the cross section (depth and width) is considered as a degree of freedom, while slope, discharge and surface material will be imposed to the channel. This assumption will be test with three regime models: Millar (2005), Parker et al. (2007) and Ikeda et al (1982). All of them include a criterion for bank stability (details in Chapter 2). Furthermore, two modified models are proposed introducing explicitly the slope as an independent variable in the aforementioned models (the calibrated values to be used in eq. 2.9 are : $a = 4{,}39$; $n = 0{,}210$.

The first modified model (hereafter MM1) is based on Parker et al.`s (2007), but slope is introduced as an external control instead of being correlated against liquid discharge as in the original model. Therefore, the same relation is used for the stability criterion and equation 45 of Parker et al. (2007) is used for the flow resistance because it was calibrated using S as an independent variable.

The second modified model (hereafter MM2) is based on Millar's (2005). It considers the Keulegan's (1938) equation for energy dissipation with Bray's (1979) calibration for roughness height. The stability criterion consists on a comparison between mean shear stress and the reference shear stress for sediment transport, as used by Parker et al. (2007), but introducing the dependence of the reference shear stress with slope as proposed by Muller et al. (2005).

Table 8.2. Summary of the properties of river reaches selected used in this study including data from literature.

Dataset	Depth (m)		Width (m)		Discharge ($m^3 s^{-1}$)		Surface D_{50} (m)		Slope (m m^{-1})		Reference
	min	max	min	max	min	Max	min	max	min	max	
Patagonia	0.28	1.81	10.38	64.11	4.2	129.2	0.020	0.067	0.0008	0.0185	This study
Italy	0.59	1.42	37.58	99.90	57.0	350.0	0.036	0.050	0.0022	0.0060	This study
Britain	0.77	5.25	12.30	77.10	7.1	424.0	0.020	0.091	0.0012	0.0109	Hey & Thorne (1986)
Colorado	0.34	1.85	7.25	83.80	2.2	255.0	0.023	0.122	0.0009	0.0110	Andrews (1984)
Idaho	0.24	2.78	2.80	89.20	0.6	652.0	0.027	0.207	0.0005	0.0509	Mueller et al. (2005)
Alberta	0.71	6.83	26.21	544.68	23.8	7220.8	0.026	0.117	0.0007	0.0059	Bray (1979)
Alberta	0.58	6.95	18.00	280.00	11.9	5440.0	0.027	0.145	0.0004	0.0150	Kellerhals et al. (1972)
Lab. Nº 1	0.013	0.017	0.48	0.99	0.0030	0.0043	0.0014	0.0018	0.0096	0.0118	Eaton & Church (2004)
Lab. Nº 2	0.028	0.049	0.52	0.70	0.0055	0.0107	0.0013	0.0015	0.0020	0.0034	Ikeda et al. (1988)

Data for the test is provided by this study and an extra published dataset composed of hydraulic geometry data of gravel-bed rivers in other geographical regions in the world. The selected rivers fulfill the following requirements: scarce bank vegetation, complete description of surface grain size distribution (at least D_{50} and D_{90}) and channel geometry. The database is composed of 33 river reaches from Alberta, Canada (Bray 1979, and Kellerhals et al., 1972), 13 reaches from Britain (Hey and Thorne, 1986), 32 from Idaho, USA (Mueller et al., 2005), 14 from Colorado, USA (Andrews, 1984), and 36 small laboratory streams (Ikeda et al., 1988; Eaton and Church, 2004). A summary of the principal features for each dataset is presented in table 8.2.

8.2.1 Performance of regime models

Figure 8.5 shows the comparison of dimensionless predicted parameters H* and B* against observed values. A quick visual inspection reveals that Parker et al.'s model provides the best performance, and good results are also attained by Millar's and Ikeda et al's models. However, when slope is introduced as an external control in Parker et al.'s model the prediction capacity is lower and scatter is higher (MM1, Figure 8.5, d). On the other hand, the second modified model (MM2 based on Millar's model) presents an evident systematic deviation.

Model's performance was quantified using two indices: the average deviation (AD) defined as the mean value of the relative difference between predicted and observed values, and the mean square-root deviation (RMD) which expresses the scatter of predicted values with regards to the mean prediction:

$$AD = \frac{1}{N}\sum_{k=1}^{N}\frac{x_k^{pred} - x_k^{obs}}{x_k^{obs}} \qquad 8.7$$

$$RMD = \sqrt{\frac{1}{N-1}\sum_{k=1}^{N}\left(\frac{x_k^{pred} - x_k^{obs}}{x_k^{obs}} - AD\right)^2} \qquad 8.8$$

Table 8.3 contains the results of the predictions of dimensionless depth applying both indexes to each data set, and to the whole data base. The table also contains the correlation coefficient between predicted and observed values and its standard error. Millar's model shows the best performance, being the mean predicted depth 2.4% lower than observed, while Ikeda et al.'s model and the MM1, also give good predictions (AD equal +4.3% and -5%, respectively). However, this statistics refer to the overall data. A closer inspection to models performances on each data set reveals that Britain streams are largely underpredicted. Ikeda et al.'s model predicts fairly well each dataset giving more uniform values of AD, however the scatter is larger within each dataset (see RMD and SE). Parker et al's model presents some discrepancies as results from Italy, Britain and Alberta datasets. On the contrary the overall performance is good. A zero value of AD was obtained with the MM2 calibrating the stability criterion. For the whole database, the mean shear stress results to be 1.38 times the references shear stress. The scatter is quite similar among models, with a lowest RMD value of 0.26 (Parker et al.'s model) and highest value of 0.56 (MM1).

With regards to width (Table 8.4), Ikeda et al.'s model and Parker et al.'s model give the best prediction for the whole data set with AD values of -2% and -6%, respectively. Although AD values are very similar, Parker et al's model presents the lowest RMD value and SE, as well. Millar's model also has a good performance. Width is overpredicted by 15%, and fails particularly in laboratory

cases. However, if only natural stream are considered its performance is better: AD=0.07 and RMD = 0.22. The performance of modified methods is lower than aforementioned models, having larger values of AD and scatter, as well.

Table 8.3. Performance indexes (Average deviation AD, and Mean square-root deviation RMD) applied to predictions of dimensionless depth. Correlation coefficient (Cor) with its standard error (SE_{cor}) are also included for the whole dataset. Underlined values indicate the lowest AD value for each dataset.

Streams	Millar (2005)		Parker et al. (2007)		Ikeda et al. (1988)		MM1 (after Parker's)		MM2 (after Millar's)	
	AD	RMD	AD	RMD	AD	RMD	AD	RMD	AD	RMD
Patagonia	0.08	0.30	0.29	0.26	0.19	0.41	0.08	0.50	**0.01**	0.31
Italy	0.14	0.23	0.88	0.28	0.18	0.28	**-0.10**	0.22	-0.13	0.24
Idaho	-0.02	0.51	**0.01**	0.21	0.14	0.64	-0.01	0.91	0.35	0.63
Britain	-0.40	0.19	-0.41	0.10	**-0.29**	0.24	-0.37	0.31	-0.35	0.33
Colorado	0.13	0.16	**0.10**	0.19	0.24	0.23	0.15	0.25	0.17	0.21
Alberta	0.09	0.33	0.39	0.24	**0.08**	0.44	0.10	0.61	-0.11	0.44
Laboratory	-0.10	0.07	0.22	0.37	**-0.08**	0.09	-0.21	0.17	-0.13	0.10
All Data	**-0.02**	**0.31**	**0.17**	**0.26**	**0.04**	**0.40**	**-0.05**	**0.56**	**0.00**	**0.40**
Cor (SE_{cor})	**0.941**	**(0.026)**	**0.951**	**(0.026)**	**0.911**	**(0.035)**	**0.870**	**(0.042)**	**0.886**	**(0.039)**

Table 8.4. Performance indexes (Average deviation AD, and Mean square-root deviation RMD) applied to predictions of dimensionless width. The last row contains the correlation coefficient (Cor) with its standard error (SE_{cor}) for the whole dataset. Underlined values indicate the lowest RMD value for each dataset.

Streams	Millar (2005)		Parker et al. (2007)		Ikeda et al. (1988)		MM1 (after Parker's)		MM2 (after Millar's)	
	AD	RMD	AD	RMD	AD	RMD	AD	RMD	AD	RMD
Patagonia	-0.13	0.39	-0.31	0.18	-0.28	0.41	0.23	0.91	**-0.01**	0.52
Italy	0.26	0.52	-0.26	0.16	**0.14**	0.66	1.19	1.39	1.14	1.21
Idaho	0.19	0.50	**-0.01**	0.21	-0.10	0.43	0.72	1.18	-0.36	0.36
Britain	**-0.02**	0.36	-0.07	0.12	-0.25	0.34	0.12	0.68	0.07	0.78
Colorado	-0.08	0.13	**-0.04**	0.14	-0.34	0.12	**-0.07**	0.23	-0.14	0.33
Alberta	**0.07**	0.59	-0.24	0.16	0.16	0.95	0.70	1.73	0.96	1.68
Laboratory	0.41	0.15	0.16	0.36	**0.14**	0.17	0.92	0.65	0.44	0.27
All Data	**0.15**	**0.41**	**-0.06**	**0.23**	**-0.02**	**0.53**	**0.62**	**1.11**	**0.29**	**0.89**
Cor (SE_{cor})	**0.942**	**(0.028)**	**0.973**	**(0.020)**	**0.894**	**(0.038)**	**0.787**	**(0.052)**	**0.92**	**(0.033)**

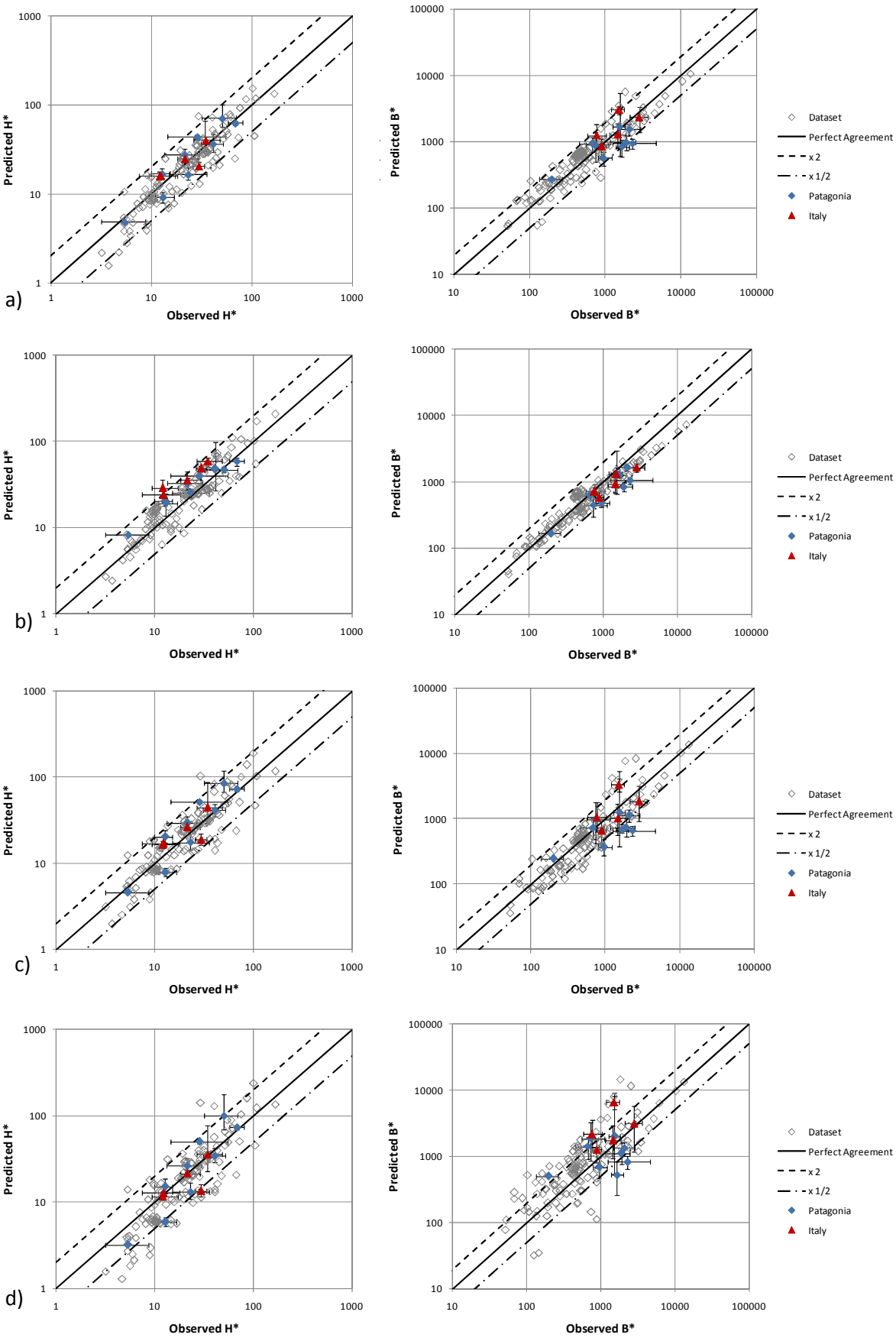
a)
Predicted H*
Observed H*
1000
100
10
1
Predicted B*
Observed B*
100000
10000
1000
100
10
Dataset
Perfect Agreement
x 2
x 1/2
Patagonia
Italy
b)
c)
d)

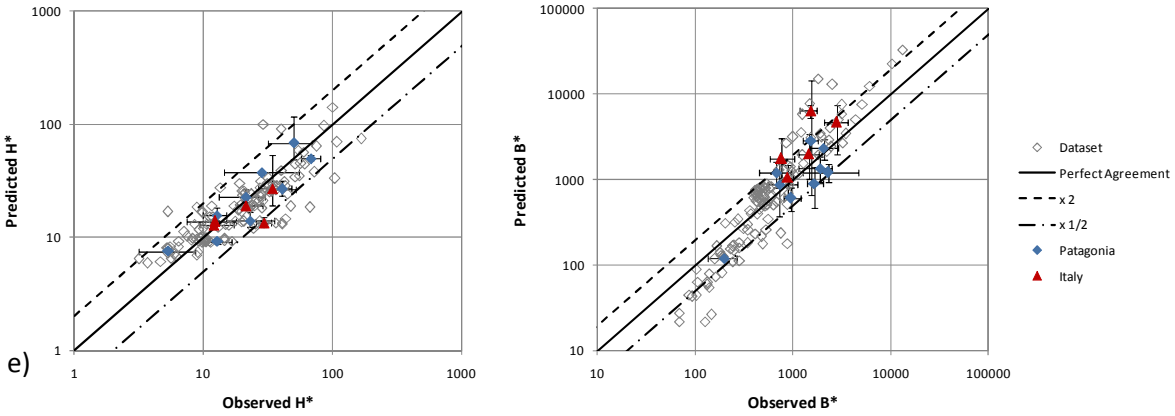

Figure 8.5. Performances of regime models: a) Millar's model; b) Parker et al.'s model; c) Ikeda et al.'s model; d) MM1 after Parker's; and e) MM2 after Millar's. Graphs show on the left: dimensionless water depth (H*); and on the right: dimensionless channel width (B*). Dashed lines indicate a two-time overprediction and one half-time underprediction. Bars represent the confidence interval (with a probability of 95%) associated with data (horizontal bar) and its propagation into predicted values (vertical bar).

8.2.2 Variability in source data and propagation into models

The natural variability of hydraulic geometry parameters is propagated into dimensionless parameters H*, B* and Q*. Confidence intervals for each parameter are shown in Figure 8.5. On the mean, dimensionless depth is expected to be found within a relative range of -28% to 40%; dimensionless width has also a similar interval: -26% to 35%. On the contrary, dimensionless discharge has a wider range between -34% to 45%. Data variability can be used to assess the confidence interval for predictions. This task is accomplished performing a Monte Carlo approach. Section 6.3 exposes the procedure for computing the confidence interval of dimensionless parameters. The procedure used here is similar but the functions that relate source data with dimensionless parameters (equations 6.30 and 6.31) are changed by more complex functions according to each theoretical model. The incidence of data variability in the prediction accuracy is also shown in Figure 8.5. The horizontal bars are the confidence interval for dimensionless parameters as results from observed variability in H, B and D_{50}. The vertical bars indicate the confidence interval for the determination of H* and B* subject to the variability in independent variables, i.e., bankfull discharge, mean diameter and slope. It is evident how the variability in source data affects the prediction's accuracy. Furthermore, confidence intervals cover an area similar to the scatter in the reference dataset. Table 8.5 reports the mean confidence interval for predicted H* and B* considering data from Patagonian and Italian streams. Almost all the models seem to have the same sensibility to source data variability. In particular, Parker et al.'s model has the narrowest confidence interval for B* prediction (-19%; 25%), however, when the slope is introduced (MM1 model), that interval is the widest (-41%; 71%). In the case of H* all the models exhibit similar performances, on the mean it is between -14% and 23%.

Table 8.5. Mean confidence interval (95%) for predicted variables H* and B* according to different regime models.

Model	H* (2.5%)	H* (97.5%)	B* (2.5%)	B* (97.5%)
Millar	-12%	19%	-31%	45%
Parker et al.	-17%	21%	-19%	25%
Ikeda et al.	-13%	22%	-35%	66%
MM1	-15%	28%	-41%	71%
MM2	-11%	22%	-41%	74%

8.2.3 The slope as an external control at the reach scale.

When the slope is introduced as an independent variable in Parker et al.'s model (2007), its performance decreases abruptly (as inferred from Figure 8.5d), and the scatter (RMD) for B* and H* increases (Tables 8.3 and 8.4). In Parker et al.'s model S is a dependent variable related with the dimensionless discharge Q*. The dependence of H*, B* and S with Q* is explained by the physical constrains: flow resistance (eq. 2.9), channel stability (eq. 2.11), sediment transport (eq. 2.10), and sediment supply (2.12); the last one been a relation between sediment transport at bankfull discharge and the bankfull discharge. For convenience these relations are reproduced again in an arranged form:

$$Q = a\left(\frac{H}{D_{50}}\right)^{n}\sqrt{gHS}(HB) \qquad 8.9$$

$$\tau^{*} = \frac{HS}{R_s D_{50}} = r\tau_c^{*} \qquad 8.10$$

$$q_b^{*} = 11{,}2(\tau^{*})^{3/2}\left(1-\frac{\tau_c^{*}}{\tau^{*}}\right)^{4{,}5} = a_q(Q^{*})^{n_q} \qquad 8.11$$

This set of equations constitutes the heart of Parker et al.'s model. But in order to solve them an extra empirical relation is added for the critical shear stress: the authors proposed that τ_c^{*} is a power function of dimensionless discharge[20]. This additional expression was dictated by the particular way the authors defined dimensionless parameters (see section 6.3). Then, it is plain to see that all the three variables: depth, width and slope, must be a function of discharge.

This way of elaborating the theory, i.e, the choice of dimensionless parameters and the discharge dependence is not trivial. Assuming S as a dependent variable the model filters the noise in S with the relationship S-Q*, and in this way, reduces the deviations in B* and H*. It is not the same to have the actual value of slope as observed in the field that to have a value from a fitted model. It can be said that the model is weak in this respect.

What would be the performance of Parker et al.'s model if the actual slope value was used instead of the fitted model? Modified Model 1 was defined so as to answer this question. MM1 incorporates a resistance law calibrated by Parker et al. using information about width, depth, discharge and slope.

[20] The authors indicate that it is a weak relation. In fact, the exponent n_q is 0,057 and a t-test with a null hypothesis n_q= 0 gives a p-value of 0,068. Then the information is not enough to render significant this relationship.

This means that the modified model considers the slope as an external control and does not use the resistance law calibrated by these authors where S is related with Q (equation 44 in Parker et al., 2007). However, the modified model also adopts the same stability criterion relating the critical shear stress with dimensionless discharge. This model has the worst performance for predicting B*, as results from the highest values of AD and RMD (Table 8.4) and has a good performance only in the case of Colorado dataset. With regards to depth, although the overall result seems quite good (AD value of -0.05) the RMD index evidence a wide variability (RMD = 0.26).

Modified Model 2 presents a systematic deviation as is evident from the slopes in Figure 8.5e: 0.70 for H* and 1.39 for B*; both of them are significantly different to 1 with a p-value below 0.01. This deviation is a result of the model structure and can be explained linking predicted and observed dimensionless depth (hereafter H^*_{pred} and H^*_{obs}). Mueller et al. (2005) proposed a linear relationship between the reference Shields stress and the channel slope.

$$\tau^*_r = 2.18S + 0.021 \qquad 8.12$$

Shear stress is linked to water depth (H^*_{pred}) using the uniform flow approximation.

$$\tau^* = \frac{H^*_{pred} S}{R_s} \qquad 8.13$$

Replacing eq. 8.12 and eq. 8.13 into eq. 8.10, and solving for H^*_{pred} it results an expression like this one:

$$H^*_{pred} = a + bS^{-1} \qquad 8.14$$

wherein a and b are two coefficients. On the other hand, a regression model relating Slope and observed values of depth (H^*_{obs}) can be fitted showing that the slope is nearly inversely proportional to H^*_{obs}.

$$S = 0{,}084 H^{*-1.02}_{obs} \qquad 8.15$$

Finally, adopting a unit exponent and including 8.15 into 8.14, a linear relationship is found between H^*_{pred} and H^*_{obs} with a slope coefficient below 1:

$$H^*_{pred} = 0{,}56 H^*_{obs} + 4{,}96 \qquad 8.16$$

This expression indicates that there will be underestimations when $H^*_{obs} > 11.3$. Finally, an error in the determination of H* affects B* estimation. An underestimation in H* will required a wider channel in order to verify the flow resistance equation. That's why the slope in the width scatterplot is higher than 1 (figure 8.5e).

8.2.4 Interpretation of recent channel changes in the Piave and Brenta rivers.

As most of Italian rivers, the Piave and Brenta rivers have experienced dramatic morphological changes due to human interventions, extensively studied by means of historical maps and aerial photos (Surian, 1999; Comiti et al., 2011; Surian and Cisotto, 2007)[21]. Evidence support the hypothesis that sediment supply rather than flow regime was the key factor driving the narrowing

[21] A brief history of recent morphological changes of Piave and Brenta rivers has been presented in Chapter 5.

trends of both rivers (e.g. Surian et al., 2009; Comiti et al., 2011). Regime models are here used to interpret recent channel changes. However, it must be pointed out that, because regime models suppose channel equilibrium, a condition not satisfied in these rivers, the interpretation and management extrapolations have to be considered and used cautiously.

Millar's (2005) regime model has been chosen because it incorporates sediment supply as an independent variable. On the contrary, Ikeda et al.'s model do not invocate any sediment transport model and in Parker et al.'s model the sediment supply depends on water discharge, assumed to remain constant (see later).

Millar's model relates dimensionless width (B*) with dimensionless, discharge (Q*), sediment concentration C and bank strength (μ'):

$$B^* = 28{,}1Q^{*0.50}C^{*-1.12}\mu'^{-1.66} \qquad 8.17$$

where C* is a log-transformation variable for C ($C* = -log\ C$). This formula indicates that the channel will enlarge if sediment supply raises or bank strength decreases. Millar (2005) also proposed a criterion to distinguish between single thread (meandering) and braided channels. A river reach will develop a single-thread meandering pattern only in two situations, a) the valley slope is higher than the minimum slope required to convey sediment load; or b) the required channel slope is below the meandering-braided transition slope. When condition a) is not verified the channel aggrades and a braided patter may emerge. In the second case, the channel is too steep and flow-sediment instability drives channel to a braided configuration (Parker, 1976). Millar's equation for meandering-braided transition slope reads as follows:

$$S^* = 0{,}0975Q^{*-0.25}\mu' \qquad 8.18$$

These two expressions will be used to interpret Piave and Brenta rivers recent changes. In order to apply these equations, has the channel-forming discharge remained constant along the study period? For both rivers by the end of the fifty's all the major dams where already constructed and since then, discharges have been regulated. Because channel forming discharges occur only during flood events, an analysis of flood frequency can reveal the possible interference due to dam regulation. Figure 8.6 shows the annual probability of maximum peak discharges for Piave and Brenta rivers. Records were divided into two groups: pre- and post-dams (following Da Canal, 2006; and Surian, 1999).

A visual inspection of figure 8.6 suggests that curves overlap quite well and dams should not change peak discharges. This conclusion is supported also in quantitative terms applying the Mann-Whitney non-parametric test. The null hypothesis to be tested states that the two samples come from identical populations. In the case of Piave River, a p-value of 0.90 was found indicating that the null hypothesis is accepted. Also in the case of Brenta River a high p-value was found (0.94). Then, it can be assumed that the channel-forming discharge has remained constant along the study period because dams have not significantly altered flow regime.

Mean grain diameter is also assumed to remain constant. Although this assumption can be questioned because the surface grain size distribution does change with sediment supply (see comments in section 7.6), there is not information that can be used to describe this change. The research conducted by Surian (1999) in the Piave River provides a detailed description of morphological and geometrical changes, stressing the role of various types and degree of human

impacts on this river. However, there are no references to grain size changes overtime. Later Surian (2002) focused on sediment size and showed that grain size can change substantially due to the presence of human disturbances and structures and natural tributaries. Because of the high spatial variability and the lack of evidence of temporal variability, the simple assumption of grain size constancy at large spatial scale is considered in this analysis.

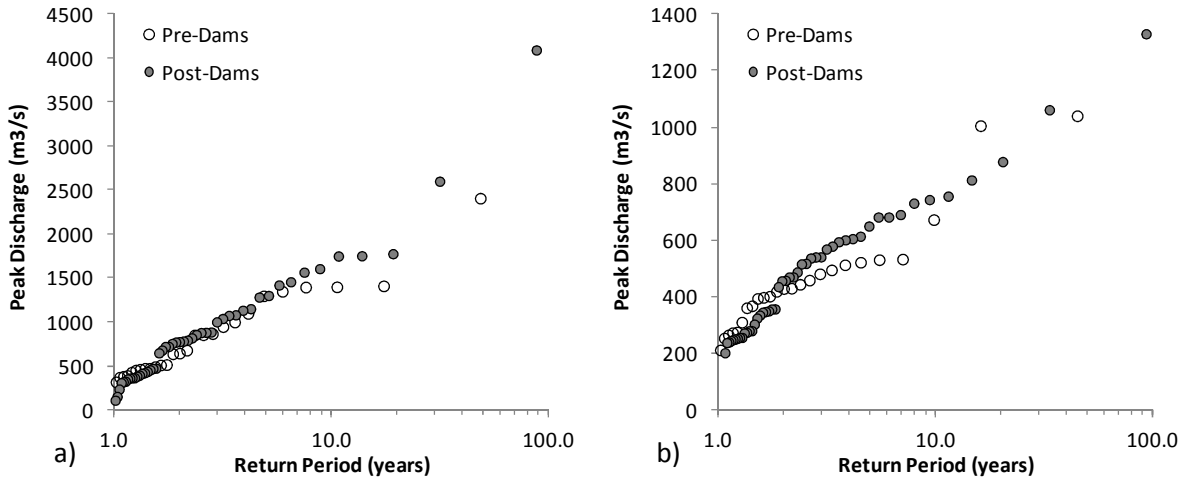

Figure 8.6. Comparison of probability curves for peak discharges before and after dams construction in Piave (a) and Brenta (b) rivers.

Consequently, keeping discharge and grain size constant, a change in width must only be a consequence of an alteration in sediment supply or bank strength. Millar (2005) calibrated the μ' parameter against Hey and Thorne's (1986) and Andrews's (1984) data. A condition of scarce vegetation, i.e., lowest strength, corresponds to μ' = 1. On the contrary, in the case of thick vegetation (type IV for Hey and Thorne) μ' assumes a maximum value of 1.50, approximately.

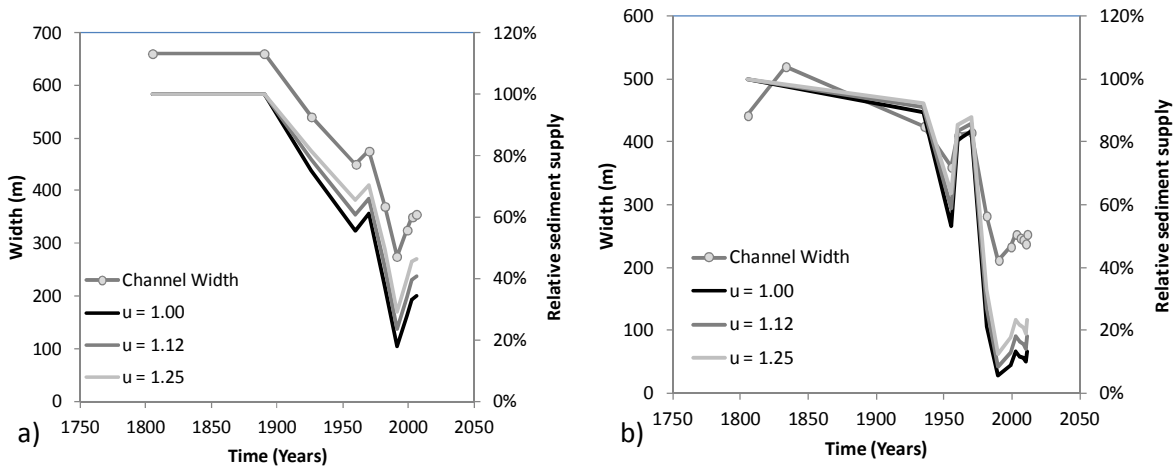

Figure 8.7. Morphological changes in the Piave (a) and Brenta (b) rivers and the corresponding sediment supply variation as calculated applying Millar's model. Calculi have been made for different values of bank strength (μ), between sparse vegetation (μ = 1) to moderate bank density vegetation (between categories II and III according Hey and Thorne, 1986).

The overtime change in sediment supply has been back-calculated from reach average values of width, under scenarios of different bank strengths. In the Brenta River there is a clear reduction in

sediment supply since 1930 up to the end of 20th century, but interrupted in the 60's with a peak in supply (Figure 8.7b). The lowest value is attained in 1990 (between 5% and 12%). After that there is a low recovery been the load in the last surveys (2011) between 13 – 25% of the initial one. Bank strength seems to have a minor role in explaining width change.

With regards to Piave River, a similar trend has been found, with a first reduction phase from 1930 to 1960 where sediment supply decreases 40%, and a second phase after a low increase in the 60's, from 1970 to 1990 with a reduction of 42% (Figure 8.7a). The lowest sediment supply is attained in 1991, 24% of sediment supply of the initial situation. After 1990 there is a low recovery reaching 40% by 2006.

As documented by historical maps and aerial photos, Piave River exhibited a braided pattern until 1930 (Comiti et al., 2011). During the narrowing phases channel configuration gradually migrated from braiding to a wandering pattern (see channel extent in Figure 8.8). Besides, the braiding index (the mean of the number of channels) reduced from about 3.4 to 1.5 (Surian, 1999). Equation 8.18 has been used to check if a morphological pattern adjustment was related to a change in sediment supply, and results show that the threshold slope for Piave River is about 0.0060 m m^{-1}. On the other hand, the actual slope of the Piave River within the study reach is 0.0045 m m^{-1}, i.e., the 75% of threshold value. This would entail that the original braided pattern should be attributed to a condition of sediment overloading, i.e the channel was not steep enough to convey sediment supply and the channel aggraded. As a consequence, a reduction in sediment supply would imply a direct change in channel pattern because a single-thread channel would be hydraulically stable for that slope. In the case of Brenta River, its mean slope is 0.0036 m m^{-1} while the threshold slope is between 0.0036 m m^{-1} (for μ' = 1.0) and 0.0045 m m^{-1} (for μ' = 1.25). The threshold value is much closer to the actual mean slope. Sub-reaches with slope above the threshold are expected to remain in a multi-thread configuration even under conditions of sediment supply reduction.

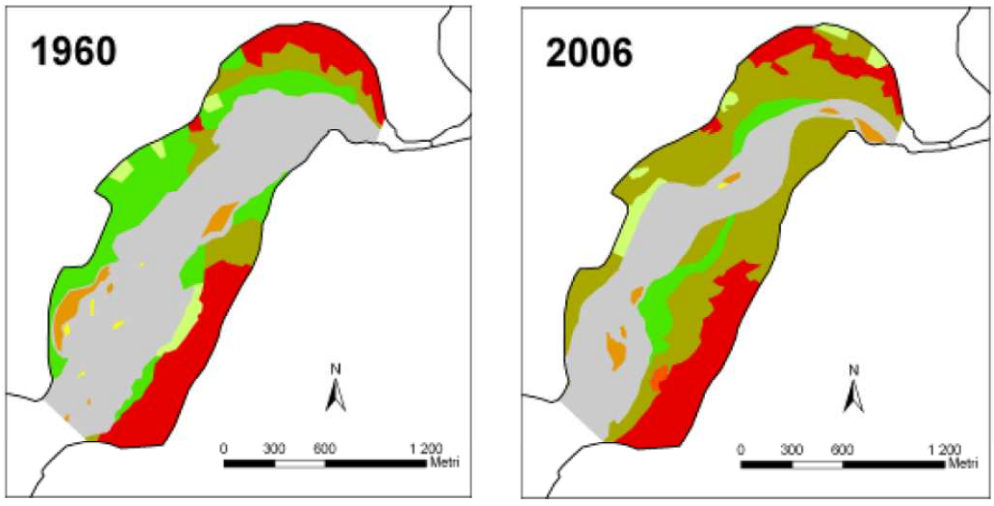

Figure 8.8. Morphological evolution of a Piave River reach near Belluno (between Ponte nelle Alpi and Sagrogna) in the period 1960-2006. Colors indicate: Gray, active channel; brown, sectors covered by threes; red, crops; green, bushes; orange, islands with threes (from Da Canal, 2011). Note the dramatic narrowing and the colonization by threes (and hence, stabilization) of extensive areas previously been active channel.

An interesting question regards the role of gravel mining in the narrowing of Piave River. Gravel mining basically stopped by 1990 (Figure 8.9), and soon a channel width recovery has been observed afterwards. However, the complete recovery of the channel width at the 1800 conditions would be impossible to be reached. In fact, the recovery is seriously conditioned by the presence of dams and by long-term land use changes at the basin scale. Near 73% of the drainage area upstream (1965 km^2) of the study reach is under dam regulation. In any case along the study reach there are 6 unregulated tributaries that still furnish sediments into the river (drainage area 269 km^2). Supposing similar basin conditions now and before the closure of major dams (around 1950 according to Surian, 1999), the actual available sediment supply would be around 63% of the sediment supply in 1950. Under these conditions, channel width should be around 250 - 300m (depending on the chosen value of μ'). The fact that the Piave River is actually wider than these estimation arise the question if the observed recovery phase is just a transitional adjustment, after the end of gravel-mining, and if a channel narrowing is to be expected in the future (see figure 8.9). Surian et al. (2009) hypothesized that the Piave River in the study reach should have the potential for a further widening even without direct intervention at the reach or the basin scale. The presented analysis seems to suggest the contrary, but further modeling efforts are to be carried out.

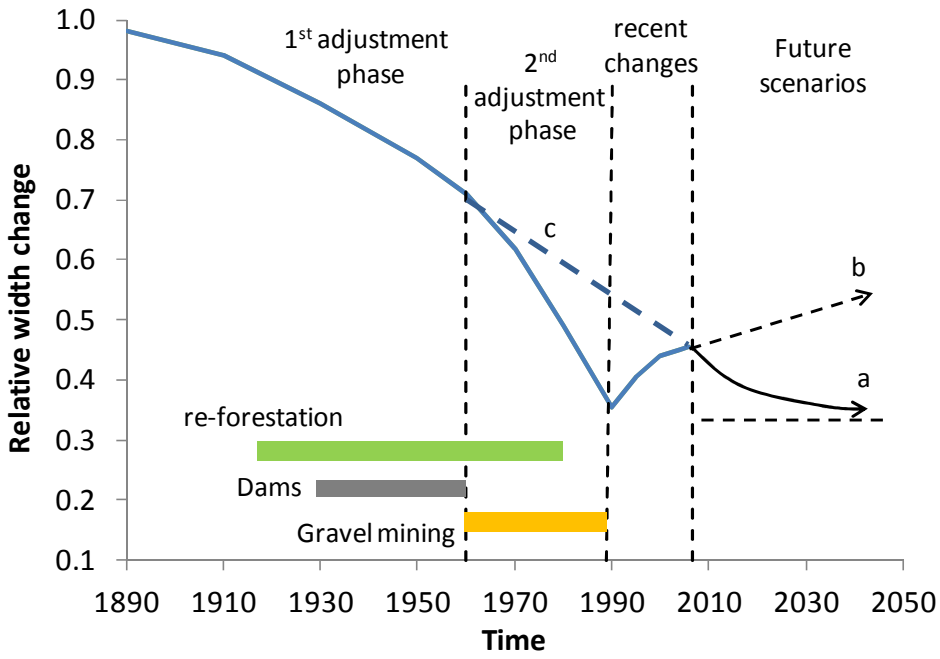

Figure 8.9. Possible scenarios of Piave River change. According to this study recent changes are transitory and a new narrowing phase should follow approaching a new equilibrium width (line a). Instead, Surian et al. (2009) have suggested a discrete channel widening according to different strategies of sediment management; line b indicates a no intervention scenario (modified from Surian et al. 2009). The dashed line c may represent an interpretation of the possible channel evolution without the perturbation introduced by gravel mining. Blocks indicate the period of major human activities that have influenced channel evolution (simplified from Comiti et al. 2011). Channel width is expressed relative to the reference width observed in the 19th century.

Sediment mobility and transport has been recently measured in the field using sediment tracers and evaluating morphological changes at the cross-section scale. These estimations have the potential of quantifying the actual sediment budget at the reach scale, and inform further modeling efforts being able to estimate future morphological tendencies of the river reach under different scenarios of sediment supply from the upstream reaches.

Section Three

Numerical Simulations

"Los planetas no hablan: primero, porque no tienen nada que decir; segundo, porque no tienen tiempo; tercero, porque se los ha hecho callar (…) Nunca se sabe lo que puede ocurrir con una realidad, hasta el momento en que se la ha reducido definitivamente inscribiéndola en un lenguaje (…) la ley de la gravitación, que consiste esencialmente en que hay una fórmula que mantiene todo esto unido, en un lenguaje ultra simple constituido por tres letras".

Jaques Lacan
El Seminario II.

9 LICAN-LEUFU: A NEW 2D DEPTH-AVERAGE HYDRODYNAMIC-SEDIMENTOLOGICAL MODEL FOR GRAVEL BED RIVERS

In this section I will present a hydrodynamic-sedimentological model especially designed for simulating the evolution of gravel bed rivers. I started working with Bernard's (1993) STREMR, a numerical model that generates discrete solution of the incompressible Navier-Stokes equations for depth-averaged 2-D flows. Then I continued progressively modifying and adding new modulus. As a result, a new model has been created, named LICAN-LEUFU[22]. The new model is intended to simulate the change in the shape of gravel bed rivers during long and short time intervals.

STREMR has been extensively tested with laboratory and field measurements (see Bernard, 1993). The secondary current model introduced by Bernard enabled the depth-average model to properly describe the flow in meandering channels (Rodriguez et al., 2004). But the more interesting validations came from field tests conducted in a pro-glacial gravel bed stream (Lane and Richards, 1998). In this case, bed roughness played a determinant role in flow patter while other aspects had little effect, such as the side-wall effects. I have introduced the following modifications: a) water surface elevation is treated as a dependent variable (instead of pressure); b) secondary current correction is discarded because it has negligible effects in low-sinuosity gravel bed rivers; c) side-wall effects are also negligible; d) Keulegan's resistance law is used instead of Manning's equation (as established in STREMR), and the roughness height is related to surface grain size distribution using Kamphuis's (1974) results.

Recently, Abad et al. (2008) have also presented an enlarged version named STREMR HySeD. It consists on the original hydrodynamic model STREMR and incorporates a sediment transport model and a bed-morphology model. The depth-averaged sediment transport model is based on 3D dilute, multiphase flow equations. The suspended sediment load can be subdivided into different size classes using the continuum approach but only one bed sediment size is used. In contrast, the model presented in this work is mainly directed to gravel bed rivers and hence it has important differences to that proposed by Abad et al. (2008). In the new model, a special attention is paid to bed processes: a) suspended sediment load is not considered, b) bed load is subdivided into different size classes, c) the bed is composed of a mixture of gravels and sands, d) the bed surface is organized exhibiting a coarser armour layer. LICAN-LEUFU model also includes a morphological modulus that simulates bank failures and channel widening.

9.1 Hydrodynamic model

The governing equations for the flow of water are composed of the 2D depth-averaged expressions of mass conservation and momentum balance:

$$\frac{\partial z_{ws}}{\partial t} + \frac{\partial (hU)}{\partial x} + \frac{\partial (hV)}{\partial y} = 0 \qquad 9.1$$

[22] I chose these two words of the Mapuche language, the native inhabitants of Central Patagonia. The words indicate the two key aspects of the new model: the flow of water (Leufu = river) and the processes related with gravel transport (Lican = pebble). The word Mapuche means: people (che) of the Earth (mapu).

$$\frac{\partial U}{\partial t} + \mathrm{U}\frac{\partial U}{\partial x} + \mathrm{V}\frac{\partial U}{\partial y} = -\mathrm{g}\frac{\partial z_{ws}}{\partial x} + T_x - Ch^{-1}\mathrm{U}|\mathbf{U}| \quad 9.2$$

$$\frac{\partial V}{\partial t} + \mathrm{U}\frac{\partial V}{\partial x} + \mathrm{V}\frac{\partial V}{\partial y} = -\mathrm{g}\frac{\partial z_{ws}}{\partial y} + T_y - Ch^{-1}\mathrm{V}|\mathbf{U}| \quad 9.3$$

Wherein z_{ws} is the water surface elevation, h is the flow depth, U and V are the depth-average quantities of local velocities $\bar{u}$ and $\bar{v}$, $|\mathbf{U}|$ is the modulus of the depth-averaged velocity vector, T is the force due to viscous effects, and C, a friction factor. This coefficient is related to the bed roughness using Keulegan's equation and Kamphius's (1974) experimental results supported by field measures from this study (see section 8.1).

$$C^{-2} = 2.5ln\left(11\frac{h}{k_s}\right) \quad 9.4$$

$$k_s = 2D_{90} \quad 9.5$$

Viscous forces are the result of turbulent flow. Turbulence effects on the mean flow is included by means of a viscous force T that is parameterized as follows (Bernard, 1993):

$$T_{\mathrm{x}} \approx h^{-1}\nu_t\nabla\cdot(h\nabla\mathrm{U}) + 2\frac{\partial\nu_t}{\partial x}\frac{\partial U}{\partial x} + \frac{\partial\nu_t}{\partial y}\left(\frac{\partial U}{\partial y} + \frac{\partial V}{\partial x}\right) \quad 9.6$$

$$T_{\mathrm{y}} \approx h^{-1}\nu_t\nabla\cdot(h\nabla\mathrm{V}) + 2\frac{\partial\nu_t}{\partial y}\frac{\partial V}{\partial y} + \frac{\partial\nu_t}{\partial x}\left(\frac{\partial U}{\partial y} + \frac{\partial V}{\partial x}\right) \quad 9.7$$

Where ν_t represents the depth-averaged kinematic eddy viscosity. The standard k-ε model is used for the turbulence closure. The kinematic eddy viscosity is evaluated by an empirical formula in terms of the turbulent kinetic energy (k) and the energy dissipation rate (ε) (Bernard, 1993):

$$\nu_t = C_\mu f(R_k)\frac{k^2}{\varepsilon} \quad 9.8$$

Where f is a correction that reduces the eddy viscosity in case of recirculating flow (Bernard 1991, 1993).

$$f(R_k) = \frac{1}{R_C} + \left(1 - \frac{1}{R_C}\right)tanh\left(\frac{{R_k}^2}{{R_0}^2}\right) \quad 9.9$$

Where R_C is the maximum reduction factor of value between 1.5-2.0; $R_k = |\boldsymbol{U}|^2/k$ and $R_0 = 65$, based on calibration.

The transport equations for k and ε are given by:

$$\frac{\partial k}{\partial t} + U\frac{\partial k}{\partial x} + V\frac{\partial k}{\partial y} = \nu_t\,\Gamma - \varepsilon + \sigma_k^{-1}\left[\frac{\nu_t}{h}\nabla(h\nabla\mathrm{k}) + \nabla\nu_t\cdot\nabla\mathrm{k}\right] \quad 9.10$$

$$\frac{\partial \varepsilon}{\partial t} + U\frac{\partial \varepsilon}{\partial x} + V\frac{\partial \varepsilon}{\partial y} = \frac{C_{\varepsilon 1}\nu_t}{k}\,\Gamma - C_{\varepsilon 2}\frac{\varepsilon^2}{k} + \sigma_\varepsilon^{-1}\left[\frac{\nu_t}{h}\nabla(h\nabla\varepsilon) + \nabla\nu_t\cdot\nabla\varepsilon\right] \quad 9.11$$

in which

$$\Gamma = 2\left[\left(\frac{\partial \mathrm{U}}{\partial x}\right)^2 + \left(\frac{\partial V}{\partial y}\right)^2\right] + \left(\frac{\partial U}{\partial y} + \frac{\partial V}{\partial x}\right)^2 \quad 9.12$$

In the standard model the constants assume the following values: c_μ = 0.09, $c_{\varepsilon 1}$ = 1.44, $c_{\varepsilon 2}$ = 1.92, σ_k = 1.0, σ_ε = 1.3 (see Chapter 3 for details).

Near the lateral walls high gradients of turbulence and mean flow are found. This is considered in STREMR introducing a resisting shear stress assuming a power-law velocity distribution. Vertical and high walls are expected in meandering channels with small shape factor (width/depth). Instead, gravel bed rivers are wide and shallow and banks can only be as steep as the response friction angle (been in general below 40º). Taking into consideration these facts I simplified STREMR eliminating the side-wall effects.

Secondary circulations occur wherever the streamlines are curved and produce a net transfer of momentum at right angles to the direction of the primary flow. Results from field study conducted by Lane and Richards (1998) suggest that the secondary circulation correction in STREMR has little effect upon the velocity predictions in a gravel bed stream. Based on this result I further simplified STREMR eliminating the secondary circulation correction. However, the stream line curvature is considered later for estimating the near bed velocity that drives the motion of gravels on the bed (Nagata et al. 2000).

9.2 Sedimentologic model

The governing equations describe the temporal evolution of bed elevation and the surface grain size distribution. The equilibrium sediment transport model is used, thus local sediment transport is assumed to attain a condition of equilibrium (see Chapter 4). The Exner's equation relates spatial changes in sediment transport with temporal variation of bed elevation. It is expressed in the following way:

$$\left(1-\lambda_p\right)\frac{\partial z_b}{\partial t} = -\sum_k \nabla \cdot \mathbf{q}_k \qquad 9.13$$

where λ_p Is the bed material porosity, z_b is the bed elevation and $\mathbf{q}_k$ is the sediment transport vector for the k^{th} grain size class, which is evaluated with a sediment transport model. The sum on the right side indicates that the divergence must be evaluated for all the grain size classes.

The temporal evolution of the surface grain size distribution is described using the active layer approach (Hirano, 1971; Parker and Southerland, 1990). The mass balance is applied to analyze interactions between sediment transport, active layer and sublayer:

$$\frac{\partial (L_a F_k)}{\partial t} = \frac{-\nabla \cdot \mathbf{q}_k}{(1-\lambda_p)} + f_{Ik}\left(\frac{\partial L_a}{\partial t} - \frac{\partial z_b}{\partial t}\right) \qquad 9.14$$

wherein L_a is the height of the active layer, F_k and f_{Ik} are the surface and interface exchange grain fractions (for the k^{th} grain size class), respectively.

The active layer has a height of the same order that the largest particles: $L_a = 2D_{90}$. The interface grain size distribution f_{Ik} depends on whether the bed is degrading or aggrading. When the bed degrades f_{Ik} is equal to the substrate grain size distribution. On the contrary, when bed aggrades a mixture between the bed load and the active layer material is adopted.

$$f_{Ik} = \begin{cases} f_{ssk} & when\ bed\ degrades \\ \alpha F_k + (1-\alpha) f_{bk} & when\ bed\ aggrades \end{cases} \quad 9.15$$

where f_{ssk} is the substrate k[th] grain size fraction. Following Parker et al. (2006), I adopted $\alpha = 0.5$.

The evaluation of the sediment transport vector $\mathbf{q}_k$ requires the definition of its modulus (transport intensity) and then its direction, i.e., the components along the x and y directions. The bulk transport of the k[th] grain size class is calculated using the Wilcock and Crowe's (2003) model (see Chapter 4 for details and discussion):

$$\mathrm{q_k} = \frac{\mathrm{F_k u_*^3}}{\mathrm{g R_s}} \mathrm{G}(\phi) \quad 9.16$$

$$G(\phi) = \begin{cases} 14\left(1 - \frac{0{,}894}{\phi^{0,5}}\right)^{4,5} & for\ \phi \geq 1{,}35 \\ 0{,}002\phi^{7,5} & for\ \phi < 1{,}35 \end{cases} \quad 9.17$$

where

$$\phi = \frac{\tau_g^*}{\tau_{ssrg}^*}\left(\frac{D_k}{D_g}\right)^{-b} \quad 9.18$$

$$\tau_{ssrg}^* = 0{,}021 + 0{,}015e^{-20Fs} \quad 9.19$$

$$b = \frac{0{,}67}{1+\exp\left(1{,}5 - D_i/D_g\right)} \quad 9.20$$

In which, q_k is the bulk sediment transport per unit width, for the k[th] grain size class ($m^2 s^{-1}$); τ_g^* is the dimensionless shear stress for the mean geometric diameter; u^* is the shear velocity; R_s is the submerge relative specific weight of sediments; Fs is the sand fraction content; F_k is the partial frequency of the k[th] grain size class; D_g is the mean geometric diameter; D_k is the mean diameter of the k[th] grain size class.

Shear stress due to bottom roughness is evaluated using the Darcy-Weissbach equation.

$$\tau = \rho C |\mathbf{U}|^2 \quad 9.21$$

Where the friction factor C is evaluated using equation 9.4.

The direction of sediment transport depends on the direction of the main flow, the presence of secondary currents and bed topography (Figure 9.1). First, the direction of near bed flow relative to the main flow is calculated using the secondary flow correction:

$$\tan\delta = \frac{A}{r} h \quad 9.22$$

Factor A is assumed to be constant (with a value of 7) and r is the radius of curvature:

$$r = \frac{|\mathrm{U}|^3}{UV\left(\frac{\partial V}{\partial y} - \frac{\partial U}{\partial x}\right) + U^2\frac{\partial V}{\partial x} - V^2\frac{\partial U}{\partial y}} \quad 9.23$$

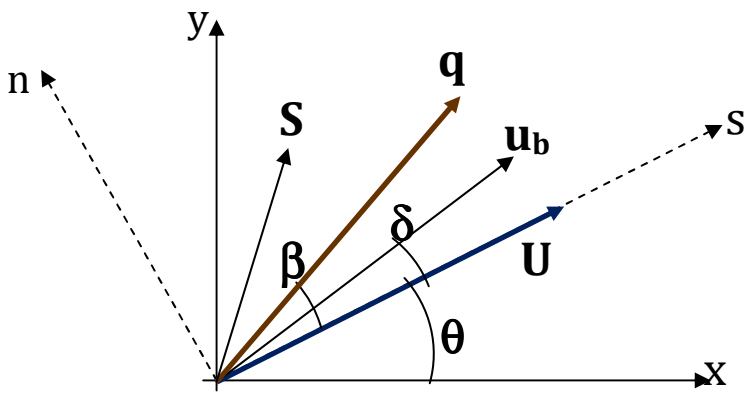

Figure 9.1. Scheme indicating the direction of main flow that defines the streamwise coordinate system (axes s and n). The bed current ($\mathbf{u_b}$) has a deviation angle δ with respect to the main flow (**U**). Near bed currents and bed slope deviate sediment transport an angle β with regards to the main flow.

A major influence is due to the action of gravity that deviate the trajectory of gravels that moves on the bed. The bed load direction (β, relative to the main flow direction) for the kth grain size class is given by:

$$\tan\beta = \frac{\sin\delta + K_k S_n}{\cos\delta + K_k S_s} \qquad 9.24$$

Where S_s and S_n are the components of the highest (negative) bed slope along the streamwise direction and the normal direction, respectively (it will be discussed later).

$$K_k = \frac{1+r\mu_d}{\mu_d}\left(\frac{\tau_k^*}{\tau_{ck}^*}\right)^{-n_t} \qquad 9.25$$

$$n_t = \frac{1}{2} \qquad 9.26$$

$$\tau_k^* = \frac{\tau_b}{\rho g R D_k} \qquad 9.27$$

Finally, τ_{ck}^* is the adimensional critical shear stress computed with the modified Egianzaroff exposure/hiding relation:

$$\frac{\tau_{ck}^*}{\tau_{cg}^*} = \left[\frac{\log 19}{\log\left(19\frac{D_k}{D_g}\right)}\right]^2 \qquad 9.28$$

And for $D_k/D_g \leq 0{,}40$,

$$\frac{\tau_{ck}^*}{\tau_{cg}^*} = 0{,}843\left(\frac{D_k}{D_g}\right)^{-1} \qquad 9.29$$

where D_g is the mean geometric diameter and τ_{cg}^* is the corresponding dimensionless critical shear stress ($\tau_{cg}^* = 0{,}03$).

On the base of field data, Johansen and Parker (1989) obtained the following values for the dimensionless coefficient of dynamic Coulomb friction for bed particles, μ_d = 0,43 and the lift/drag ration r = 0,85.

Then, the bed load components in the streamwise and normal directions are:

$$q_{k_s} = q_k \cos\beta \tag{9.30}$$

$$q_{k_n} = q_k \sin\beta \tag{9.31}$$

For the x and y components, a rotation is performed:

$$q_{k_x} = q_{k_s} \cos\theta - q_{k_n} \sin\theta \tag{9.32}$$

$$q_{k_y} = q_{k_s} \sin\theta + q_{k_n} \cos\theta \tag{9.33}$$

9.3 Bank evolution model

Sediment transport near the banks is expected to produce local erosion. This process increases the bank slope beyond the response angle, hence it is necessary to establish a mechanism for bank failure. This is a critical point that has been resolved by heuristic models such as those proposed by Pizzuto (1990), and Jang and Shimizu (2005). Let's consider the profile near the bank where it is expected to find the highest slopes within the channel (Figure 9.2). If at some point or region of the bank, the slope exceeds the angle of repose (assumed to be $\phi = \mu_d$, the dynamic Coulomb coefficient) a failure surface inclined at the angle of repose is extended up to the floodplain surface. All the sediment above the failure lines moves downslope to form a deposit with a linear upper surface. The highest point of the deposition surface is the lowest point of the failure surface. More details will be given in section 9.5.

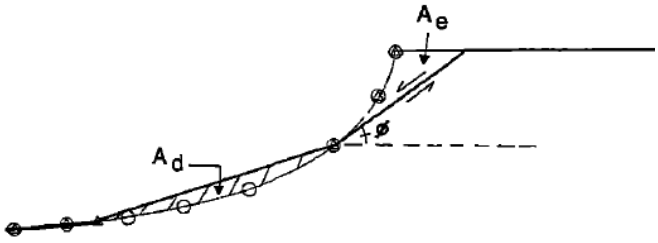

Figure 9.2. Heuristic model for bank failure. A_d is the deposition area that must be equal to the erosion area A_e (modified from Pizzuto, 1990).

The new surface grain size distributions for deposited and eroded areas are evaluated considering a mixture between the previous surface layer and the substrate material:

$$F_k^{new} = (1-\alpha)F_k + \alpha f_{ssk} \tag{9.34}$$

Where the mixing factor α depends on the bed elevation variation (Δz) and a mixing depth l_m.

$$\alpha = \left|\frac{\Delta z}{l_m}\right| \tag{9.35}$$

The mixing factor must fulfill the constrain: $\alpha \leq 1$. The mixing depth is equal to the active layer thickness, i.e., $l_m = 2D_{90}$. The proposed model works in this way: when the depth of erosion is higher than the armour layer the material exposed is equal to the substrate, the same occurs when deposition takes place and the armour layer is completely buried. When the deposition/erosion depth is lower, a mixture is assumed. Note that stratification is not kept and hence depositional history is lost.

9.4 Boundary conditions

The solution of the governing equations requires the specification of the boundary conditions and the initial condition. The boundary conditions consist of the fluxes and their distribution along the upstream cross section and water level at the downstream end. Furthermore, flow through the lateral boundaries is not allowed. Because flow is unsteady, a specific treatment (drying/wetting processes) must be considered for inner and lateral boundaries.

9.4.1 Inlet boundary conditions

Inlet boundary conditions are specified at the upstream end of the reach. They consist on the temporal variation of the input flows: water discharge and sediment supply. Both the amount and the distribution across the upstream cross section have to be provided. Water flow is distributed using the Keulegan's resistance law assuming a constant energy gradient across the section. Given a known water surface elevation, for each inlet boundary cell, the flow velocity (U_j') and face-centered discharge can be calculated. Then, summing all these discharges the total incoming discharge (Q') is:

$$Q' = \sum_j U_j' h_j l_j^w \tag{9.36}$$

Where h_j is the cell's depth, l_j^w is the length of the western face. Because this discharge is not equal to the imposed discharge Q, a renormalization has to be applied for mean velocities at the western face:

$$U_j^w = U_j' \frac{Q}{Q'} \tag{9.37}$$

Face-center discharges at the western faces are:

$$q_{Uj}^w = U_j^w h_j l_j^w \tag{9.38}$$

The criterion for the sediment supply distribution is similar. In this case the Wilcock and Crowe's (2003) sediment transport model is used. A specific sediment input is imposed to the river reach, Qs. On the other hand, if the sediment transport model is used, a different sediment load can be calculated Qs':

$$Q_s' = \sum_j \sum_k q_{jk}' \, l_j^w \tag{9.39}$$

Where q_{jk}' is the sediment transport of the kth grain size class calculated with the flow properties of the jth cell. Therefore, the second sum is along all the size classes and the first one sums the contributions of each cell across the first cross section. Again, the fluxe through the western face is calculated renormalizing with the true value of sediment supply:

$$Q_{sj} = \frac{Q_s}{Q_s'} \sum_k q'_{jk}\, l_j^w \qquad 9.40$$

The bed load grain size distribution is supposed to be known (f_{bk}) and then, the bed load of each class (Q_{sj}^k) can be calculated as:

$$Q_{sj}^k = f_{bk} Q_{sj} \qquad 9.41$$

9.4.2 Outlet boundary

Because an arbitrary cut is performed in the river reach, so as to define the study system, the influence that the downstream reach would exert to the system has to be introduced as a boundary condition. With regards to the water flow two possible situations have been considered: a) fixed water surface elevation, and b) an open boundary.

Fixed water surface elevation. The water surface elevation is calculated assuming a condition of uniform flow at the downstream end. Given an energy dissipation slope, the resistance equation is solved to back-calculate the flow depth. Recalling the momentum equation (eq. 9.2), the acceleration is null and viscous forces are neglected ($T_x \approx 0$), then:

$$-\mathrm{g}\frac{\partial z_{ws}}{\partial x} - Ch^{-1}\mathrm{U}^2 = 0 \qquad 9.42$$

The water surface gradient $\frac{\partial z_{ws}}{\partial x}$ is replaced by the imposed energy dissipation slope, because flow has been assumed uniform.

The continuity equation (9.1) reduces to $\nabla \cdot (h\mathbf{U}) = 0$, and in terms of a finite volume discretization scheme it means that the sum of all the fluxes through the control volume surface has to be null.

$$Q_U^e = Q_U^w + Q_V^s - Q_V^n \qquad 9.43$$

where Q_U^e, Q_U^w, Q_V^s, Q_V^n, are face-center fluxes through the eastern, western, southern and northern faces, respectively. Fluxes on the right side are calculated with the momentum equations 9.2 and 9.3.

Open boundary. An open boundary condition allows phenomena generated in the domain of interest to pass through the boundary without undergoing significant distortion and without influencing the interior solution. Orlaski (1976) applied the Sommerfeld radiation condition to hyperbolic differential equations and proposed a discretization scheme. The boundary condition for open channel flow is given by:

$$\frac{\partial z_{ws}}{\partial t} + c\left(\frac{\partial z_{ws}}{\partial x} + S_f\right) = 0 \qquad 9.44$$

Where c is the phase velocity of the waves. This equations is somewhat different to that employed by Bernard (1993) in STREMR in that water surface elevation (z_{ws}) is used instead of water velocity (U). An additional term has been added, the water surface slope S_f because when the steady state is achieved the flow should be uniform: $\frac{\partial z_{ws}}{\partial x} + S_f = 0$, i.e., it is the result found in the former boundary condition (eq. 9.42). Although the final state are equal during the unsteady phase in the open boundary waves will pass the boundary without producing reflections.

The condition defines, then, the water surface elevation. Water fluxes are calculated using the continuity equation (9.43).

With regards to the sedimentological model, the downstream boundary condition states that bed can aggrade freely but erosion is limited by a minimum bed elevation. It is equivalent to put a check dam that prevents bed from erosion.

9.4.3 Dry-wet cells and Islands

In the unsteady simulation velocity components and water surface evolve until a steady state is attained. During this period some cells that did not initially constitute the flow domain can be wetted due to a rise in water surface elevation. On the contrary, initially wetted cells could be eliminated from the flow domain due to an erroneously high water surface elevation, as calculated by the 1D hydraulic model (see initial condition below). A cell is considered wet when its depth (h) is above a user-defined threshold value ($h_{\min\ \_hyd}$).

$$\text{Wet cell if } h > h_{\min\ \_hyd} \tag{9.45}$$

It follows that a criterion for wetting and drying cells is needed. The criterion is very simple and can be stated in this way: a dry cell can receive water only from a wetted cell (Jang and Shimizu, 2005; Bradford and Sander, 2002). Let's consider a dry cell surrounded by wet cells (Figure 9.3). The central dry cell can receive water from the eastern cell when its water surface elevation is lower than the eastern one and flux is negative; otherwise a null flux is imposed.

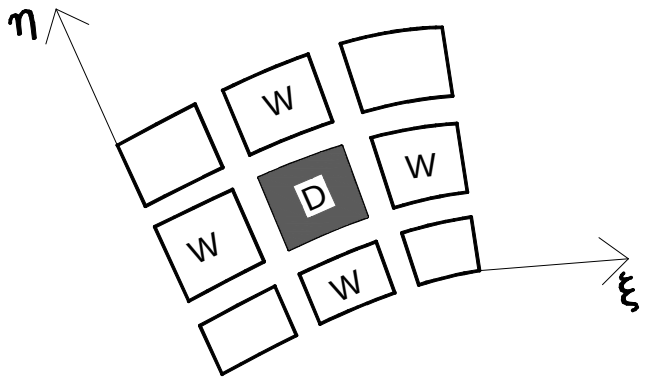

Figure 9.3. The central cell is dry and will receive water from the surrounding cells when their water surface elevations are higher and face flux is toward the dry cell.

The proposed rule imposes the following constrains:

$$\text{Face EAST: If not } \left(\left.\frac{\partial z_{ws}}{\partial \xi}\right|_E > 0 \quad and \quad Q_{U\,i,j} < 0\right) \text{ then } Q_{U\,i,j} = 0 \tag{9.46}$$

$$\text{Face NORTH: If not } \left(\left.\frac{\partial z_{ws}}{\partial \eta}\right|_N > 0 \quad and \quad Q_{V\,i,j} < 0\right) \text{ then } Q_{V\,i,j} = 0 \tag{9.47}$$

$$\text{Face WEST: If not } \left(\left.\frac{\partial z_{ws}}{\partial \xi}\right|_W < 0 \quad and \quad Q_{U\,i-1,j} > 0\right) \text{ then } Q_{U\,i-1,j} = 0 \tag{9.48}$$

$$\text{Face SOUTH: If not } \left(\left.\frac{\partial z_{ws}}{\partial \eta}\right|_S < 0 \quad and \quad Q_{V\,i,j-1} > 0\right) \text{ then } Q_{V\,i,j-1} = 0 \tag{9.49}$$

When the sedimentological model runs the Exner equation for bed elevation variation is applied to wet cells. However, here a different threshold value is defined:

$$\text{Wet cell if } h > h_{\min\ \_sed} \qquad 9.50$$

Because the sedimentological model runs after the hydrodynamic model, $h_{\min\ \_sed}$ must be higher than $h_{\min\ \_hyd}$. It is important to underline that the momentum equations (9.1, 9.2 and 9.3) are solved only in wet cells. The continuity equation is also applied to dry cells only in those cases allowed by rules 9.46-9.49, i.e., when there is an incoming flow. Similarly, the sedimentological model applies also to wet cells until $h < h_{\min\ \_sed}$ and since then it is considered a bank/island and excluded from calculus. In this case, sediment transport in all the faces of a wet cell that is in contact with dry cells (banks or islands) is forced to be null.

9.4.4 Initial conditions

Before performing the hydrodynamic model initial values for the dependent variables, i.e., face-centered fluxes (Q_U and Q_V) and water surface elevation, have to be provided. There are two situations **Cold start** and a **Hot start**. Under the condition of Cold start initial values of water surface elevations are calculated using a 1D gradually varied flow model (see section 6.4). Assuming that curvilinear axes ξ define curves nearly perpendicular to actual flow lines, the downstream face-centered flux $Q_U$can be estimated using the Keulegan's equation. After that, perpendicular fluxes $Q_V$are estimated using the continuity equation with the condition of no-flux through boundaries.

The Hot start simply uses the provided initial values that may be the result of a previous simulation.

9.5 Discretization, numerical methods and algorithms

9.5.1 Discretization

LICAN-LEUFU uses the same discretization scheme as implemented in STREMR (Bernard, 1993), i.e., a finite-volume discretization scheme with curvilinear boundary-fitted grids. The governing equations (depth-average water flow equations and Exner equation) are transformed from Cartesian (x, y) coordinates to curvilinear coordinates $\xi = \xi(x,y)$ and $\eta = \eta(x,y)$. Each cell is composed of four nodes that can be placed arbitrarily, so spacing Δx and Δy are variable. Conversely, in the computational domain the spacing is constant: $\Delta\xi = 1$ and $\Delta\eta = 1$. It follows that the curvilinear grid in the Cartesian system has been converted to a regular one in the computational system (Figure 9.4).

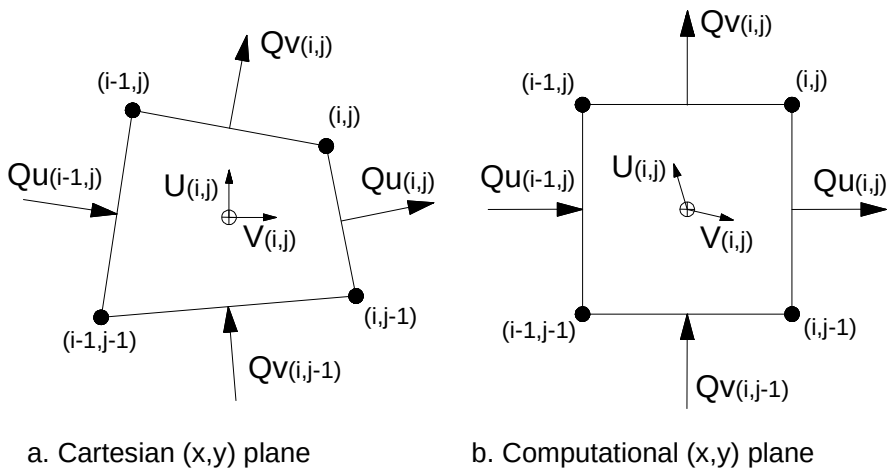

Figure 9.4. Discretization of flow domain and coordinate transformation from the Cartesian system (a) to the computational system (b). Placement of face-centered volumetric fluxes (Q_U and Q_V) and cell-centered depth-average velocities U and V (modified from Bernard, 1993).

Although the location of grid nodes is arbitrary there are several rules that must be considered in order to avoid numerical instabilities (Bernard, 1993):

a. **Low skewness**: the angle between intersecting grid lines should be kept between 45° and 135°.
b. **Gentle variation**: the local change in grid spacing should be no more than 30 per cent from one cell to the next.
c. **Aspect ratio**: the ration length/width should be no greater than 10 whenever strong flow gradients may occur in the lengthwise direction.
d. **Orientation**: cells should be oriented so that the grid spacing is finest in the direction of strongest depth or velocity gradients.
e. **Bathymetry**: depth-average approximation for bottom friction requires gentle variation in depth, and hence the bottom slope should be less than 45°. Side slopes greater than 45° should be replaced with vertical walls.

In keeping with the logic of STREMR, the location of dependent variables is specified according to a staggered grid: fluxes (Q_U and Q_V) are calculated at face-centers, and scalar variables (water elevation, turbulent kinetic energy k, and dissipation rate ε) are calculated at cell-centers. The cell-centered depth-averaged velocities U and V are computed from Q_U and Q_V only when they are needed, for instance, to compute the viscous and friction forces. In the case of the sedimentologic model, the dependent variable set is compost of cell's elevations z and the cell's surface grain size distributions F_i that are calculated at cell centers. Bed load fluxes are not actually dependent variables because a sediment equilibrium models was chosen. These quantities are calculated at cell-center and after face-centered values are interpolated as required for the finite volume element scheme (see section 9.5.4).

Using the coordinate transformation $\xi = \xi(x,y)$ and $\eta = \eta(x,y)$ it is possible to obtain the corresponding expression for each differential operator in the governing equations (Bernard, 1993). Let F be any arbitrary scalar function.

Gradient:

$$\nabla F = \left(F_x; F_y\right) \qquad F_x = J^{-1}\left(y_\eta F_\xi - y_\xi F_\eta\right) \qquad F_y = J^{-1}\left(x_\xi F_\eta - x_\eta F_\xi\right) \tag{9.51}$$

Divergence:

$$\nabla \cdot (hQ_i) = J^{-1}\left(Q_{U\xi} + Q_{V\eta}\right) \tag{9.52}$$

Laplacian Operator:

$$\nabla \cdot (h\nabla F) = J^{-1}\left[\frac{\partial}{\partial \xi}\left(y_\eta F_x - x_\eta F_y\right) + \frac{\partial}{\partial \eta}\left(x_\xi F_y - y_\xi F_x\right)\right] \tag{9.53}$$

where J is the jacobian of the coordinate transformation:

$$J = x_\xi y_\eta - x_\eta y_\xi \tag{9.54}$$

And, Q_U and Q_V are the volumetric fluxes:

$$Q_U = h\left(y_\eta U - x_\eta V\right) \tag{9.55}$$

$$Q_V = h\left(x_\xi V - y_\xi U\right) \tag{9.56}$$

wherein subindeces x, y, ξ and η indicate partial derivatives. Advection terms in equations 9.2, 9.3 require specific numerical methods in order to avoid instabilities: a) the momentum equation is solved applying the MacCormack's predictor-corrector scheme; b) the transport equations of the Standard k-ε model are solved using the Euler (first order) upwind scheme; and c) the Exner equations (for bed elevation and grain size distribution) employ the Euler scheme with the HLPA interpolation method for the divergence term.

9.5.2 Euler`s method for time integration

The Euler's upwind method is a very simple first-order method that is used for solving the transport equations of kinetic energy (k) and the dissipation rate (ε). In convection problems information propagates from either the left or the right side of the solution point depending on whether U > 0 or U < 0, respectively. In the first-order upwind method time derivative is replaced by the first-order forward-difference approximation. Figure 9.5 shows the stencil for the finite difference scheme.

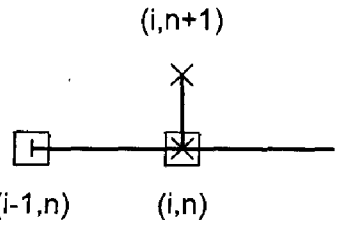

Figure 9.5. Stencil of the Euler first-order upwind method. Dots indicate the points used for spatial derivatives (U > 0) while crosses indicate time derivative (Hoffman, 2001).

Bernard (1993) adapted this method for the 2D hydrodynamic model STREMR. The upwind scheme is used to calculate the advection term. For instance, let's consider that the kinetic energy (k) is the dependent variable. The advection term in curvilinear coordinates is discretized as follows:

$$A = h^{-1}J^{-1}\left[Q_U^+\left(k_{i,j} - k_{i+1,j}\right) + Q_U^-\left(k_{i-1,j} - k_{i,j}\right) + Q_V^+\left(k_{i,j} - k_{i,j+1}\right) + Q_V^-\left(k_{i,j-1} - k_{i,j}\right)\right] \quad 9.57$$

where

$$Q_U^+ = \frac{(\mathrm{Q_U} - |\mathrm{Q_U}|)_\mathrm{E}}{2} \quad 9.58$$

$$Q_U^- = \frac{(\mathrm{Q_U} + |\mathrm{Q_U}|)_\mathrm{W}}{2} \quad 9.59$$

$$Q_V^+ = \frac{(\mathrm{Q_V} - |\mathrm{Q_V}|)_\mathrm{N}}{2} \quad 9.60$$

$$Q_U^- = \frac{(\mathrm{Q_V} + |\mathrm{Q_V}|)_\mathrm{S}}{2} \quad 9.61$$

Indeces E, W, N, and S indicate the face to be considered for face-centered fluxes $\mathrm{Q_U}$ and $\mathrm{Q_V}$. Note that when flow is positive (U > 0, i.e., from left to right) Q_U^+ = 0 and Q_U^- = $(\mathrm{Q_U})_\mathrm{W}$, i.e, information comes from the western face.

The full transport equation is discretized as follows:

$$k^{n+1} = k^n + \Delta t\left[P - D - A + \frac{\nu_t}{h}\nabla\cdot(h\nabla k) + \nabla\nu_t\cdot\nabla k\right] \quad 9.62$$

where P is the production term, D the diffusion term and A, the advection term. All the terms inside the brackets are calculated with old data. Advection is discretized using the Euler upwind scheme (eq. 9.57), and cell-centered discretization is used for the diffusion term and for the gradient terms (see Bernard, 1993, for details).

9.5.3 MacCormack's method for time integration

MacCormack (1969) proposed a simple second-order scheme that has been widely used to solve non-linear differential equations. The solution is split into two steps a predictor-corrector procedure. In the first phase, provisional (i.e., predicted) values of the dependent variable are calculated using first-order forward-space-difference approximations based on old data (time t_n in Figure 9.6). After, the correction applies a first-order backward-space approximation for derivatives using old data and predicted values. The method was adapted by Bernard (1993) to be used in hydrodynamic problems. Here, a summary is presented with modifications to the original Bernard's scheme.

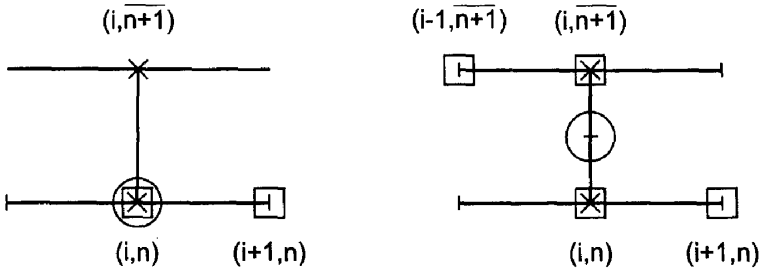

Figure 9.6. Stencil of MacCormack's method. On the right, predictor phase and on the left, corrector phase. Dots indicate points used for spatial derivatives; crosses, points for time derivative, and circle, the point at which the temporal derivative is calculated. Note that at the predictor phase backward-space is used for derivatives, and it is reversed in the corrector

phase (Hoffman, 2001). Index I is used for spatial points and index n indicates the temporal step.

The **predictor phase** starts with old data consisting on face-centered fluxes (Q_U^n and Q_V^n) and water surface elevation (z_{ws}^n), where the upper index (n) refers to the previous time step. The momentum equation for the predictor phase is given by

$$U_p^{n+1} = U^n + \Delta t(F^n - A_{rs}^n) - g\Delta t \nabla_{rs} z_{ws,p}^{n+1} \quad 9.63$$

where F stands for the friction and viscuous forces and A is the advection term, r and s are indeces that indicate the sense of the space-derivative approximation, index p indicates that these provisional values belong to the predictor phase. Note that the water surface elevation to be considered is at time n+1, which has not already been calculated. It is approximated by:

$$z_{ws,p}^{n+1} = z_{ws}^n + \varphi_p \quad 9.64$$

Where φ_p is the change in the water surface elevation during the predictor phase. Replacing eq. 9.64 into eq. 9.63, two equations are composed: one that calculates an intermediate velocity U_p^* using old data of water surface elevation (z_{ws}^n) and a corrective equation that takes into account φ_p:

$$U_p^* = U_p^n + \Delta t(F^n - A_{rs}^n) - g\Delta t \nabla_{rs} z_{ws,p}^n \quad 9.65$$

$$U_p^{n+1} = U_p^* - g\Delta t \nabla_{rs} \varphi_p \quad 9.66$$

The change in water surface elevation (φ_p) is calculated solving the continuity equation using flow data at time n+1 (U_p^{n+1}):

$$\frac{\varphi_p}{g\Delta t^2} - \nabla \cdot \left(h \nabla \varphi_p\right) = \frac{-1}{g\Delta t} \nabla \cdot \left(h U_p^*\right) \quad 9.67$$

This is the Poisson equation which after discretization results in a linear system of equations. It is solved using the Conjugate Gradient Method (Kapitza and Eppel, 1987).

The **corrector phase** uses original data and the provisional values calculated in the predictor phase. This time, space derivatives are reversed: $r^* = 1 - r$ and $s^* = 1 - s$; and temporal derivative is evaluated at moment t + Δt/2. A provisional velocity is first calculated using existing information on water surface elevation:

$$U_c^* = U^{n+1/2} + \Delta t\left(F_p^{n+1} - A_{p,r*s*}^{n+1}\right) - g\Delta t \nabla_{r*s*} z_{ws}^{n+1/2} \quad 9.68$$

Where some quantities have been evaluated at the instant t + Δt/2:

$$U^{n+1/2} = \frac{U^n + U_p^{n+1}}{2} \quad 9.69$$

$$z_{ws}^{n+1/2} = \frac{z_{ws}^n + z_{ws,p}^{n+1}}{2} \quad 9.70$$

And then, the velocity at time t + Δt is calculated correcting U_c^* with the change in water surface:

$$U^{n+1} = U_c^* - g\Delta t \nabla_{rs} \varphi_c \quad 9.71$$

$$\frac{4\varphi_c}{g\Delta t^2} - \nabla \cdot (h\nabla\varphi_c) = \frac{-2}{g\Delta t}\nabla \cdot (hU_c^*) \quad 9.72$$

The aforementioned development has been done considering cell-centered velocities. However it has to be underlined that face-centered fluxes are the actual dependent variables. Details about the transformation between face and cell centered velocities can be found in Bernard (1993).

The index pair (r, s) is change at the beginning of predictor phase so as to reduce bias. The sequence is (0,0) (0,1) (1,0) (1,1).

The water surface gradient is not calculated with central difference; instead it also follows the derivative direction as dictated by MacCormack's scheme. First, the gradient is calculated in the computational system according to the current derivative direction (pairs r and s, or r* and s*):

$$z_{ws,\xi} = z_{ws}(i + r, j) - z_{ws}(i + r - 1, j) \quad 9.73$$

$$z_{ws,\eta} = z_{ws}(i, j + s) - z_{ws}(i+, j + s - 1) \quad 9.74$$

And then, the gradient is transformed into Cartesian coordinates:

$$z_{ws,x} = J^{-1}\left(y_\eta z_{ws,\xi} - y_\xi z_{ws,\eta}\right) \quad 9.75$$

$$z_{ws,y} = J^{-1}\left(x_\xi z_{ws,\eta} - x_\eta z_{ws,\xi}\right) \quad 9.76$$

For details on the spatial derivatives x_ξ, y_η, y_ξ, y_η , see Bernard (1993).

9.5.4 Open boundary and MacCormack's method

Orlanski (1976) proposed a discrete version of the Sommerfeld radiation condition and Bernard (1993) applied the scheme to his finite-volume model. I have ntroduced little modifications for using the scheme with the equation 9.44.

For the predictor phase the provisional water surface elevation ($z^p_{ws,i}$) and Courant number ($C = c\frac{\Delta t}{\Delta x}$) are given by:

$$Z^p_{ws,i} = (1 - C^p)Z^n_{ws,i} + C^p Z^n_{ws,i-1} - C^p S_f \Delta x \quad 9.77$$

$$C^p = \frac{Z^n_{ws,i-1} - Z^{n-1}_{ws,i-1} + Z^n_{ws,i-2} - Z^{n-1}_{ws,i-2}}{Z^n_{ws,i-2} + Z^{n-1}_{ws,i-2} - Z^n_{ws,i-1} - Z^{n-1}_{ws,i-1} - 2S_f\Delta x} \quad 9.78$$

And in the corrector phase:

$$Z^{n+1}_{ws,i} = \frac{1}{2}\left[Z^n_{ws,i} + (1 - C^c)Z^p_{ws,i} + C^c Z^p_{ws,i-1} - C^c S_f \Delta x\right] \quad 9.79$$

$$C^c = \frac{Z^p_{ws,i-1} - Z^n_{ws,i-1} + Z^p_{ws,i-2} - Z^n_{ws,i-2}}{Z^p_{ws,i-2} + Z^n_{ws,i-2} - Z^p_{ws,i-1} - Z^n_{ws,i-1} - 2S_f\Delta x} \quad 9.80$$

Velocities at the downstream boundary are evaluated using the continuity equation.

9.5.5 HLPA method for convective terms

The divergence terms in equation 9.13 and 9.14 need a special treatment. When the central scheme is used numerical oscillations arise due to the assumption that the convected property, the sediment load, at-a-cell face is given by the averages at two neighboring points. Several schemes are available to overcome this problem, such as: Upwind, Quick, Soucup and HLPA (Wu, 2007, p.143). In this case, the HLPA (Hybrid Linear/Parabolic Approximation) has been chosen. Let's consider that fluxes have to be evaluated at faces around cell c (Figure 9.7), and that main flow is from left to right (U>0). The HLPA approximates the face value q_w as:

$$q_w = q_W + \gamma_w (q_C - q_W) \frac{q_W - q_{WW}}{q_C - q_{WW}} \qquad 9.81$$

where $\gamma_w = 1$ if $0 \leq \varphi_w \leq 1$; otherwise $\gamma_w = 0$. φ_w is defined as follows:

$$\varphi_w = \frac{q_W - q_{WW}}{q_C - q_{WW}} \qquad 9.82$$

When flow is from right to left (U<0) the cells to be used are W, C and E, changing C by W, W by C and WW by E.

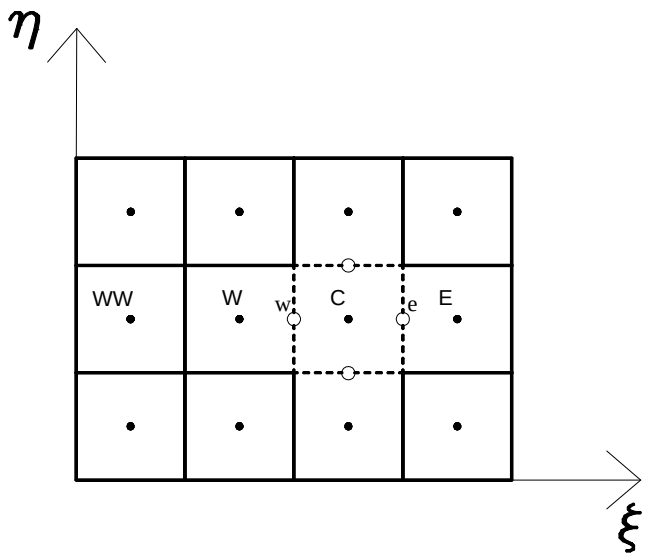

Figure 9.7. Sediment transport vectors are evaluated at cell-centers (W, C, E). Divergence terms require face-centered values (at w and e faces) that have to be evaluated by interpolation.

The procedure is as follows:

1. Cell-centered fractional sediment transports (for each grain size class) are calculated and also their components in the Cartesian plane (x, y), i.e, $q_{x,k}$ and $q_{y,k}$ (section 9.2). The transport rate calculation uses known values of grain size distribution (cell-center), water depth and depth-averaged velocities U and V (cell-centered). The sediment transport direction is corrected taking into account gravity and secondary current effects.

2. Face-centered values are evaluated using the HLPA method, for instance, in the case of the western face: $q_{x,k}^w$ and $q_{y,k}^w$.

3. Cartesian components $q_{x,k}^{w}$ and $q_{y,k}^{w}$ are projected along the normal direction to the face ($q_{n,k}^{w}$). If resulting normal flow direction is contrary to that assumed in the interpolation, then the interpolation has to be done again with opposite cells as described above.

4. Normal components of unit-with sediment transport rates ($q_{n,k}$) are then converted into bulk rates ($Q_{n,k}$) multiplying by the respecting face lengths and after that the divergence terms in equations 9.13 and 9.14 can be calculated:

$$\nabla \cdot \mathbf{q}_k = \frac{Q_{n,k}^{e} - Q_{n,k}^{w} + Q_{n,k}^{n} - Q_{n,k}^{s}}{A} \qquad 9.83$$

Wherein A is the area of the cell.

9.5.6 Minimum bed slope for sediment transport

The correction of sediment transport direction due to the action of gravity requires the determination of the bed slope. A simple way consists on using a central difference scheme for spatial derivatives $\partial z_{ws}/\partial n$ and $\partial z_{ws}/\partial s$, where s is the streamwise direction and n the perpendicular direction. When this approach was implemented bed instability appreared. In order to overcome this problem a different approach was developed. The slope is not evaluated along arbitrary x-y axes but along the direction of maximum change. This means that gravels are directed towards the deepest cells nearest to the central cell.

$$S = min\left(\frac{z_{b,j} - z_{b,c}}{L_{jc}}\right) \qquad 9.84$$

For each cell "j" placed around cell "c" (i.e., j=N, NE, E, ecc. according Figure 9.8), the elevation difference is taken and the distance between the respective cell's centers is calculated (L_{jc}). The slope must also satisfy the constrain that S ≤ 0. The angle φ is also calculated and then the slope can be projected on any axes. For instance, in the x-y coordinate system it is (see Figure 9.8):

$$S_x = S\cos\varphi \qquad 9.85$$

$$S_y = S\sin\varphi \qquad 9.86$$

With this approach instabilities were reduced because gravels tended to fill and raise the deepest cells while lowering the highest cells.

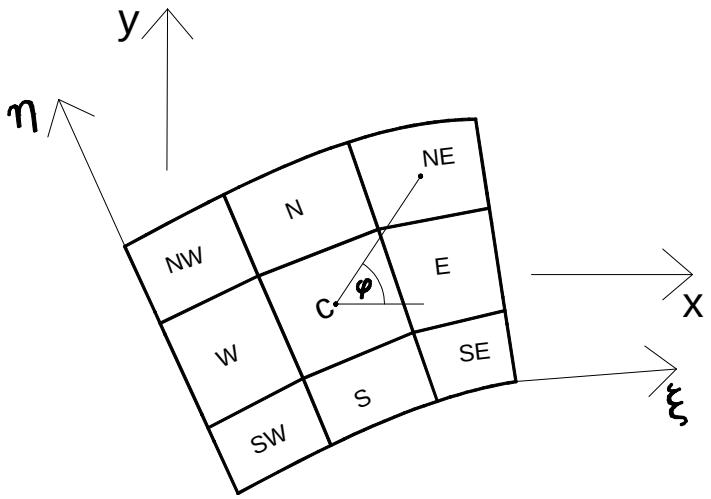

Figure 9.8. Determination of the magnitude (S) and direction (φ) of the minimum bed slope.

9.5.7 Bank slides and grid construction

The general criterion exposed in section 9.3 describes the slide affecting the entire bank region. After discretization, the criterion has to be applied considering individual cells. The domain is scanned along the cross sections, i.e, slides are expected across the section and not in the downstream direction. At each cell, its elevation is compared against the northern cell. If the slope is greater than the maximum allowed (the response friction angle) then an instantaneous slide takes place, and new elevations are calculated defining a failure plane with a slope equal to the maximum value.

The heuristic procedure will be explained following a possible situation. Figure 9.8 shows the bank profile with black dots indicating the cell center elevation at the beginning of the simulation. Considering cell C, because the angle between cells C-N (θ) is higher than the angle of response (φ), a bank slide will occur causing a change in elevation (white dots: C' and N') until a new angle φ is reached. The formulas for the bed elevation changes are given by:

$$\Delta z_{b,N} = \frac{z_{b,C} - z_{b,N} - L_{C,N} \tan \varphi}{1 + \frac{A_N}{A_C}} \qquad 9.87$$

$$\Delta z_{b,C} = \Delta z_{b,N} \frac{A_N}{A_C} \qquad 9.88$$

wherein subindexes indicate the cells according to figure 9.9, A is the cell's area and $L_{c,N}$ is the distance between cell centers. This formula applies when there is erosion at cell C and deposition at cell N, and subindexes are permuted in the opposite case.

This procedure is applied for all the cells in the domain (j = 0 ... J_{max}) several times until no more slides will occur. In the example, the first cell (j=0), that belongs to the floodplain, has also been eroded (point S'). In this case a new boundary line has to be defined so as to reestablish the floodplain elevation at point S (point S'' in figure 9.9). The bank retreats a distance S''-S which is calculated assuming a slope equal to $\tan \varphi$.

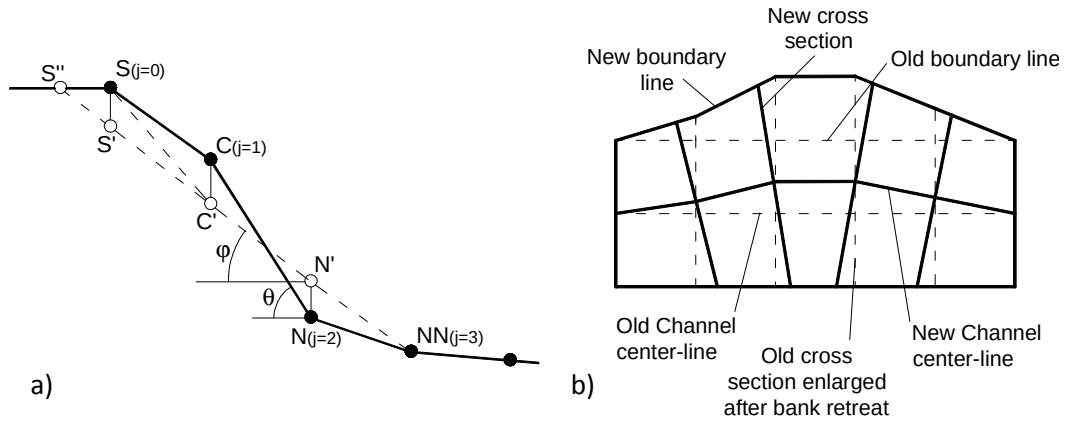

Figure 9.9. Sketch of bank retreat model. A) When the angle (θ) between two neighboring cells surpasses the angle of response (φ) a slide take place and cells elevations are changed. If the first cell (j=0) is affected then there is also a bank retreat. B) When cross sections are enlarged due to bank retreat a new computational grid is generated.

When boundary lines change a new mesh has to be generated: 1) a new central line is set passing through the center of the enlarged old cross sections; 2) new cross sections are placed equally spaced along the new central line and oriented perpendicular to the central line; 3) cross sections are divided into equal spacing nodes. With the new computational grid surface grain size distribution and elevations are assigned by linear interpolation.

9.5.8 Variable time step

The hydrodynamic model uses MacCormack's and Euler's schemes which are both explicit. The new values are computed from the existing values at the previous time step. When the time step is too large the method can become unstable. Numerical stability requires that each flow variable must keep its sign during a single time step. In order to analyze this point let's consider the governing equation for U, written in the discrete form:

$$\frac{\Delta U}{\Delta t} = -A(U) - F(U) + T(U) + other\ terms \qquad 9.89$$

where A is the advection term, F is the fiction force and T is the viscous force. All these terms are functions of U and can be written in the following way: "constant · U + other terms". Therefore, the above equation can be simplified as follows:

$$\frac{\Delta U}{\Delta t} = -\lambda \cdot U + other\ terms \qquad 9.90$$

In this equation λ contains the sum of the absolute values of all coefficients that multiply U. The first term in the right side is the most important, while "other terms" also affect numerical stability but are less important[23], and hence, can be neglected. Applying the stability criterion it follows that the time step should be:

$$\Delta t < \frac{1}{\lambda} \qquad 9.91$$

[23] Bernard (2010) personal communication.

Developing each term it is possible to show that λ at cell (i,j) is:

$$\lambda_{i,j} = \left|\frac{Q_{Ur}}{hJ_c}\right| + \left|\frac{Q_{Vs}}{hJ_c}\right| + \left|\frac{C|\mathbf{U}|}{h}\right| + \left|\frac{\upsilon_t A_{cc}}{J_c}\right| \quad 9.92$$

where, h is the mean depth of the cell; J_c is the Jacobian evaluated at cell center; Acc is a coefficient that appears during the discretization of the Lapacian operator (eq. 9.54); Q_{Ur} is the volumetric flux for cell (i + r – 1, j) and Q_{Vs} is the volumetric flux for cell (i, j + s – 1). Coefficient λ is evaluated for each cell and the highest value defines the maximum allowable time step.

The sedimentological model also employs a maximum time step but in this case the user fixes the maximum change in bed elevation: $\Delta z_b \leq TOL_z h$. The maximum time step is evaluated using the Exner equation (9.13):

$$\Delta t(i,j) = -\left(1-\lambda_p\right)\frac{\Delta z_b}{\sum \nabla\cdot\mathbf{q}_k} \quad 9.93$$

The time step is evaluated in all the cells and the minimum value is chosen. This assures that the required tolerance is not exceeded. Furthermore, the user can fix a maximum time step (Δt_{max}), and hence the time step for calculation is evaluated with the following rule:

$$\Delta t = \min\left[\Delta t_{max}; \max\left(\Delta t(i,j)\right)\right] \quad 9.94$$

9.5.9 Steady state flow convergence

Hydrodynamic model and sedimentologic model are decoupled. Water flow is assumed steady because the river reach is not long enough to develop dynamic waves. Unsteady flow is only a consequence of the numeric strategy adopted to solve the governing equations. However, a criterion has to be defined for stopping the calculation when unsteady flow is nearly steady, i.e., it has converged. Convergence is defined with the Relative discharge error (ε_Q):

$$\varepsilon_Q = \frac{max(|Q_i - Q|)}{Q} \quad 9.95$$

wherein Q is the incoming discharge and Q_i is the discharge through the i^{th} cross section. The criterion is as follows: the steady state is said to be reached when $\varepsilon_Q \leq TOL_Q$ during a period of time T_c, where TOL_Q is the tolerance. Both T_c and TOL_Q are defined by the user.

9.5.10 Approximation of shear stress variation

Because the governing equations are not linear, a change in bed elevation will modified the water flow and then the sediment transport. The hydrodynamic and sedimentological models are not coupled, which means that when performing the hydrodynamic simulation bed properties are kept fixed, because bed changes much slowly than the hydrodynamic variables. On the contrary, when running the sedimentological model water surface elevation and face fluxes are kept constant. What happens with the bed shear stress? Two approaches are proposed, one for “Medium-term” simulations and another for “short-term” simulations.

Case 1. Medium-term simulation. This is the situation of long simulations lasting several years and discharges are supplied daily. The flow is calculated ones per the whole day. Water surface elevation and face fluxes are kept constant but as bed elevation changes, the flow depth and depth-averaged

velocity also change. The shear stress is calculated for each time step using expression 9.21. It is recognized that this approach promotes stabilization because when bed aggrades the shear stress increases and reduces the aggradation rate. During the sedimentological model, time step is calculated with eq. 9.94.

Case 2. Short-term simulation. Before the tolerance for bed changes is achieved shear stress is approximated with the aforementioned approach, but after, the hydrodynamic models starts and new flow variables are calculated.

9.5.11 Algorithms

The main routine is composed of four modulus (see figure 9.10): 1) a 1D hydrodynamic modulus that calculate initial approximate values of water surface elevation, 2) the 2D hydrodynamic modulus solves the unsteady flow until convergence is achieved giving as a result steady flow parameters (velocity components and water surface elevation); 3) the sediment transport modulus calculates the bed change until the tolerance is achieved; in this case the next modulus (4) calculate morphological changes due to bank slides.

The routine is intended to work with a series of discharges that constitute a hydrograph. Given a discharge, modulus 2, 3 and 4 run in a loop until the simulation time is achieved. In this case a new discharge is taken and the loop starts again. Figures 9.11 to 9.12 show the detailed flow chart for each modulus.

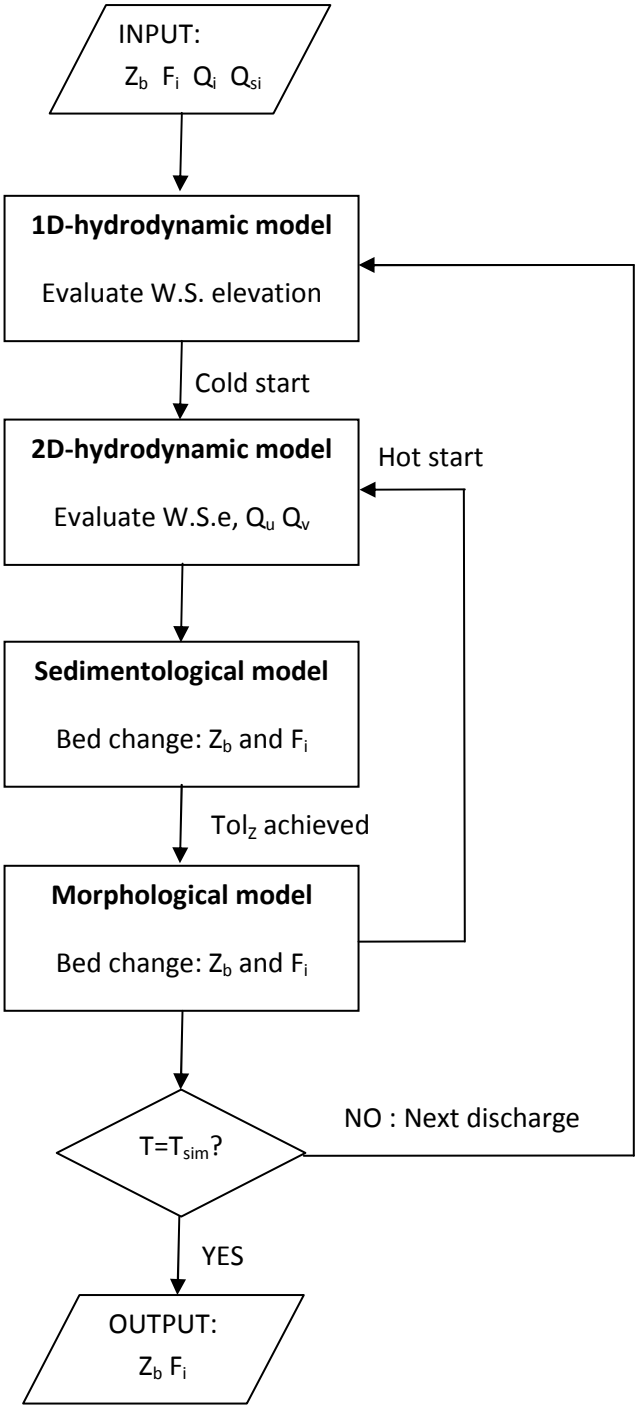

Figure 9.10. Flow chart of the main routine of LICAN-LEUFU. This routine is intended to calculate the bed change considering a set of discharges that compose a hydrograph.

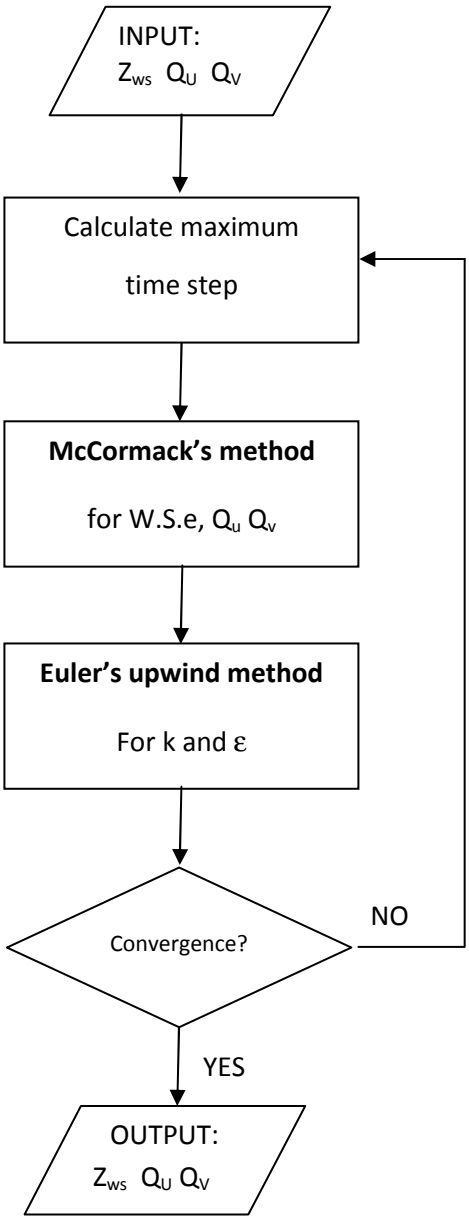

Figure 9.11. Flow chart of the 2D hydrodynamic modulus. It is in charge of solving the unsteady 2D flow considering water surface elevation and flow components as dependent variables. It is based on the routine STREMR developed by Bernard (1993).

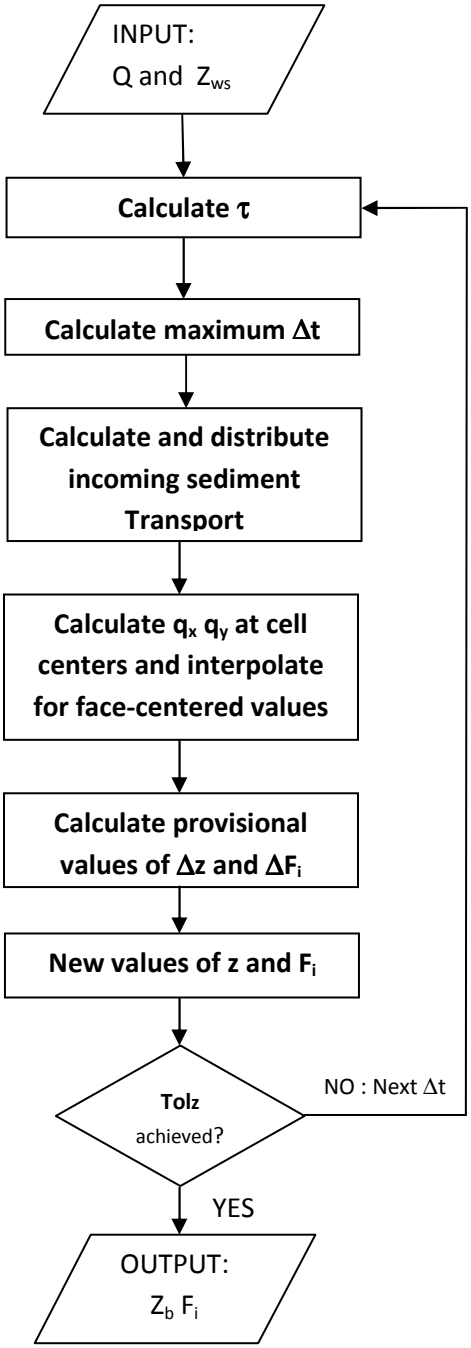

Figure 9.12. Flow chart of the sediment transport modulus. The routine calculates the maximum time step that would be necessary for achieving the established tolerance, but the user can reduce it by multiplying factor. Therefore, more than one loop may be necessary before achieving the tolerance. This routine is used when accurate results are required (see short-term simulations in the text).

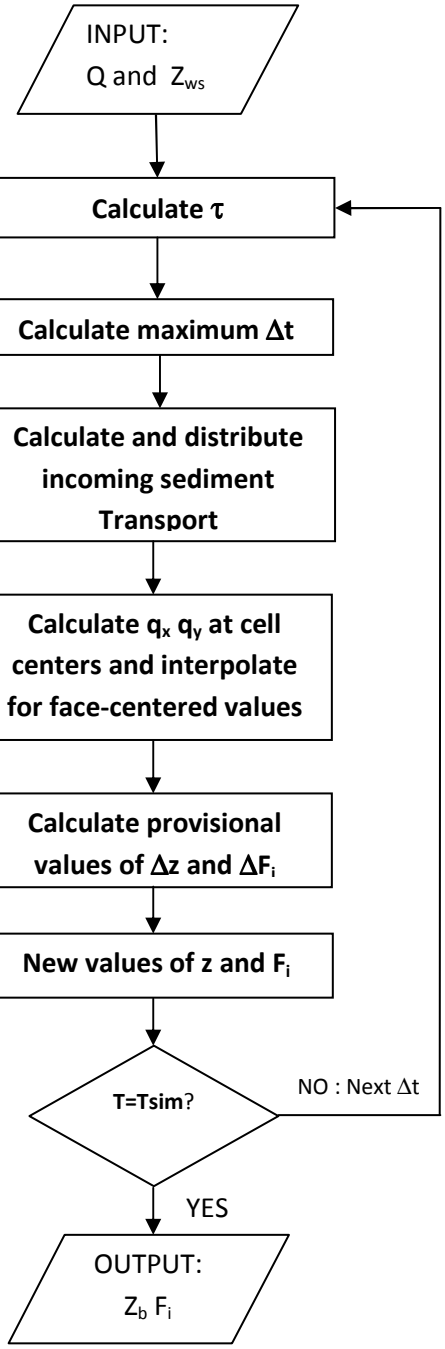

Figure 9.13. Flow chart of the sediment transport modulus. This routine is used when approximate solutions are required. In this case the maximum time step is calculated according to the bed-change tolerance. Hydraulic parameters are not re-calculated but approximate values of shear stress are used considering a fixed water surface elevation (see long-term simulation in the text).

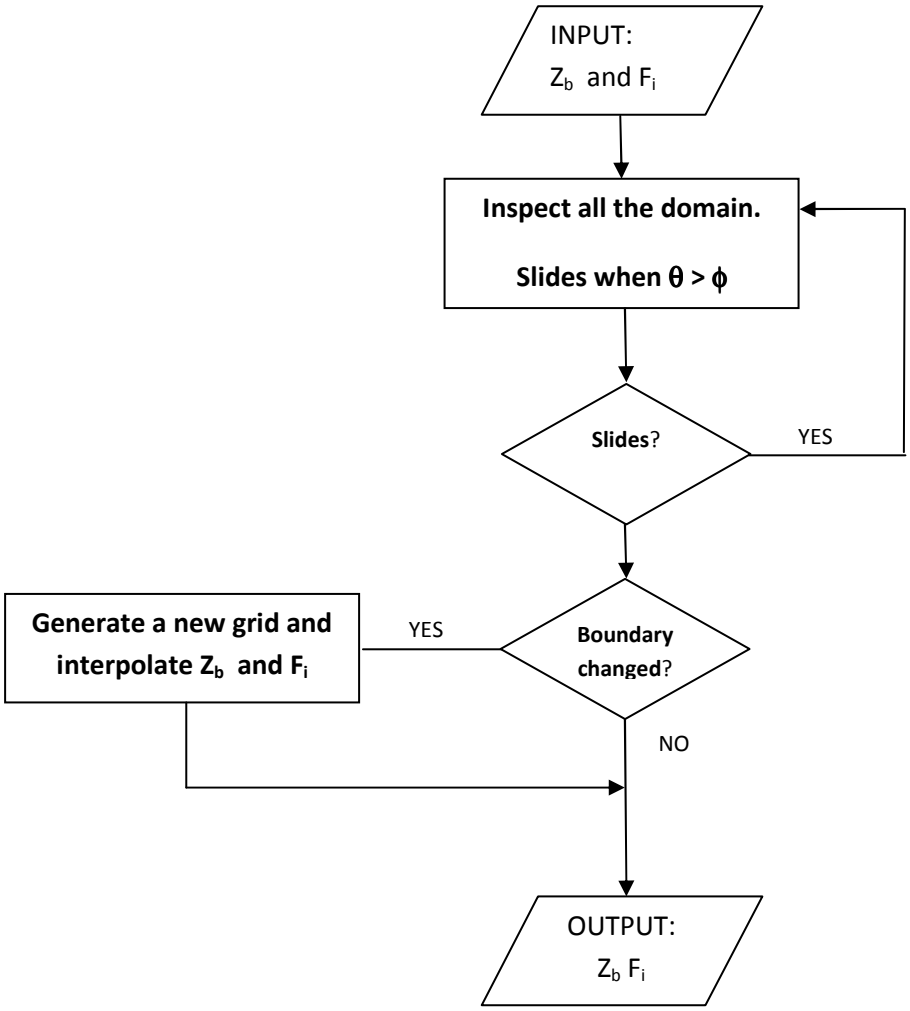

Figure 9.14. Flow chart of the morphological modulus. This routine verifies that bed slope in the domain is below the friction angle of response. When it is not verified an iterative routine generate local slides until the criterion is verified. In some cases, the slide may affect the boundary cells and hence there is a channel widening that requires the generation of a new grid.

10 APPLICATIONS OF LICAN-LEUFU 2D-MODEL

In this Chapter three study cases are presented where Lican-Leufu model is applied so as to test the hypothesis of this study. In the first case study results from the model are compared against laboratory measurements in a flume with mobile bed. The comparison is intended to validate the model and then, the second case study explores the application of the model in the context of regime theories. Finally, the third case study seeks to foretell the possible evolutional trend of Brenta River in the Nove reach.

10.1 Methodology

Let's see in detail the methodology for testing the hypothesis proposed in this study. The hypothesis states that: ***the channel morphology is driven by and is a consequence of within-channel processes; and a 2D depth-averaged model describes better the morphology and structure of the channel than 1D or aggregated regime models.*** The first part of the hypothesis states that processes are the responsible of observed forms. This hypothesis is formulated in the context of the debate on regime models (see Chapter 1). However, it should not be interpreted that extremal hypotheses are not necessary for predicting the channel shape. As has been proposed in this study, extremal hypotheses express the behaviour at the reach scale while here, reach-scale features will be explained by processes acting at a lower spatial scale. The second part of the hypothesis relates to regime theory and states that a 2D model should do better in predicting channel morphology than 1D or aggregated, as described in Chapter 2. What does better mean? It means that the 2D model is capable of predicting the reach-average form (width and depth) and also within channel structure (pools and riffles, armour layer) that are not within the capabilities of 1D or aggregated models.

Observational consequences, i.e. predictions, have been derived from the hypothesis by means of LICAN-LEUFU model, a 2D fully processes-based model as required by the hypothesis. When developing the model a series of statetments have been implicitly assumed as true:

a) Sidewall effects are negligible in shallow water flows.

b) Bed roughness is correctly predicted by Kamphuis's (1974) results.

c) The standard k-e model describes correctly the influence of turbulence on mean-flow properties.

d) Secondary currents are negligible in shallow water flows.

e) The equilibrium sediment transport model describes correctly the interaction between bed load and bed elevation changes.

f) The two-layer model (active layer and substratum) is sufficient for modeling the vertical grain size variability in gravel bed rivers.

g) The Wilcock-Crowe's (2003) formula correctly predicts the sediment transport rate.

h) Channel widening is due to bank failures.

i) Numerical methods do not introduce significant bias when approximating the differential equations by difference schemes.

Each component has extensively been discussed in previous chapters. Therefore, assuming valid all the components, the application of the model to particular situations providing also adecuate boundary conditions should produce observational consequences that can be compared against measurements. Three different scenarios have been studied:

1) **A flume experiment**. The model is used to predict the response of a laboratory flume that develops a static armour under conditions of sediment starvation. The observational consequences consist on the bed change, surface grain size distribution change, outgoing sediment transport (bulk and grain size distribution).

2) **A middle-term simulation**. The model has to predict the shape and bed structure of Azul River providing the actual water discharges, bed material, and an estimated sediment supply.

3) **A field case-study**. In this case the model has to predict the change in bed elevation in the Brenta River (Nove reach) after the passage of several floods during the period 23/8/2010 – 24/4/2011. The model is used to assess the channel behaviour if sediment supplied is provided and results are compared against measurements to assess the possible evolution of the reach.

10.2 A flume experiment

LICAN-LEUFU has been tested using the results from a flume experiment carried on to develop a static armour layer under conditions of sediment starvation. This situation represents a good opportunity for testing the model because it comprises a change in bed elevation, as incision takes place, also a change in surface grain size distribution, owing to armour development, and changes in hydrodynamics due to both aforementioned changes.

Four parameters are available for the comparison: load and grain size distribution of the outgoing sediment transport during the armouring process, and the final bed elevation and surface grain size distribution. Besides, numerical modeling has been conducted changing systematically a set of parameters so as to assess the model sensibility.

10.2.1 Experimental settings

The physical experiment was conducted at the laboratory of the University of Hull (U.K.), within the facilities of the Total Environmental Simulator (TES). The TES was designed for modeling sediment transport and flow dynamics under a range of environmental conditions. Flow can be produced using three different mechanisms: unidirectional currents, waves and rainfall. An integrated suite of high-resolution monitoring equipment is also available for measuring fluid dynamics and sediment fluxes. The effective length of the flume is 11 m with additional inlet and outlet tanks to service the flow and sediment recirculation system. The maximum operating width of the flume is 6 m, although internal walls can be used to change the working section to any width. The internal depth of the flume is 1.6 m, which permits both large lateral bed slopes to be constructed and waves of up to 0.5 m to be generated in flow depths of 1 m. Two pumps located in a pit beneath the flume tank recirculate

water. Each pump delivers up to 500 liters of water per second and when operated together can deliver 1000 liters per second. As well as recirculating water in the flume, the pumps can also recirculate sediment up to 3 mm in size through the system.

Internal walls were placed in the TES so as to create a 2 m wide and 11 m long flume with a longitudinal slope of 0.005 m m^{-1}. At its downstream end, eight traps covering the whole flume width were used to collect the transported sediment. Traps were collected and emptied at variable intervals in order to derive bedload transport rates and grain size. The bulk gravel-sand mixture had the following percentiles: D_{16} = 4.1 mm, D_{50} = 6.4 mm and D_{84} = 13.1 mm. At the beginning of the experiment sediments were screeded flat to the specified bed slope. Only one run was performed in this flume with a water discharge of 340 l s^{-1} m^{-1}. Pressure transducers were placed beneath the sediments along the channel center for measuring the water surface elevation.

Figure 10.1. View of the flume constructed inside the Total Environment Simulator. University of Hull, Department of Geography (U.K.)

The experiment run until the outgoing sediment transport was 1% the initial value. At this moment photographs of the bed surface were taken and after, the grid-by-number approach was used to evaluate the average surface grain size distribution[24]. A total of 10 photographs covered an area of 3,6 m^2. Bed elevations were also measured along the left wall of the flume.

10.2.2 Numerical method settings

Initial conditions.

Because there was no armour at the initial state the surface grain size distribution was assumed equal to the bulk sand-gravel mixture. The initial water surface elevation was calibrated against measurements so as to assure similar hydrodynamic conditions in the flume and in the model. For each selected grid (table 10.1) the hydrodynamic model was run with different downstream water surface elevations. Then, the water profile was compared against measurements and a downstream elevation was selected. Figure 10.1 shows an example of the calibration technique applied with Δx = 0.25. In this case the best water surface profile is obtained for a downstream depth H = 0,190 m.

[24] More details on the choice of this methodology can be found in a previous work of Mao et al. (2011).

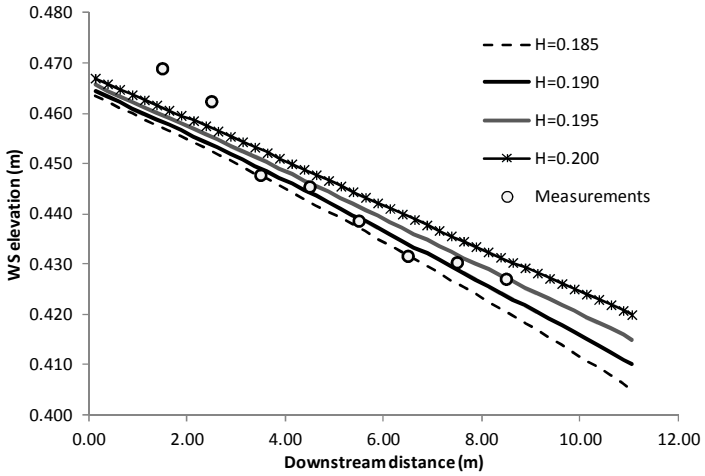

Figure 10.2. Calibration of downstream water surface elevation using measured initial water surface profile.

The porosity of the mixture was not measured. Instead it was calculated using an empirical formula proposed by Wu and Wang (2006):

$$\lambda_p = 0.13 + \frac{0.21}{(D_{50}+0.002)^{0.21}} \qquad 10.1$$

where D_{50} is in mm. For the present study case, the bed porosity evaluated with 10.1 is $\lambda_p = 0.27$.

Boundary conditions.

The boundary conditions assumed for the simulations are: a) Fixed downstream water surface elevation; b) Constant upstream incoming water discharge; c) Null sediment supply; and d) Fixed bed elevation at the downstream end.

Sensibility analysis.

Several parameters were selected for analyzing the model sensibility. They belong to three groups: a) the mesh density represented with the downstream spacing (Δx), b) hydrodynamic parameters including the convergence tolerance (Tol_Q) and the downstream water surface elevation (H_{dw}); and c) sedimentological parameters including the tolerance for bed elevation change (Tol_Z) and bed porosity (λ_p).

Table 10.1 shows the values selected for each parameter. Combining the different possibilities it results that 10 runs had to be accomplished. Runs W1, W2 and W3 show the model's sensibility with Δx. Runs W2, W6 and W7 evidence the sensibility with H_{dw}. Runs W2, W9 and W10 evidence variations in Tol_Q while runs W3, W4 and W5, show variations in Tol_Z. Finally, two runs, W3 and W8 were designed for analyzing the model sensibility to bed porosity changes.

Table 10.1. Variation in selected parameters for model sensibility analysis.

Run	Δx (m)	Δy (m)	H_{dw} (m)	Tol_Q	Tol_Z	Porosity
W1	0.500	0.125	0.195	1%	2%	0.27
W2	0.250	0.125	0.190	1%	2%	0.27
W3	0.125	0.125	0.185	1%	2%	0.27
W4	0.125	0.125	0.185	1%	5%	0.27
W5	0.125	0.125	0.185	1%	10%	0.27
W6	0.250	0.125	0.200	1%	2%	0.27
W7	0.250	0.125	0.210	1%	2%	0.27
W8	0.125	0.125	0.185	1%	2%	0.34
W9	0.250	0.125	0.190	2%	2%	0.27
W10	0.250	0.125	0.190	5%	2%	0.27

10.2.3 Results

During the experiment, the bed experienced a degradation in its upstream end and afterwards the bed surface coarsened. An erosion scour formed at the upstream end due to the presence of a fixed weir that produced a local step and a hydraulic jump (Figure 10.3). As expected, sediment transport rate reached the highest intensity at the beginning of the experiments (53 gr m^{-1} s^{-1}) and decreased quickly with an exponential-type tendency. Sediment transport rate diminished to less than 1% of the initial rate after 45 hr. Bed elevation was measured along the left wall only, however it was evident that bed elevation was not uniform across the flume and that it was lower nearer the right wall (between 1,5 and 2 cm).

Figure 10.3. Formation of a step and hydraulic jump at the upstream end of the flume (a). It promoted local erosion creating a pool (b).

Outgoing sediment transport.

All the numerical runs exhibit the exponential-type tendency previously observed during the experiment. In general, the model reproduces very well the overall behaviour, with a good agreement for peak discharge and timing. It is also evident that the peak in bed load, the predicted transport rate overestimates measurements (Figure 10.4).

The grid spacing affects little the predicted outgoing sediment flow. Some differences are observed at the beginning of the run: the finer the grid, the higher is the initial transport rate. It is noted that the solution is not grid-independent (Figure 10.4 a) because the solution does not converge when

grid is densified. A similar trend is observed when Tol_Q is changed; lower initial transport rates are found when the tolerance is relaxed (figure 10.4 c). The model is quite sensitive to changes in the downstream water surface elevation: when the depth is increased the transport rate decreases significantly, being the best agreement found for the calibrated boundary condition (figure 10.4 b). Finally, the change in Tol_Z does not affect the exiting sediment transport (figure 10.4 d).

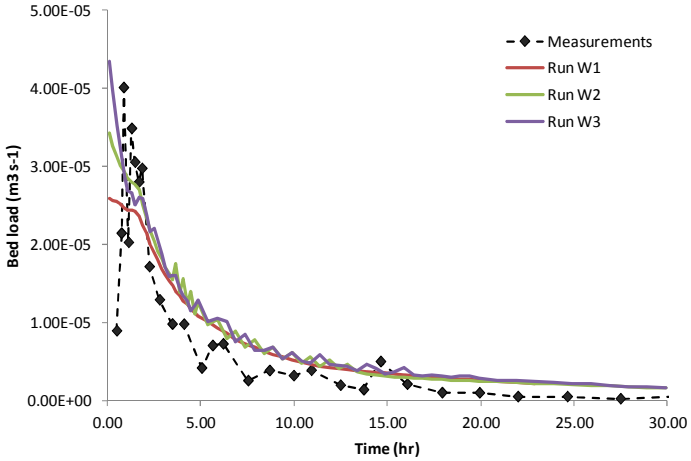

a)

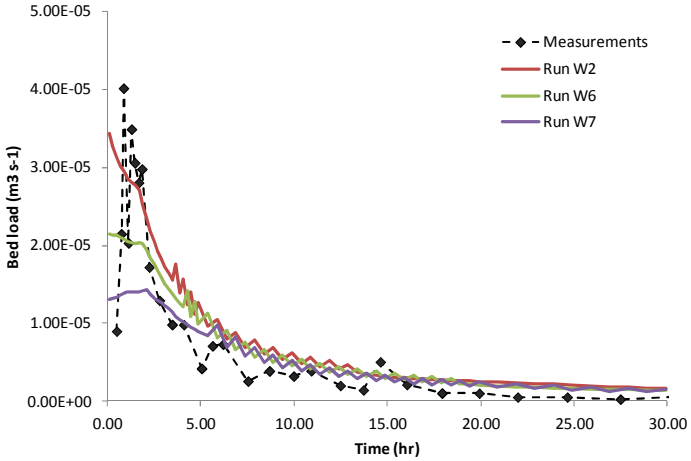

b)

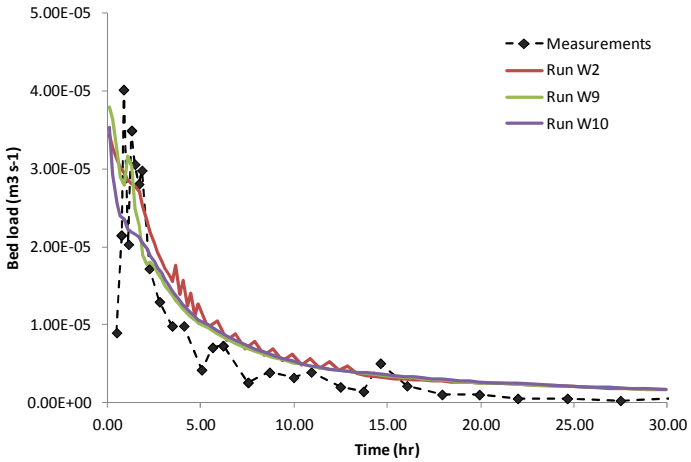

c)

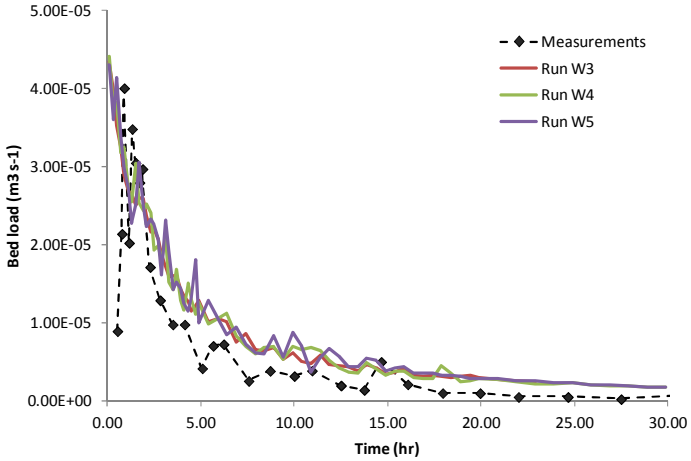

d)

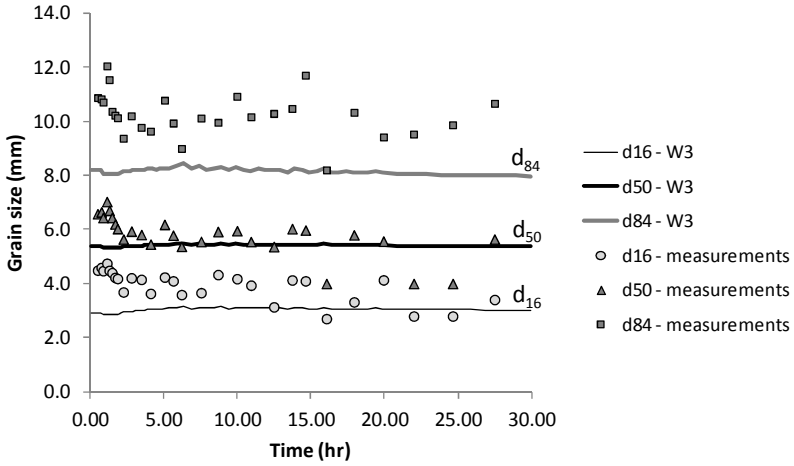

e)

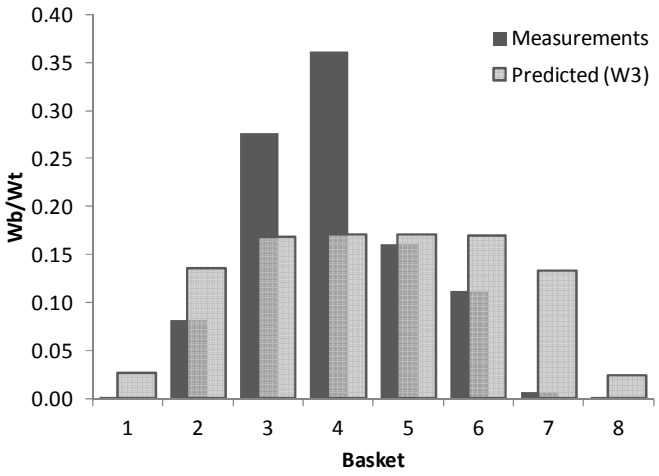

f)

Figure 10.4. Sensibility analysis of model predictions for outgoing sediment transport rate when a) grid downstream-spacing is reduced; b) downstream water surface elevation is raised; c) discharge convergence tolerance is relaxed, and d) bed change tolerance is relaxed. Furthermore, the grain size distribution of leaving load (e) and lateral transport distribution (f) are reported for W3 only because all the runs have identical predictions. In (f) W_b is the weight of material collected in individual baskets and W_t is the total weight.

The grain size distribution of outgoing bed load is shown in figure 10.4e. Because all the runs predict the same distribution only that belonging to Run W3 is exposed in the figure. Measurements shows scatter in the selected percentiles (16%, 50% and 84%). The mean mixture has the following percentiles: D_{16} = 3.6 mm, D_{50} = 5.5 mm and D_{84} = 10.3 mm. Note that the transported material is finer than the original bulk material, and the coarser transported fraction is much finer than the initial bed material (4.1 mm, D_{50} = 6.4 mm and D_{84} = 13.1 mm). With regards to the predicted grain size distribution, it approximates very well the observed one for the lower percentiles (D_{16} = 3.0 mm and D_{50} = 5.4 mm), i.e, the predicted median diameter is very near the observed mean value. There is a clear discrepancy for the coarser fractions: the predicted percentile 84 % is much lower than observations (predicted D_{84} is 8.0 mm).

Sediment transport is not uniform across the flume: it is lower near the sidewalls and higher in the channel center (Figure 10.4f). Numerical results show a symmetrical distribution of bed load with an almost uniform sediment transport rate at the channel center. This result is the same for all the runs. In particular, according to run W3, the central relative rate (basket weight divided the total transport) was 17,8%. On the contrary, measurements indicate that bed load was asymmetrical in the flume. It was higher towards the right sidewall. Bulk collected in basket 3 and 4 summed 63,7% of the total transport (see Figure 10.4f).

Bed elevation.

Figure 10.5 shows the effect in predicted bed elevations when the selected parameters were changed. In general, bed was incised not uniformly across the flume, with the deepest sector in the channel center and almost no erosion at the sidewalls. With regards to the longitudinal profile, erosion was higher at the downstream end in contradiction with observations. Moreover, at the downstream end an erosion of 2cm was predicted.

When grid spacing was reduced the final bed elevation changes but convergences was not achieved for the proposed values ($\triangle$x = 0,50; 0,25 and 0,125m) because results from run W3 did not match those from run W2 (10.3a). However, when mean bed elevations (across the flume) are considered, it is seen that the three runs give very similar results. When the tolerance Tol_z was relaxed (Tol_z= 2%, 5% and 10%) there were slight differences at the downstream end channels center (Figure 10.5b). On the contrary, the model is more sensible to changes in boundary conditions. The rise in the downstream water surface elevation (H = 0.19; 0.20 and 0.21 m) reduced the amount of erosion and the final bed profile was progressively at higher levels (Figure 10.5c). The model was also sensible to changes in the discharge convergence tolerance (Tol_Q). When the tolerance was relaxed (Tol_Q= 1%; 2% and 5%) the deepest zone migrated upstream as indicated by the channel center profile. However, cross section mean elevation remained unchanged (Figure 10.5d). Finally, the change in porosity did not modify significantly the model results.

a)

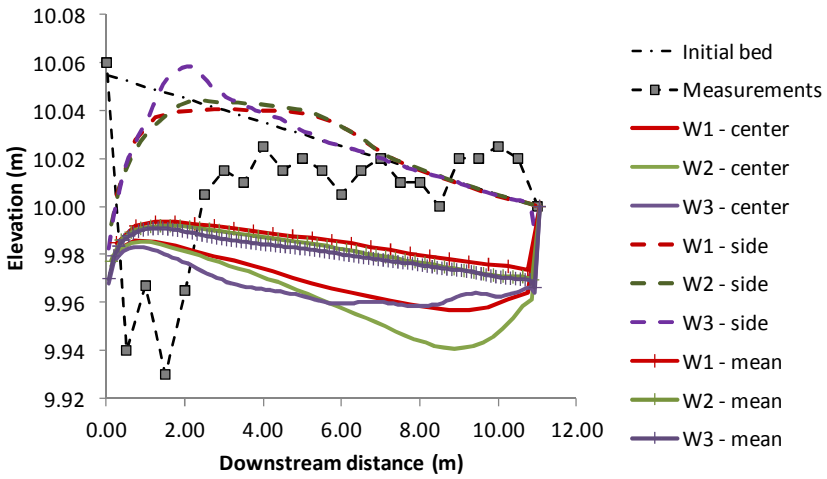
10.08
10.06
10.04
10.02
10.00
9.98
9.96
9.94
9.92
Elevation (m)
0.00
2.00
4.00
6.00
8.00
10.00
12.00
Downstream distance (m)
Initial bed
Measurements
W1 - center
W2 - center
W3 - center
W1 - side
W2 - side
W3 - side
W1 - mean
W2 - mean
W3 - mean

b)

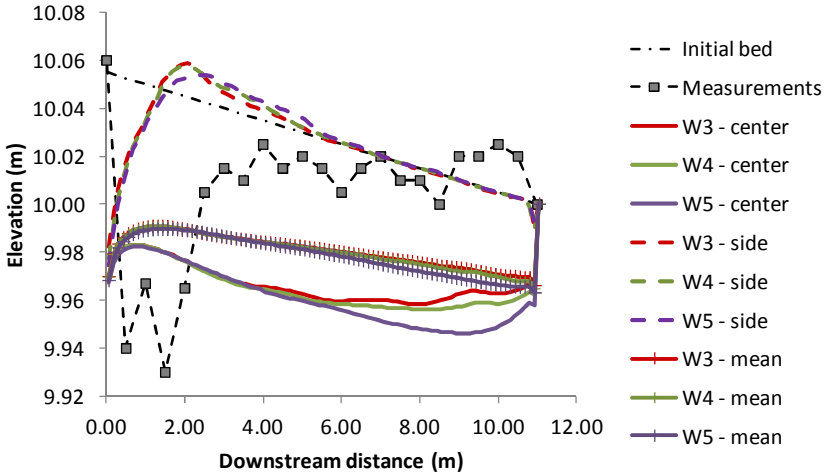
10.08
10.06
10.04
10.02
10.00
9.98
9.96
9.94
9.92
Elevation (m)
0.00
2.00
4.00
6.00
8.00
10.00
12.00
Downstream distance (m)
Initial bed
Measurements
W3 - center
W4 - center
W5 - center
W3 - side
W4 - side
W5 - side
W3 - mean
W4 - mean
W5 - mean

c)

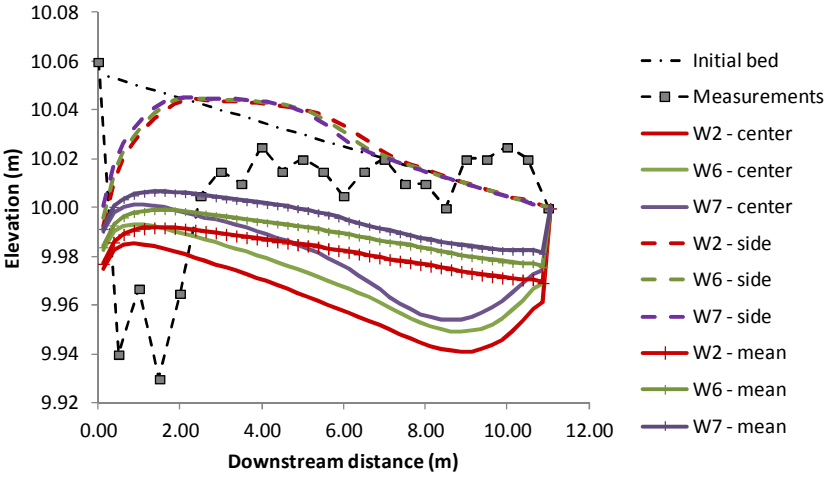
10.08
10.06
10.04
10.02
10.00
9.98
9.96
9.94
9.92
Elevation (m)
0.00
2.00
4.00
6.00
8.00
10.00
12.00
Downstream distance (m)
Initial bed
Measurements
W2 - center
W6 - center
W7 - center
W2 - side
W6 - side
W7 - side
W2 - mean
W6 - mean
W7 - mean

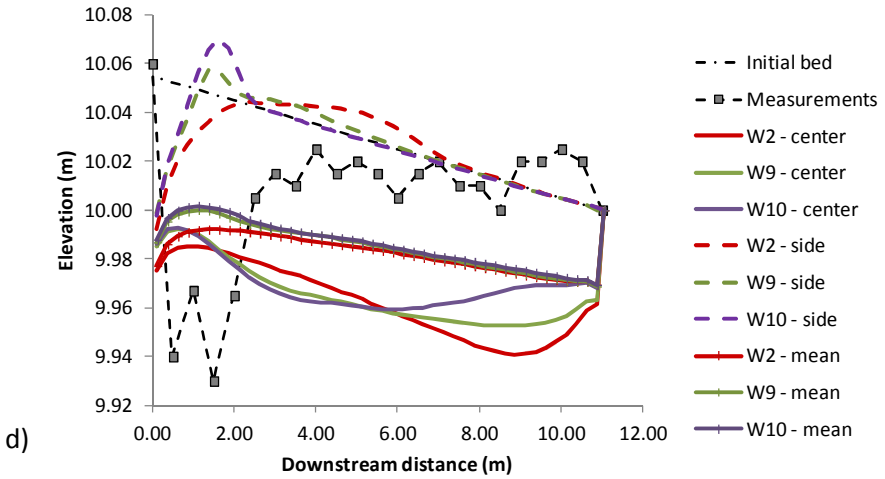

d)

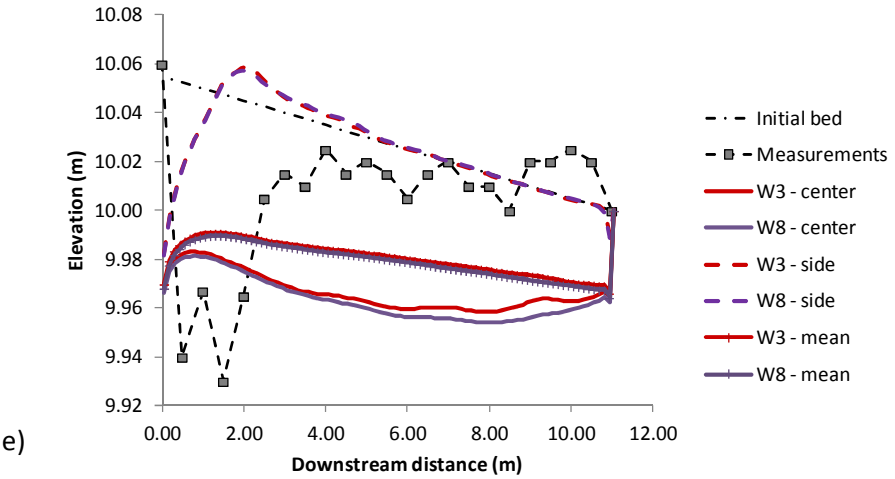

e)

Figure 10.5. Sensibility analysis of model predictions for bed elevation when a) grid downstream spacing is reduced; b) bed change tolerance is relaxed; c) downstream water surface elevation is raised; d) discharge convergence tolerance is relaxed, and e) bulk material porosity is changed. For further details see table 10.1

Final static armour.

Figure 10.5 shows the final surface grain size distribution as results from measurements and numerical modeling. With regards to measurements, the figure shows the mean distribution from 10 photographs; it has the following percentiles: D_{16} = 4,1 mm, D_{50} = 8,1 mm and D_{84} = 17,7 mm. The figure also exposes a band with maximum and minimum enveloping curves. It is noted that the predicted grain size distribution is very similar to that measured and is within the aforementioned band. The predicted percentiles are: D_{16} = 4,5 mm, D_{50} = 7,5 mm and D_{84} = 16,1 mm. These values belong to run W3 but all the runs have produced the same results.

The measured distribution is clearly bimodal (modes in D_1 = 4,8 mm and D_2 = 13,4 mm). The predicted distribution has only one mode in D = 6,7 mm. Figure 10,6 also shows the initial grain size distribution, where two classes are most frequent: 4,0-5,7 mm and 5,7-8,0 mm. These fractions exhibit also a clear reduction of their frequencies in the final state (especially the class 5,7-8,0). It is consistent with the fact that the median grain size of the transported material was 5,5 mm.

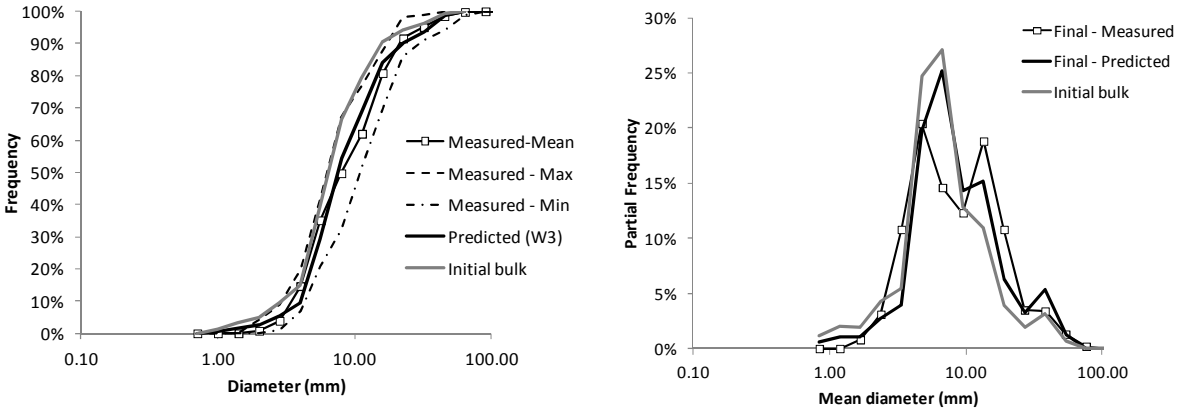

Figure 10.6. Initial and final surface grain size distribution. On the left: cumulative frequencies, dashed lines indicate envelope of measured distribution curves from 10 photographs. On the right, partial frequencies evidence modes: the final surface material has two modes while the predicted distribution has one clear mode.

10.2.4 Discussion

LICAN-LEUFU predictions have been tested against a flume experiment that involves a change in bed elevation, surface grain size distribution, flow hydraulics and sediment transport as well. Because all these factors are tightly related the experiment constitutes a good opportunity to assess the model capabilities. The overall model performance was very good because: a) the outgoing sediment flux was correctly predicted in terms of transport rate (Figure 10.4 a) and caliber (Figure 10.4e); b) final mean bed elevation was very similar to that measured (considering that only near sidewalls elevations were available); and c) the predicted surface grain size distribution is in agreement with observations.

The model is most sensitive to boundary conditions. Changing slightly the downstream water surface elevation an evident effect is observed in outgoing sediment flux and final bed elevation. This is so because rising the water surface reduces flow velocity and bottom shear stress. Then, as there is a no-linear relation between shear stress and sediment transport, a small reduction in τ is amplified into the transport rate. The higher the water surface elevation, the lower the shear stress, sediment transport and hence, the final bed elevation is higher.

There are two situations that were not considered by the model. The upstream disturbance created in the flume, due to the presence of a weir, produced a local scour that explains discrepancies in the upstream end of bed profiles (Figure 10.4). Secondly, the model was developed for wide/shallow channels with typical shape factors width/depth above 40. In this situation sidewall effects are negligible. Instead, walls do disturb the across-section discharge distribution in the “narrow” flume ($B/H \approx 10$) promoting flow concentration near the channel center. This may explain why there was almost null material collected in the lateral baskets (number 1 and 8 in Figure 10.4f), and the discrepancy with predicted lateral transport rate distribution.

Inspecting Figure 10.6 it seems as if the bed surface had not develop an armour layer because the final and initial surface grain size distribution are only slightly different. So, why does sediment transport follow an exponential-type tendency? Does it depend on hydraulics or on the development of the armour layer? Previous researches have shown that there is a first phase were bed degrades and then a second phase where the surface coarsens due to selective transport of fine sediments at

flows below the threshold for entrainment of larger grain sizes, such that the bed surface is winnowed of the most easily moved fine sediment (Mao et al. 2011; Wilcock et al., 2001; Church et al. 1998). When the static armour layer has developed sediment transport vanishes.

In order to answer the proposed questions a very simple model was implemented. The water surface elevation is calculated only at the middle of the channel, i.e., x = 5,5m; using a gradually varied flow model:

$$\frac{dh}{dx} = \frac{S_b - S_f}{1 - F_r^2} \qquad 10.2$$

where h is the water depth, $S_b$is the bed slope, S_f is the energy grade line slope and F_r is the Froude number. Friction losses are calculated using the Keulegan's equation with $k_s = 2 \cdot D_{90}$. The differential equation is easily solved applying the Runge-Kutta (third order) method.

Depth at x = 5,5 m is then used for evaluating local shear stress and sediment transport rate. These local quantities are loosely considered as flume-averaged values. Bed degrades pivoting around the fixed downstream end and hence for each time step a change of bed slope is calculated:

$$\Delta S_b = -\left[\frac{2}{(1-\lambda_p) b L^2}\right] q \Delta t \qquad 10.3$$

wherein L and b are the flume length and width, respectively, and q is the transport rate calculated with Wilcock-Crowe´s (2003) model using the bulk grains size distribution. The armouring process is not considered so the surface grain size distribution is hold constant.

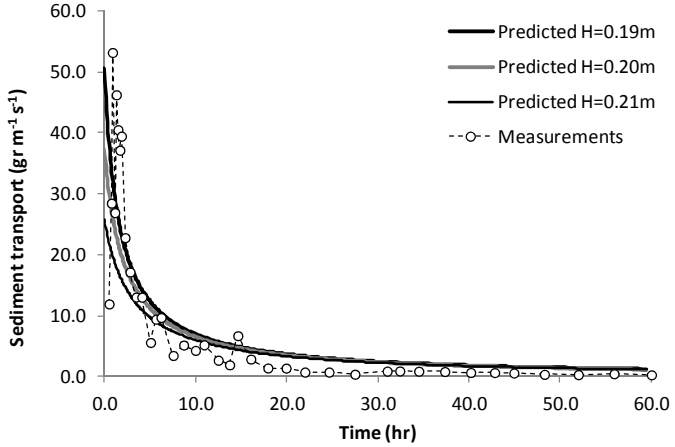

Figure 10.7. Comparison between measured sediment transport rates and predicted values with the simplified aggregated model (predictions have been made with different downstream depth: 0,19m, 0,20m and 0,21m). Because the model does not take into account the armouring process, the reduction in the transport rate is wholly attributable to bed degradation and consequent changes in hydraulics.

Figure 10.7 shows the model results obtained using several downstream water depth: 0,19 m, 0,20m and 0,21 m (as previously used in the 2D model). The result is remarkable because of the simplicity of the model. The best agreement corresponds with H = 0,19 m, the same result obtained when calibrating run W3. Because the armouring process has not been included into the model, the results indicate that the temporal trend observed in the outgoing sediment transport is entirely governed by hydraulics: as bed degrades, the slope reduces, depth increases, shear stress reduces and so does the

transport rate. Extrapolating this result to the 2D model, it is clear that the model should be more sensitive to changes in hydraulic parameters: downstream water surface elevation and discharge tolerance. Both parameters affect the flow characteristics.

Previously I pointed out that two phases have been observed in this kind of experiments: degrading and coarsening. With regards to the second phase, although the final surface grain size distribution is slightly coarser than the initial one, an incipient static armour has developed. The measured absolute degree of armouring is D_{50}/D_{50ss} = 1.26, while the predicted one is 1.17. This indicates that selective transport took place in the flume. In order to verify this affirmation, fractional rates were calculated using sediment transport rates at the beginning and the end of the experiment. For the initial state, the initial bulk grain size distribution was considered, while the final surface grain size distribution was considered for the final fractional rate. Figure 10.7 shows that at the beginning of the experiment, when there was no armour layer, all the grain fractions were transported (full transport). On the contrary, by the end of the experiment partial transport occurred. Coarse material remained in the bed while fine grains were winnowed. The figure also includes the predicted fractional ratios. The Wilcock-Crowe model describes quite well the partial transport state at the end of the experiment but it incorrectly predicts partial transport at the initial state.

It can be concluded that the interaction between hydraulic and bed degrading was the main factor driving sediment transport and full transport prevail in the initial phase of the experiment. By the end of the experiment, partial transport occurred due to bed coarsening, coarse material remain in the flume and fine sediments were winnowed.

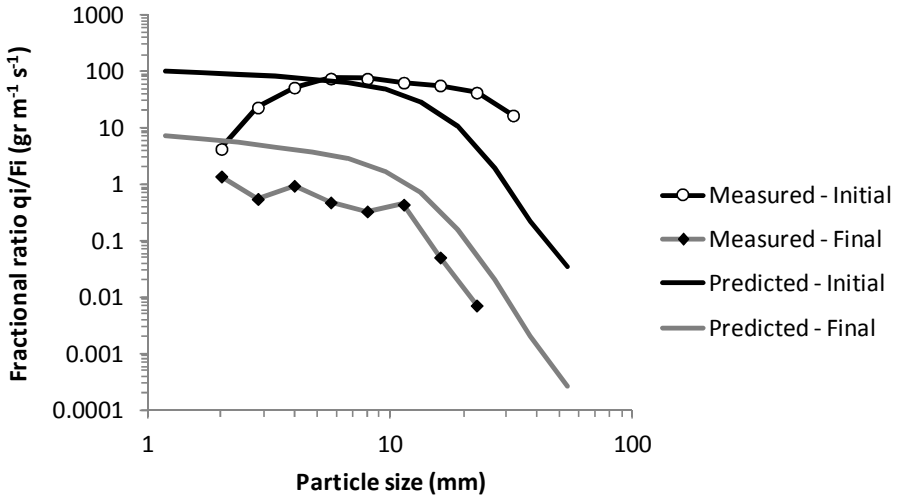

Figure 10.8 Measured fractional transport rates divided by the grain size frequency in the bed surface. At the beginning of the experiment full transport took place while by the end, partial transport occurred. The figure also includes predicted fractional ratios with the Wilcock and Crowe's (2003) sediment transport model.

10.3 A Medium-term simulation

This test concerns the application of LICAN-LEUFU 2D model in the context of regime theories, i.e., the model has been used to predict the shape of a channel (width, depth) providing water discharge and sediment supply. There are several differences with regards to previous works. The surface grain size distribution is treated as a degree of freedom instead of been an independent variable as normally used in regime models (see Chapter 2). The material on the channel surface is left to evolve freely in response to sediment supply and local flow properties. Another important difference is that water discharge is not constant. Aggregated and 1D regime models use a constant discharge equal to the bankfull discharge observed in the field. Instead, I have not supposed any bankfull discharge for this simulation; the model simulates the passage of 10 floods that corresponds to nearly 10 hydrological years.

10.3.1 Material and Methods

Case study: The Azul River

The Azul River was selected for this test because it has a very well developed riffle-pool morphology with alternate bars. The river reach is 890 m long, 64 m wide, has a slope of 0,0044 and a mean depth of 0,86 m but maximum depth at pools is 1,67 m. Bed material (substrate) is composed of gravel-sand mixture with D_{50} = 38,8 mm and a sand content of 14,3%. The bed is armoured and the surface is coarser; the representative percentiles are: D_{16} = 21,8 mm, D_{50} = 67,3 mm, D_{84} = 166,8 mm.

Description of cross section geometry

In order to describe the channel geometry three parameters are defined, one for each spatial dimension: cross section lateral asymmetry (a), vertical depth deviation (σ_h) and for the streamwise direction, two parameters are proposed: the thalweg slope (s_b) and the change in lateral asymmetry.

The asymmetry is defined as the distance from the channel center to the centroid of the cross section:

$$a = \frac{\int_0^B h(x-B/2)dx}{A} \tag{10.4}$$

with

$$A = \int_0^B h dx \tag{10.5}$$

wherein B is the channel width, A is the cross section area, x is the distance from the right bank. The relative asymmetry (a_r) results from dividing the asymmetry by half the channel width.

$$a_r = \frac{2a}{B} \tag{10.6}$$

The pool cross section with the deepest sector along the left bank will produce a positive asymmetry, while for the crossover, it should be zero (symmetrical section). Then, this parameter quantifies the lateral displacement of the thalweg in the alternating sequence: pool/bar, riffle, and bar/pool. Although the maximum variation range is (-1, +1), a triangular cross section with one vertical bank would have an asymmetry of ±B/6, and hence a_r = ±1/3.

The depth deviation describes the variability of the cross section in the vertical direction. It is defined using the standard deviation of depth with respect to the mean depth (H):

$$H = \frac{A}{B} \tag{10.7}$$

$$\sigma_h = \sqrt{\frac{1}{B}\int_0^B (h - H)^2 dx} \tag{10.8}$$

And the relative depth deviation is

$$\sigma_{hr} = \frac{\sigma_h}{H} \tag{10.9}$$

The lowest value of σ_{hr}, i.e., zero, is obtained in a rectangular cross section. Therefore, crossovers are expected to have lowest deviation while maximum values will be found at pool where vertical variability is highest.

The bottom channel slope is defined in terms of the thalweg slope:

$$s_b = \frac{dh_{th}}{dx} \tag{10.10}$$

A positive value indicates that the local bed slope is greater than the flood plain, i.e., depth is increasing.

Bankfull discharge and reach-average hydraulic geometry determination

Bankfull discharge has been evaluated using a similar procedures applied in the field, as described in section 6.1.3. First, bankfull level was recognized as the maximum bar elevation. Then, a 1D hydrodynamic model was run for different discharges and predicted water levels were compared against bankfull levels. The bankfull discharge was the discharge that minimized the square differences between predicted water surface elevations and observed bankfull levels (see calibration procedure exposed in section 6.4).

10.3.2 Numerical method settings

Initial configuration

The initial channel reach had a uniform geometry, i.e., the cross section remained constant along the reach. The channel was 1,50 m deep, 50 m wide, had a slope of 0,0044 and was 1200 m long. The width was chosen lower than the actual value so as to promote channel widening. In order to perturb the flow, a bar was placed along the right bank. The bank was 0,50 m high, 120 long and 20 m wide.

A rectangular mesh was constructed with cell sizes of 12 m x 1,67 m. As a result, the cross section was represented with 35 cells while 100 cells were needed in the downstream direction.

The initial surface grain size distribution was set equal to the mean distribution found at pools in the field, with a distribution: D_{16} = 19,5 mm, D_{50} = 51,0 mm, D_{84} = 157,6 mm. Instead, the bar was given a coarser distribution so as to enhance stability. In this case the grain size distribution measured at riffles was assigned: D_{16} = 31,5 mm, D_{50} = 83,1 mm, D_{84} = 172,8 mm. The substrate had a finer material as found in the field: D_{16} = 3,1 mm, D_{50} = 41,6 mm, D_{84} = 150,2 mm. The grain size

distribution were represented by 18 classes covering the range 1 mm – 512 mm. The material porosity was calculated with eq. 10.1 giving $\lambda = 0{,}54$. The angle of response was set equal to 37°.

Sediment supply

Assuming that the Azul River is at grade (as comes out from the stability verification done in section 5.4), the sediment supply was estimated as the reach-average sediment transport capacity. A DTM was constructed interpolating 5 cross sections surveyed in the field (see Chapter 6). The surface grain size distribution was also interpolated using the distributions from each cross section. The model was run with a range of discharges and sediment transport was calculated at each cell giving the reach-averaged sediment transport (Figure 10.9). The fitted polynomial curve was used to calculate the supply for each discharge. The supply grain size distribution was set equal to the subsurface distribution (Parker and Toro-Escobar, 2002).

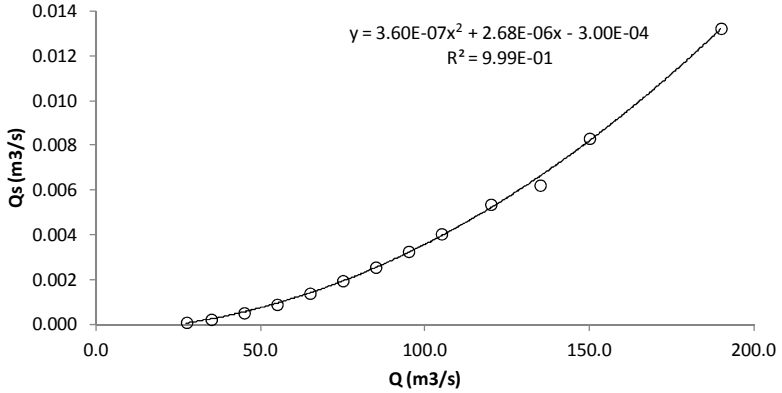

Figure 10.9. Reach-averaged sediment transport evaluated at the Azul River using LICAN-LEUFU 2D model. The fitted curve is used to calculate the supply assumed to be equal to the current transport capacity of the river.

Water discharge

Inspecting Figure 10.9, it is evident that it would not be efficient to simulate flows that transport low or negligible sediment loads, for instance, discharges below 40 m^3/s. In order to define the lowest discharge (Q_{min}) a quantitative criterion was assumed: the amount of sediments transported by discharges lower than or equal to Q_{min} should be below 25% of the annual yield; and Q_{min} should have a competence equal to D_{30}.

For each discharge the reach-averaged shear stress was calculated and the flow competence was estimated using $\tau_c^* = 0{,}047$; the competent diameter was compared against the mean grain size distribution for evaluating the corresponding percentile (Table 10.2). A discharge of 50 m^3/s fulfilled well the requirement aforementioned: 77% (i.e. 1 – 0,23) of the annual yield will be loaded to channel and low discharges are able to move percentile 29% of the surface material.

Table 10.2. Selection of minimum discharge based on flow competence and volume of transported material as a percentage of annual yield.

Discharge	**Mean Shear stress**	**Percentile moved**	**Annual Yield**
(m3/s)	(Pa)	(%)	(%)
80	34.1	36	55
70	32.0	34	46
60	29.8	32	35
50	27.1	29	23
40	24.2	26	11
30	20.5	21	2
25	18.3	18	0

Daily mean discharges were available for the period 1/4/1970 – 31/3/2009. However, only the last 20 years were used for the simulations as had already been used in the stability verification (Chapter 6). Selecting discharges above the threshold of 50 m^3/s, the record was reduced to 562 days, i.e., 28 days per year, approximately.

Numerical scheme settings – boundary conditions

LICAN-LEUFU 2D model was run under the medium-term configuration. Discharge-tolerance was 10% and tolerance for bed elevation change was set at 5%. At the downstream boundary a minimum bed elevation was imposed (no erosion could take place below this level) and the water surface elevation was fixed at the uniform-flow depth (see section 9.4.2). The minimum water depth was set at 0,10 m for the hydrodynamic model and 0,15 m for the sedimentological routine.

10.3.3 Results

The model simulated the first 102 days covering the range of discharges 50 – 250 m^3/s, and 10 floods were present. At the end of the period the hydrodynamic model encountered difficulties to converge for low discharges and hence the simulation was stopped. This is the reason why the actual simulated period is lower than the proposed period (562 days). Nevertheless, the results are discussed keeping in mind that this drawback can limit the applicability of the experiment to test the hypothesis.

Bed armour

A first analysis of the bed structure consists on inspecting the change of the reach-average median diameter. Figure 10.9 shows the temporal trend of the median diameter. It is evident that the major change took place during the first flood. At the beginning of the simulation D_{50} was 57 mm and it quickly coarsened up to 88 mm. Afterward, the diameter increased very slowly during the first half of the simulation period and decreased during the second half. On average, after the first two floods the diameter remained around to 95mm. The same picture also shows the outlet caliber. Comparing both diameters (bed and outlet), while sediment transport caliber depended on the flow intensity, bed grains size distribution remained nearly constant.

At the end of the ninth flood (the last complete flood) the reach-average surface grain size distribution had the following percentiles: D_{16} = 20.4 mm, D_{50} = 92.4 mm, D_{84} = 204.7 mm. Figure 10.10 compares the grain size distributions as measured in the field and that predicted by the model. Predicted surface material is coarser that the observed reach-average curve (D_{50} = 67.3 mm) and is nearer the curve at riffles (D_{50} = 83.1 mm).

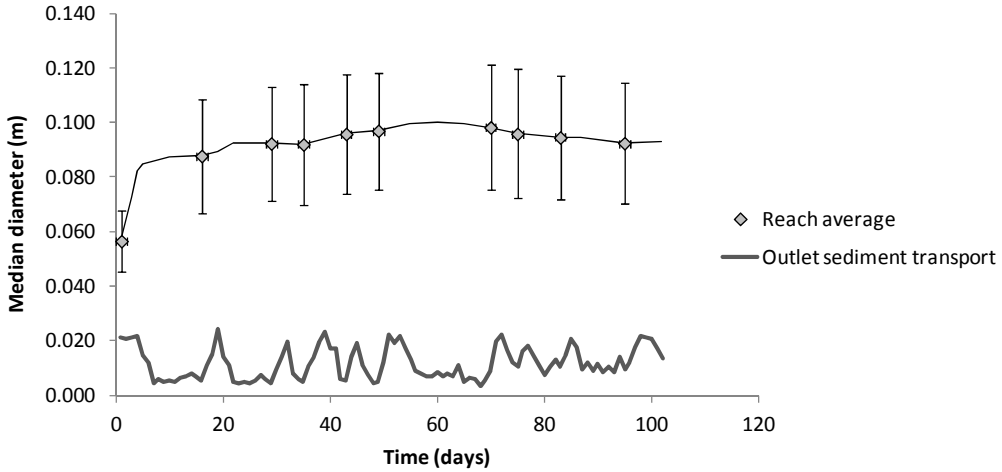

Figure 10.10. Temporal change in surface reach-average median grain size. The error bars represent the standard deviation in median grain size variability along the reach.

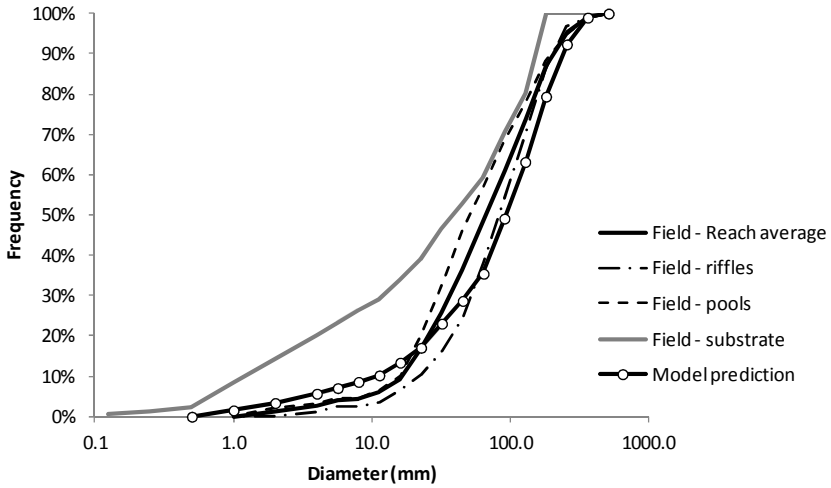

Figure 10.11. Comparison of grain size distributions including field measurements (reach average at pool, riffles, and substrate) and the reach-average model prediction after the ninth flood.

The degree of armouring is not constant along the reach. Figure 10.10 also includes error bars that represent the standard deviation in median diameter. The length of the bars is nearly equal indicating that spatial variability remained constant during the repeated passage of floods. However, variability is not random but is tightly related to bed topography. Figure 10.12a shows the spatial variability of the surface grain size at the end of the simulated period (figure 10.12b includes bed

topography for enhancing comparison). The coarser material is found at the feet of the bank in contact with pools (armour index near 5) and extends over the bar bends. These areas extend downstream covering the head of the bars. Finer material is placed on the central part of the bars and their tails. Within the channel, finer material is found at the deep places while coarser sediments are clearly seen at the sides of crossovers.

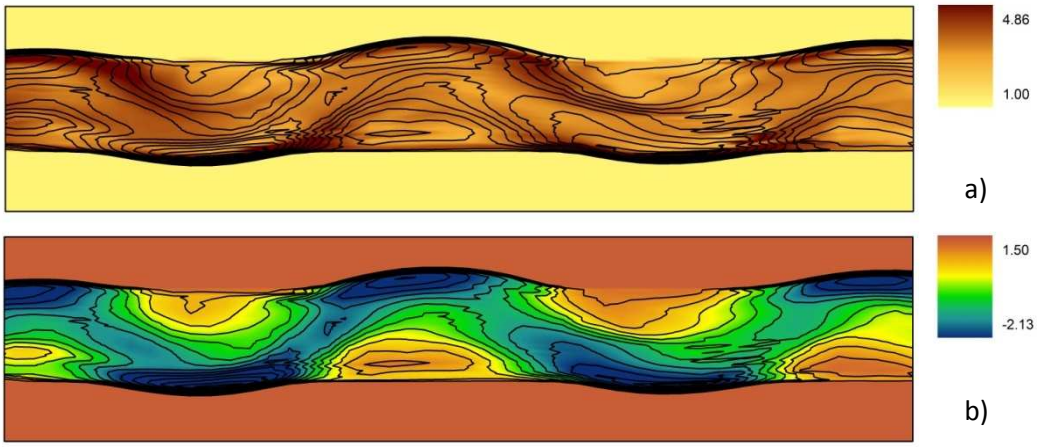

Figure 10.12. Comparison between the absolute armour index (above) and channel morphology (below). Dark lines representing contour levels have been included for enhancing the comparison (spacing equal to 0.25 m). Flow is from left to right.

Changes in channel morphology

Figure 10.13 shows a sequence of ten pictures corresponding to the end of each flood. A flood event starts when the discharge rises, then the peak discharge is attained, and it further extends including the recession period up to the beginning of the next event. For instance, the first flood lasted 17 days (see Figure 10.10).

During the first flood erosion took place at the opposite bank of the initial bar, and bed elevation decreased to 0,61 m. Downstream this pool sediment was deposited raising the level by 0,24 m. In this way the initial perturbation generated another one on the opposite bank. The subsequent floods accentuated this process creating alternate banks along the channel reaching the downstream end by the end of the 6th flood. The original bar migrated downstream and was finally replaced by a pool.

The first reaction of the channel was to change the bed form. Bank migration was low during this phase. Since the 6th flood, pools were deep enough to promote bank slides when the inclination angle exceeded the response friction angle. Figure 10.14 shows the sequence of cross section A (see figure 10.13 for location). The initial width was 47,3 m while after 10 floods it enlarged up to 65,3 m – both values evaluated at the final bankfull level. Note that pool depth remained nearly constant while channel widened.

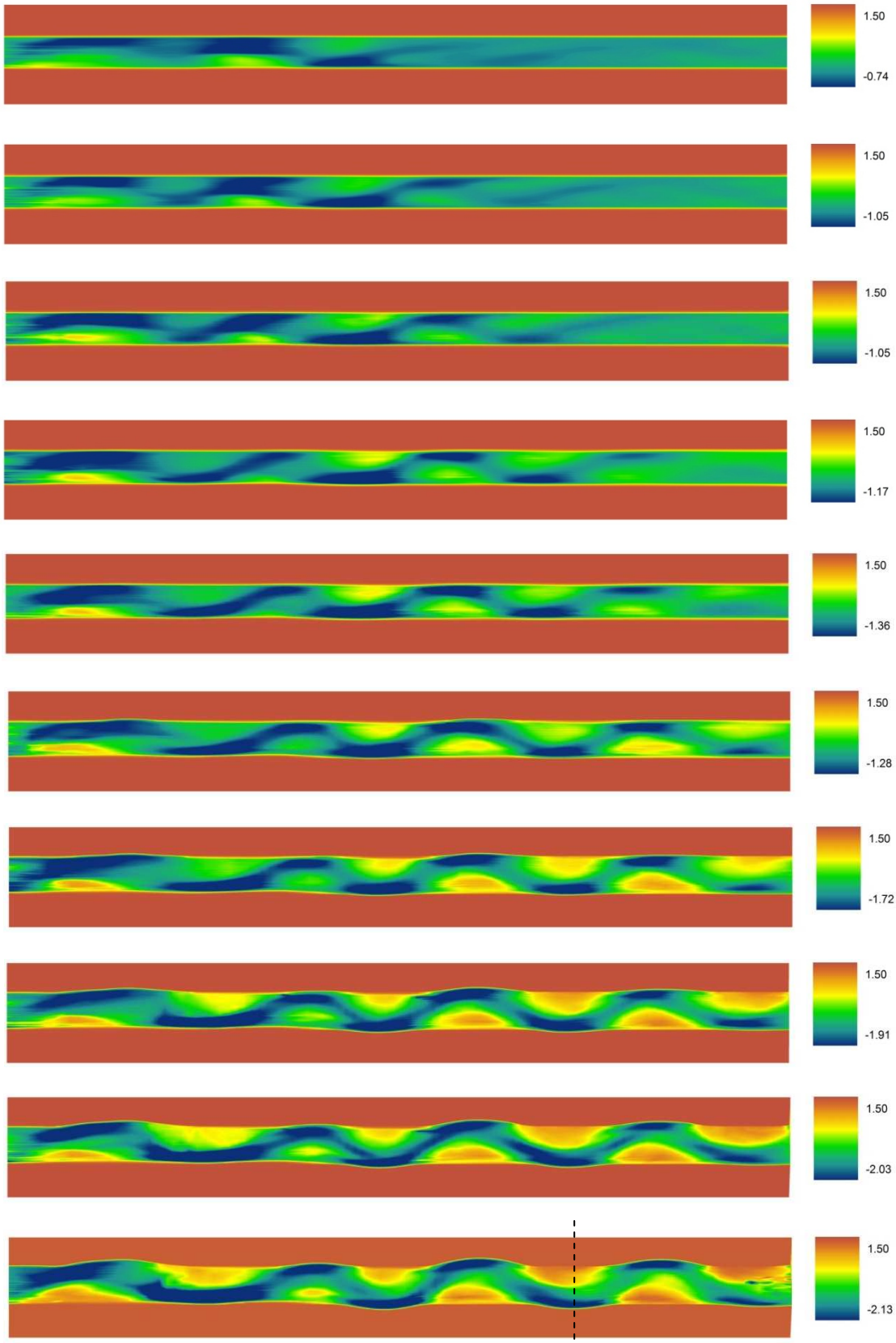

Figure 10.13. Sequence of channel planform after the passage of each flood. Elevations have been slope-detrended for enhancing the visualization of bed forms. The dashed line indicates the location of the cross section analyzed in Figure 10.14 (see text).

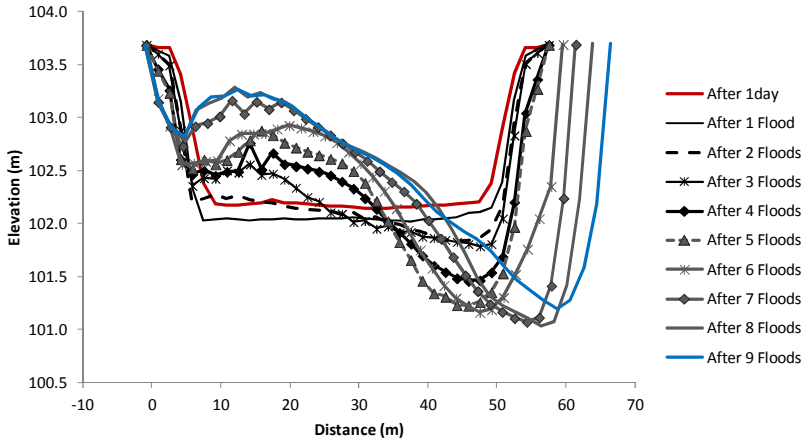

Figure 10.14. Temporal change of a cross section place at x=700 m from the upstream end. See dashed line in Figure 10.13 for location.

As aforementioned, the channel evolved towards a more asymmetrical shape (wider relative asymmetry range) and higher downstream depth variation. However, this trend seems to arrive to a stable configuration by the ninth flood. In fact, the system spatial evolution for the seventh and ninth floods is very similar. The relative asymmetry varies in the range $\pm$ 0,32, that corresponds to an asymmetry of $\pm$ 10,2 m.

Now, considering the proposed geometrical parameters, the initial state of the channel is presented by two points in the phase space defined by a_r and s_{hr} (Figure 10.15). The central point indicates the symmetrical part of the reach ($a_r = 0$), while the second red point corresponds to the lateral bar imposed as an initial perturbation. Because there is a sudden change between these cross sections, the entire channel is represented by two discrete points. This situation changed as the channel evolved and the points transformed into a continuous line that indicates a continuous and related change between asymmetry and bed elevation variability. This change was small for the first floods but wide for the ninth flood. The V shape developed in the phase space is a clear demonstration of the interrelation of depth and asymmetry between riffle and pools: pools are represented by the extremes of the V where asymmetry and depth deviation are highest; and riffles are placed at the center ($a_r = 0$) where the depth deviation is lowest.

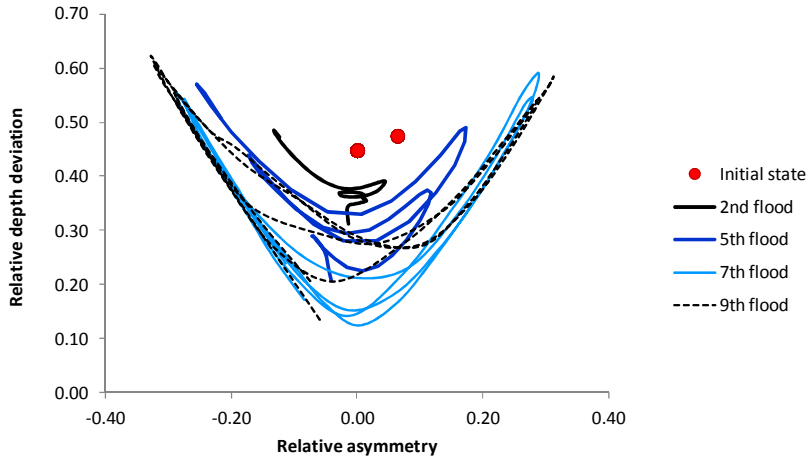

Figure 10.15. Channel shape evolution as represented in the phase space. Red points indicate the initial state, lines belongs to the channel state after selected flood events.

The shape parameters (a_r, s_{hr}, and s_b) have also been used to describe the change of the cross section in the streamwise direction for a particular moment, at the end of the ninth flood (Figure 10.16). Along the first 500 m of the channel there is a transition as observed in the irregular variation in σ_{hr}. Downstream this point the channel attains a cyclic variation in shape, and both a_r and s_{hr} follows a cosine trend. The length wave for asymmetry is nearly 270 m while σ_{hr} has a one-half wave length as required for attaining the minimum depth deviation at each crossover. It is also evident that both parameters are at face, i.e., sections with highest depth deviation occur at most asymmetrical locations.

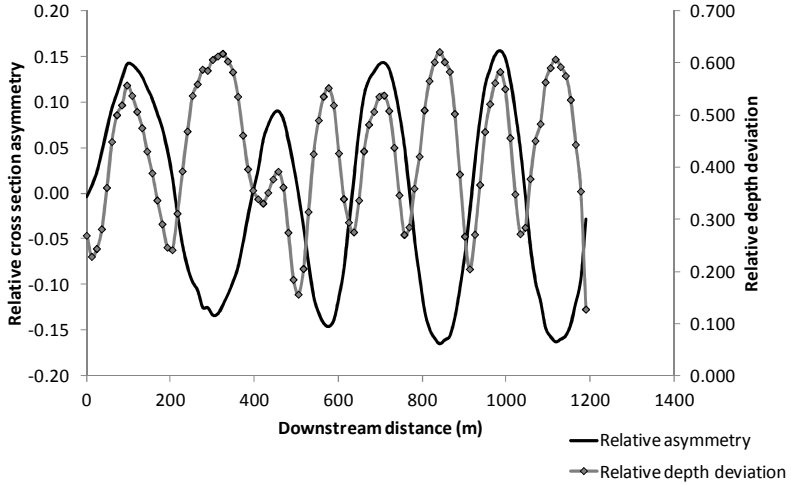

Figure 10.16. Spatial variability of cross shape parameters. Relative asymmetry changes sign in a cyclic way in response to the alternating bar-pool morphology. Depth deviation is maximum at pools and lowest at crossovers.

The channel bed can also be described with the thalweg slope. Figure 10.17 shows the variation of this parameter along the channel. There is a similar situation as aforementioned: along the first 500 m an irregular pattern is observed, but downstream this progressive a cyclical feature develops. At crossovers the detrended slope is positive meaning that riffles are steeper than the mean reach slope. Then, s_b is zero at the most asymmetrical section, i.e., the pools, and changes sign downstream indicating that the bed slope between pool-riffle is below the mean reach slope.

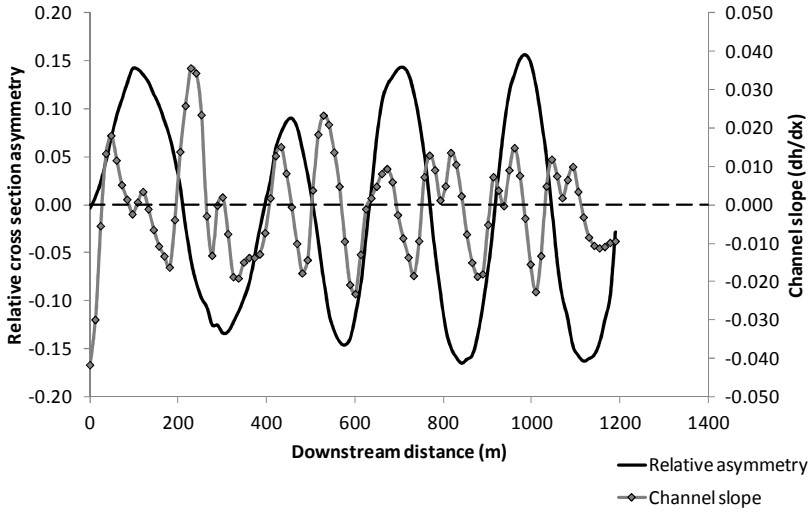

Figure 10.17. Spatial variation of relative asymmetry and bed slope detrended with the valley slope.

Sediment transport and mass balance

Mass balance was computed as the difference between incoming and outgoing sediment volumes at the reach extremes. Bank failure was not considered because it represents a lateral displacement of material, i.e., it is within the reach. Figure 10.17 shows the reach mass balance. During the first flood channel incision took place and the channel lost 4000 m^3 of material, approximately. This erosion is also evident in Figure 10.14, comparing the cross sections before and after the first flood. The erosion due to subsequent floods was more moderate. Two phases are distinguished: a first phase of incision for high discharges (transport capacity is higher than supply) followed by a deposition phase for low discharges (transport capacity is lower than supply). For the second flood this tendencies almost balanced, but in the subsequent events it depended on the duration of low discharges with capacity below to the imposed supply.

Figure 10.19 shows a comparison between the incoming and outgoing sediment transports. Discharges above 100 m^3/s have a transport capacity higher than supply. Although there is a clear tendency between bedload and water discharge, the response of the system was not always the same. The scatter in bedload indicates that the outgoing sediment transport was a complex output of the system that depended on within-reach features such as bed armour and morphology. In order to evidence a possible time-dependence, the scatterplot has been classified according to the flood event. Figure 10.19 also shows that points overlap and that there is not systematic reduction of transport capacity as time goes by. In order to quantify this observation sediment transport from the first and ninth flood were considered. The analysis of regression provided the following functions:

First flood: $$\log Q_b = 3.13 \log Q - 8.51 \quad (10.11a)$$

Ninth flood: $$\log Q_b = 3.09 \log Q - 8.62 \quad (10.11b)$$

The analysis of covariance indicated that the null hypothesis that there was no difference between regressions lines can be accepted with a p-value of 0.042. In this sense, although slope has been reduced due to the deficit in mass balance, it has not affected significantly the output of the system.

The simulation period is not long enough to answer the question whether the reach has attained a mass balance (in the sense explained in Chapter 1). The last flood was intense and produced a significant loose of material, but the recession, and hence deposition phase, was incomplete.

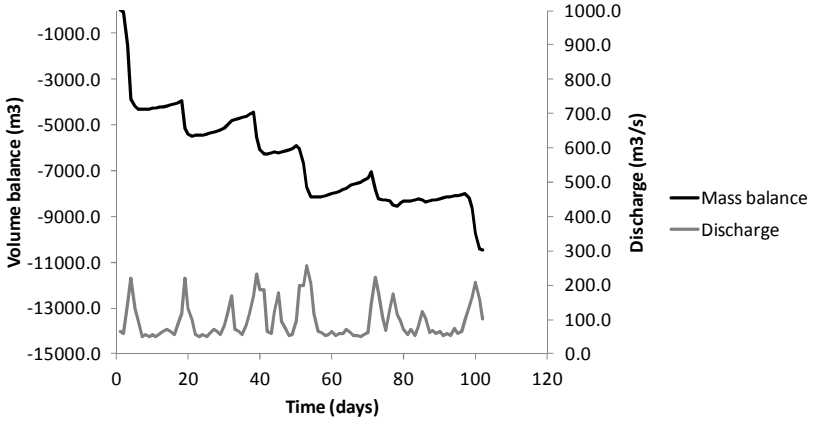

Figure 10.18. Mass balance evolution with the passage of floods. Mass balance is evaluated as the difference between volumes due to sediment supply and outlet transport.

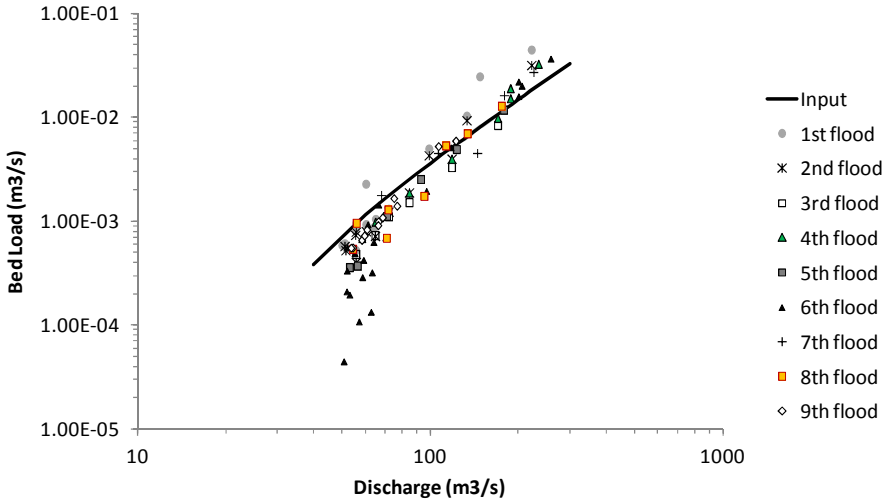

Figure 10.19. The outlet sediment transport of the system follows nearly the input signal but scatter is evident indicating that the system response depends on channel structure (morphology and armour state).

Hydraulic geometry

The calibrated bankfull discharge was 95m^3/s, which is 23% higher than the measured in the field, 77 m^3/s , but falls within the confidence interval (95%): 56.1 – 102.6 m^3/s. Shape parameters were calculated considering bankfull stages as the reference elevation (instead of flood plain as previously used). The observed shape parameters were also calculated using the bankfull stage as measured in the field. The predicted channel geometry is very similar to that observed in the field; this refers to width, depth, asymmetry and depth deviation (see table 10.3). However, predicted riffle spacing, 132 m, is very much lower than the actual spacing of 444 m.

Table 10.3. Comparison of hydraulic geometry parameters predicted by the model and measured in Azul River.

	Model predictions **Mean** (st.dev.) **(m)**	**Field measurements Mean (m)**
Reach average geometry		
Width	63.96 (4.73)	64.11
Depth	0.92 (0.08)	0.86
Riffle spacing	132.1	444.6
Pool geometry		
Asymmetry	14.88 (1.42)	8.96
Depth deviation	0.66 (0.06)	0.60
Mean depth	0.87 (0.07)	0.93
Maximum depth	2.06 (0.16)	1.67
Riffle geometry		
Asymmetry	3.17 (1.51)	-1.39
Depth deviation	0.33 (0.03)	0.38
Mean depth	1.03 (0.06)	0.82
Maximum depth	1.49 (0.09)	1.30

10.3.4 Discussion

Did the 2D-model describe better the channel geometry than aggregated or 1D- models? Do different spatial scales require different morphological parameters?

The 2D-model performs better than a 1D or aggregated model if it predicts the width and depth of the channel, as the regime theories do, but also within channel bed forms. Then, two different spatial scales are applied. Regime theories work at the reach-scale that can be defined with a length in the order of 10^2 channel widths (Ferguson, 2008; Weichert et al., 2009). Instead, the scale of applicability of the 2-D model is lower, the macro-scale proposed by Weichert et al. (2009), with a length of 10^1 channel widths. At this scale, other parameters have to be invocated for describing the channel cross section. In this study three parameters have been proposed, one for each spatial direction: lateral asymmetry, vertical deviation, and in the case of the streamwise direction, the rhythmic change in the alternating bar can be describes in term of riffle spacing, bed slope or downstream change in asymmetry (see Table 10.4 for a summary).

Table 10.4. Morphological parameter that describes the shape of the channel at different spatial scales.

Spatial scale	Length	Morphological parameters
Reach-scale	10^2 B	Width, Depth
Macro-scale	10^1 B	Asymmetry, Depth deviation, Riffle spacing

Table 10.3 shows a comparison of predicted and observed parameters for the Azul River. With regards to the reach-scale, it can be said that the model predicted very well the width and depth of the channel, and in this sense it provided the answer expected from a regime model. Now, inspecting parameters at the macro-scale, good agreement was also found for depth (mean and maximum) for riffles and pool cross sections. Asymmetry was somewhat overpredicted at pools and riffle, but the deviation is also important. Figure 10.20 compares model predictions against field measurements in the phase space. There are five points that represent the cross sections in the sequence riffle-pool-riffle-pool-riffle, as measured in Azul River. It is observed that points are placed within the region of variation of predicted asymmetry and depth deviation. In the case of the streamwise channel properties, the predicted riffle spacing was significant lower than measurements. It is also evident in the phase space when the derivative of the asymmetry is used (Figure 10.20). The predicted trajectory is wider indicating a lower wave length. This discrepancy will be discussed later in the context of channel response and spatial- temporal- scales

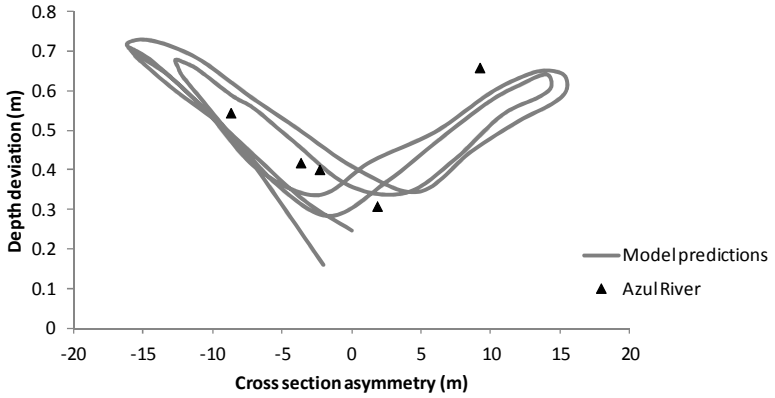

Figure 10.20. Phase-space portrait of the streamwise variation in lateral asymmetry and depth deviation. Dots indicate field measurements in Azul River.

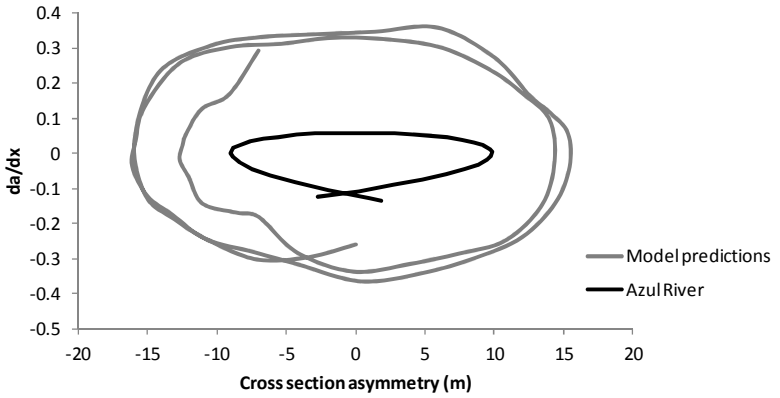

Figure 10.21. Phase-space portrait of the streamwise variation in lateral asymmetry and its downstream variation. The gray line represents the model predictions and the black line, an estimation from field measurements. The higher the vertical amplitude of the curve indicates the lower spacing between riffles.

State diagrams have been used to describe alluvial systems at grade. Eaton et al. (2004) proposed a state space (B/H, D/H and S or τ^*) where the range of alluvial states for constant values of relative bank strength forms a single plain in the space (Figure 10.22). State plots represent the state of the system when it has attained equilibrium, and then there is no more "change". In the context of fluviomorphology, it means that it has attained a statistically stable state (or steady state): mean values of the variables that describe the system do not change with time (see Chapter 1). In all the cases, time does not play any role in the system. The neglection of time has also been used in the description of dynamic systems that are far away from equilibrium, the so called, chaotic systems. In this new brand of physics the evolution of the system is portrayed by means of the phase space: "*the set of all possible states of the system determined by the values of all variables which specify its state of motion*" (Cencini, et al., 2010, p.11). The trajectories depicted in the phase space represent the phase-space portrait of the system. The set of points asymptotically reached by the trajectories in a space of dimensions smaller than the original phase-space is called *attractor* (Cencini, et al., 2010, p.15).

Now, Figure 10.20 and 10.21 can be interpreted as plane projections of the system trajectories in a phase space defined by asymmetry, depth deviation and da/dx. Figure 10.22 gives a qualitative interpretation of the previous figures as a phase-space portrait of the channel evolution in the streamwise direction. The attractors of this system consist of two points with maximum asymmetry and depth variance. Then, while Eaton et al.'s (2004) diagram represents all the river states at the reach-scale, the phase-space portrait represents all the cross section configurations possible, at the macro-scale.

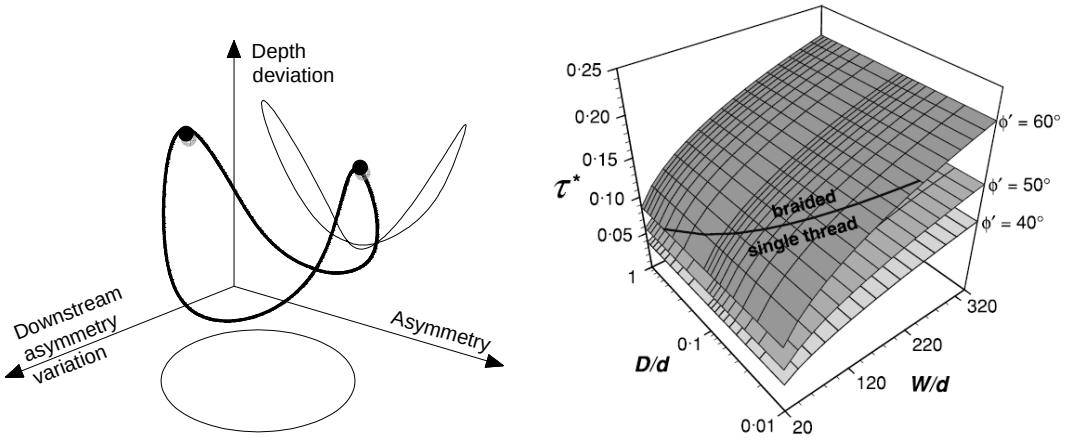

Figure 10.22. Left: Conceptual interpretation of morphological change as a phase-space portrait. Each cross section in the field represents a point the phase-space. The two black points represent attractors with maximum lateral asymmetry and depth variance. Right: state diagram of the channel morphology at the reach-scale prposed by Eaton et al. (2004).

Eaton et al. (2006) presented a simple analytical model for explaining the reach-scale river behaviour (expressed as extremal hypothesis) in terms of feedback processes acting at the scale of a channel width. They showed that due to a positive feedback an initial perturbation developed pools with maximum cross sectional shear stress variance, which represent attractor states where sediment continuity is satisfied using the least possible energy expenditure per unit length of channel. At crossovers the stream occupies a metastable state, with lower variance and requiring greater energy expenditure to transport the same volume of sediment. These extreme situations are clearly seen in the phase-space portrait.

Does the coarse surface material, observed during low discharges, persist during very large floods capable of moving the bed material?

The problem about the persistence of the amour layer is crucial because surveys are easily performed during low discharges, but the scenarios of interest are those of high discharge. Field evidence based on direct observation demonstrates that in fact, the armour layer persists (Andrews and Erman, 1986; Clayton and Pitlick, 2008). The analysis of bed load with a sediment transport formula also confirmed the persistence of the amour layer (Wilcock and DeTemple 2005). Recent flume experiments confirm the persistence or the armour layer and the constancy of the surface grain size throughout the hydrographs (Mao, 2012).

Parker et al. (2006) followed a different approach, investigated the characteristics of the armour layer using a 1D model. As a result of the simulations, they found that there was a "boundary layer" at the upstream part of the flume where bed elevation changed in response to the hydrograph, but downstream bed elevation and surface size distribution became invariant in time. However, the bed transport rate and size distribution changed according to the hydrograph[25].

In this study the channel adjustment in bed elevation, bed form development, channel widening, and sediment sorting, have been considered. Hence, the new simulation includes 2D-complexities that had to be neglected in a 1D model. Nevertheless, the same conclusion can be affirmed: the reach average grain size distribution has remained unchanged during the passage of floods (see Figure 10.10); and given a fixed sediment input (caliber and amount) the channel responded in terms of bedload transport rate and bedload size distribution (see Figures 10.19 and 10.10, respectively).

Because Parker et al. (2006) analyzed results from a 1D model, it is clear that there would not be a downstream variation in grain size if a uniform flow condition was established. In the 2D-model, flow is not uniform, instead a gradually varied flow occurs depending on bed forms and bars. Then, it would be expected to observe some kind of spatial variability. Figure 10.23 shows the evolution in bed elevation and surface grain size for the riffle-pool sequence of the second half of the channel. During the phase of increasing discharge, erosion took place downstream the pools (sections with highest absolute asymmetry) while deposition occurred upstream the pools. There was also a change in grain size been erosion linked with a coarsening process and deposition with fining (Figure 10.23a). During the recession phase of the hydrograph erosion and deposition were located at different places: deepest points were filled with fine material and riffles degrade and got coarser (Figure 10.23b). The overall result was a trend for aggradation at the riffle/pool-head sector with a reduction in grain size while low erosion and small coarsening took place at the pool-tail.

Sear (1996) examined riffle-pools sequences on the basis of their sediment transport characteristics. He characterized riffles sectors by coarser surface material and exhibiting an aggradation tendency during bankfull floods. On the contrary, pools showed a downstream fining of surface sediments and were characterized by degrading, though the pool-tail may aggrade.

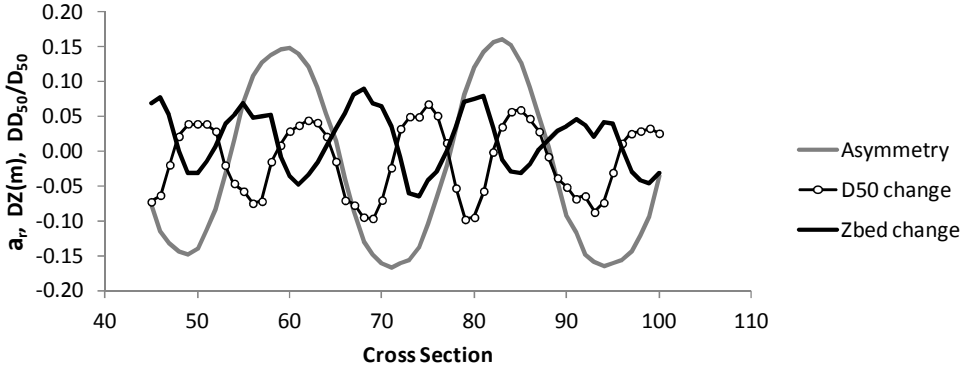

[25] This topic on the persistence of the amour layer has been exposed in detail in Section 4.1.

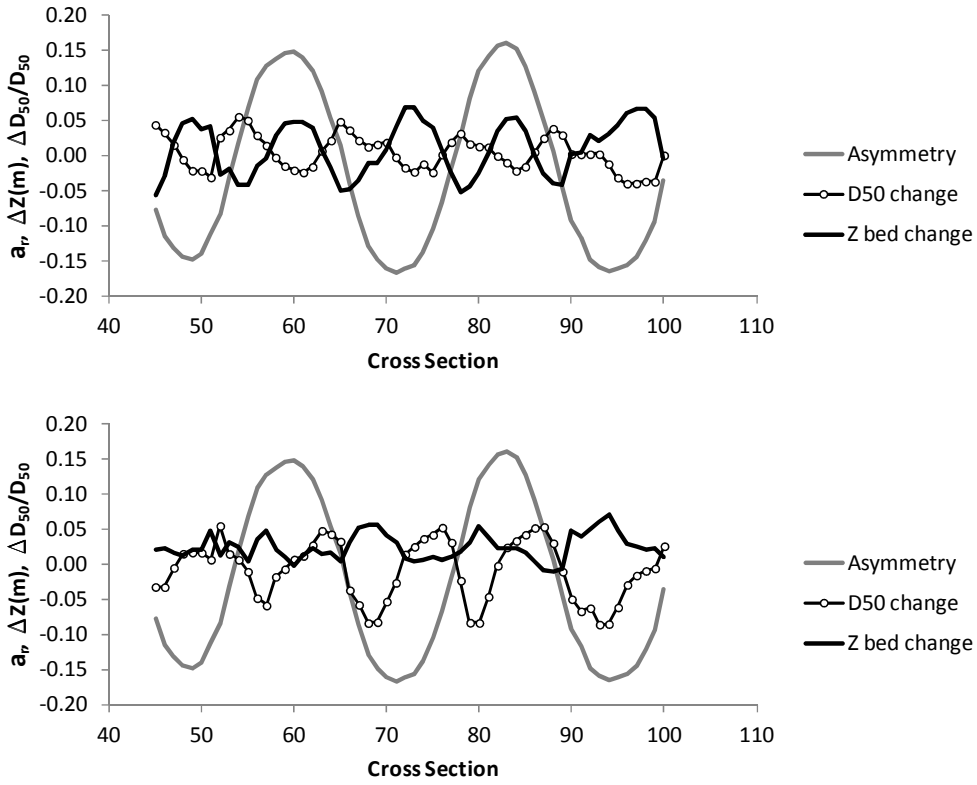

Figure 10.23. Downstream variation of bed elevation and surface grain size during the phase of increasing discharge (a), then during the recession limb (b), and the comparison between pre-and post flood conditions (c).

Although the results from the numerical simulation indicate a significant relation between bed form and armour response there are differences with field observations. In general, riffles are not coarser than pools according to the simulation, in clear contradiction with field observations. Sears (1996) points out that hydraulic hypotheses are not necessary, such as velocity reversal, for explaining the formation of riffle-pool sequences. Instead, he suggests that crucial difference may be found in the chaotic turbulence on riffles that develops particle structures during low flows. As a result, riffles tend to have a well structured armour layer with higher critical shear stress that renders them more stable. On the contrary, the lack of vibration in pools leaves loose material easily movable during floods. This process occurs at a scale lower than that adopted for this study. The development of the alternating bar morphology with riffle pools observed in the simulation results is a consequence of the interaction of water flow, sediment transport and channel shape, but bed structures has only been represented by the armour layer, i.e, the grain size distribution property. The discrepancy between Sear's (1996) observations and the results from this study may put in evidence the importance of at-low-scale grain structure in the development of macro- and meso-scale structures, such as riffle-pools sequences, and the role of low discharges for its development.

Which are the channel response styles at different spatial and temporal scales?

According to Weichert et al. (2009), at the micro scale the reach response consists on adapting the surface roughness (see table 2.1). This scale is dominated by individual particles and hence it has a reduced spatial extension (in the order of 10^{-1} – 10^{-2} channel widths) and also a small temporal

characteristic span. The formation of the armour layer can take place by winnowing of fine fractions - with de development of a static armour- or in the context of mobile amour as explained by the equal mobility hypothesis (see Chapter 4 for details). At the so-called macro-scale (10^1 channel widths), riffles and pools are the dominating bed structures. When the paved bed is not strong enough, the channel responds by erosion and deposition at the next spatial scale developing bed forms. Eaton et al. (2006) have pointed out that this response depends to the excess in shear stress ($\tau - \tau_c$). When the excess is very high there are few possibilities for the growth and persistence of a disturbance because sediment transport rate is so high that the perturbation is swept. On the contrary, when the excess is low, which is the case of most gravel bed rivers (see Andrews, 1984), and initial perturbation is amplified and the channel necessary deforms through erosion and deposition. At the largest spatial scale, the so-called reach scale (10^2 channel widths), the bed restabilizes by reducing the slope due to a rotational erosion around a pivot point (Figure 10.24).

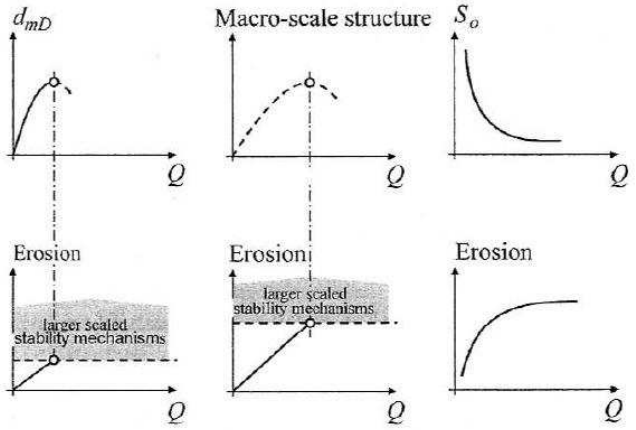

Figure 10.24. Self-stabilization mechanisms in different geomorphologic scales accompanied by bed erosion in every scale: micro-scale (left), macro-scale (center) and reach-scale (right) (after Weichert et al., 2009).

Results from this study support the idea that there is a relation between spatial-scale and channel style of response, as aforementioned, but also they are related with a time span or a characteristic morphological period of adjustment. The change of surface grain size took place mostly during the passage of the first flood, while minor adjustments were present during subsequent events (Figure 10.25). Hence, the micro-scale has the lowest morphological response period. At the next spatial-scale, the macro-scale, the cross section adjusted in two ways. First, bed deformed as a result of the initial perturbation developing alternating bars, as was qualitative evident in Figure 10.13, or by means of the increase in the depth standard deviation (Figure 10.25). Ones pools were deep enough, bank erosion took place and the channel got wider. This process took place much later, been evident after 70 days. According to Figure 10.25, width does not seams to arrive to a statistically constant value but the relation between asymmetry an depth deviation (Figure 10.15) suggests that the reach arrived to a stable state. The period was not long enough for assessing the stability with regards to the slope. The mass balance (Figures 10.18) and the trend in slope (Figure 10.25) suggest that the slope has not attained a constant value, i.e., mass balance has not been achieved still. Finally, the mean depth did not change significantly during the simulation period.

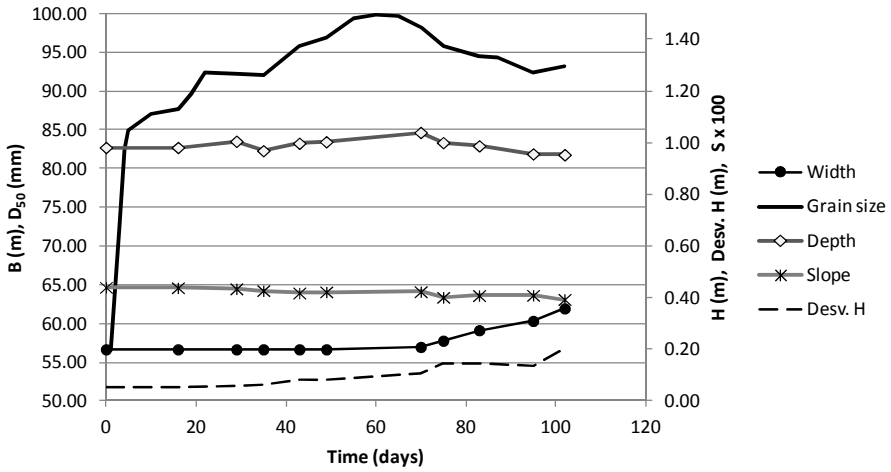

Figure 10.25. Temporal evolution of reach average geomorphologic parameters: width, mean depth, slope, median grain size and the standard deviation in mean depth.

The relation between channel response and spatial scale has already been presented in Section 5.2.3 with regards to Brenta and Piave rivers, in Italy. In these cases, several human interventions (gravel mining, bank protection works, ecc.) impacted on the river equilibrium. The response has been observed mainly in the channel width that reduced almost 49% in Brenta River during the last century. On the contrary, the slope has only changed by an amount of 9%. These observations indicate that while channel width adjusts quickly, the channel slope requires longer temporal spans.

The previous discussion poses the question on the relevant variable that a regime model should treat as dependent and independent. The published hydraulic geometry and that provided by this study is based on field surveys that usually extend along a wave length, i.e., a reach 10^1 channel width long. Therefore, parameters are evaluated at the macro-scale wherein the channel responses adjusting the cross section, and hence width and depth should be used as dependent variables. Slope belongs to a wider scale and requires longer time spans for its adjustment, and then, it represents an independent variable for the reach (marco-scale). Surface grain size has normally been assumed as a dependent variable. In fact, this parameter can adjust very quickly but ones the armour layer has developed, the channel responses by changing the sediment transport rate and its caliber. Table 10.5 summaries qualitatively the results of this discussion.

Table 10.5. Comparison of different spatial and temporal scales in the river system with indication of response style.

Spatial Scale	Length	Morphological time response	Response style
Reach-scale	10^2 widths	10^2 years	Slope reduction
Macro-scale	10^1 widths	10^1 years	Bed form development and channel widening
Micro-scale	10^{-1} – 10^0 widths	10^0 year	Armour layer

A final remark is conceded to the discrepancy in the riffle spacing. The predicted riffle spacing is 132m much lower that the measured value of 444.6m. Furthermore, the predicted value is below the

lowest observation of 4 · B (equal to 256m), as derived from field observations (see Figure 7.20). The hypothesis proposed for explaining this discrepancy states that riffle spacing has a morphological time longer than the simulation period. Figure 10.26 shows the evolution of the bed form as indicated by the lateral asymmetry. By the end of the ninth flood the second half of the channel had developed a well sinusoidal configuration. A downstream migration of the patter is evident, however it is not clear from the figure whether the wave length is increasing or this configuration has attained a stable state. In order to answer this question a part of the reach between progressives 500 m to 1200 m was selected, and a sinusoidal function was fitted:

$$a = A \sin\left(\frac{\pi}{L}x + \alpha\right) \qquad 10.12$$

wherein A is the amplitude, L is the riffle spacing and α is a phase constant. The calibration indicates that L is 135 m after the fifth flood, while it is 145 m, at the end of the 9th flood. Remembering that the initial bar length was 120m, it is clear that riffle spacing is increasing and the riffle-pool morphology is enlarging. It is not surprising this low rate of increase because the riffle development is constrained by the bank erosion process.

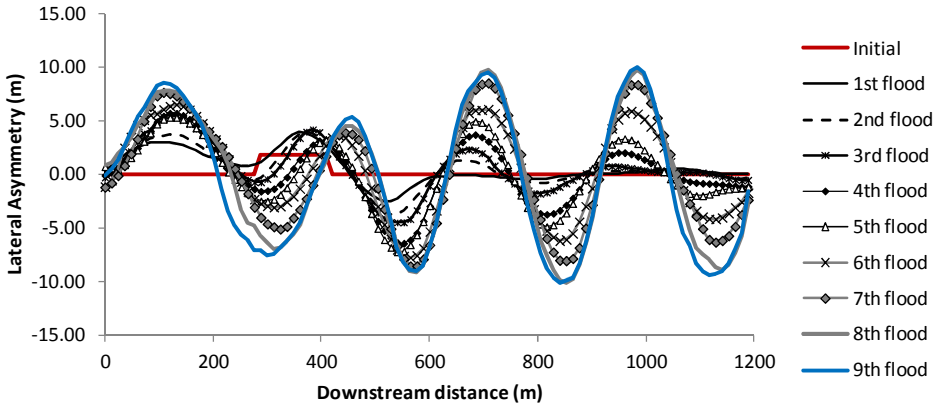

Figure 10.26. Temporal change in the asymmetry spatial variation that illustrates the formation of the riffle-pool morphology.

To sum up, the riffle spacing requires a longer time span than the simulation period, it may depends on the initial perturbation length, and the growth rate is slow because it depends on bank failures, channel widening and bar migration.

10.4 A field case study: the Brenta River.

In the last test, LICAN-LEUFU 2D model was used to predict the morphological change of the Brenta River after the passage of several floods. During the period between August 2010 – April 2011 three intense floods occurred in the Brenta River with the highest peak discharge of 755 m^3/s (RI 9 years, Figure 10.27), i.e., more than twice the bankfull discharge (350 m^3/s). The available data for this test consists on high resolution DTMs of the channel at the beginning and end of the period, the surface and substrate grain size distribution as sampled in the field and the discharges measured at Barzizza gauging station. Sediment transport data was not available. The model simulated a condition of mass

balance (supply equal the reach transport capacity) so as to assess the state of Brenta River and its possible evolution.

Figure 10.27. The Brenta River near Nove Town. Top: view of the study reach from the downstream end during the summer of 2009; note the terrace on the right side of the channel which is 2,50m above the water surface. Bottom: peak discharge of 755 m^3/s (R.I. 9 years) during the flood of November, 2011. Water surface elevation is almost at the terrace level (Photo courtesy, Emanuel Rigon).

10.4.1 Material and methods

Case Study: The Brenta River

The river reach is 1400 m long, the active channel is 73 m wide, has a slope of 0,0056 and a mean depth of 1,42 m but maximum depth at pools is 2,80 m. Bed material (substrate) is composed of a gravel-sand mixture with D_{50} = 20,8 mm and a sand content of 15,1%. The bed is armoured and the surface layer is coarser than substrate material; the representative percentiles are: D_{16} = 16,0 mm, D_{50} = 48,2 mm, D_{84} = 136,5 mm.

Digital terrain model

DTMs were available for two dates: 23/8/2010 and 24/4/2011 (Figure 10.28). The data was produced integrating LiDAR-derived elevations of dry surfaces, water depth of wetted areas derived from aerial photos and a predictive depth-color relationship derived from field DGPS measurements (Moretto et al., 2012). From the data collected through channel field surveys, a regression model was fitted linking depths and the intensity of three color bands. LiDAR and depth points were then merged and interpolated into a DTM. It was estimated an error of ±18 cm in bed elevations.

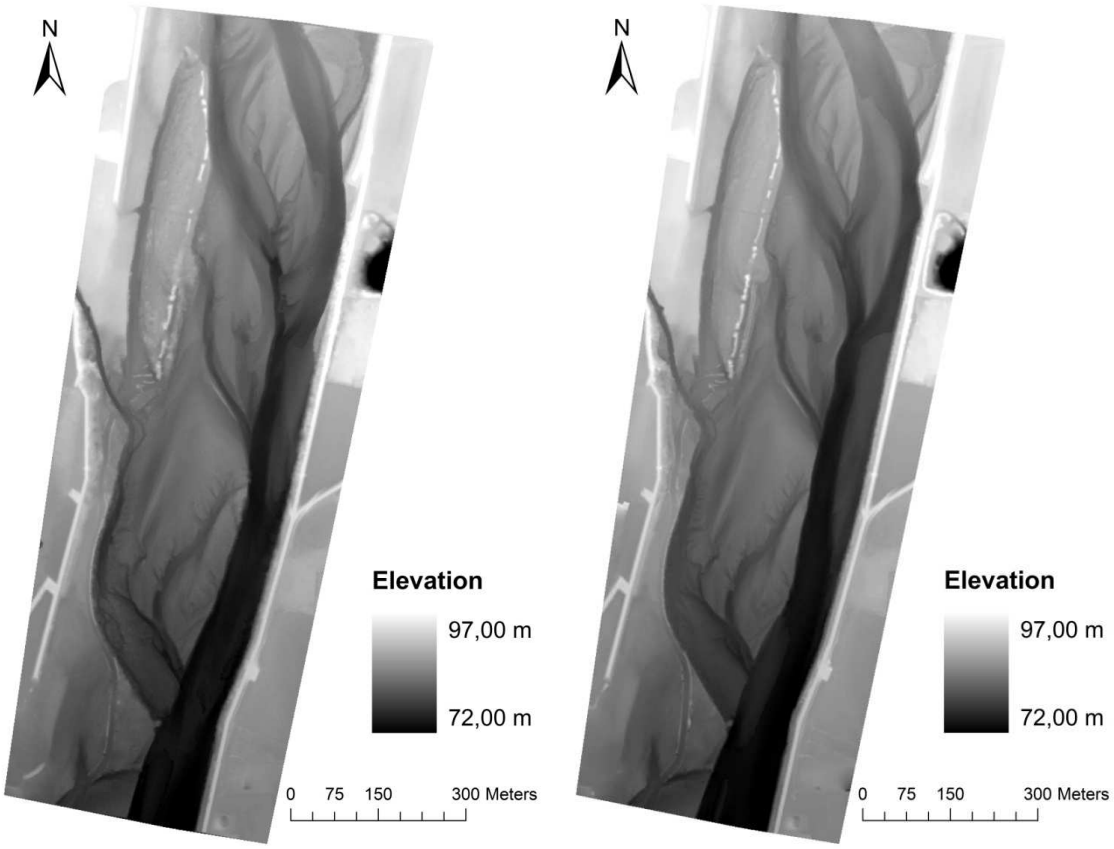

Figure 10.28. Digital terrain models elaborated with a hybrid technique that combines LiDAR data and the chromatic analysis of aerial photos (Moretto et al., 2012).

Grain size distribution

Samples of surface material were taken at 5 cross sections (see Chapter 6). Then grain size distribution at the other cross sections were estimated by interpolation. For this purpose I adopted the Sear's (1996) field observations: the coarser material is found on riffles, there is a gradual reduction up to the downstream next pool and since this point, the material remains fine up to the head of the next riffle. Figure 10.31 shows the spatial variability of surface mediam diameter used as the initial condition for the model.

The first run (Run 1) adopted the spatial variability aforementioned. A second run was simulated using directly a uniform surface material equal to the reach-average material (Run 2).

Sediment supply

There is no information available on the sediment transport rate in the studied reach. Surian and Cisotto (2007) analyzed mass balance in a 20 km long reach of Brenta River and concluded that at the upstream extreme (that includes the studied reach of Nove) the supply may be 0 – 12.200 m^3/year of gravel material (d > 2mm). I adopted a recirculation scheme so as to simulate a condition of mass balance, i.e., the reach can transport all the sediment supplied. Then, considering model results as a reference of equilibrium, the state of the actual River Brenta can be assessed.

Water discharge

The lowest water discharge was selected following a similar methodology explained for the case of Azul River. Table 10.55 shows the reach-average shear stress and competence calculated for different discharges. The minimum discharge was fixed at 150 m^3/s, which can entrain at least 41% of the bed material (considering a reference shear stress of 0,045). The competence is higher than the value assumed for Azul River (30%). It is so because the discharge (150 m^3/s) was the minimum for which the model was able to solve the hydrodynamic equations.

Table 10.55. Comparison of calculated reach-average shear stress and competence for different discharges.

Discharge	Shear Stress (mode)	Maximum percentile moved	
(m3/s)	(Pa)	τ^*_{ref} = 0.045	τ^*_{ref} = 0.057
150	25	41%	33%
200	35	51%	45%
300	55	68%	58%

The data available for the period 23/8/2010 - 24/4/2011 consists on mean daily discharges. The length of the period is 244 days but imposing a minimum discharge of 150 m^3/s it reduces to 35 days. Discharges below this threshold were erased from the original record and hence the sequence is conserved (Figure 10.29).

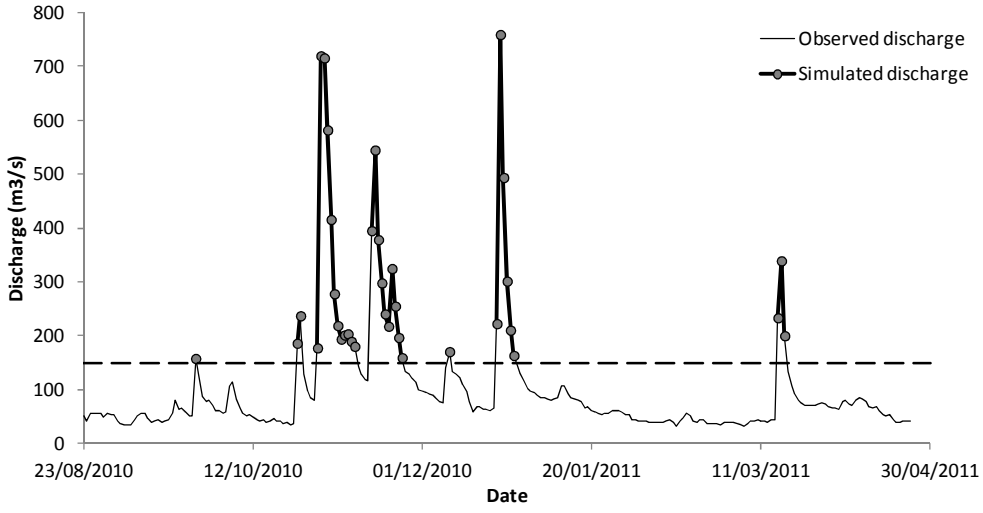

Figure 10.29. Hydrograph measured during the period 23/8/2010 – 24/4/2011 at Barziza gauging station, and used in the calculation assuming a minimum discharge of 150 m^3/s (dashed line). Dots indicate the value of mean daily discharge.

Boundary conditions

Because banks are protected with rip-rap, and to prevent erosion at these places, a high friction angle was selected (e.g. 89°).

Numerical settings.

The domain was divided in 111 cells in the downstream direction and 60 cells across the channel. Cells size varies but on the mean it was 12,60m long and the width was between 2,00 to 4,00 m.

Although a short period of 35 days was simulated, the model was run under the "medium-term" scheme, as explained in the previous chapter. Discharge-tolerance was 10% and tolerance for bed elevation change was set at 5%. At the downstream boundary a minimum bed elevation was imposed (no erosion could take place below this level) and the water surface elevation was fixed at the uniform-flow depth (see section 9.4.2). The minimum water depth was set at 0,25 m for the hydrodynamic model and 0,30 m for the sedimentological routine.

10.4.2 Results

Water surface elevation

According to the photographic documents (Figure 10.27), water surface elevation during the peak discharge of December 2010 did not surpassed the terrace level at the right side of the channel. The hydrodynamic model predicted a water surface elevation of 82,28 m which is below the terrace level of 82,50 m. This indicates that the downstream boundary condition of uniform flow was adequate.

Another verification was possible thanks to the measurement of maximum water surface levels as indicated with post-events signs[26]. At the historical cross section (see cross section 30 in Figure 10.31), the maximum water elevation was near 85,4 m, and the model predicted an elevation of 85,51 m. Therefore, friction losses have been described adequately with the Keulegan's (1938) equation and Kamphius' (1974) parameterization of bed roughness.

Comparison of mass balance

At the reach-scale, a first comparison between predicted and observed channel changes can be assessed by means of the elevation frequencies of the active channel. Elevation has been detrended using a plain that represents the mean surface of the channel bed. At the beginning of the simulation, the mean bottom elevation was -0,35 m bellow the reference plane. At the end of the period it was -0,60 m, indicating that there was a general degradation of the reach. Figure 10.29 shows the frequency of elevations for these moments. A shift of the frequency curve towards lower elevations is evident. On the other hand, the predicted final mean elevation was -0,08 m, indicating a low aggradation in the channel. In the simulation was necessary to add a transition channel upstream which experimented bed degradation, however this part was not considered for the comparison.

Computing solid volumes, i.e., correcting for material porosity, it comes out that the reach lost 59.210 m^3 of material while the variation according to the model was +10.420 m^3.

[26] Emmanuel Rigon (2012) personal communication.

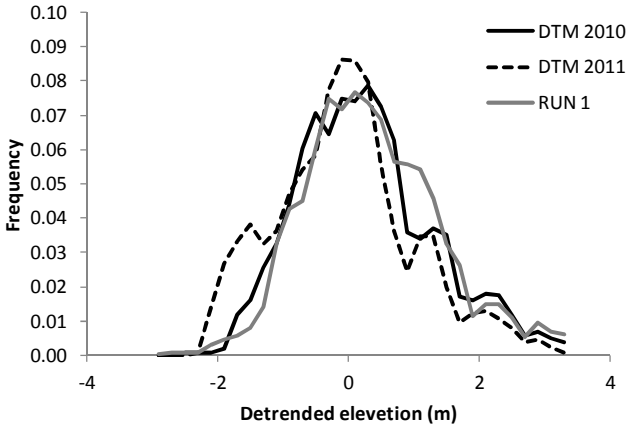

Figure 10.30 Comparison of bed elevation frequencies for the active channel.

A more detailed evaluation requires the comparison at a lower spatial scale. In this case cross sections were analyzed computing the volume difference between final and initial elevations. The difference has been expressed in terms of volumes (Figure 10.31). The net degradation observed in the field and detected in figure 10.30, is now distributed along the channel; sectors with higher and lower volume deficit are detected in Figure 10.31. The predicted variation of volumes relies above the observed one, however both curves exhibit similar patterns. In order to evidence this fact the output of run 1 was adjusted with a constant equal to the difference in predicted and observed total volumes. The dashed line in figure 10.31 shows a good agreement at the first part (cross sections between 15 and 55) and better for the following part of the reach. The figure also shows the result for Run 2. Although Run 2 used a uniform grain size distribution, the final output DTM has almost equal volume variation that Run 1 for which one a spatial variability in surface grain sizes was introduced.

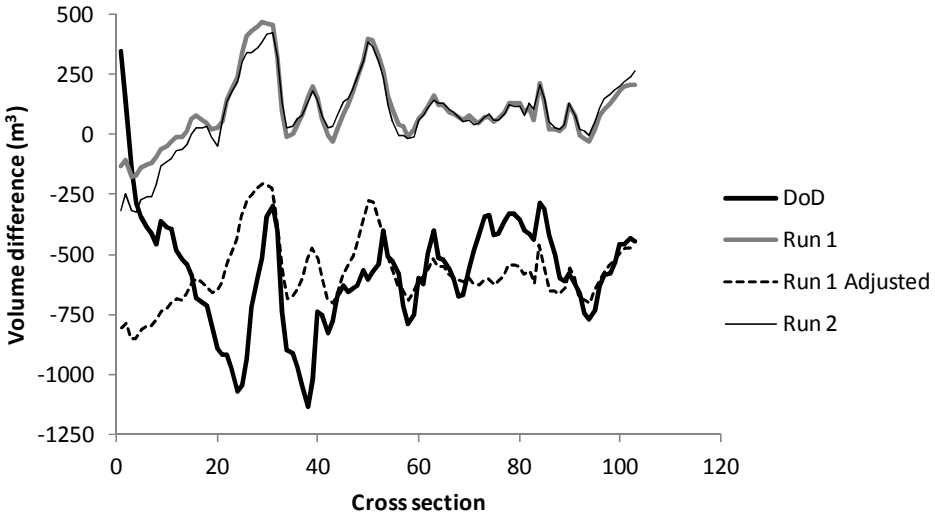

Figure 10.31. Comparison of volume differences at cross sections (see text).

Comparison of spatial patterns

The difference of DTMs (DoD) was calculated with the available DTM of Brenta River (Moretto et al. 2012) and the results of simulation Run 1. At this scale, pattern of deposition/erosion can be compared not only in the streamwise direction but also across the channel (Figure 10.32). The flow in Brenta River was mainly concentrated in the active channel as is indicated by the pattern of erosion/deposition, while all over the lateral floodplain a small deposition took place indicating conditions of low flow. On the contrary, the lateral channel was activated in the simulation and a high erosion process took place at the upstream end.

Due to the passage of these high floods bank erosion occurred along the pool sectors, i.e., the upper left bank (cross section 30) and the subsequent in the right bank (cross section 70). There should have been erosion on the next left side near cross section 90 but at this place bank was protected with rip-rap. Erosion was also important on the right bank between sections 20 and 30 (see also Figure 10.37). This bank was not eroded in the simulation but at the same place erosion was present within the channel. However, it is evident the coincidence at erosion pattern with alternating sides, between observations and simulation.

Although the net mass balance is negative in the Brenta River, the DoD reveals that siltation also occurred within the channel. There was a large supply of material deposited at the upstream end of the reach, with positive mass balance at the beginning of the reach and modest net erosion downstream (see in Figure 10.31 the first 10 cross sections). Furthermore, downstream deposits were also generated immediately downstream the eroded sectors in the same side of the channel (see cross sections 70 and 90 in Figure 10.32). Because sediment was recirculated in the simulation more material was available for bar formation and hence deposition sectors are more frequent in the predicted DoD. Those sectors observed in the field were siltation or low erosion occurred are instead now covered with sediments in the simulation. It is evident between cross sections 50 and 100.

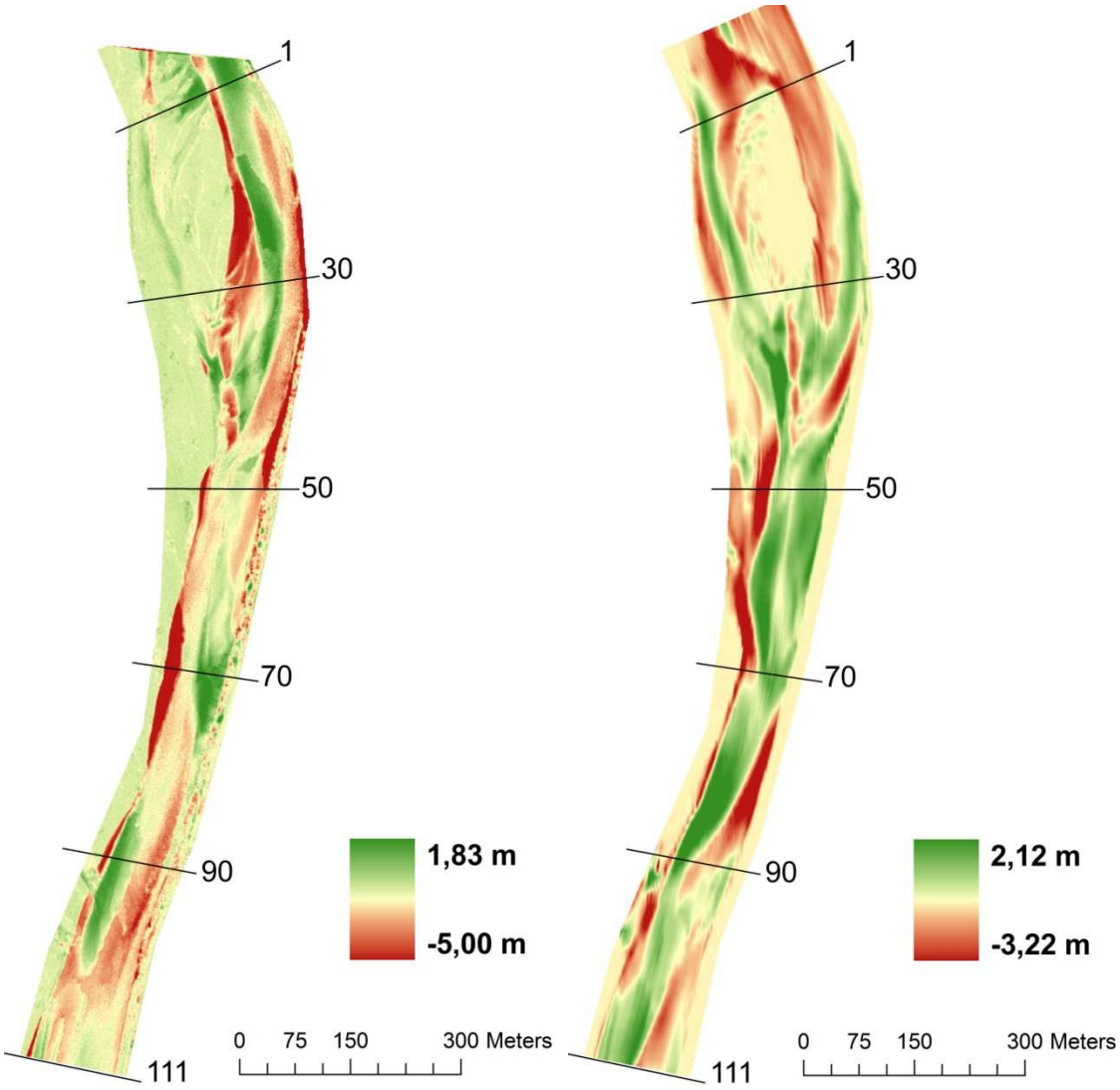

Figure 10.32. Left: comparison of DoD as observed in the field (Moretto et al., 2012); and right: simulated from Run 1.

Sediment transport and surface grain size

Although there are not measurements of surface grain size distribution post events and the output sediment transport, the results obtained with the model are also included. Figure 10.32 shows the spatial variability of surface median diameter as results at the end of runs 1 and 2. Both simulations predicted similar spatial distributions. The initial reach-averaged caliber was 54 mm in the active channel sector, while the predicted final states were both near 80 mm. Then, although there was sediment supply the model predicted a coarsening of the channel bed.

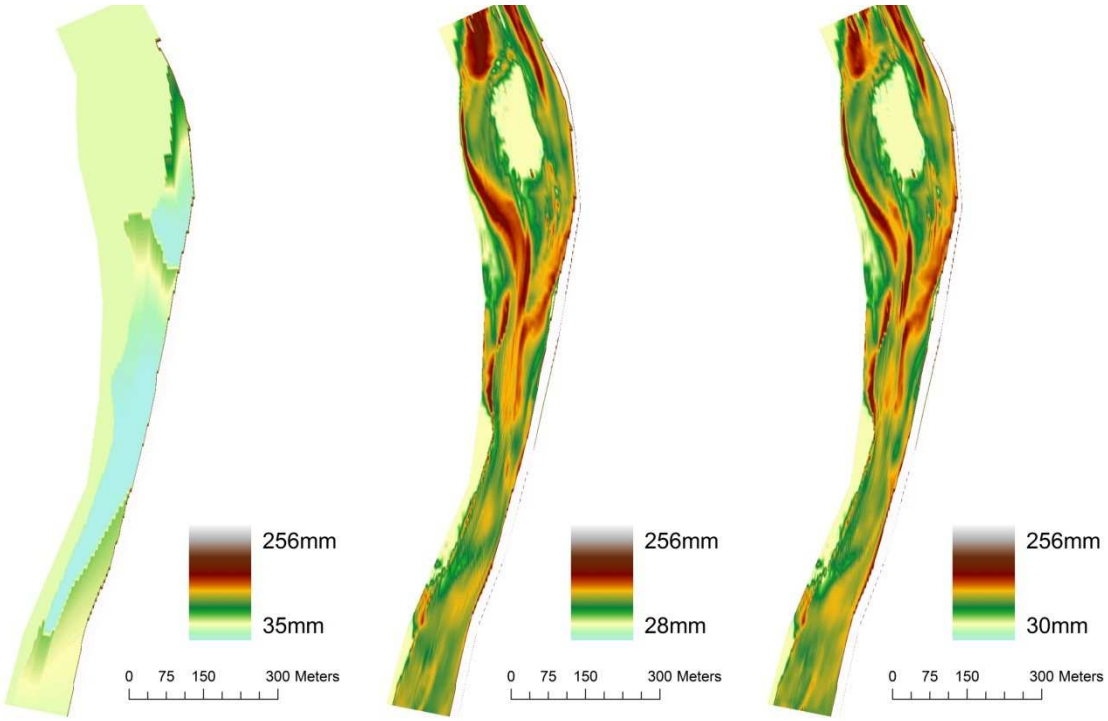

Figure 10.33. Variation in surface median diameter. Right: initial distribution of sizes along the reach used in Run 1; center) final result from Run 1; and left) final result from Run 2.

Coarser sectors are located mostly where erosion occurred, especially in the upper extreme of the reach and the confluence with the lateral channel. In these sectors mediam diameter is as high as 130 mm.

The armouring process is also evident from the comparison of outgoing sediment transport caliber and bed material size (Figure 10.34). For almost all the discharge range, the transported material was finer than the substrate and surface material. Moreover, bedload caliber increased with transport rate reaching a distribution similar to that of substrate with the highest discharge. At low discharges, the median grain size was in the range of fine gravels (6 mm) and it passed to coarse gravels (25 mm) for the peak discharge.

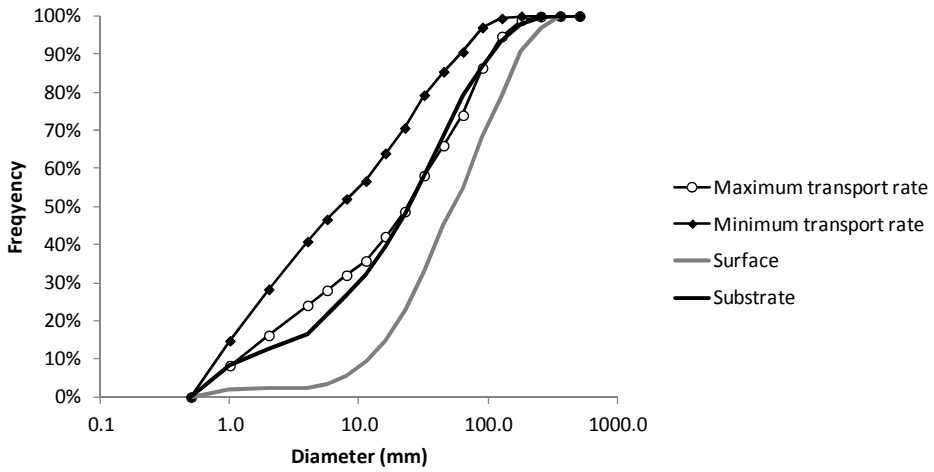

Figure 10.34. Comparison of grain size of transported material and initial bed grain size distribution.

10.4.3 Discussion

How was the performance of the 2D model for predicting locations of erosion and siltation?

The comparison of maximum water surface elevations surveyed after the event with predicted elevations for the peak discharge validated the hydrodynamic model with regards to the choose of uniform flow at the downstream boundary condition and the adopted resistance law. This validation is intended at the reach scale, and it is plain that the correctness of within channel flow patter remains still uncertain.

The simulations was designed for assessing the channel behaviour under condition of mass balance so as to compared the results against current processes in Brenta River and hence to provide indications of the possible future trend. This implied that recirculation was imposed to the system and 57.400 m^3 of material were provided to the reach. Field measurements indicate that it lost 59.200 m^3 (see the following discussion). Although, a low sediment supply (but not zero) may have occurred, the volumes referred are of the same magnitude, and can be concluded that the Wilcock-Crowe (2003) model gave good predictions of bed load transport rates.

Although the simulated reach has an excess of sediment supply with regards to the current reach, a comparison of deposition and erosion areas can still be assessed. Dowsntream cross section 50 (Figure 10.31) there is a good agreement between the predicted location of bank erosion and the observed case. Depositional features are also similar, been placed mostly downstream the eroded banks and on the same side of the channel. Figure 10.35 shows the channel change at cross section 92, a particular interesting location because of the protection works present along the left bank. Degradation occurred in the channel but the toe of both banks were most affected. The model also predicted that erosion would be higher on the sides of the channel, while deposition took place at the center. This agreement is interpreted as a validation of the flow pattern properties (flow direction and shear stress intensity) simulated by the model and the actual flow that changed the shape of Brenta River.

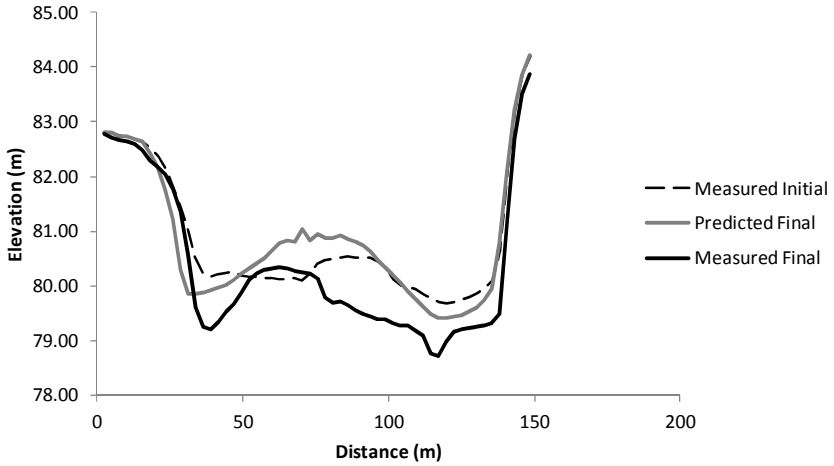

Figure 10.35. Comparison of a cross section with protection works on the right bank (see cross section 92 in Figure 10.32 for location)

On the other hand, upstream cross section 50 comparison is difficult because the secondary channel was activated during the simulation diverting discharge and reducing the flow in the main channel.

This, aside the imposition of a high friction angle for bank stability may be the reason of the lack of bank erosion sectors in the predicted cross section (Figure 10.36).

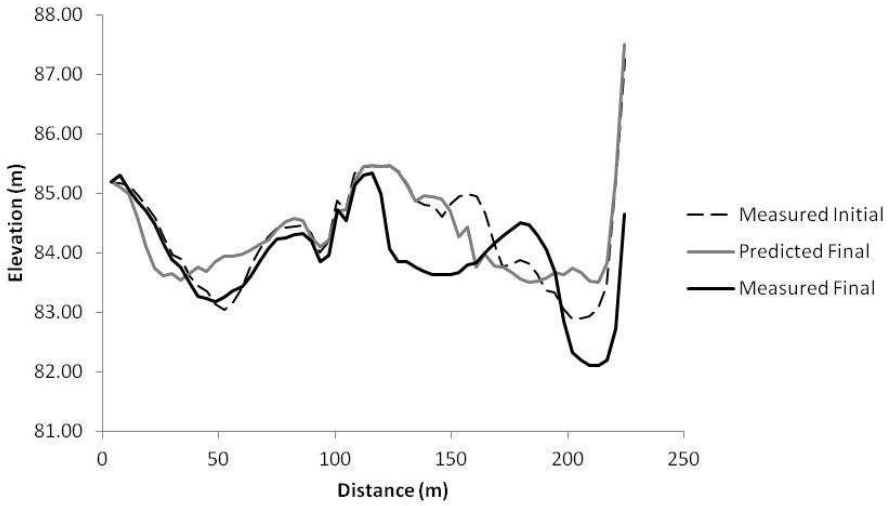

Figure 10.36. Evolution of the historical cross section after the passage of floods in the period 2010-2011. See cross section 30 in Figure 10.31 for location.

Which is the possible evolutionary trend of the Brenta River at the Nove reach?

The Brenta River has been dramatically disturbed by human activities during the last decades (see Chapter 7). Dams built in the upper basin have retained sediments in the catchment, protections works along the banks have limited the local sources of sediments and in-channel gravel mining has produced a deficit in sediment balance. The sediment dynamics in the lower reach of the Brenta River has recently been studied by Surian and Cisotto (2007). These researchers compared cross sections and aerial photographs and calculated sediment transport rates within the channel. As a result, they concluded that transport rate may be 0 – 12.200 m^3/year of gravels in the upstream end of the reach, it attains a highest intensity in the middle of the reach (73.200 – 85.400 m^3/year of gravels) and falls to zero at the downstream end where the river transforms into a sand-bed meandering channel. The reach studied here is located at the upstream part of the 23 km long reach analyzed by Surian and Cisotto (starting near their 2nd cross section and finishing upstream the 3rd cross section).

There are some issues that have to be considered before attending a comparison of results. Firstly, there are spatial scales and data resolution differences between this study and the previous aforementioned that have to be underlined. Surian and Cisotto evaluated sediment transport analyzing changes in 12 cross sections distributed along a reach 23 km long. In this study high resolution DTMs were employed covering a shorter reach 1.400 m long. Secondly, these researchers did not consider the sand content because they assumed it was wash material. Substrate surveys were conducted in this study taking two samples at two lateral bars. The sand content were 11,4% and 18,8%, respectively with a mean of 15,1%. Moreover, sediment transport and bed changes were computed using Wilcock and Crowe (2003) model that included the sand fractions. Finally, the aforementioned input annual bulk of 12.200 m^3 was added by the authors to the budget so as to have positive sediment transport; and they further indicated that at the Barziza gauging station the

total load was estimated in 37.000 m^3/year. Therefore, budgets provided by Surian and Cisotto and will be considered as indication of "order of magnitude" and corrected to incorporate the sand content.

Total sediment volumes (V_{Ts}) are related with gravel volumes (V_{gravel}) by means of:

$$V_{Ts} = \frac{V_{gravel}}{(1 - SF)}$$

wherein SF is the sand content. DoD volumes (V) are also corrected to take into consideration porosity:

$$V_{Ts} = (1 - \lambda) \cdot V$$

Surian and Cisotto reported a sand content of 20,8% and hence their informed volumes were multiplied by 1,263. The bed porosity was estimate using eq. 10.1, and is 0,223, hence volume differences have to be multiplied by the factor 0,777.

The difference in DTMs indicates that the reach lost 59.200 m^3 which is higher than the Surian and Cisotto estimation for the annual transport rate of 15.400 m^3 / 37.000 m^3, or the evaluated annual rate of 31.700 m^3 according to this study (see below). These differences may be attributed to the high intensity of the flood events. There were five events in the period 2010-2011: two of them with nearly bankfull discharges (325 m^3/s and 340m^3/s) and the others three with higher magnitude, 760 m^3/s, 544 m^3/s and 719 m^3/s (been the return intervals equal to 9,5 3,2 and 7,7 years, respectively). The high discharge produced also a high sediment transport rate.

The model was run under conditions of mass balance, i.e., the reach transport capacity was equal to the sediment supply. The comparison of sediment transport capacities done in the preceding discussion validated the model and now its results will be used as a reference of the reach behaviour at equilibrium (in the sense of mass balance and steady state). Figure 10.37 shows the sediment transport rate for different discharges as predicted by the model. It is interesting to note that, according to the model, transport rate increases lowly up to discharges above bankfull, but surpassing a discharge of 420m^3/s, transport rate goes up quickly.

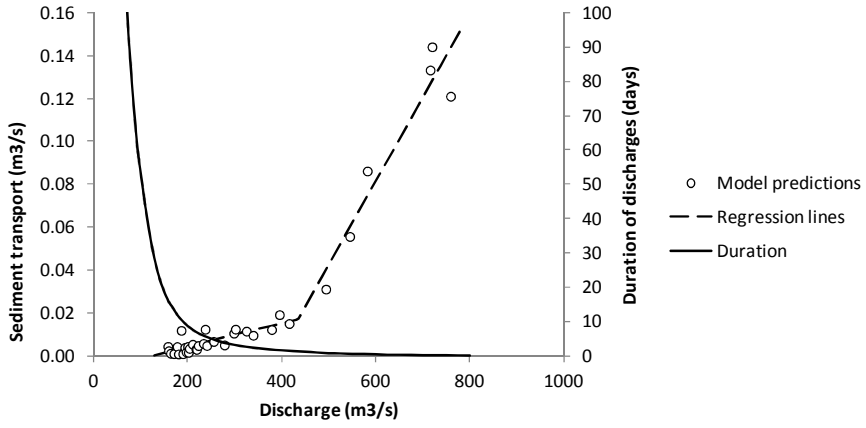

Figure 10.37. Predicted sediment transport rate in the Brenta River for the simulated period. Frequency of discharges was calculated using records from the last 50 years.

The mean annual sediment transport rate was calculated using the duration curve of discharges for the last 50 years. The annual bulk was 31.700 m^3 which is below the transported material for this event 57.400 m^3. This indicates that a mass balance state has not been achieved by the reach yet, and the future evolution of the reach may be characterized by net erosion within the channel and along banks.

Erosion along the active channel may be conditioned by several factors: channel widening, the development of a static armour, or by fixing the boundary conditions at the bridge located near downstream of the reach (located upstream the cross section 3 of Surian and Cisotto, 2007). Figure 10.31 shows that most of the material deficit was due to erosion along the banks of the channel. Computing volumes it turns out that bank erosion furnished 21.750 m3 of material during the floods, which is 38% of the total mass deficit. If protection works should be removed (mainly along the right bank at the downstream part of the reach27) channel widening would promote channel stability by providing material and reducing the transport capacity as shear stress is reduced. A recent research carried on by Rigon et al., (2012) has pointed out the relation between flood magnitude and channel widening, and stressed the role of riparian vegetation. In general, a higher magnitude of flooding corresponds to a higher active channel widening; and reduction of the active channel width is due to the expansion of riparian vegetation establishing in floodplains and islands during periods lacking major disturbance processes.

The development of a static armour is crucial for the channel stability. Laboratory experiments revel that two phases are present during the development of the armour: a first phase of incision and a second phase of coarsening (see section 10.2.4). Furthermore, static amour layers are highly structurated and imbrincated with higher thresholds for entrainment. The Brenta River is highly armoured, with an reach-average absolute armouring index of 2,32 (3.58 at riffles and 1.72 at pools). Considering reach-average values, the surface D_{90} is nearly 181 mm and the maximum diameter (D_{99}) is 335 mm. This surface material is much coarser than the competence of high flows (RI > 9 years) which according to the model is D_{90} = 110 mm and D_{99} = 181 mm. This difference may be and indication that the surface has developed a static armour that is resistant to high floods.

As a conclusion, the response of the channel in the medium-term has to distinguish ordinary events (above bankfull discharge, with Q = 450 m^3/s and R.I. ≈ 2 years) and high floods with recurrence interval above 9 to 10 years. With regards to ordinary events, due to the presence of a well armoured bed and low transport rates (Figure 10.37) not significant or negligible changes are expected to be observed in the channel bed (considering also errors in determination of volume changes that render difficult to discern small changes). On the other hand, high floods are expected to focalized erosion on banks instead on channel bed. Widening is the main process to stabilize the channel owing to the reduction in shear stress and the delivery of sediments into the channel.

[27] It is posible moving two or three houses and building a new levee 100 m to 150 m apart from the current bank position.

Section Four

Conclusions

“Quienes recorran este artículo, deben considerar que no registra sino las conclusiones de Runeber, no su dialéctica y sus pruebas. Alguien observará que la conclusión precedió sin dudas a las “pruebas”. ¿Quién se resigna a buscar pruebas de algo no creído por él o cuya predica no le importa?”

Jorge Luis Borges
Tres versiones de Judas.

“Adieu, dit le renard. Voici mon secret. Il est très simple: on ne voit bien qu`avec le cour. L`essentiel est invisible pour les yeux.”

Antoine de Saint-Exupery
Le Petit Prince

11 CONCLUSIONS AND NEW CHALLENGES

In this research I've worked on an ancient topic in fluvial studies, the problem of explaining and predicting the shape of a river. When analyzing the problems involved in current regime theories I proposed the general assumption that ***physical laws and constrains described the behaviour of a population of river reaches, instead of describing the exact processes within a single river reach***. Furthermore, each object contained in the population ***had uncertain boundaries (width, depth) and uncertain properties (median grain size, slope, bankfull discharge).*** This starting point open the study of rivers at the reach-scale with the analysis of variability in hydraulic geometry parameters, the comparison of disturbed and natural rivers, and the performance of regimen theories. On the other hand, the current extent of regime theories, mainly based on 1D or aggregated models which applied to the reach-scale, indicated that it was time to make a step forward passing to the macro-scale for which a 2D model was required. Then I based the work on the assumption that ***the channel morphology was driven by and was a consequence of active processes; and a 2D-depth-averaged model described best both morphology and processes of the channel***. This chapter presents the conclusions arrived in this study.

11.1 Theoretical aspects on regimen theories

Regime theories were created for the design of stable canals of irrigation by the end of the nineteenth century. It was shown that this context was determinant in the transposition of regime theories into the study of rivers because several points of view were inherited: one single water discharge acting as an external control, geometry of the channel described by a handful of variables (width, depth and slope) which variability was not considered. Furthermore, the concept of scale was not relevant in the context of irrigation canals, but crucial for the stability analysis of gravel bed rivers.

Space-scale was introduced to distinguish levels of organization in the fluvial system. Following Weichert et al. (2009) three levels were recognized: micro-scale; macro-scale and reach-scale. Each level was defined by a characteristic length, but mainly by the response style of the system. Furthermore, specific parameters and ways of modeling were associated with scales. Table 11.1 provides a synthesis of conclusions arrived in the study.

A classification system of regime theories was proposed based on the number of dimensions and the way of modeling. With regards to the number of dimensions three classes were recognized: aggregated models, 1D models and 2D models. Most of previous research has concentrated in aggregated and 1D models that are suitable for predicting the slope, width and depth of the channel, i.e., parameters belonging to the reach-scale. This study has introduced 2D models in the context of regime theories for analyzing the channel evolution at the macro-scale. At this scale, not only the model predicted the parameters at the higher level (reach-scale) but also macro-scale features such as the lateral asymmetry, depth deviation and riffle-spacing.

The classification based on the way of modeling identified processes-based models, constrains based models and those based on behaviours. In previous studies, aggregated models were mostly based

on constrains because bankfull discharge was treated as an independent variable at the reach-scale which the channel is compelled to convey. The stability of the river was formulated in terms of constrains. Behaviour-based models recognized a particular organization principle of the system at the reach scale, this was the case of the so-called extremal hypothesis. In this study, it is concluded that behaviour- and constrain-based model are acceptable for aggregated and 1D schemes that describe river shape at the reach-scale. Macro-scale features require a 2D processes-based models. The concept of space-scale enabled to recognize different levels of organizations within the fluvial system, and at each level different laws describe complex interactions. In this way have been interpreted Millar's (2005) extremal hypothesis-bases model acting at the reach-scale and Parker et al.'s (2007) constrain-based model that proposes an organization at the basin level.

Table 11.1 Summary of relationship of space-scales, levels of organization and description of the fluvial system.

	Space- scale		
	Reach-scale	**Macro-scale**	**Micro-scale**
Length	10^2 widths	10^1 widths	10^{-1} – 10^0 widths
Morphological time response	10^2 years	10^1 years	10^0 year
Response style	Slope reduction	Bed form development and channel widening	Armouring
Geometrical parameters	Slope, width and depth	Lateral asymmetry, depth deviation and riffle spacing	Surface grain size distribution
Independent variables	Bankfull discharge	Slope	Slope, width, depth
Dependent variables	Slope, width, depth	Width, depth, Bankfull discharge	Surface grain size distribution
Regime model	Aggregated and 1D	2D	
	Extremal hypothesis and constrain based	Processes based	

A novel fully processes-based model was proposed for the macro-scale in two dimensions. At this level, bankfull discharge was treated as a dependent variable, and new geometry parameters were used for describing morphological features specific of this scale (see below).

The review of regime theories also analyzed some arguments proposed for giving physical based to extremal hypothesis models. Nanson and Huang (2008) justification based on the least action principle was showed to confuse scales in the fluvial system and to be of no application at the reach-scale.

Field evidence indicates that there is a relationship between sediment supply and bankfull discharge as proposed by the basin organization scheme of Parker et al.'s (2007). However, the model proposed by these researches has a week performance when compared against field data.

11.2 Performance of regimen models

Models that assumed slope as a control (Ikeda et al., 1988; or Millar, 2005, as used in this study) were capable of predicting channel depth and width reasonably well. Best results were obtained by Parker et al.'s (2007) model when used in the original version, however when slope was introduced as an independent variable its performances decreased significantly. The original model proposed by Parker et al. provided good results because it filtered the scatter in slope data with a slope-discharge relation.

The second modified model, that introduced the dependence of reference shear stress with channel slope, showed a systematic error due to the very structure of the model.

11.3 Variability of river reach parameters

Considering a confidence interval of 95%, width varies 27% around the mean value, with a minimum in Piave River at Perarolo (±11%) and the widest range observed in the Mayo River with: -46%, +99%. Depth has a similar confidence interval to the width; it is 30% around the mean value. The lowest variation is found in the Brenta River (-6%, 8%). Conversely, the Mayo River displays again the widest variation in depth (-49%, 91%). The mean range for the confidence interval of the slope is ±16%.

The major source of surface grain size variability comes from the local sorting with fine material in pools and coarse material in riffles. But if the reach-averaged grain size distribution is considered, the confidence interval for the median diameter is ±10% in Italian rivers and ±7% for Patagonian rivers.

The estimation of bankfull discharge is severally conditioned by errors in the identification of bankfull levels and also scatter in the rating curve at gauging stations. The best estimation corresponds to Mayo River for which the extremes of the confidence interval are ±25% around the mean value while the other gauging stations present wider ranges: Chubut River at El Maitén (-76%, 334%) and Alto Chubut River (-60%; 192%).

Variability on hydraulic geometry parameters propagates into dimensionless parameters normally used in regime models. On the mean, dimensionless depth has a relative range of -28% to 40%; dimensionless width has also a similar interval: -26% to 35%, and dimensionless discharge has a wider range: -34%, 45%.

11.4 Comparison between disturbed and natural gravel bed rivers

The comparison of average parameters from natural rivers in Patagonia and disturbed rivers in Italy indicated that floods affecting Italian rivers are more torrential and high discharges have lower durations (flash floods) than in Patagonia. On the contrary, the average frequencies of bankfull discharge (return interval) are identical and also its intensity in terms of shear stress. Furthermore, during half of the year discharges are much lower (almost one-half) in Italian rivers than in Patagonia.

With regards to the morphology, it can be affirmed that the spatial variability of the shape factor is higher in Italian streams because the parameter B/H_{riffle} / B/H_{pool} is higher. Another significant differentiation is found for the surface grain size variability. Rivers in Italy exhibit a wider range of variability, i.e., riffles are much coarser than pools than what is observed in Patagonian rivers.

Vertical sorting is also a factor of difference: the armour layer in Italian streams is much coarser than that in Patagonian rivers.

Both populations have similar riffle spacing, reach average shape factor and bankfull dimensionless shear stress. Therefore, it can be said that Italian and Argentine rivers are similar when observed at the macro-scale, i.e., Italian rivers seem at this scale as stable as the reference natural river set in Argentina.

11.5 Friction losses in gravel bed rivers

The use of reach average hydraulic geometry parameters introduces bias in the determination of friction factor which is overestimated when mean depth and width are used. Instead, good results are obtained when mean velocity is used, i.e., taking the average of A^{-1}.

The roughness height of the studied gravel bed rivers turned out to be $k_s = 2\,D_{90}$, considering bankfull flow conditions. The result supports previous Kamphuis's (1974) observation on laboratory flume and suggests that skin resistance is the main source of energy losses in gravel bed rivers at bankfull discharge.

11.6 Performance of Lican-Leufu processed-based model

With regards to the flume experiment, the overall model performance was very good because: a) the outgoing sediment flux was correctly predicted in terms of transport rate and caliber; b) final mean bed elevation was very similar to that measured; and c) the predicted surface grain size distribution was in agreement with observations. The model was most sensitive to the downstream water surface elevation imposed as a boundary condition. The interaction between hydraulic and bed degradation was the main factor driving sediment transport and full transport prevail in the initial phase of the experiment. By the end of the experiment, partial transport occurred due to bed coarsening, coarse material remained in the flume and fine sediments were winnowed.

The second test consisted on the comparison of model predictions against a field case study: the Azul River. The model predicted very well reach-scale variables such as width and depth of the channel, and in this sense it gave the answer expected from a regime model. With regards to macro-scale parameters, again a good agreement was found for depth (mean and maximum) at riffles and pool cross sections. Asymmetry was somewhat overpredicted at pools and riffle, but measured points fell within predicted variability in the phase-space. The predicted riffle spacing was significant lower than measurements because the simulation period was not long enough.

In the second simulation bankfull discharge was also predicted. It was higher than the observed value but within its confidence interval. Then it gives support to the statement that ***bankfull discharge is a dependent variable at the macro-scale.***

In order to describe the hydraulic geometry variation along the reach the phase-space concept was applied using three variables: lateral asymmetry, depth deviation and streamwise variation in asymmetry. The phase-space portrait represents all the cross section configurations possible and is proposed to be equivalent, at the macro-scale, of the state diagram proposed by Eaton et al. (2004) for the reach scale.

Finally, the application of Lican-Leufu to the Brenta river gave good results in the sense that: a) water surface elevation was correctly predicted; b) total sediment transport was of the same magnitude that the volume lost by the river; and c) there was good agreement of location of areas of erosion and siltation.

On the based of the good results obtained in these three tests it can be sustain that ***the channel morphology was driven by and was a consequence of activing processes; and a 2D-depth-averaged model described best both morphology and processes of the channel***.

11.7 Stability analysis of the Brenta and Piave rivers

The application of a regime model to the Piave River related recent morphological responses to changes in sediment supply: a first reduction phase took place from 1930 to 1960 where sediment supply decreased 40%, and a second phase after a low increase in the 60's, from 1970 to 1990 with a reduction of 42%. The lowest sediment supply was attained in 1991, 24% of sediment supply of the initial situation. After 1990 there was a low recovery reaching 40% by 2006. The braided patter in the Piave River is related to an excess in sediment supply. As a consequence, a reduction in sediment supply may be the cause of the observed change into a single-thread pattern. The fact that the Piave River is actually wider than the predicted width of equilibrium under current sediment supply conditions suggests that the recent observed recovery phase may be a transitional adjustment, after the end of gravel-mining, and that channel may continue narrowing in the future.

With regards to the Brenta River, the application of the model gave a similar interpretation. There was reduction in sediment supply since 1930 up to the end of 20^{th} century, but interrupted in the 60's with a peak in supply. The lowest value was attained in 1990 (between 5% and 12%). After that there was a low recovery been the load in the last surveys (2011) between 13 – 25% of the initial one. Bank strength seemed to have a minor role in explaining width change. The threshold value of meandering-braided transition is closer to the actual mean slope. Sub-reaches with slope above the threshold are expected to remain in a multi-thread configuration even under conditions of sediment supply reduction.

The application of Lican-Leufu model to simulate the Brenta River (reach at Nove) indicates that the response of the channel in the medium-term depends on the intensity of floods. Ordinary events (discharges below 450 m^3/s and R.I. $\approx$ 2 years) will produce not significant or negligible changes within the channel bed. On the other hand, high floods (RI near 9 years) are expected to focalized erosion on banks instead on channel bed. Widening is the main process to stabilize the channel owing to the reduction in shear stress and the delivery of sediments into the channel.

11.8 New challenges

During the work some issues were detected and new questions were encountered. The McCormack's scheme was employed for solving the Reynolds equations in the hydrodynamic model. During the simulation of Azul River the scheme experienced some difficulties for converging and the simulation had to be stopped. Further work is needed to improve this modulus incorporating numerical schemes more robust.

The simulation of Brenta River was done under conditions of unlimited sediment supply so as to assess the “at-equilibrium” response of the reach. A more realistic simulation would consider a sediment supply in the order of 28.700 m^3 of gravel, which is 50% of the recirculated volume. The model can also be used to assess the stability of other reaches of Brenta River located downstream.

Regime theories were used in the analysis of Piave and Brenta rivers for explaining recent morphological changes and to predict possible medium-term trends. The analysis considered the reach-scale (more than 10^2 channel widths long), and hence differential local trends may take place. The future work should consider a smaller partial scale to analyze the response of indivifual sub-reaches.

The last topic concerns the relationship between chaos and order. Macro-scale features have been adequately described by averaged processes such as depth average velocities and sediment transport formulas. Turbulent chaotic behaviour has been considered by means of the standard k-e model, that predicts the influence of turbulence in time-averaged velocities distributions, i.e., turbulence itself is not modeled. Sear (1996) pointed out that vibration may play a key role in rendering more stable riffles than pools. How much micro-scale random processes are important for the macro-scale channel behaviour?

APPENDIX A: SUMMARY TABLES WITH MORPHOLOGICAL, SEDIMETOLOGICAL AND HYDROLOGICAL INFORMATION.

Table A1. Hydraulic geometry of studied river reaches in Argentina and Italy.

Code	Stream	Slope	Conf. Interval		Depth	Conf. Interval		Width	Conf. Interval	
		m/m	2.5%	97.5%	m	2.5%	97.5%	m	2.5%	97.5%
2211	Gualjaina River	**0.0011**	0.0010	0.0011	**1.33**	1.16	1.55	**40.55**	29.46	56.25
2228	Lepà Creek	**0.0027**	0.0022	0.0032	**0.57**	0.36	0.80	**51.15**	31.53	65.40
2206	Chubut River	**0.0022**	0.0018	0.0026	**1.18**	0.90	1.47	**44.60**	36.95	50.55
2204	Carrileufu River	**0.0008**	0.0004	0.0011	**1.81**	1.15	2.46	**59.89**	51.64	73.21
2230	Cohihues Creek	**0.0185**	0.0144	0.0226	**0.28**	0.16	0.45	**10.38**	7.03	13.79
2212	Mayo River	**0.0015**	0.0014	0.0015	**0.77**	0.39	1.47	**61.93**	33.39	123.10
2267	Alto Chubut River	**0.0079**	0.0055	0.0103	**0.88**	0.63	1.06	**51.45**	38.07	57.54
1811	Quemquemtreu River	**0.0113**	0.0100	0.0126	**0.78**	0.67	1.00	**44.29**	33.64	66.63
1817	Azul River	**0.0044**	0.0036	0.0053	**0.86**	0.67	0.97	**64.11**	57.11	80.51
2208	Epuyén River	**0.0053**	0.0041	0.0065	**1.01**	0.66	1.53	**29.58**	20.02	40.38
IT101	Piave River (P)	**0.0054**	0.0051	0.0056	**0.62**	0.38	0.88	**44.60**	39.63	49.54
IT102	Piave River (BL)	**0.0034**	0.0031	0.0037	**0.91**	0.78	1.24	**62.21**	49.46	78.48
IT103	Piave River (S)	**0.0022**	0.0010	0.0034	**1.23**	0.99	1.66	**99.90**	77.45	123.24
IT201	Brenta River	**0.0056**	0.0047	0.0065	**1.42**	1.33	1.53	**73.15**	58.26	78.24
IT301	Cordevole River	**0.0060**	0.0054	0.0066	**0.59**	0.48	0.84	**37.58**	29.17	49.57

Table A2. Hydraulic geometry parameters of studied river reaches.

Code	Wetted Perimeter	Hydraulic Radius	Pool Depth	Riffle Depth	Riffle spacing	Invers. Area
	m	m	m	m	m	m-2
2211	41.38	1.29	2.13	2.05	379.8	0.0196
2228	51.53	0.57	1.57	1.12	353.6	0.0396
2206	45.22	1.16	2.47	1.51	173.7	0.0197
2204	63.30	1.70	2.33	2.11	630.6	0.0098
2230	10.49	0.28	0.52	0.41	70.0	0.4079
2212	62.28	0.76	2.07	1.31	316.1	0.0254
2267	51.74	0.87	1.66	1.19	210.4	0.0235
1811	44.95	0.77	1.74	1.38	166.6	0.0317
1817	64.67	0.85	1.67	1.30	444.6	0.0186
2208	30.04	0.99	2.00	1.30	203.8	0.0378
IT101	45.15	0.61	1.46	1.22	277.7	0.0402
IT102	62.76	0.90	1.77	1.13	514.9	0.0186
IT103	100.91	1.21	2.50	1.58	599.7	0.0086
IT201	73.91	1.40	2.78	2.52	338.6	0.0098
IT301	37.87	0.59	1.24	1.10	200.4	0.0486

Table A3. Hydrological parameters of studied reaches.

Code	Bankfull discharge	Conf.Interval		Return period	Duration	Mean Annual discharge	Median discharge	Maximum discharge	Minimum discharge	Torrential Index
	(m3/s)	(2,5%)	(97,5%)	(years)	(days)	(m3/s)	(m3/s)	(95%)	(5%)	
2211	**49.8**	62.7	37.2	1.3	13.3	14.94	8.45	44.34	1.87	1.06
2228	**25.6**	35.0	18.3	2.0	12.8	6.03	2.97	22.54	0.00	1.07
2206	**78.4**	340.0	18.6	1.3	5.3	19.75	15.11	50.48	3.72	1.08
2204	**129.2**	154.3	107.6	1.2	11.3	49.11	40.34	105.93	17.01	1.05
2230	**4.2**	N/D	N/D	2.4	2.5	1.20	1.03	2.58	0.39	1.10
2212	**41.7**	51.2	31.9	1.3	12.5	8.17	3.15	34.35	0.06	1.09
2267	**19.5**	56.8	7.7	1.2	16.2	7.97	7.32	18.86	0.97	1.07
1811	**49.8**	92.0	22.4	2.4	1.3	9.37	7.95	20.85	2.61	1.05
1817	**77.1**	102.6	56.1	1.1	10.3	24.00	19.19	58.21	4.72	1.13
2208	**45.5**	60.4	34.7	1.6	6.3	15.01	13.24	32.67	4.22	1.06
IT101	**57.0**	N/D	N/D	1.3	5.9	8.13	4.65	25.94	1.81	1.71
IT102	**100.0**	N/D	N/D	1.3	7.2	18.58	11.89	46.83	6.10	1.49
IT103	**220.4**	N/D	N/D	1.3	3.5	29.68	20.17	78.97	10.74	1.60
IT201	**298.0**	N/D	N/D	1.3	3.5	66.89	47.54	167.26	22.22	1.24
IT301	**83.0**	N/D	N/D	1.3	4.3	7.22	3.23	21.72	0.45	1.77

Table A4. Sedimentological parameters of studied reaches.

	Surface material									Subsurface material		Armouring	
Code	D_{50}	Confidence interval		D_{84}	D_{90}	sg	$\frac{D_{90}}{D_{50}}$	D_{50} Riffle	D_{50} Pool	D_{50ss}	Sand	$\frac{D_{50}}{D_{50ss}}$	q*
	(mm)	2,5%	97,5%	(mm)	(mm)			(mm)	(mm)	(mm)	Fraction		
2211	19.5	18.4	20.7	38.4	44.8	2.47	2.3	24.3	19.2	14.6	17.2%	1.34	0.52
2228	26.9	25.3	28.6	52.0	59.3	2.54	2.2	32.6	19.7	14.0	13.0%	1.91	0.13
2206	28.8	26.8	31.3	65.3	81.1	3.30	2.8	32.3	27.2	17.4	15.2%	1.66	0.55
2204	36.0	33.7	38.4	68.4	81.0	1.88	2.3	34.6	37.4	12.9	28.8%	2.79	0.00
2230	52.1	49.0	55.5	103.5	122.4	2.23	2.3	55.8	47.2	30.2	13.7%	1.72	0.76
2212	27.0	25.1	28.9	56.7	64.0	2.64	2.4	34.2	18.8	10.2	30.2%	2.66	0.00
2267	93.4	78.0	118.6	299.8	367.4	2.76	3.9	104.1	85.4	N/D	N/D	N/D	N/D
1811	60.1	56.3	64.8	124.3	148.0	2.00	2.5	68.8	54.1	52.7	14.7%	1.14	0.91
1817	67.3	61.3	73.7	166.8	204.0	2.94	3.0	83.1	51.0	38.8	14.3%	1.74	0.13
2208	43.7	39.8	48.9	106.5	124.6	2.52	2.9	64.2	32.7	25.4	15.2%	1.72	0.69
IT101	50.3	46.3	54.2	115.2	139.4	2.39	2.8	72.8	31.3	22.3	16.6%	2.26	0.23
IT102	42.7	40.2	45.6	92.8	112.2	2.26	2.6	53.8	43.8	15.0	20.3%	2.84	0.79
IT103	35.6	31.9	39.5	89.4	110.5	2.19	3.1	54.2	24.3	16.1	14.3%	2.22	0.34
IT201	48.2	43.2	54.1	136.5	166.8	3.03	3.5	74.5	35.8	20.8	15.1%	2.32	0.72
IT301	49.1	43.9	54.9	126.5	156.8	2.92	3.2	59.2	33.4	24.8	17.8%	1.98	0.34

APPENDIX B: PICTURES OF STUDIED RIVER REACHES

Figure B1. Quemquemtreu River (Argentina).View from the right bank towards upstream.

Figure B2. Azul River (Argentina). View from right bank towards downstream.

Figure B3. Carrileufu River (Argentina). View of the river towards upstream.

Figure B4. Chubut River near El Maitén Town (Argentina). View from the right bank towards upstream.

Figure B5. Epuyen River near the gauging station at “La Angostura” (Argentina). View from the channel center towards upstream.

Figure B6. Gualjaina River (Argentina), looking downstream from the bridge at Provincial Route Nº 12.

Figure B7. Mayo River near the gauging station at Paso Rio Mayo town (Patagonia). View from the center of the channel towards downstream.

Figure B8. Lepá Creek at the cross section of the gauging station (Gualjaina Town, Argentina).

Figure B9. Cohihues Creek at the entrance of Los Alerces National Park (Argentina). View from the right bank towards upstream.

Figure B10. Alto Chubut River (Argentina) near the gauging station, looking towards upstream.

Figure B11. Brenta River near Cartigliano Town and downstream the gauging station at Bassano del Grappa (Italy). View from the left bank looking upstream.

Figure B12. Cordevole River near Peron Town (Italy), upstream the gauging station at Ponte Mas. View from the left bank towards upstream.

Figure B13. Piave River at Belluno (Italy). The study stream is downstream near the gauging station. View from the center of the channel looking upstream.

Figure B14. Piave River at Ospitale di Cadore Town (Italy). The study reach is downstream the gauging station placed at Perarolo di Cadore Town. View looking upstream.

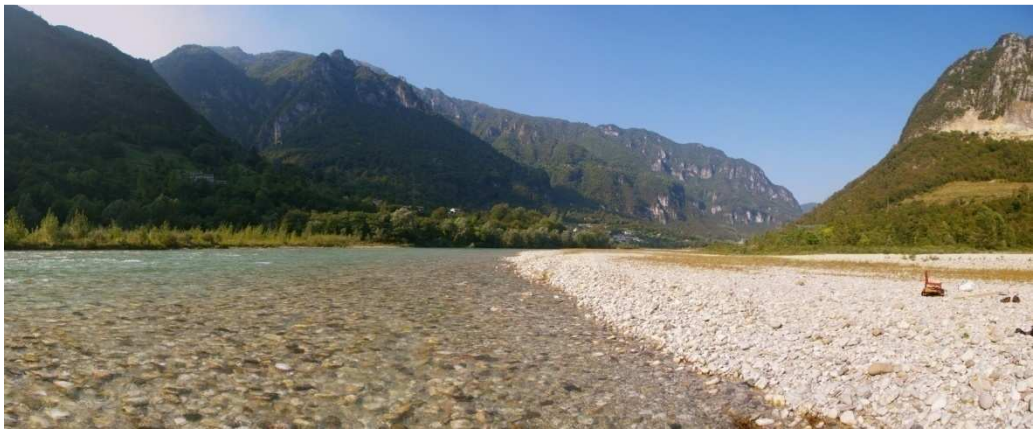

Figure B15. Piave River at Santa Maria Town (Italy), upstream the gauging station at Segusino Town. View from left bank towards upstream.

BIBLIOGRAPHIC REFERENCES

Abad, J. D., Buscaglia G. C., and Garcial M. H. (2008), 2D stream hydrodynamic, sediment transport and bed morphology model for engineering applications. Hydrological Processes, 22, 1443-1459.

Abril, J. B. (1995), Numerical Modelling of Turbulent Flow in Compound Channels by the Finite Element Method. Hydra 2000, Proceedings of the 26th Congress of the International Association for Hydraulic Research, A. Ervine and T. Telford (Eds), London, U.K., Vol. 5, 1–6.

Abril, J. B., and Knight W. D. (2004), Stage-discharge prediction for rivers in flood applying a depth-averaged model, Journal of Hydraulic Research, 42(6), 616–629.

Ackers, P. and White W. R. (1973), Sediment transport: a new approach and analysis, Journal of Hydraulic Engineering, 99(11), 2041-2060.

Afzalimehr, H. and Anctil, F. (1998), Estimation of gravel-bed river flow resistance, Journal of Hydraulic Engineering, 124(10), 1054-1058.

Andrews, E. D. (1980), Effective and bankfull discharges of streams in the Yampa River basin, Colorado and Wyoming. Journal of Hydrology, 46, 311-330.

Andrews, E. D. (1983), Entrainment of gravel from naturally sorted riverbed material, Geol. Soc. Am. Bull., 94, 1225– 1231.

Andrews, E. D. (1984), Bed material entrainment and hydraulic geometry of gravel-bed rivers in Colorado, Geol. Soc. Am. Bull., 95, 371– 378.

Andrews, E.D. and Erman D.C. (1986), Persistence in the size distribution of surficial bed material during an extreme snowmelt flood, Water Resources Research 22: 191–197.

ASCE Task Committee on hydraulics, banks mechanics, and modeling of river adjustment (1998), River width adjustment (I-II), Journal of Hydraulic Engineering, 124(9) 881-917.

ASCE Task Committee on turbulence Models in Hydraulics Computation, (1988) Turbulence modelling of surface water flow and transport. Parts I-IV, Journal of Hydraulic Engineering, 114(9), 970-1073.

Bagnold, R. A. (1956), The flow of cohesionless grains in fluids. Philosophical Transactions Royal Society of London, A 249, 235-297.

Bagnold, R. A. (1980), An empirical correlation of bedload transport rates in flumes and natural rivers, Proc. R. Soc. Longon, Ser. A, 405, 369-374.

Barnes, H. H. Jr (1967), Roughness characteristics of natural channels, Geological Survery Water-Supply Paper 1849, Washington, 219p.

Barry, J. J., Buffington, J. M. and King, J. G. (2004), A general power equation for predicting bed load transport rates in gravel bed rivers. Water Resources Research, 40, Doi:10.1029/2004WR003190.

Barry, J. J., Buffington, J. M, and King, J. G. (2007), Correction to “A general power equation for predicting bed load transport rates in gravel bed rivers”. Water Resources Research, 43, Doi:10.1029/2007WR006103.

Basile, P. A. (2005), Dinámica del flujo de fluidos viscosos incompresibles, Centro Universitario Rosario de Investigaciones Hidro Ambientales, ICD 0305, Argentina, 43pp.

Bathurst, J.C. (2002), At-a-site variation and minimum flow resistance for mountain rivers. Journal of Hydrology, 269, 11-26.

Bathurst, J. C. (2007), Effect of coarse surface layer on bed-load transport, Journal of Hydraulic Engineering, 133(119. Doi: 10.1061/(ASCE)0733-9429(2007)133:11(1192)

Bernard, R. S. (1993), Numerical model for depth-averaged incompressible flow. US Army Corp of Engineers, Waterways Experimental Station, Technical Report REMR-HY-11.

Boussinesq, J. (1877), Essai sur la théorie des eaux courantes. Memoires Academie Sciences-Institut de France, 24.

Bradford, S. F., and B. F. Sander (2002) Finite-volume model for shallow-water flooding of arbitrary topography. Journal of Hydraulic Engineering, 128(3), 289-298.

Bravo-Espinosa, M., Osterkamp, W- R- and Lopes V. L. (2003), Bedload transport in alluvial channels, Journal of Hydraulic Engineering, 129(10), 783-795.

Bray, D. I. (1979), Estimating average velocity in gravel-bed rivers. Journal of Hydraulic Division ASCE, 105(9), 1103-1122.

Bray, D. I. (1982), Regime relations for gravel-bed rivers, in Gravel-Bed Rivers, edited by R. D. Hey, J. C. Bathurst, and C. R. Thorne, pp. 517–542, John Wiley, Chichester, U. K.

Brebner A, and Wilson K.C. (1967). Derivation of the regime equations from relationships for pressurized flow by use of the principle of minimum energy – degradation rate. ICE Proceedings, 36(1) : 47-62.

Buffington, J. M. (1995). Effects of hydraulic roughness and sediment supply on surface textures of gravel-bedded rivers [thesis]: Seatle, University of Washington, 184 p.

Bunte, K. and Abt S. (2001), Sampling surface and subsurface particle-size distributions in wadable gavel-and cobble-bed streams for analyses in sediment transport, hydraulics, and streambed monitoring. Gen. Tech. Rep. RMRS-GTS-74. Fort Collins. U.S. Department of Agriculture, Forest Service, Rocky Mountain Research Station. 428 p.

Cao S. and Knight D.W. (1998) Desing for hydraulic geometry of alluvial channels, Journal of Hydraulic Engineering, 124 (5), 484-492.

Cao, S. and D. W. Knight (1997), Entropy-based design approach of threshold alluvial channels. Journal of Hydraulic Research, 35(4), 1-21.

Cao, S. and Knight D. W., (1998), Design for hydraulic geometry of alluvial channels, Journal of Hydraulic Engineering, 124(5), 484-492.

Cencini, M., Cecconi, F. and Vuppiani, A. (2010) Chaos, from simple models to complex systems. Series on Advances in Statistical Mechanics – Vol. 17. World Scientific, 460p.

Cereijido, M. (2009). Elogio del desequilibrio, en busca del orden y el desorden en la vida. Colección Ciencia que ladra. Siglo veintiuno Editores, Argentina.

Chang H.H. (1980). Geometry of gravel streams. Journal of the Hydraulics Division, ASCE 106 : 1443-1456.

Charlton, F. G., Brown, P. M. and Benson, R. W. (1978) The hydraulic geometry of some gravel rivers in Britain. Hydraulic Research Station Report IT 180.

Chen, L. and Stone, M. C. (2008) Influence of bed material size heterogeneity on bedload transport uncertainty. Water Resources Research, 44, W01405, doi:10.1029/2006WR005483.

Chew LC, Ashmore PE. (2001) Channel adjustment and a test of rational regime theory in a proglacial braided stream. Geomorphology 37: 43-63.

Chow, V. T. (1994), Hidráulica de canales abiertos, McGraw Hill, Colombia, 337p.

Chow, V. T., D. R. Maidment and L. W. Mays (1994), Hidrología Aplicada. McGraw Hill, Colombia. 584 pp.

Church M., (2006), Bed material transport and the morphology of alluvial river channels, The Annual Review of Earth and Planetary Science, 34, 325-54.

Church, M. and D. Jones (1982), Channel bars in gravel-bed rivers. In: Gravel-bed Rivers. Fluvial Processes, Engineering and Management. R.D. Hey, J.C. Bathurst and C.R.Thorne (Eds), Chichester, United Kingdom, John Wiley and Sons, 291-338.

Church, M., M. A. Hassan and J. F. Wolcott (1998), Stabilizing self-organized structures in gravel-bed stream channels: field and experimental observations, Water Resources Research, 34(11), 3169-3179.

Church, M., M.A. Hassan and J.F. Wolcott (1998). Stabilizing self-organized structures in gravel-bed stream channels: Field and experimental observations. Water Resources Research 34(11): 3169–3179.

Clayton, J. A. and J. Pitlick (2007), Persistence of the surface texture of a gravel-bed river during a large flood. Earth Surface Processes and Landforms, 33, 661-673. Doi: 10.1002/esp.1567

Clifford, N. J. and J. R. French (1993), Monitoring and modelling turbulent flows: historical and contemporary perspectives, In: Turbulence, perspective on flow and sediment transport, N.J. Clifford, J. R. French and J. Hardisty (Eds), Chichester, U.K., John Wiley and Sons, 1-34.

Colosino, C., V. A. Copertino and M. Veltri (1988), Friction factor evaluation in gravel-bed rivers, Journal of Hydraulic Engineering, 14(8), 861-876.

Comiti F., M. Da Canal, N. Surian, L. Mao, L. Picco, and M. A. Lenzi (2011), Channel adjustments and vegetation cover dynamics in a large gravel bed river over the last 200 years, Geomorphology, doi: 10.1016/j.geomorph.2010.09.011

Coulthard, T. J. and Van De Wiel, M. J. (2006). A cellular model of river meandering. Earth Surface Processes and Landforms, 31, 123-132.

Coulthard, T.J., Kirkby, M.J. and Macklin, M.G. (1997). Modeling hydraulic, sediment transport and slope processes, at a catchment scale, using a cellular automaton approach. Proceedings of GeoComputation ’97 & SIRC ’97, 15-24.

Coulthard, T.J., Lewin, J. and Macklin, M.G. (2005). Modeling differential catchment response to environmental change. Geomorphology, 69, 222-241.

Da Canal, M (2011) Analisi della dinamica passata ed attuale del fiume Piave nel Vallone Bellunese finalizzata ad una gestione integrata del suo corridoio fluviale. PhD Thesis, Università degli studi di Padova.

Da Canal, M. (2006). Studio delle variazioni morfologiche del Fiume Piave nel Vallone Bellunese durante gli ultimi duecento anni. Università degli Studi di Padova.

D'Agostino, V. And Lenzi, M. A. (1999). Bedload transport in the instrumented catchment of the Rio Cordon, Part II: Analysis of bedload rate. Catena, 36, 191-204.

Davies T.R.H., and Sutherland AJ. (1983) Extremal hypotheses for river behavior. Water Resources Research 19(1) : 141-148.

Davis, W. M. (1899). Topograhical development of the Triassic formation of the Connecticut Valley. Am. J. Sci., 37: 423-434.

Davis, W. M. (1902). Base-level, grade, and peneplain. Journal of Geology, Vol. 10, 77-111.

Dietrich, W.E., J. W. Kirchner, H. Ikeda and F. Iseya (1989), Sediment supply and the development of the coarse surface layer in gravel–bedded rivers, Nature, 340, 215–217.

Diplas, P. (1990), Characteristics of self-formed straight channels, Journal of Hydraulic Engineering, 116(5), 707-728.

Diplas, P. and G. Vigilar (1992), Hydraulic geometry of threshold channels. Journal of Hydraulic Engineering, 118(4), 597-614.

Duan J. G. and Julien, P. Y. (2005). Numerical simulation of the inception of channel meandering. Earth Surface Processes and Landforms, 30, 1093-1110.

Eaton, B. C. and M. Church (2004), A graded stream response relation for bedload dominated streams. Journal of Geophysical Research – Earth Surface 109(F03011). Doi: 10.1029/2003JF000062.

Eaton B.C., Church M, and Millar R.G. (2004). Rational regime model of alluvial channel morphology and response. Earth Surface Processes and Landforms 29 : 511-529. DOI: 10.1002/esp.1062.

Eaton B.C., Church M, and Davis TRH. (2006). A conceptual model for meander initiation in bedload dominant streams. Earth Surfaces Processes and Landforms 31 : 875-891.

Efron, B. (1979). Bootstrap Methods: Another Look at the Jackknife. The Annals of Statistics 7 (1): 1–26. doi:10.1214/aos/1176344552.

Einstein, H. A. (1950), The bed-load function for sediment transportation in open channel flows, Tech. Bull. 1026, Soil Conserv. Serv., U.S. Dep. Of the Army, Washington, D. C.

Einstein, H. a. and Shen, S. W. (1964). A study of meandering in straight alluvial channels. Journal of Geophysics Research, 69, 5239-5247.

Emment, W. M. and M. G. Wolman (2001), Effective discharge and gravel-bed rivers. Earth Surface Processes and Landforms 26, 1369-1380.

Fergunson, R.I. (1986) Hydraulics and hydraulic geometry. Progress in Physical Geography 10, 1-31.

Fergunson, R.I. (2008). Gravel-bed rivers at the reach scale. In Gravel-bed rivers VI: from processes understanding to river restoration, J.F. Shroder Jr (Ed.), Elsevier, 817p.

Feynmann R. P., Leighton, R. B., and Sand M. (1964), The Feynman lectures on physics: Mainly electromagnetism and matter (Vol. 2). Addison-Wesley.

Flintham, T.P., and Carling P.A. (1988), The prediction of mean bed and wall boundary shear in uniform and compositely roughened channels. In: White, W.P. (Ed.), International Conference on River Regime. John Wiley and Sons, Chichester, England, pp. 267–287.

Garcia, M. H. (2008). Chapter 1: Sediment transport and morphodynamics, In: Sedimentation Engineering, ASCE Manuals and reports on Engineering Practice no. 110, M. H. Garcia (Ed), ASCE, 21-165.

Garcia-Martinez, R., Espinoza R., Valera E., and Gonzalez G. (2005), An explicit two-dimensional finite element model to simulate short- and long-term bed evolution in alluvial rivers. Journal of Hydraulic Research, 44(6), 755-766.

Garret, P. W. and Wolman M. G. (1984) Downstream effects of dams on alluvial rivers. Geological Survey Profressional Paper 1296, pp. 83.

Gomez, B. and Church M. (1989), An assessment of bed load sediment transport formulae for gravel bed rivers, Water Resources Research 25, 1161– 1186.

Habersack, H. M. and Laronne J. B. (2002), Evolution and improvement of bed load discharge formulas on Helley-Smith sampling in an Alpine gravel bed river. Journal of Hydraulic Engineering, 128(5), 484-499.

Hassan, M.A., Egozi R. and Parker G. (2006). Experiments on the effect of hydrograph characteristics on vertical grain sorting in gravel bed rivers. Water Resources Research 42: W09408. DOI: 10.1029/2005WR004707

Hey R.D., and Thorne C.R. (1986). Stable channels with mobile gravel beds, Journal of Hydraulics Engineering 112(8) : 671-689.

Hey, R. D., (1988), Bar form resistance in gravel-bed rivers, Journal of Hydraulic Engineering, 114(12), 1498-1508.

Hirano, M. (1971). River bed degradation with armouring. Proceedings of the Japan Society of Civil Engineering, 195, 55-65.

Hoey, T. B. and Ferguson R. I. (1994), Numerical simulation of downstream fining by selective transport in gravel bed rivers: Model development and illustration, Water Resources Research, 30, 2251-2260.

Hoffman, J. D. (2001) Numerical methods for engineers and scientists.Marcel Dekker Inc, New York, 825pp.

Huang, H.Q. and Nanson A. (2002) A stability criterion inherent in laws governing alluvial channel flow. Earth Surface Processes and Landforms, 2002, 27, 929-944.

Hunziker, R. and Jaeggi M. N. R. (2002), Grain sorting processes, Journal of Hydraulic Engineering, 128(12), 1060-1068.

Ikeda, S. (1981), Self-formed straight channels in sandy beds, Journal of Hydraulic Engineering, 107, 389-406.

Ikeda, S. and Izumi N. (1990), Width and depth of self-formed straight gravel rivers with bank vegetation, Water Resources Research, 26(10), 2353-2364.

Ikeda, S., Parker G. and Kimura Y. (1988), Stable width and depth of straight gravel rivers with heterogeneous bank materials, Water Resources Research, 24, 713-722.

Jaeggi, M. (1984), Abflussberechnung in kiesfuehrenden fluessen. Wasserwirtschaft, Friedrich Vieweg, Wiesbaden, Germany, 24(5), 263–267.

Jang C-L. and Shimizu Y. (2005), Numerical simulation of relative wide, shallow channels with erodible banks, Journal of Hydraulic Engineering, 131(7), 565-575.

Jia, Y. and Wang, S.S.Y. (1999). Numerical model for channel flow and morphological change studies. Journal of Hydraulic Engineering, 125(9), 924-933.

Johansen, H. and Parker G. (1989), Linear theory of river meanders. In S. Ikeda and G. Parker (Eds.) River Meandering. AGU Water Resources Monograph 12, 181-213.

Julien, P. Y. and Wargadalam J. (1995), Alluvial channel geometry: theory and applications. Journal of Hydraulic Engineering, 121(4), 312-325.

Kamphuis, J. W. (1974), Determination of sand roughness for fixed beds. Journal of Hydraulic Research, 12(2), 193–203.

Kapitza, H and Eppel D. (1987), A 3-D Poisson solver based on conjugate gradients compared to standard iterative methods and is performance on vector computers. Journal of Computational Physics, 68, 474-484.

Keller, E. A. and Melhorn W. N. (1973), Bedforms and fluvial processes in alluvial stream channels: selected observations, in M. Morisawa (Ed.) Fluvial geomorphology: SUNY-Binghamton, N.Y., Proc. Fourth Annual Geomorphology Symposium, Pub. Geomorphology, p 253-283.

Kellerhals, R. (1967), Stable channels with paved gravel beds. J. Waterw. Harb. Div., ASCE 93 (1), 63–83.

Kellerhals, R., Neill C. R. and Bray D. I. (1972), Hydraulic and geomorphic characteristics of rivers in Alberta, River Engineering and Surface Hydrology Report No. 72-1, Research Council of Alberta, Edmonton, Alberta, CanadaCharlton et al (1978).

Kennedy, R.G. (1895), The prevention of silting in irrigated channels. Proc. Inst. of Civil Engrs., London, England, Vol. CXIX.

Keulegan, G. H. (1938), Laws of turbulent flow in open channels, National Bureau of Standards Research Paper RP 1151, Washington, D.C.

King, J. G., Emmett, W. W. Whiting, P. J. Kenworthy, R. P. and Barry J. J. (2004), Sediment transport data and related information for selected coarse-bed streams and rivers in Idaho, Gen. Tech. Rep. RMRS-GTR 131, 26 pp., Rocky Mt. Res. Stn., U.S. Dep. of Agric. For. Serv., Fort Collins, Colo.

Klingeman, P. C., Chaquette, C. J. and Hammond S. B. (1979), Bed Material Characteristics near Oak Creek Sediment Transport Research Facilities, 1978-1979, Oak Creek Sediment Transport Report No. BM3, Water Resources Research Institute, Oregon State University, Corvallis, Oregon, June.

Knight, D. W. (1981), Boundary shear in smooth and rough channels. Journal of the Hydraulics Division, 107, HY7, 839–851.

Knight, D. W. and Patel H. S. (1985), Boundary shear in smooth rectangular ducts. Journal of Hydraulic Engineering, 111(1), 29–47.

Knight, D. W., and Yu G. (1995), A geometric model for self-formed channels in uniform sand. Hydra 2000, Proceedings of the 26th Congress of the International Association for Hydraulic Research, A. Ervine and T. Telford (Eds), London, U.K., Vol. 1, 354-359.

Knighton, D. (1998), Fluvial forms and processes: a new perspective, John Wiley & Sons, New York, 383pp.

Kovacs, A. and Parker G. (1994), A new vectorial bedload formulation and its application to the time evolution of straight river channels, Journal of Fluid Mechanics, 267, 153-183.

Kuhnle, R.A. (1992), Fractional transport rates of bedload on Goodwin Creek. In Dynamics of Gravel-Bed Rivers, P. Billi, R. D. Hey, C. R. Thorne, T. Tacconi (Eds). Wiley, New York, 141–155.

Kuhnle, R. A. (1993), Fluvial transport of sand and gravel mixtures with bimodal distributions, Sedimentary Geology, 85, 17-24.

Lacey, G. (1930) Stable channel in alluvium. Minutes of the Proceedings, 229, 259-292.

Lane E. W. (1957). A study of the shape of channels formed by natural streams flowing in erodible material. U.S. Army Engineer Division, Missouri River, Corps of Engineering.

Lane, E.W. and Carlson E.J. (1953), Some factors affecting the stability of canals constructed in coarse granular material. Proceedings of the 5th Congress of the International Association for Hydraulic Research, 37-48.

Lane S. N. and Richards K. S. (1997). Linking river channel form and process: time, space and causality revisited. Earth Surface Processes and Landforms, 22, 249-260.

Lane, S. N. and Richards K. S. (1998), High resolution, two-dimensional spatial modeling of flow processes in a multi-tread channel. Hydrological Processes 12, 1279-1298.

Langbein, W. B. and Leopold L. B. (1968), River channel bars and dunes: Theory of kinematic waves, Geological Survey Professional Paper 422-L, 23p.

Lenzi, M. A., D'Agostino, V. and Billi P. (1999). Bedload transport in the instrumented catchment of the Rio Cordon, Part I: Analysis of bedload records, conditions and threshold of bedload entrainment. Catena. 36, 171-190.

Lenzi, M. A., D'Agostino V. and D. Sonda (2000), Ricostruzione morfologica e recupero ambientale dei torrenti. Editoriale Bios. Cosenza, Italia.

Leopold, L. B. (1982). Water surface topography in river channels and implications for meander development. In Gravel-bed Rivers, R. D. Hey, J. C. Bathurst and C. R. Thorne (Eds.), John Wiley $ Sons, 359-388.

Leopold L. B. (1994). River morphology as an analog to Darwin's theory of natural selection. Proceeding of the American Philosophical Society, 138 (1), 31-47.

Leopold, L. B. (1994). A View of the River. Harvard University Press, Cambridge, Massachusetts USA, 298p.

Leopold L. B., and Maddock T. (1953) The hydraulic geometry of streams channels and some physiographic implications, U. S. Geological Survey Professional Paper, 252, 56p.

Leopold, L. B., Wolman M. G. and J. P. Miller (1964), Fluvial Processes in Geomorphology, W. H. Freeman and Company, San Francisco, 522p.

Li R., Simons M. and Stevens M. A. (1976). Morphology of cobble streams in small watersheds. Journal of Hydraulics Division, Vol. 102, HY8, 1101-1117.

Li, S. S. and Millar R.G. (2007), Simulating bed-load transport in a complex gravel-bed river. Journal of Hydraulic Engineering, 133(3), Doi:10.1061/(ASCE)0733- 9429(2007)133:3(323).

Liao, H. and D. W. Kinght (2007), Analytic stage-discharge formulas for flow in straight prismatic channels. Journal of Hydraulic Engineering, 133(10), Doi: 10.1061/(ASCE)0733-9429(2007)133:10(1111).

Limerinos, J. T. (1970), Determination of the Manning coefficient for measured bed toughness in natural channels. Water Supply paper 1898-B, U.S. Geological Survey, Washington D.C.

Lindley E.S. 1919. Regime Channels. Proceedings Punjab Engineering Congress, Vol Vii, p. 63.

Lisle, T.E. (1995), Particle size variations between bed load and bed material in natural gravel bed channels. Water Resources Research, 31(4), 1107-1118.

Lisle, T.E., J. M. Nelson, J. Pitlick, M. A. Madej, B. L. Barkett (2000), Variability of bed mobility in natural, gravel-bed channels and adjustments to sediment load at local and reach scales. Water Resources Research 36, 3743– 3755.

Lopez, R., and Barragan J. (2008), Equivalent roughness of gravel-bed rivers, Journal of Hydraulic Engineering, 134(6), Doi: 10.1061/(ASCE)0733-9429(2008)134:6(847).

Lu, X. L. (1986), Nonuniform bed load transport rate and coarsening stabilization. Thesis for Master Degree of Chengdu University of Technology.

Lundgren, H. and Jonsson I. G. (1964), Shear and velocity distribution in shallow channels, Journal of Hydraulic Engineering, 90, 1-21.

Mackin, J. H. (1948), Concept of the graded river, Geol. Soc. Am. Bull., 59, 463-512.

Manning, G. (1889). On the flow of water in open channels and pipes. Transaccions of the Institution of Civil engineers of Ireland, 24, 179-207.

Mao L., Cooper, J. & Frostick, L. (2011) Grain size and topographical differences between static and mobile armour layers. Earth surface Processes and Landforms, DOI: 10.1002/esp.2156.

Mao, L., (2012). The effect of hydrographs on bed load transport and bed sediment spatial arrangement. Journal of Geophysical Research, 117, F03024, doi:10.1029/2012F002428.

McCandless, T. L. (2003), Maryland stream survey: Bankfull discharge and channel characteristics of streams in the Allegheny Plateau and the Valley and Ridge hydrologic regions, Rep. CBFO-S03-01, 33 pp., Chesapeake Bay Field Off., U.S. Fish and Wildlife Serv., Annapolis, Md.

McCormack, R. W. (1969), The effect of viscosity in hypervelocity impact cratering. AIAA Paper 69-354, American Institute Aeronautics and Asutronautics, Cincinnati, OH.

Meyer-Peter, E. and Müller R. (1948), Formulas for bed-load transport. International Association for Hydraulic Structures Research, 2nd Meeting, Proceedings. Stockholm.

Milhous, R. T. (1973), Sediment transport in a gravel-bottomed stream, Ph.D. thesis, Oregon State University, Corvallis.

Millar, R. G. (1999), Grain and form resistance in gravel bed rivers, Journal of Hydraulic Research, 37, 303–312.

Millar R.G. (2005) Theoretical regime equations for mobile gravel-bed rivers with stable banks, Geomorphology 64 : 207-220.

Millar R.G., and Quick M.C. (1993). Effect of bank stability on geometry of gravel rivers. Journal of Hydraulic Engineering, ASCE 119: 1343-1363.

Miller, B. A. and Wenzel H. G. (1985), Analysis and simulation of low flow hydraulics, Journal of Hydraulic Engineering, 111(12).

Montgomery, D. R. and Buffington J. M. (1997), Channel-reach morphology in mountain drainage basins, Geol. Soc. Am. Bull., 109, 596–611, doi:10.1130/0016-7606(1997)109<0596:CRMIMD>2.3.CO;2.

Moretto J., Rigon, E. Mao, L. Delai, F. Picco L. and Lenzi M. A. (2012) Assessing morphological changes in gravel bed rivers using LiDAR data and colour bathymetry. Erosion and Sediments Yields in the Changing Environments, Proceedings of a symposium held at the Institute of Mountain Hazards and Environment, China. IAHS Publ. 356, 419-427.

Mueller, E. R. and Pitlick J. (2005), Morphologically based model of bed load transport capacity in a headwater stream, Journal of Geophysical Research, 110, F02016, doi:10.1029/2003JF000117.

Mueller, E.R., Pitlick, J. and Nelson J. (2005) Variation in the reference shear stress for bedload transport in gravel bed streams and rivers, Water Resources Research, 41,W04006, doi:101029/2004WR003692.

Murray, A. B. and Paola, C. (1994). A cellular model of braided rivers. Nature 371, 54-57.

Murray, A. B. and Paola, C. (1997). Properties of a cellular braided-stream model. Earth Surface Processes and Landforms, 22, 1001-1025.

Nagata, N., Hosoda T. and Muramato Y. (2000), Numerical analysis of river channel processes with bank erosion. Journal of Hydraulic Engineering, 126(4), 243-252

Nanson, G. C., and Huang H. Q. (2008), Least action principle, equilibrium states, iterative adjustment and the stability alluvial channels. Earth Surface Processes and Landforms 33, 923-942.

Orlanski, I. (1976). A simple boundary condition for unbounded hyperbolic flows. Journal of computational physics 21, 251-269.

Paintal, A. S. (1971), Concept of critical shear stress in loose boundary open channels, Journal of Hydraulic Research, 9: 91-113.

Paola C. and Seal R. (1995), Grain size patchiness as a cause of selective deposition and downstream fining. Water Resources Research 31: 1395–1407.

Parker G. (1976). On the cause and characteristics scales of meandering and braiding in rivers, Journal of Fluvial Mechanics, 76, 457-480.

Parker, G. (1978), Self-formed straight rivers with equilibrium mobile bed, 2, the gravel river, Journal of Fluid Mechanics, 89, 127-146.

Parker, G. (1979). Hydraulic geometry of active gravel rivers. Journal of the Hydraulics Division, ASCE, Vol. 105, HY9, Proc. Paper 14841, 1185-1201.

Parker, G. (1983), Discussion of “Lateral bed load transport on side slopes”, Journal of Hydraulic Engineering, 109, 197-199.

Parker, G. (1990), Surface-based bedload transport relation for gravel rivers, Journal Hydraulic Research, 28(4), 417–436.

Parker, G. (1991a), Selective sorting and abrasion of river gravel. I: Theory, Journal of Hydraulic Engineering, 117(2): 131-149.

Parker, G. (1991b), Selective sorting and abrasion of river gravel. II: Application, Journal of Hydraulic Engineering, 117(2): 150-171.

Parker, G. (2008). Chapter 3: Transport of gravel and sediment mixtures, in Sedimentation Engineering: Processes, measurements, modeling and practice. Garcia, M. H. (Editor). ASCE Manuals and Reports on Engineering Practice No. 110.

Parker, G. and Peterson A. W. (1980), Bar resistance of gravel bed streams, Journal of the Hydraulics Division Am. Soc. Civ. Eng., 106, 1559– 1575.

Parker, G, and Klingeman P. C. (1982), On why gravel bed rivers are paved. Water Resources Research, 18(5), 1409–1423.

Parker, G., Klingeman P. C. and McLean D. G. (1982a), Bed load and size distribution in paved gravel-bed streams, Journal of Hydraulic Engineering, 108(4), 544–571.

Parker, G., Dhamotharan S. and Stefan H. (1982b), Model experiments on mobile, paved gravel bed streams, Water Resources Research, 18, 1395– 1408, doi: 10.1029/ WR018i005p01395.

Parker, G. and Sutherland A. J. (1990), Fluvial armor, Journal of Hydraulic Research, 28(5), 529-544.

Parker, G. and Wilcock P. R. (1993), Sediment feed and recirculating flumes: fundamental difference. Journal of Hydraulic Engineering, 119(11), 1192-1204.

Parker, G. and Toro-Escobar C. M. (2002), Equal mobility of gravel in streams: the remains of the day, Water Resources Research, 38(11), 1264.

Parker, G., Toro-Escobar C. M., Ramey M. and Beck S. (2003), The effect of floodwater extraction on the morphology of mountain streams, Journal of Hydraulic Engineering, 129(11), 885-895.

Parker, G., Wilcock, P.R., Paola, C., Dietrich, W., and Pitlick, J. (2007) Physical basis for Quasi universal relations describing bankfull hydraulic geometry of single-thread gravel bed rivers, Journal of Geophysical Research, 112, Doi: 10.1029/2006JF000549.

Parker G., Hassan M. and Wilcock P. (2008), Adjustment of the bed surface size distribution of gravel-bed rivers in response to cycled hydrographs, In: Gravel Bed Rivers 6: From process understanding to river restoration, H. Habersack, H. Piegay and M. Rionaldi (Eds), Elsevier, 836p.

Pellegrini, G. B., Surian N., and Urbinati C. (2004). Dating and explanation of Late Glacial – Holocene landslides: a case study from Southern Alps, Italy. Zeitschrift für Geomorphologie, 48, 245-258.

Petit, F. and Pauquet, A. (19979. Bankfull discharge recurrence intervalle in gravel-bed rivers. Earth Surface Processes and Landforms, 22, 685-693.

Philips, J. D. (1992). Non-linear dynamical systems in geomorphology: revolution or evolution. Geomorphology, 5, 219-229.

Pitlick, J. (1992), Flow resistance under conditions of intense gravel transport, Water Resources Research, 28(3), 891-903.

Pitlick, J. and Cress R. (2002), Downstream changes in the channel geometry of a large gravel bed river, Water Resources Research, 38, Doi: 10.1029/2001WR000898.

Pizzuto, J. E. (1990), Numerical simulation of gravel river widening, Water Resources Research, 26(9), 1971-1980.

Pizzuto, J. E. and the ASCE Task Committee on hydraulic, bank mechanics and modelin of river width adjustment (2008). Chapter 7: Streambank erosion and river width adjustment. In Sedimentation Engineering: Processes, measurements, modeling and practice. Garcia, M. H. (Editor). ASCE Manuals and Reports on Engineering Practice No. 110.

Powell, D.M., Reid, I. Laronne J. B. (2001), Evolution of bed load grain size distribution with increasing flow strength and the effect of flow duration on the calibre of bed load sediment yield in ephemeral gravel bed rivers. Water Resources Research 37: 1463 –1474.

Powell, D. M., Laronne, J. B., and Reid, I. (2003) The dynamics of bedload sediment transport in low-order, upland, ephemeral gravel-bed rivers, Advances in Environmental Monitoring and Modelling, 1(2), http://www.kcl/ac/uk/advances/.

Prandtl, L. (1925), Bericht über utersuchungen zur ausgebildeten turbulenz, Z. Angew. Math. Meth., 5, 136-139.

Prestegaard, K. (1983), Bar resistance in gravel bed streams at bankfull stage. Water Resources Research, 19(2), 472-476.

Proffitt, G.T. (1980) Selective Transport and Armoring of Nonuniform Alluvial Sediments, Report No. 80/22. Department of Civil Engineering, University of Canterbury: Christchurch; 203.

Pyrce, R. S and Ashmore P. E. (2003), The relation between particle path length distribution and channel morphology in gravel-bed streams: a synthesis. Geomorphology, 56, 167-187.

Rabassa, J. and Clapperton C. M. (1990). Quaternary glaciations of the southern Andes. Quaternary Science Reviews, 9, 153-174.

Reid, I., Laronne, J. B. and Powell D. M. (1995), The Nahal Yatir bedload database: sediment dynamics in a gravel-bed ephemeral stream, Earth Surface Processes and Landforms, 20, 845-857.

Reid, I., Powell, D. M. and Laronne, J.B. (1996), Prediction of bed-load transport by desert flash floods, Journal of Hydraulic Engineering, 122, 170–173.

Reynolds, C. W. (1987), Flocks, herds, and schools: a distributed behavioral model. Computer Graphics 21(4), M. C. Stone (Ed), 25-34.

Reynolds, O. (1883). An experimental investigation of the circumstances which determine whether the motion of water shall be direct or sinuous, and the law of resistance in parallel channels. Philosophical Transactions of the Royal Society of London, 174, 935-982.

Reynolds, O. (1895). On the dynamical theory of incompressible viscous fluids and the determination of the criterion. Philosophical Transactions of the Royal Society of London, 186, 123-164.

Rhodes, D. G. and Knight D. W. (1994), Distribution of shear force on boundary of smooth rectangular duct, Journal of Hydraulic Engineering, 120(7), 787– 807.

Rice, S. And Church M. (1996), Sampling surficial fluvial gravels: the precision of size distribution percentile estimates. Journal of Sedimentary Research, 66(3), 654-665.

Rickenmann, D. (1991). Hyperconcentrated flow and sediment transport at steep slopes. Journal of Hydraulic Engineering. 117(11), 1419-1439.

Rigon, E., Moretto, J., Mao, L., Picco, L., Delai, F., Ravazzolo, D., Lenzi,I M.A., and Kaless G. (2012). Thirty years of vegetation cover dynamics and planform changes in the Brenta River (Italy): implications for channel recovery. IAHS Publication 356, 178-186; ISSN 0144-7815.

Rodi, W. (1993), Turbulent models and their applications in hydraulics, A state-of-the-art review, 3rd Edition. IAHR Monograph Series, Taylor & Francis, New York, 104p.

Rodriguez, J. F., Bombardelli, F. A. García, M. H. Frothingham, K. M. Rhoads B.L. and Abad J. D. (2004), High-resolution numerical simulation of flow through a highly sinuously river reach. Water Resources Management, 18, 177-199.

Rozovskii, I. L. (1961), Flow of water in bends of open channels. Translated by Y. Prushansky, Israel Program Sci. Translation, Jerusalem, Israel.

Schoklitsch, A. (1962), Handbuch des wasserbaues, 3rd Ed., Springer, Vienna, Austria.

Sear, D. A. (1996), Sediment transport processes in pool-riffle sequences. Earth Surface Processes and Landforms 21, 241-262.

Shames, I.H. (1995) Mecánica de fluidos. 3rd Edition. McGraw-Hill, Colombia, pp.829.

Shin Y.H., and Julien P.Y. (2010). Changes in hydraulic geometry of the Hwang River below the Hapcheon Re-regulation dam, South Korea. International Journal of River Basin Management 8(2) : 139-150. DOI 10.1080/15715121003651252

Shiono, K. and Knight, D. W. (1991), Turbulent open channel flows with variable depth across the channel. Journal of Fluid Mechanics, 222, 617-646.

Sime, L. C., Ferguson R. I. and Church M. (2007), Estimating shear stress from moving boat acoustic dopper velocity measurements in a large gravel bed river. Water Resources Research, 43. Doi: 10.1029/2006WR005069.

Smart, G. M. and Jaeggi M. N. R. (1983), Sediment transport on steep slopes, Mitteilungen 64 der Versuchsanstalt für Wasserbau, Hydrologie und Glaziologie, ETH Zurich, 19-76.

SsRRHH: Subsecretaría de Recursos Hídricos, (2002), Atlas Digital de los recursos Hídricos Superficiales de la República Argentina, CD-ROM, Buenos Aires, Argentina. Also available in the web-site: www.hidricosargentina.gov.ar.

Strickler, A. (1923), Beitrage zur Frage der Geschwindigkeitsformel und der Rauhigkeitszahlen fur Strome, Kanale und geschlossene Leitungen. Mitteilungen des Eidgenossischen Amtes fur Wasserwirtschaft 16, Bern, Switzerland (Translated as ‘‘Contributions to the question of a velocity formula and roughness data for streams, channels and closed pipelines.’’ by T. Roesgan and W. R. Brownie, Translation T-10, W. M. Keck Lab of Hydraulics and Water Resources, Calif. Inst. Tech., Pasadena, Calif. January 1981).

Sun Z. and Donahue J. (2000), Statistically derived bedload formula for any fraction of nonuniform sediment, Journal of Hydraulic Engineering, 126(2), 105-111.

Surian, N. (1998), Fluvial processes in the alpine environment during the last 15.000 years: a case study from the Venetian Alps, Italy. Géomorphologie : relief, processus, environment, nº 1, 17-25.

Surian, N. (1999). Channel changes due to river retulation: the case of the Piave River, Italy. Earth Surface Processes and Landforms, 24, 1135-1151.

Surian, N. and Pellegrini, G. B. (2000). Paraglacial sedimentation in the Piave valley (Eastern Alps, Italy): an example of fluvial processes conditionated by glaciations. Geografia Fisica e Dinamica Quaternaria, 23, 87-92.

Surian, N. and Rinaldi M. (2003). Morphological response to river engineering and management in alluvial channels in Italy. Geomorphology, 50, 307-326.

Surian N, and Rinaldi M. (2004). Channel Adjustments in response to human alteration of sediment fluxes: examples from Italy rivers. In: Golosov, V., Belyaev, V., Walling, E.E (Eds.) Sediment Transfer Trhough the Fluvial System, . IAHS Public. 288, 276-282.

Surian, N. and Cisotto A. (2007), Channel adjustments, bedload transport and sediment sources in a gravel-bed river, Brenta River, Italy. Earth Surface Processes and Landforms 32, 1641-1656.

Surian, N., Ziliani, L. Comiti, F. Lenzi M. A. and Mao L. (2009), Channel adjustments and alteration of sediment fluxes in gravel-bed rivers of North-Eastern Italy: potentials and limitations for channel recovery. River Research and Applications. DOI: 10.1002/rra.1231.

Suzuki, K., and Hano A. (1992), Grain size change of bed surface layer and sediment discharge of an equilibrium river bed. Proc., Int. Seminar on Grain Sorting, Ascona, Mitteilungen Nr. 117 der Versuchsanstalt fu¨r Wasserbau, Hydrologie und Glaziologie, ETH, Zuerich.

Suzuki, K., and Kato K. (1991), Mobile bed armouring of bed surface in a steep slope river with gravel and sand mixture, Proc., Int. Workshop on Fluvial Hydraulics of Mountain Regions, Trento, Lecture Notes in Earth Sciences No. 37, Springer Verlag, Berlin, 393–404.

Thompson A. (1986), Secondary flows and the pool–riffle unit – a case-study of the processes of meander development. Earth Surface Processes and Landforms 11(6): 631–641.

Thorn, C. E. and Welford M. R. (1994). The equilibrium concept in geomorphology. Annals of the Association of American Geographers, 84, 4, 666-696.

Tominaga, A., Nezu I., Ezaki K. and Nakagawa H. (1989), Turbulent structure in straight open channel flows, Journal of Hydraulic Research, 27(1), 149–173.

Venditti, J. G., Church M. A. and Bennet S. J. (2005), Bed form initiation from a flat sand bed, Journal of Geophysical Research, 110, Doi:10.1029/2004JF000149

Weichert, R. b., Bezzola G. R. and Minor H. E. (2009), Bed erosion in steep open channel. Journal of Hydraulic Research, 47(3), 360-371.

White, W.R., Bettess R. and Paris, E. (1982), Analytical approach to river regime. Journal of Hydraulics Division American Society of Civil Engineers 108, 1179-1193.

Whiting, P. J. and Dietrich W. E. (1990), Boundary shear stress and roughness over mobile alluvial beds, Journal of Hydraulic Engineering, 116(12), 1495-1511.

Whiting, P. J., Stamm, J. F. Moog D. B. and Orndorff R. L. (1999), Sediment-transporting flows in headwater streams, Geological Society American Bulletin, 111, 450-466.

Wilcock, P. R. (1997), The components of fractional transport rate, Water Resources Research, 33(1), 247-258.

Wilcock, P. R. and Southard J. B. (1988), Experimental study of incipient motion in mixed-size sediment, Water Resources Research, 24(7), 1137-1151.

Wilcock, P. R. and McArdell B. W. (1993), Surface-based fractional transport rates: mobilization thresholds and partial transport of a sand-gravel sediment. Water Resources Research 29(4), 1297–1312.

Wilcock, P. R., Kenworthy, S. T. and Crowe, J. (2001). Experimental study of the transport of mixed sand and gravel. Water Resources Research, 37(12), 3349-3358.

Wilcock, P. R. and Crowe J. C. (2003), Surface-based transport model for mixed-size sediment, Journal of Hydraulic Engineering, 129(2), 120-128.

Wilcock, P.R. and DeTemple B.T. (2005), Persistence of armor layers in gravel-bed streams. Geophysical Research Letters, 32, L08402. DOI: 10.1029/2004GL021772.

Williams G. P. (1978) Bank-full discharge of rivers. Water Resources Research, 14(6), 1141-1154.

Williams, G. P. and Rosgen D. L. (1989), Measured total sediment load (suspended load and bed load) for 93 United States streams, Open-File Report 89-67, USGS.

Wolman, M. G. (1954) A method of sampling coarse bed material. American Geophysical Union, Transactions, 35, 951-956.

Wolman, M. G. and Millar, J. P. (1960). Magnitude and frequency of forces in geomorphic processes. Journal of Geology, 68, 54-74.

Wong M. and Parker G. (2003), Reanalysis and correction of bed-load relation of Meyer-Peter and Müller using their own database. Journal of Hydraulic Engineering, 132(11). Doi: 10.1061/(ASCE)0733-9429(2006)132:11(1159).

Wong, M. and Parker, G. (2006). One-dimensional modeling of bed evolution in a gravel bed river subject to a cycled flood hydrograph. Journal of Geophysical Research, 111, FO3018, doi:1029/2006JF000478.

Woods, W. (1917). Normal data of design for “Kennedy” channels. Punjab Irrigation Branch, Lahore.

Wu, W. (2008) Computational river dynamics. Taylor and Francis, 494p.

Wu, W. (2004). Depth-average two-dimensional numerical modeling of unsteady flow and nonuniform sediment transport in open channels. Journal of Hydraulic Engineering, 130(10), 1013-1024.

Wu, W., Wang S. S. Y. and Jia Y. (2000), Nonuniform sediment transport in alluvial rivers, Journal of Hydraulic Research, 38(6), 427-434.

Yang C.T, Song C.C.S., and Woldenberg M.J. (1981). Hydraulic geometry and minimum rate of energy dissipation. Water Resources Research 14(4): 1014-1018.

Yang, C.T. and Song CCS. 1979. Theory of minimum rate of energy dissipation. Journal of the Hydraulics Division, ASCE 105 : 759-784.

Yang, C. T. (1971), Potential energy and stream morphology. Water Resources Research 7, 311-322.

Yen, B. C. (1992), Dimensionally Homogeneous Manning’s formula. Journal of Hydraulic Engineering, 118(9), 1326-1332.

Yen, B. C. (2002), Open Channel Flow Resistance, Journal of Hydraulic Engineering, 128(1), Doi:10.1061/(ASCE)0733-9429(2002)128:1(20).

Zadeh, L. A. (1965). Fuzzy sets. Information and control, Vol. 8, 338-353.

ACKNOWLEDGEMENTS

I gratefully acknowledge Mario Lenzi, Luca Mao and Juan Serra for the supervision of my work; their careful reading and useful comments have greatly improved the original manuscript.

I specially thank Johnny Moretto and Anna Simonetto for supporting the extensive field survey measurements in the Patagonian gravel bed rivers; and Emanuel Rigon and Marco Da Canal for supporting the measurements in Italy.

I thank Andrés Malnero, Chief of the Department of Civil and Hydraulic Engineering (Universidad Nacional de la Patagonia San Juan Bosco, Argentina), for providing all the equipment needed for the field surveys in Argentina. I also thank the *Subsecretaria de Recursos Hídricos de Nación* for providing the hydrologic data of the studied gauging stations in Argentina, and the *Azienda Regionale per la Protezione Ambientale (Veneto)* for providing the hydrologic data of the Italian gauging stations.

I'm warmly grateful to Nadia Donati who has showed me the historical dimension and the importance of social context in the development of ideas, and the fascinating world of epistemology.